NOVEL METABOLITES OF ACETATE AND LIPIDIC ALDEHYDES IN MICE AND PIGS THROUGH METABOLOMICS-BASED IDENTIFICATION AND CHARACTERIZATION

A Dissertation

SUBMITTED TO THE FACULTY OF THE

UNIVERSITY OF MINNESOTA

BY

Qingqing Mao

IN PARTIAL FULFILLMENT OF THE REQUIRMENTS

FOR THE DEGREE OF

DOCTOR OF PHILOSOPHY

DR. CHI CHEN, ADVISOR

March, 2025

Acknowledgement

My time at the University of Minnesota is coming to its final chapter, following my first arrival on campus in August 2012. A decade ago, I could not have imagined delving so deeply into the research and science of nutrition. This journey has felt long, yet time has flown by. It has been both challenging and rewarding. With the generous and kind support of the loving people and community around me, I have reached this significant milestone. Throughout my time here in Minnesota, I have not only gained invaluable knowledge and training, but I have also discovered more about myself and the person I aspire to be.

First and foremost, I would like to express my deepest gratitude to my advisor, Dr. Chi Chen, for the dedicated guidance and encouragement throughout my academic journey. His expertise and insight have been invaluable in shaping my research and my growth as a scientist.

I am also grateful to the mentors, cohort students, staff, and collaborators, who have been a constant source of support and inspiration - Committee members: Dr. Brian J Kerr, Dr. Daniel Gallaher, Dr. Xiaoli Chen; students and staff: Dana Yao, Andrew Howe, Theresa Bushman, Wes Mosher, Rachel Su, Junwei Zhang, Dr. Yuyin Zhou, Dr. Yue Guo, Dr. Jieyao Yuan, Dr. Yiwei Ma, Dr. Yuwei Lu, Dr. Xiaolei Shi, Dr. Lei Wang, Makayla Maher, Dr. Edward Yang, Dr. Yuan-Tai Hung.

To my dearest family, thank you for your love, encouragement, understanding, and patience. Despite the long distance between us and the time difference, your belief in me has been my greatest motivation. To my friends, thank you for your understanding and for always being there to offer a listening ear and a comforting presence.

Last but not least, I want to express my heartfelt gratitude to my husband, Zhe Zhang. Without your unwavering support, I could not have made it this far.

Dedication

This dissertation is dedicated to my late grandparents,

Lanzhen Gu and Huaixing Zhang,

who ignited my passion for science, nutrition, and health.
I shall always carry your love and wisdom in my heart as I continue on this life journey.

Abstract

This dissertation explores the identification and characterization of novel metabolites of acetate and lipidic aldehydes in animal models. Advanced metabolomics techniques are utilized to elucidate the metabolic pathways and health impacts of these compounds, which are significant due to their presence in common foods and endogenous production.

Acetate, a vital metabolite involved in numerous metabolic processes, serves as a precursor for acetyl-CoA, essential for energy production and biosynthesis. This research validates urinary N-acetyltaurine (NAT) as a potential biomarker for hyperacetatemia, providing a non-invasive method to monitor circulating acetate levels.

Lipidic aldehydes, formed during the thermal oxidation of lipids and fats, are highly reactive and have been shown to substantially influence cellular metabolism and the health of humans and animals. This study investigates the disposition of aldehydes in the gastrointestinal tract of pigs fed oxidized oils, assessing their biotransformation and influence on nutrient digestion. The findings revealed the importance and potential contribution of *de-novo* aldehyde formation within the gastrointestinal tract to host health. Additionally, urinary markers responsive to lipidic aldehyde intake were characterized and identified in a mouse model. The results demonstrated the potential for new methods of assessing dietary aldehyde intake. Additional lipidomic analysis of the oils highlights the broader impacts of other lipid oxidation products in thermally oxidized oils on the host metabolism and health.

All these insights enhance the understanding of acetate and lipidic aldehyde metabolism, offering new biomarkers for monitoring their dietary intake and metabolic states. Meanwhile, the findings call for further investigation into the comprehensive profiling of lipid oxidation products in oils, and their respective disposition and metabolic consequences.

Table of Contents

List of Tables

List of Figures

Chapter 1 Literature review

As targets of investigation in this dissertation research, acetate and lipidic aldehydes are broadly present in common foods and actively produced within the endogenous metabolic system. Acetate, a vital metabolite, plays numerous roles in metabolic processes, serving as a precursor for acetyl-CoA, essential for energy production and biosynthesis. Meanwhile, lipidic aldehydes, formed during the thermal oxidation of fats, have been implicated in various adverse health effects due to their highly reactive nature and potential to cause cellular damage. Additionally, they are associated with adverse growth performance in production animals fed oxidized oils. Understanding the impact of these compounds, both from dietary intake and endogenous production, is crucial for elucidating their roles in health and disease. This dissertation aims to: 1) review the current knowledge and identify gaps in the research areas associated with acetate and lipidic aldehyde metabolism; 2) examine and validate a potential urinary marker for circulating acetate; 3) investigate the disposition of lipidic aldehydes in the gastrointestinal tract of pigs fed oxidized oils; and 4) characterize and identify aldehyde-responsive urinary markers in a mouse model. Ultimately, this dissertation seeks to contribute to the broader field of nutritional science and metabolic health.

1.1 ACETATE

1.1.1 Sources of acetate

Acetate is an important intermediate metabolite that can originate from both exogenous and endogenous sources. Exogenously, acetate could come from dietary

sources, such as the consumption of fermented food (e.g., kimchi[1]) and apple cider vinegar.[2] Medical procedures may introduce exogenous acetate into the circulation, such as using acetate as a buffer in hemodialysis.[3] Besides the direct input, alcohol intake could be an indirect source of acetate. The acetaldehyde, a toxic intermediate metabolite of alcohol, is detoxified by aldehyde dehydrogenase and transformed to acetate.[4] On the other hand, there are several pathways for endogenous acetate production. In the liver, acetate can stem from acetyl-CoA hydrolysis by cytoplasmic acylthioesterase-12 (ACOT12) during the lipid β-oxidation process. This metabolic pathway frees coenzyme A for other metabolic activities[5], and may be heightened by starvation.[6] For cells with adequate nutrition supply, pyruvate could be converted to acetate via oxidative decarboxylation in mitochondria. This is, in fact, an acetyl-CoA-independent metabolic activity of keto acid dehydrogenases, through either thiamine- or reactive oxygen species (ROS)-dependent pathways.[7,8] Additionally, acetate could be released from the acetylated metabolites within the system, such as acetylated proteins.[9] Another source of acetate is the gut microbiome. Acetate is a major microbial fermentation product on indigested carbohydrate, which is then extensively absorbed and uptaken by the liver.[10,11]

1.1.2 Disposition and metabolism

Acetate plays versatile roles in human health and disease. It is transported into cells by both passive diffusion and monocarboxylate transporters-mediated facilitated diffusion.[12] The disposition and metabolism of acetate have been extensively studied and summarized in reviews.[10,13]

Acetate is an immediate precursor of acetyl-CoA, which is an essential intermediate in both catabolic and anabolic processes of macronutrient metabolism, as well as the cofactor for the acetylation of protein, nucleotides, and other amino-containing metabolites.[14] Acetyl-CoA plays a role in the intersection of nutrient sensing, energy metabolism, and stress response. The acyl-CoA short-chain synthetase member 1 (ACSS1), located in the mitochondria, esterifies acetate and CoA to supply the citric acid cycle.[15] The muscle, heart, and brown adipose tissue had higher expression of ACSS1.[15] The ACSS2, on the other hand, is primarily distributed in the nucleus and cytoplasm.[16] For humans, high expression levels are found in the kidney, muscle, small and large intestine, and adipose tissue.[17] It is responsible for capturing and recycling the acetate released from histone deacetylation[18,19], and can be upregulated for cells deprived of oxygen and lipid sources.[20] Meanwhile, acetate is a ligand for free fatty acid receptors 2 (FFAR2, also known as G-protein coupled receptor 43, GPR43), which regulates pancreatic β-cell function[21,22] and mediates inflammatory responses.[23,24]

Acetate is primarily excreted via urine.[25] In the kidney, acetate is metabolized to bicarbonate, which in turn plays a role in regulating acid-base balance. Also, in the kidney, the acetate excretion depends on reabsorption via the monocarboxylic acid transporters in the renal proximal tubule.[26,27]

1.1.3 Health impacts

In many cases, acetate is considered beneficial to host health. The acetate sourced from gut microbiome fermentation was considered a main contributor to the health benefits of high dietary fiber intake, including reducing lipolysis, lowering blood

cholesterol, and enhancing insulin sensitivity [11,28]. Additional benefits in body weight reduction [29], expedited fatty acid oxidation[30], and reduced pro-inflammatory cytokines [31] were also observed. Dietary acetate supplementation also showed desirable health effects, such as improved glucose uptake and lowered blood glucose levels.[32,33] Researchers have shown a notable interest in the consumption of apple cider vinegar. Clinical trials have been conducted worldwide to investigate the health benefits for overweight and obese[2], diabetic[34], dyslipidemic patients[35], and women with polycystic ovary syndrome (PCOS) [36]. The efficacy of the clinical application of apple cider vinegar is being actively studied. Discussions on vinegar consumption for its health-promoting benefits have also spanned in media platforms.

However, discrepancies have been reported as well.[10] Perry et al. observed hyperinsulinemia, increased fat deposition, and weight gain in rats that experienced chronic elevations in gut microbiome-derived acetate, accompanied by increased plasma acetate levels. Notably, such findings were observed from animal models maintained on a high-fat and high-calorie diet.[37] Additionally, acetate reportedly has a pro-cancer effect, utilized as an energy source and a substrate for lipogenesis and biomass accumulation for cancer cells, especially the aggressive types.[20,38] In fact, a recent metabolomic study associated higher blood acetate levels with an increased risk of breast cancer.[39] Additionally, the usage of acetate as the hemodialysis buffer has been associated with the development of hypotension and hypoxemia through its vasodilatory effect.[40] Considering the double-edged effects of acetate on health, monitoring systematic acetate levels potentially pertains to research and clinical importance.

Currently, acetate level is assessed via blood acetate. However, blood samples are not always available and require invasive procedures to acquire. A previous study identified elevated urinary *N*-acetyltaurine (NAT) as a metabolite in response to the increased circulating acetate from the metabolism of alcohol in mice dosed with ethanol.[41] Hence, investigating the efficacy of NAT as a urinary biomarker for NAT may provide a non-invasive predictor for monitoring acetate levels.

1.2 LIPIDIC ALDEHYDES

1.2.1 Structural xlassification of aldehydes

Aldehydes are a group of organic compounds containing a polarized carbon-oxygen double bond (-CH=O), known as the aldehyde group.[42] Based on their structures and functional groups, they can be further classified mainly into two major categories: A) aromatic aldehydes, containing an aromatic ring structure; B) aliphatic aldehyde, with the aldehyde group (-CHO) directly attached to the aliphatic chain. The aliphatic aldehydes can be further characterized into the following sub-categories: i) alkanals, saturated aldehydes; ii) alkenals, which include the α, β-unsaturated aldehydes, substituted alkenals, bis-alkenals, and epoxy aldehydes.[43]

Aromatic aldehydes are commonly used in perfumery and organic chemistry industries. Some examples include vanillin, the major flavor component of vanilla, and benzaldehyde (C_7H_6O), a major component of almond oil and used as an almond flavor.[44,45] Alkanals contain only the saturated C-C bond, such as nonanal ($C_9H_{18}O$). Alkenals refer to the aldehydes containing unsaturated C=C bonds. Usually, in fried oils, 2-alkenals are the most common species.[43] Among alkenals, α,β-unsaturated aldehydes

have a C=C double bond between the α and β (2nd and 3rd) carbon, such as 2,4-decadienal ($C_{10}H_{16}O$). Its suffix -adienal indicates the existence of two unsaturated C=C chains. Furthermore, some alkenals with additional functional groups, including hydroxyl (-OH), hydroperoxyl (-COOH), and ketone (-C=O-) groups, are classified as substituted alkenals.[43,45] One example is 4-hydroxy-2-nonenal ($C_9H_{16}O_2$), which has been extensively studied for its toxicity and carcinogenicity.[46] Epoxy aldehydes contain an epoxy group, such as 2,3-epoxy-4-hydroxynonanal, also a lipid peroxidation product.[47] Bis-aldehydes usually contain 2 aldehyde groups (-CHO) at the terminals of the molecule, exemplified by malondialdehyde (MDA), a substrate for thiobarbituric acid reactive substance (TBARS) assay and broadly used as an oxidation indicator both *in-vivo*[48] and *in-vitro*[49].

1.2.2 Dietary sources of aldehyde

Humans and animals can encounter aldehydes via environmental exposure, dietary intake, *in-situ* generation in the gastrointestinal tract (GI), and endogenous formation in the post-absorptive systems.[44,50] The dietary source of aldehydes includes various foods and ingredients, including fruits, vegetables, meats, fish, dairy, and grain products.[44]

1.2.2.1 Naturally existing aldehydes in foods

Aldehydes are naturally found in both minimally processed (e.g., raw foods) and processed (or cooked) foods. The aldehydes naturally produced by plants are primary attributors to their sensory properties. For example, aldehydes in herbs and spices define their unique aromas, such as vanillin in vanilla beans and cinnamaldehyde in cinnamon.[51] Aldehydes are also naturally present in many fruits and vegetables. For example, *trans*-2-

hexenal is abundant in apricot, banana, and radish[52], with a fresh and leafy aroma known as the leafy aldehyde.[53] Hexanal, a saturated alkanal, is naturally produced in plants and smells like cut grass.[54] Natural-occurring lipid oxidation also yields aldehydes in foods containing oils and fats. Hexanal, as an aldehyde originated from the oxidation and decomposition of linoleic acid (LA)[55], is a good indicator for the oxidation and flavor deterioration in meat and meat products.[56]

1.2.2.2 Aldehydes produced by food processing

In addition to the inherent species, various processing methods, including cooking, produce aldehydes in foods. In fermentation, 3-methyl butanal, a microbially produced branched-chain aldehyde, is a key compound ascribing to the malty aroma of fermented black tea[51], some cheeses[57], and alcoholic beverages[58]. Fermentation also produces flavor precursors, and then heating further transforms the precursors into odorant aldehydes.[59] In chocolate production, the fermentation of raw chocolate releases amino acids, fatty acids, and reducing sugars, which are then converted to odorant aldehydes during the following heated manufacturing process.[59] Three aldehydes are responsible for the pleasing chocolate-like flavors: 2-methyl-propanal, 2-methyl-butanal, and 3-methyl-butanal.[60]

Thermal treatment of lipids is known to produce aldehydes as well.[51] When heated, especially at higher temperatures for long periods, triglycerides can undergo extensive oxidation and degradation, giving rise to more than 20 different aldehyde species.[61,62] The cooking fume contains inhalable alkanals, alkenals, and alkadienals.[63] Some of these aldehydic species are responsible for the aroma of the foods, such as 2,4-decadienal,

which gave baked wheat bread a fatty smell.[64] Heated oils and fats, especially cooking oil, are rich in aldehydes, that can be ingested[61] or transferred to food matrices. For example, potatoes contain only 0.1% fat.[65] However, in the making of French fries, diverse aldehydes formed in the frying oil, as a result of lipid peroxidation, can migrate into the potato matrix in different rates and efficiencies.[43,66]

As mentioned above, aldehydes are broadly used as flavoring agents given their volatility and odorant sensory properties.[52] Their status as Generally Regarded As Safe (GRAS) compounds is commonly reviewed by the Flavor Extract Manufacturers Association (FEMA).[52,67] In a 2008 report, a total of 91 α,β-unsaturated aldehydes were confirmed to be GRAS and used as flavoring compounds in food manufacturing.[52]

1.2.2.3 *In-situ* formation of aldehydes in the gastrointestinal tract

In addition to the presence in the foods, aldehydes can be formed in the gastrointestinal tract (GIT) during the digestion of foods, as a result of the *in-situ* transformation of dietary lipids. In the stomach, the strong acidic environment and the presence of oxygen lead to the peroxidation of dietary lipids[68] via a non-enzymatic mechanism, such as the conversion of linoleic acid (LA) to linoleic acid hydroperoxide (LA-OOH).[50,69,70] These hydroperoxides could undergo further modification and form other oxidation products, including hydroxyls, epoxyketones, and aldehydes.[71] LA-OOH was broken down to secondary oxidation products in the stomachs of rats.[50] Similar transformations were observed from *in-vitro* studies. Among the formed short-chain volatile compounds, hexanal is the main end product from the decomposition of the 13-hydroperoxide of LA.[50,72] The *in-vitro* digestion studies further demonstrated that the

production of aldehydes is positively correlated with the degree of unsaturation of the fatty acid composition of the oils.[73] In addition to hydroperoxides, hydroxy lipids in oxidized oils can decompose to aldehydes in the stomach.[50] The aldehydes could be directly absorbed in the stomach, but the rates of decomposition and absorption are dose-dependent. When rats were dosed with 18 μmol labeled linoleic acid hydroperoxides, about 50% of the decomposed products were absorbed in the stomach without transferring to the intestine. However, when the dose increased to 1 mmol, the transformation in the gastric chamber seemed to be saturated. About 8.3% of the label was recovered in the intestine.[50]

1.2.2.4 Endogenous sources of aldehyde

Besides exogenous and *in-situ* sources, aldehydes, particularly the linear aliphatic species, may be produced from the endogenous peroxidation and breakdown of unsaturated fatty acids. Lipids, either stored as non-polar triglycerides, or present as cell membrane constituents, are vastly distributed at cellular and subcellular locations. The lipid species with higher polyunsaturated fatty acid (PUFA) content are more prone to peroxidation, producing predominantly linear aliphatic alkenals, alkanal, alkadienals, and substituted alkenals.[74-76] At tissue, cellular, and subcellular levels, reactive oxygen species (ROS) are constantly produced to initiate the peroxidation of endogenous lipids and yield aldehydes, such as hexanal, 2-nonenal, acrolein, malondialdehyde, and 4-hydroxy-2-nonenal (HNE)[77-80], which may be detoxified via multiple metabolic routes.[76,81] The stressors and diseases that increase oxidative stress and ROS production, therefore, may heighten endogenous aldehyde production.[76]

1.2.3 Current understanding on the dietary intake of aldehydes

Assessing the dietary intake of aldehydes is challenging, due to the diversity in aldehyde species and food sources.

1.2.3.1 Aldehydes from food additives vs traditional foods

Among all the α,β-unsaturated aldehydes used as GRAS flavoring compounds, *trans*-2-hexenal makes up 66% of the total annual volume of commercial usage.[52] As a food additive, the estimated intake of 2-hexenal food additive was 57 μg/person/day, consisting of only a small fraction of the estimated 2,390 μg/person/day from natural foods, with the highest contribution from bananas. Other α,β-unsaturated aldehydes shared a similar pattern, with more intake from traditional food sources than in the form of additives.[52] For example, 2,4-decadienal is a GRAS flavoring compound, with intake from naturally occurring sources exceeding more than 200 fold of the additive source (0.2 μg/kg body weight/day).[52] Generally, the GRAS status is established under the consideration of the low quantity in the food matrix and the frequency of dietary intake. Therefore, aldehydes from additives account for only a shallow portion of the total aldehyde intake.[74]

1.2.3.2 Aldehyde in thermally oxidized oils

Fresh and commercially edible oils usually have very low levels of aldehydes, while the thermally oxidized oils contain diverse aldehydes. In oxidized soybean oil, the major aldehydes are made up of saturated alkanals, unsaturated alkenal (e.g., 2-decenal), substituted alkenal (e.g., 4-hydroxynonenal, HNE), and alkadienal (mostly α, β-

unsaturated aldehydes, e.g., 2,4-decadienal). The aldehyde levels are positively correlated with heating time, temperature, and unsaturation level.[66,82]

The exposure of lipidic aldehydes is related to detrimental events in human health.[44] It was estimated that an individual's daily intake of total aldehydes could reach 7 mg/kg/day, equivalent to 525 mg/day for a 75 kg adult (165 lbs). Around 70-75% of the total volume came from α,β-unsaturated aldehydes.[44,83] Three categories of aldehydes are derived from lipid peroxidation: *n*-alkanals, *trans*-2-alkenals, and alka-(*trans, trans*)-2,4-dienals.[84] The total aldehydes in heated soybean oil (HSO) may reach ~800 mg/L, with 2,4-decadienal making up to half of it.[66] In culinary oils rich in linoleoylglycerols, 20 min heating at 185 °C produced 3 mmol/L alkanals, and 13 mmol/L α,β-unsaturated aldehydes per kilogram oil.[85] The differences in dietary patterns and food/ingredient sources would lead to great individual and regional variances. Unfortunately, the threshold for maximum acceptable intake of the aldehydes has not been clearly defined.[44] Grootveld et al. provided a rational estimation of several species based on the very limited existing information in 2 separate reviews.[44,74]

Assuming hexanal, 2-octenal, and 2,4-decadienal were each class's sole and representative compounds, heated sunflower oil was estimated to contain more than 300 ppm, 1,500 ppm, and 2,000 ppm of each. Alka-(*trans, trans*)2,4-dienals are the most abundant species (e.g., 2,4-decadienal) derived from peroxidized PUFA (e.g., linoleic acid).[66,74] As a result, the proportion of alka-(*trans, trans*)2,4-dienals was even higher in PUFA-rich lipid sources, exceeding 75%, with less than 25% total aldehydes as saturated alkanals.[74] Following such calculation, in a 100 g serving of French fries that contain

15% (w/w) oil, alkadienals were estimated to be nearly 300 ppm alkadienals, approaching ~28 mg.[74]

Because the macromolecules in the food matrix can interact with aldehydes, the actual profile of oil-derived aldehydes in the food might deviate from the oils. For example, French fries, or fried potato chips, compared to their frying oils, had higher ratios of saturated alkanals over unsaturated aldehydes.[74] The ^{1}H-NMR examination of fried potato chips (10-15% oil content, w/w) revealed an approximate 1:1:1 molar ratio, around 120 μmol/kg, for each of the three aldehyde classes.[84] It is worth mentioning that the oil used in this study contained equivalent concentrations of MUFA and PUFA.[74,84] In French fries prepared in PUFA-rich oils, such as soybean oils, 2,4-decadienal alone could account for 50% of total aldehyde concentration.[66]

Acrolein, an oil-derived aldehyde, is a known toxin and has been studied extensively. It is also the simplest α,β-unsaturated aldehyde. Its daily intake was estimated from foods containing 0.05 to 1.0 mg acrolein/kg. Though only 8 common food sources were included for this evaluation, the accumulated acrolein intake was 2.35/mg/day.[86] At the same time, the Acceptable Daily Intake/Tolerable Daily Intake (ADI/TDI) for acrolein is 1.09 mg/day via oral exposure, set by the U.S. Environmental Protection Agency.[87] In Australia, the ADI for acrolein is 0.0005 mg/kg body weight/day, equivalent to 0.0375 mg for a 75 kg adult (165 lbs), and is only 3% of the U.S. standard. The estimated 2.35/mg daily intake exceeds either ADI value. Given the broad existence of acrolein in food sources[88], its actual daily intake was estimated to be even higher, reaching 5.0 mg/day[74,86], doubling the U.S. ADI. Processed and cooked foods rich in lipids, especially

Ω-3 fatty acids, are major contributors to the total acrolein intake.[44] French fries may contain 14.8 – 19.9 μg/kg acrolein, whereas the acrolein concentration could reach 7.4 – 207.4 mg/kg in frying oils.[88] Yet, the acrolein intake will vary depending on geographic locations and the population's dietary pattern. On the other hand, only very few aldehydes (metaldehyde, acrylamide) have well-recognized or established ADI/TDI.[74]

1.2.3.3 Oxidized oil in human and animal diet

Dietary fats, including triglycerides and free fatty acids, are macronutrients. Fats account for about 30% of daily energy intake in a typical Western diet in the U. S.[89], while thermally processed oils and lipids make up to half of the daily fat intake.[90] Residual frying and cooking oils from commercial food production are not deemed for human consumption. In the U.S., restaurants generate about 2.5 billion pounds of waste oils annually.[91,92] Making up 1/3 of the total annual fats and oils production, the waste oils from restaurants are economical and environment-friendly raw materials for industrial use (e.g., biodiesel production) and animal feed.[91,93]

Among the rendered grease, fats, and oils, vegetable oils are the most used for animal feed in commercial practices.[94] Although rendered fats and oils are usually further processed for quality assurance, the feed-grade fats and oils can still be significantly oxidized. Shurson et al. reported a broad range of PV (0.1 to 180.8 mEq O_2/kg) in a total of 610 oil samples obtained from a feed manufacturer.[95,96] This phenomenon was supported by another study that surveyed 41 feed-grade fat samples from across the U.S. Infrared analysis detected a wide range of active oxygen content (0.5 – 184 mEq/kg).[95,97] Additionally, seasonal variations have been observed in lipid peroxidation status, as 40-

50% of the feed-grade fats showed higher instability during the summer months.[98] Storage and feed processing procedures can also intensify the peroxidation of lipid components.[95]

Many animal feeding trials have been conducted to evaluate the potential adverse influence of oxidized oil on animal health. In pig-feeding experiments, heated soybean oil has been broadly studied at varying incorporation ratios (*wt/wt*) (e.g., 3%[99], 5%[100], 6%[101], 7.5%[102], 10%[103,104]). As summarized in a meta-analysis, in addition to soybean oil, other forms of oxidized oil were studied for swine feeding trials, including fish oil, choice white grease, corn oil, canola oil, maize oil, poultry, and beef fat.[105] In addition to swine, poultry was commonly studied for feeding oxidized soybean, sunflower, corn, and blended oils.[105] The intake of oxidized oils reduced the average daily growth (ADG) by 5%, the average daily feed intake (ADFI) by 3%, and the G:F ratio by 2%.The different oil sources, fatty acid compositions, and oxidation status of the oils result in variations in the magnitude of the growth performance changes.[105] Hung et al. also pointed out that comparing oxidized-oil-elicited impacts on animal growth remains challenging due to the lack of more accurate methods for assessing the oxidation of oils.[105] The metabolic consequences of oxidized oil consumption and the commonly used approaches for analyzing aldehydes and oil oxidation status are discuss later in this chapter.

1.2.4 Aldehydes in thermally oxidized lipids

1.2.4.1 Schemes of aldehyde formation in thermally oxidized oils

The process of forming lipid oxidation products (LOPs) in thermally oxidized oil is characterized into three stages: initiation, propagation, and termination.[106] In addition to

thermal stress, exposure to metal ions, light, and irradiation can also trigger oxidation. The initiation stage is marked by hydrogen abstraction and the formation of an alkyl radical of FA (R·). In the propagation state, oxygen reacts with the alkyl radical to form a peroxyl radical (ROO·), which then accepts a hydrogen abstracted from an unsaturated fatty acid, yielding a hydroperoxide (ROOH), a primary LOP. In the termination stage, the hydroperoxides can either react with other radicals formed in the previous stages, forming polymers, or degrade to small non-radical molecules known as secondary LOPs, including acids and aldehydes.[107] Commonly consumed vegetable oils (olive, soybean, corn, canola, and sunflower) primarily consisting of the following unsaturated fatty acids: oleic acid (C18:1, OA), linoleic acid (C18:2, LA), and linolenic acid (C18:3).[108] The routes of their oxidation under heating are discussed below.

1.2.4.2 Primary LOPs of C18 unsaturated fatty acids

Oleic acid

As the second-most abundant FA in soybean oil (~25%, weight) and the most abundant FA in olive oil (~83%, weight)[108], oleic acid is a monounsaturated fatty acid (MUFA) with a double bond between C9 and C10. Its oxidation starts with hydrogen abstracted at C8 or C11. The formed alkyl radicals undergo rearrangement and oxygen attraction, yielding four hydroperoxides of oleic acid (OA-OOH) **(Figure 1.1)**. The 8- and 11-OA-OOH are preferably produced than the 9- and 10-OA-OOH.[107]

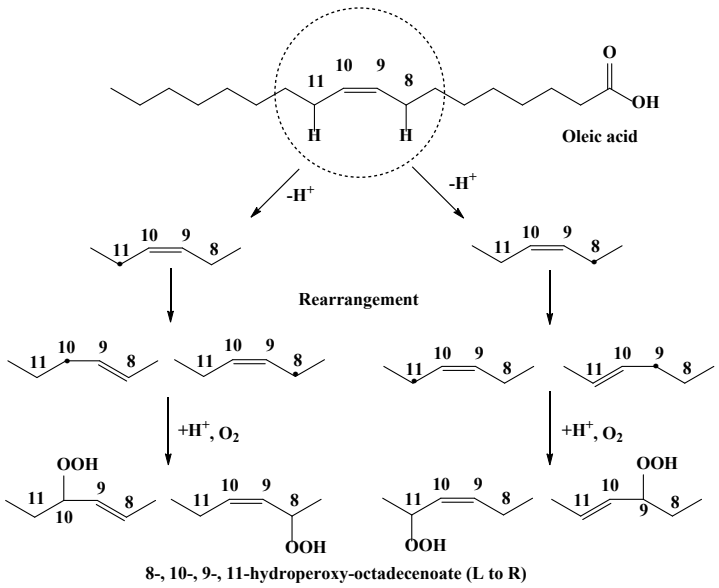

Figure 1.1 Formation of oleic acid-derived hydroperoxides.[107,109]

Linoleic acid

Linoleic acid (LA) is a poly-unsaturated fatty acid (PUFA) and is the most abundant FA in soybean oil (~63%, weight) and sunflower oil (~60%, weight), and the second most abundant in canola oil (~25%, weight). Olive oil contains only ~13% (weight) of LA.[108] It is also an Ω-6 essential fatty acid, that can only be acquired from dietary intake for humans and pigs. For LA, the hydrogen at C11 (the 1,4-diene structure) is easily lost upon oxidative stress. The radicals then form 13- and 9-LA-OOH **(Figure 1.2)**.[107] In an NMR study, Frankel et al. estimated that the two hydroperoxides are produced at about equal ratio from methyl-LA thermal oxidation.[110]

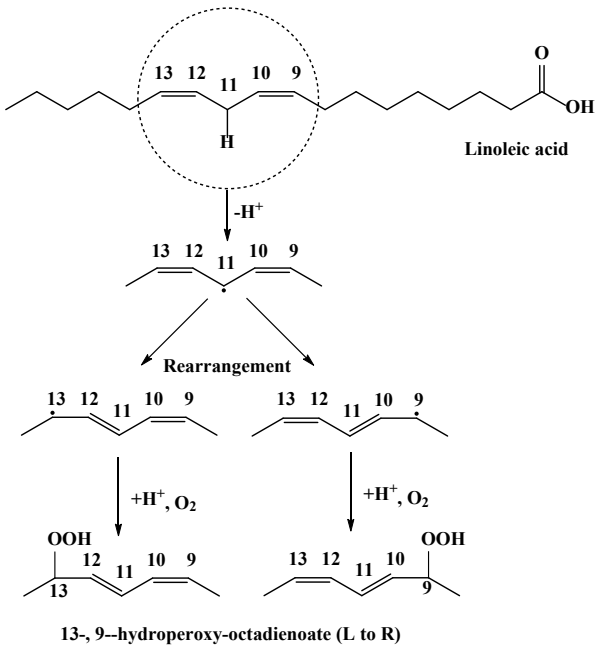

Figure 1.2 Formation of linoleic acid-derived hydroperoxides.[107,109]

Linolenic acid

Linolenic acid (LnA), specifically the α isoform (ALA), is an essential Ω-3 fatty acid for humans and pigs. It is the least abundant FA in olive, canola, soybean, and sunflower oil (~3%, ~15%, ~10%, ~1%, respectively, by weight).[108] Its oxidation mechanism is similar to LA, with the hydrogen easily abstracted from C11 and C14. The additional 1,4-diene structure (compared to LA) gives more diversity to the formed hydroperoxides of ALA **(Figure 1.3 A)**.[107] Yet, the ratio of these LnA-OOHs varies. The 16-LnA-OOH is the most dominant in the 25-80°C temperature range, making up about 48% of the total hydroperoxides of LnA. The second abundant species is 9-LnA-OOH (~30%). The 12- and 13-LnA-OOH are produced at a similar ratio of 10%.[111]

On the other hand, the γ-linolenic acid (GLA) is an essential Ω-6 fatty acid for humans, commonly found in evening primrose, borage, and black currant seed oils (9%, 21%, and 17%, respectively, by weight of total fatty acid).[112-114] Its oxidation pathway is less studied than ALA and hence not discussed further. A putative pathway is illustrated in **Figure 1.3 B** (adapted from Frankel et al.[107]).

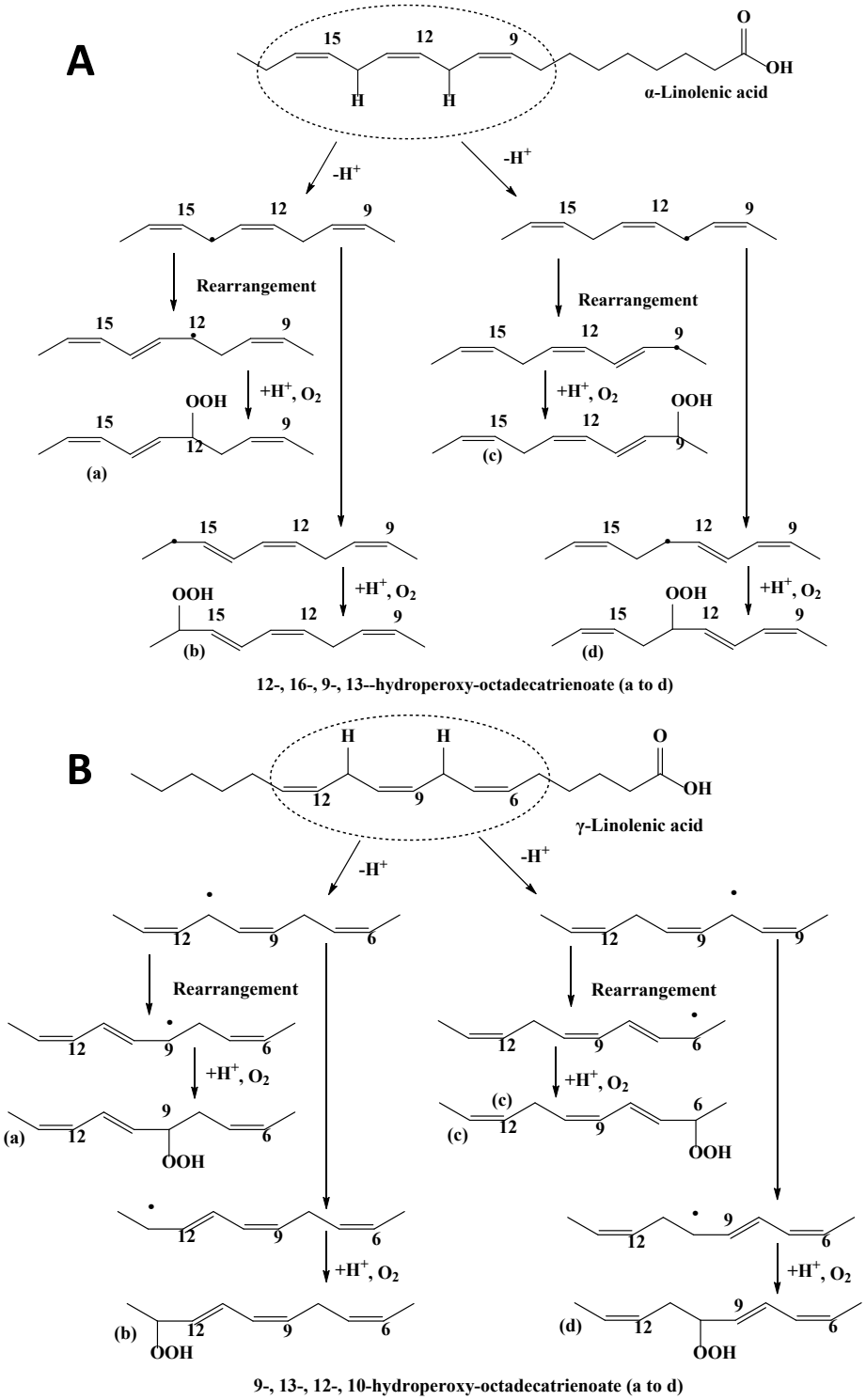

Figure 1.3 Formation of linolenic acid-derived hydroperoxides. A) From α-linolenic acid[107,109] and B) From γ-linolenic acid (putative pathway, adapted from Frankel et al.[107]).

1.2.4.3 Aldehyde formation from hydroperoxide decomposition

After extensive heating at high temperatures, the radicals continue to attack the hydroperoxides, which decompose to diverse secondary LOPs, including acids and aldehydes **(Figure 1.4)**.[43,106,115,116] For example, the loss of hydroxyl radical (OH·) from the hydroperoxide group in 9-hydroperoxide of LA **(Figure 1.4 A)**, forms an alkoxy radical (RO·). The adjacent C-C bonds to the radical are then subjected to homolytic β-scission, giving rise to smaller molecules, such as 2-nonenal and 2,4-decadienal. These products may further interact with the radicals formed from previous steps, converting to substituted alkenal, such as 4-hydroxy-2-nonenal (HNE), or breakdown to smaller aldehydes, such as 2-octenal and hexanal **(Figure 1.4 A)**. It should be noted that one aldehyde may come from multiple hydroperoxide precursors. For example, HNE can be derived additionally from the 13-hydroperoxide of linoleic acid via a dihydroperoxide intermediate **(Figure 1.4 B)**.

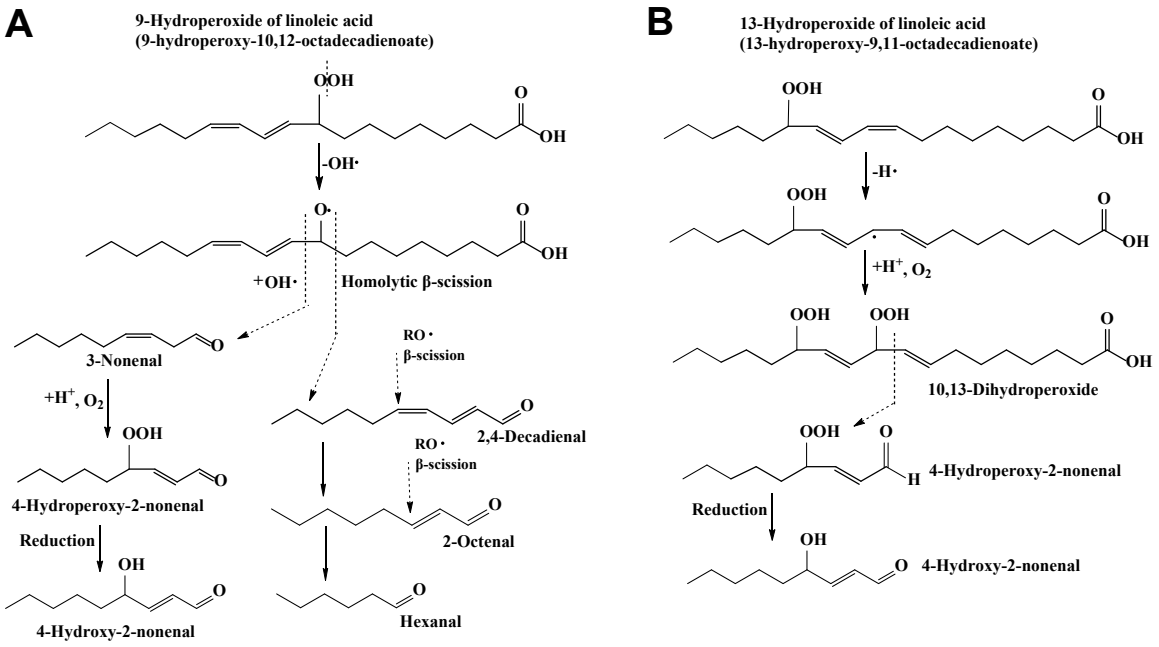

Figure 1.4 Formation of aldehydes from the 9- and 13- hydroperoxide of linoleic acid. A) Mechanisms of forming 2,4-decadienal, 2-octenal, hexanal, and 4-hydroxy-2-nonenal. B) Mechanisms of forming 4-hydroxy-2-nonenal via a dihydroperoxide intermediate.[107,109]

1.2.4.3 Factors influencing aldehyde formation in thermally oxidized oils

Fatty acid composition, temperature, and heating time are the main factors associated with the aldehyde yield in thermally oxidized oils.

Fatty acid composition

When it comes to fatty acid composition, different fatty acids, due to the different structural locations of the C=C double bonds, give rise to different aldehydes. Meanwhile, the higher degree of unsaturation is more reactive and prone to heat-induced autoxidation.[82] Oleic is the least reactive among the C18 unsaturated FAs since it only has one C=C double bond.[107] It is the precursor for C7 – C11 saturated aldehydes, as well as 2-decenal and 2-undecenal.[66,116-118] Linoleic acid has two unsaturated C=C bonds and is reportedly 40 times more reactive than oleic acid.[107] It is the precursor for pentanal, hexanal, and a series of alkenals, including 2,4-decadienal, 2,4-undecadienal, 2-octenal, 2-nonenal, and 2-heptenal.[116] Additionally, LA is responsible for forming substituted alkenals, including 4-HNE.[107] Linolenic acid, on the other hand, is more reactive than LA by 2.4 fold.[107] It is the precursor of C4-C11 unsaturated alkenals, HNE, propanal, and butanal. [66,116-118] As a result, the aldehyde generated in different oils largely depends on their fatty acid composition. Olive oil is rich in oleic acid (83% by weight).[108] After heating at 180 °C, hexanal, nonanal, and pentanal were the three most abundant

aldehyde produced.[119] Though olive oil consists of only 13% LA[108], due to much higher reactivity[107], the LA derivatives surpassed the OA derivatives by around 2 fold in olive oil heated at 180 °C.[119] Similarly, canola oil's OA and LA ratio is around 2-fold (by weight).[108] Yet, in heated canola oil, the LA-derived aldehyde could be 3 fold higher than OA-derived ones.[119] On the contrary, soybean and sunflower oils are rich in LA (~63% and ~60% by weight).[108] The most abundant aldehyde in heated soybean and sunflower oils is usually 2,4-decadienal[61,66], a characteristic aldehyde originated from LA oxidation. The known fatty acid and monohydroperoxide precursors of selected aldehydes are summarized in **Table 1.1**.

Table 1.1 The known fatty acid and monohydroperoxide precursors of selected aldehydes formed at frying temperature [43,120]

Fatty acid	**Monohydroperoxide**	**Aldehydes formed**
Oleic acid	OA-8-OOH	Decanal, 2-Undecenal
	OA-9-OOH	2-Decenal, Nonanal
	OA-10-OOH	Nonanal
	OA-11-OOH	Octanal
Linoleic acid	LA-9-OOH	2,4-Decadienal, 4-HNE, 3-Nonenal, 2-Octenal
	LA-13-OOH	Hexanal, 4-HNE, Pentanal
Linolenic acid	LnA-9-OOH	2,4,7-Decatrienal, 3,6-Nonadienal
	LnA-12-OOH	2,4-Heptadienal, 3-Hexenal
	LnA-13-OOH	3-Hexenal, 2-Pentenal
	LnA-16-OOH	Propanal

Temperature

The aldehyde is generated at a higher rate during food processing at higher temperatures. The 185 °C is a typical temperature used for frying oils. The kinetics of aldehyde formation before and after reaching this temperature displayed distinct patterns,

as revealed by Wang et al. During the ramping stage, the aldehyde production in the soybean oil was slow and minimal. However, after reaching 185 °C, the concentration of aldehydes showed a dramatically steep increase within the first hour.[66] Beyond this temperature, aldehyde production in heated oils could be accelerated. Comparing canola oils heated at 240°C and 180°C, the total aldehydes were generated much faster (about 4-fold difference) at 240°C.[119] Similar trend was reported for olive oil[119], and soybean oil[121,122].

Heating time

At frying or cooking temperatures, heating time is commonly positively correlated with aldehyde formation in the oil. However, prolonged heating (e.g. 6 hr[66], 9 hr[119], 15 hr[119]) may not increase the aldehydes concentrations and could decrease them. A kinetic study on soybean oil showed that the rate of aldehyde production was very rapid when heated at 185°C for 1 hour, reaching a total aldehyde concentration of around 600 mg/L. Nevertheless, in the following 5 hours, the aldehyde concentration increased to about 800 mg/L.[66] The canola oil heated at 180 °C showed a similar trend, as the rate of total aldehyde production was the highest in the first 9 hours, then dropped dramatically.[119] Different aldehydes also have distinct patterns of production during prolonged heating. For example, HNE continued to increase and showed a linear correlation with heating time, whereas 2,4-heptadienal and 2-heptenal decreased after 1 hour of heating in the soybean oil.[66] These phenomena have been attributed to evaporation and degradation. The boiling point increases with the number of carbons in the aldehydes. Those with carbon length less than 8 have a boiling point below 180 °C and may quickly evaporate.[61]

Their peak concentrations were reached at a lower temperature. The boiling points of C9-C11 aldehydes, on the other hand, peaked at a higher temperature. [123] In addition to evaporation, aldehydes may undergo further degradation if heated extensively, especially for long-chain alkenals. For example, 2,4-decadienal may break down at the two double bonds, yielding two smaller aldehydes: hexanal and 2-octenal.[124] Similarly, 2,4-hepadienal can degrade to propanal and 2-pentenal, and 2-pentenal to formaldehyde, and acetaldehyde.[124]

1.2.5 Approaches for analyzing aldehydes

1.2.5.1 Thiobarbituric acid reactive substance (TBARS) assay

The TBARS assay is a common approach to aldehyde analysis, applicable to not only oils but also biological specimens (e.g., muscle tissue).[125] The product of the reaction between thiobarbituric acid and malondialdehyde (MDA) has a pink color with absorbance at 532-535 nm.[125] However, the TBARS assay has its limitations. The assay could be confounded by other non-MDA compounds in the sample matrix, such as formaldehyde[126], oxidized lipids[125], and imine/amine-MDA adducts[127]. On the other hand, TBARS assay does not cover other aldehydes in oxidized oils[125], such as HNE or 2,4-decadienal. Additionally, under prolonged heating, the TBARS value tends to plateau[66], most likely due to the equilibrium of MDA formation in oils heated at high temperatures.[128] The interpretation of TBARS results may warrant further caution as well. MDA primarily derives from the oxidation of poly-unsaturated fatty acids (PUFA), such as linoleic acid.[128] Therefore, the TBARS values only partially describe the status of aldehyde production.

1.2.5.2 *p*-Anisidine value (AnV)

The *p*-anisidine value directly reflects the concentration of aldehydic compounds.[102] It relies on the color formed between the *p*-anisidine and a carbonyl group, which is measured spectrophotometrically at 350 nm.[129] In other words, AnV not only reflects the free aldehydes, but also captures the non-volatile carbonyls[129], which are likely aldehydic precursors in the form of fatty acids or triglycerides. AnV is additionally advantageous in animal feeding trials. For broilers and pigs fed oxidized oils, the AnV of the oils used for feed formulation showed the strongest inverse correlation with the growth performance, compared to other indicators of oils' oxidation status.[123] Hence, AnV is a promising predictor of animals' growth performance, with a proposed threshold of 172.[130] In general, oils with AnV greater than 172 would more likely impair the animal growth. Nevertheless, this is not without exception.[130] Further studies are still needed. On the other hand, AnV has its shortcomings. It is more sensitive to unsaturated aldehydes (2-alkenals, 2,4-dienals) than saturated aldehydes. Because the product formed between unsaturated aldehydes and *p*-anisidine reagent have stronger absorbance at 350 nm.[129,131] Furthermore, AnV lacks specificity for distinguishing the specific aldehyde specie, which is common for spectrophotometric assays.

1.2.5.3 Chromatographic approaches

Gas- and liquid-chromatography (GC, LC) based methods have been developed for detecting and quantifying lipidic aldehydes. Compared to colorimetric assays, GC- and LC are robust in separating and quantifying individual aldehydes from complex samples with higher specificity and accuracy.

Gas chromatography (GC)

GC is a powerful platform for separating and detecting volatile organic compounds, including aldehydes.[132] The target compounds need to be chemically stable. The GC mobile phase usually consists of carrier gases like nitrogen or helium. The carrier gas flows through the stationary phase, which comprises a solid coating in a GC column to separate the target compounds.[133] GC can be connected to several different detectors for compound identification and quantification, including flame ionization detector (FID)[134] and mass spectrometry (MS)[135]. GC-MS has broad application in analyzing aldehydes as flavoring compounds from various solid food matrices[136], fluids[137], and fumes[119]. Fullana et al. quantified seven alkanals, eight 2-alkenals, and 2,4-heptadienal from the cooking fumes of three different cooking oils.[119] Vegetable oils could be directly injected into GC without derivatization for analysis of aldehydes.[135] Meanwhile, headspace (HS) GC-MS is a popular technique given most aldehydes' low boiling point and volatility. Based on the HS-GC-MS platform, Liu et al. identified 21 aldehydes from 10 different types of frying oils. Additionally, the kinetics of pentanal formation during the continuous heating process was suggested as a good predictor for the oil quality.[135]

To maximize the detection of aldehydes by GC-MS, additional sample preparation techniques can be applied. Solid food matrix, such as pork, must be homogenized before loading into HS-GC vials.[136] Solvent extraction can be applied to separate and obtain the lipidic content from the sample matrix.[138] Chemical derivatization is another approach to increase the sensitivity and accuracy of aldehyde detection by GC-MS, especially for the species with longer carbon chain, higher molecular weight, and less volatility.[139] One

commonly used derivatizing reagent is *O*-2,3,4,5,6-(Pentafluorobenzyl)-hydroxylamine hydrochloride (PFBHA).[140] It reacts with the carbonyl group in aldehydes, forming aldehyde pentaflyorobenzyl oxime (PFBO) derivatives, under mild acid. Alkanals and alkenals can be detected via their characteristic $[M-181]^+$ ion.[141] For α,β-unsaturated alkenals, one additional characteristic ion with *m/z* 250 can be used for identification.[141] Schmarr et al. quantified long-chain alkanals, alkenals, 2,4-alkadienal in grape seed oil samples via PFBHA derivatization coupled with GC-MS.[142] This method can also be applied for biological samples, though less commonly, such as quantifying hexanal and heptanal in blood.[143] In addition to PFBHA, other derivatization reagents are available for GC-MS application for biological samples.[139] Taking MDA analysis for example, available reagents include 2,3,4,5,6-pentafluorobenzyl bromide (PFB-Br) and 2,4,6-trichlorophenylhydrazine (TCPH) for urine samples[144,145], and phenylhydrazine (PH) for plasma and rat liver microsomes[146]. GC-MS platform can also be coupled with 2,4-dinitrophenylhydrazine (DNPH) derivatization. Osório and Cardeal validated and quantified acrolein in French fries via this approach.[147]

Liquid chromatography (LC)

GC is commonly used for food samples, but its application on biological samples, such as tissue and serum, remains challenging due to interference from other non-aldehyde compounds (e.g., protein).[140] LC-based approaches can minimize GC's inherited shortcomings. It is additionally advantageous for longer-chain aldehydes, such as the lipidic species.[140] Reverse-phase LCs are commonly used for separating target compounds. The mobile phase is more polar than the stationary phase (packed in the LC

column). During a typical RPLC run, the ions are adsorbed to the stationary phase packed in the LC column, which is less polar than the mobile phase. Then, the mobile phase gradient changes the polarity, allowing ions to elute from the column. In general, compounds with greater hydrophobicity will have longer retention time and elute later from the RP column.[148]

LC can be coupled with an ultraviolet detector (UV) or a mass spectrometer (MS). LC-UV was one of the earliest methods developed for quantitatively analyzing aldehydes, usually from environmental sources. However, pre-column derivatization with DNPH is required. The formed carbonyl-hydrazones can be detected at 360 nm. Its application has been extended to food, beverage, and biological fluids (serum, plasma, and urine).

On the other hand, LC-MS has an even broader application for complex samples, with many developed methods with high sensitivity, selectivity, and specificity towards aldehydes.[139] Aldehydes generated in oil during the frying process were monitored via LC-MS analyses via DNPH[149] or 2-hydrazinoquinoline (HQ)[66] derivatization. The carbonyl group in aldehyde forms a hydrazine with HQ via a condensation reaction.[150] DNPH is broadly used for food samples[151] and biological samples.[152] Both approaches are more efficient than GC, as they allow for the quantification of both aldehyde and fatty acids at the same time.[66,150] For GC-MS detection, fatty acids usually need to be derivatized to methyl esters for thermal stability, especially for those longer than 10-carbon.[153] Therefore, LC-MS workflows are more rapid and have higher throughput.

1.2.5.4 Other approaches

Fourier transform infrared spectroscopy (FTIR)

FTIR can be used to detect the carbonyl functional group.[154,155] Navarra et al. monitored the change of aldehyde in thermally oxidized extra virgin olive oil by spectral change at wavelength 3530 cm^{-1}.[156] The primary LOPs, such as peroxides, can be characterized by spectral change at wavelength 3500 cm^{-1}.[157] Alshuiael et al. recorded the broader spectra corresponding to carbonyl (C=O) group in thermally oxidized sunflower and corn oil at wavelength 1743 cm^{-1}.[158] Nevertheless, FTIR is unable to distinguish the classes of carbonyl-containing compounds, such as esters, ketones, and aldehydes. The lack of specificity makes it an inferior option for comprehensive characterization of aldehydes in food and biological samples.

Proton nuclear magnetic resonance (^{1}H-NMR)

Similar to FTIR, NMR can detect both the primary and secondary LOPs in oxidized oil samples. Goicoechea and Guillen monitored the changes of hydroperoxides, conjugated dienes, di-epoxides, and aldehydes in thermally oxidized sunflower oils.[159] With the standards, NMR can also distinguish different aldehydes classes, such as identifying alkenals, alkanals, and 2,4-alkadienals.[159] Compared to LC-MS based approaches, NMR requires minimal sample preparation, but has much less sensitivity and specificity for aldehydes.

1.2.6 Current knowledge on the *in-vivo* disposition of lipidic aldehydes

Overall, lipidic aldehydes are bioavailable and are associated with many pathophysiological consequences, such as cardiovascular disease, cancer, and

Alzheimer's disease **(Figure 1.5)**[160], due to their non-enzymatic and enzymatic reactivities. In epidemiology studies, dietary intake of fried food was associated with elevated risks for cancer, cardiovascular disease, and metabolic syndrome. [161-166] In animal studies, consuming highly oxidized oil led to a series of biological implications, including depressed appetite, increased intestinal leakage, diarrhea, deterred growth performance, elevated liver and kidney weight, oxidative stress, and altered blood lipid panel.[100,103,104,167-169] The bioavailability, reactivities, and related health implications are discussed below.

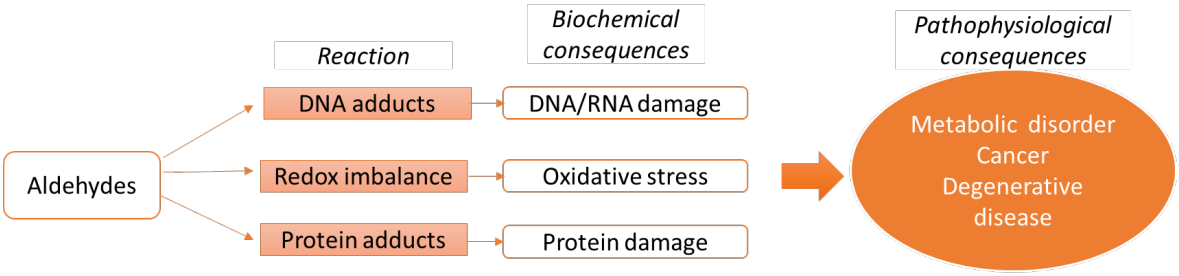

Figure 1.5 Aldehyde-related toxicity and pathogenesis in humans and animals. Modified from Laskar and Younus, 2019.[160]

1.2.6.1 Bioavailability of aldehydes

The aldehydes in heated oils are bioavailable. The octanol-water partition coefficient (Log *P*) values of major aldehydes in HSO, except acrolein, are between 1.04 and 4.23, which indicates high lipophilicity for efficient transepithelial diffusion in the intestine.[102] This statement was supported by detecting aldehydes in the chylomicrons of the pigs fed oxidized oil.[170] Additionally, after oral dosing of radioisotope labeled 4-HNE in rats,

about 50% of the radioactivity was excreted in the urine, including the detection of 9-hydroxy-nonenoic acid as a major urinary metabolite of HNE, which was in contrast to the 15% radioactivity in feces.[171] The bioavailability of aldehydes was also illustrated by the detection of mercapturic conjugates in urine after dosing the rats with 2-nonenal, a major aldehyde in heated oils.[172] Despite this evidence on the bioavailability of aldehydes, the kinetics of aldehyde absorption have not been examined in detail.

1.2.6.2 Non-enzymatic metabolism of aldehyde and its consequences

Aldehydes are electrophiles. Their reactivity is mainly contributed by the unique aldehyde group (-CH=O). The oxygen attracts the electrons of its adjacent carbon 1, increasing the polarity for reactions with nucleophiles.[45] Saturated alkanals with longer carbon chains preferably form adducts with amines via Schiff base **(Figure 1.6 A)**.[45] The amine group of the lysine side chain and the exocyclic amino group of DNA are often target sites.[45] Besides Schiff-type adducts, aldehydes can also form Michael-type adducts. For α, β-unsaturated aldehydes, the additional reactivity stems from the unsaturated C=C bond between the α and β carbon. The β-carbon can form adducts with thiol groups (-SH) in cysteine via Michael addition **(Figure 1.6 B)**.[173] Another type of Michael-type adducts can be formed by the covalent binding between the β-carbon and primary amine **(Figure 1.6 C)**, often targeting the side chain of lysine.[174] Moreover, the imidazole side chain in histidine can form Michael adducts with α, β-unsaturated aldehydes **(Figure 1.6 D)**[175], at a slower rate than the reaction with thiol.[176]

The reactivity of aldehyde can be exemplified by HNE, as it contains three functional groups for reactions: carbonyl, α-β double bond, and hydroxyl group.[175] The

terminal carbonyl group of HNE may react with the amine group. Meanwhile, its hydroxyl group is at the carbon adjacent to β carbon. It pulls the electron away from the carbon chain, making the β carbon more vulnerable to react with the thiol group.[173] The diverse reactivity allows HNE to crosslink large molecules, such as proteins and DNA, leading to biological dysfunction and toxicity.[45,177] Besides forming adducts with lysine, cysteine, and histidine, HNE also reacted with other amino acids, including arginine, threonine, tryptophan, glutamic acid, and asparagine.[178,179]

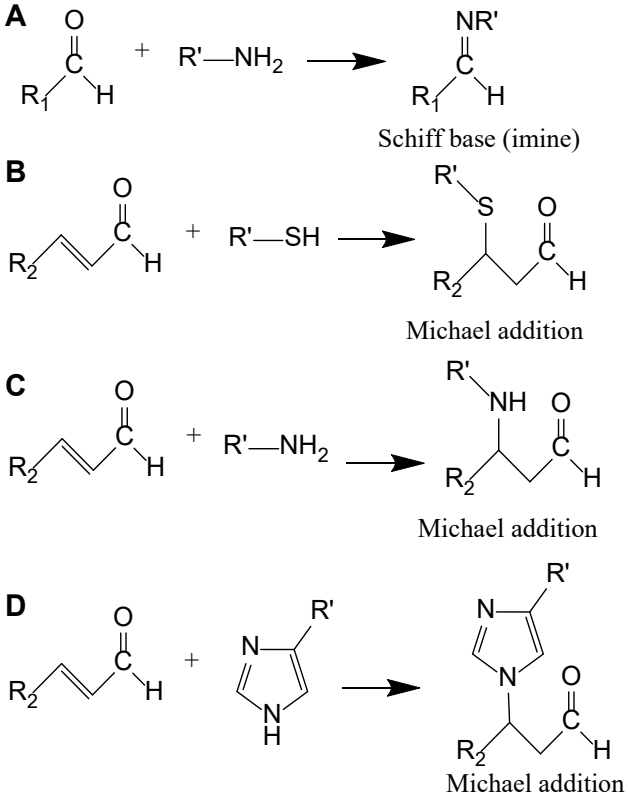

Figure 1.6 Non-enzymatic formation of adducts between aldehydes and biological molecules of different functional groups. A) Aldehyde forming Schiff base with an amine group. B) Aldehyde forming adducts via Michael addition with a thiol group. C)

Aldehyde forming adducts via Michael addition with a terminal amine group. D) Aldehyde forming adducts via Michael addition with imidazole group.

Capable of forming adducts with DNA, aldehydes are genotoxic and mutagenic. For nucleic acids, their amine groups may form diverse adducts with aldehydes, leading to point mutation, deletions, insertions, and inversions. As a result, DNA strand breakage and destabilization were observed in the cellular model.[180,181] Exposure to aldehyde also impaired DNA repair activity, an important checkpoint in carcinogenesis.[182] As a result, the genotoxicity of aldehydes can be directly reflected in the development of cancer. Prolonged inhalation of aldehyde-rich cooking oil fume has been associated with elevated risks of non-smoking lung cancer, observed in epidemiology studies.[183] Similarly, the intake of aldehyde-containing fried food is a contributor to the increased gastric[164], colorectal[165], and prostate[166] cancer.

The formation of aldehyde-amino acid adducts may lead to protein inactivation. For example, when the cysteine residue is modified, some mitochondrial enzymes, including glutathione S-transferase, are inactivated.[45,160] Furthermore, since aldehyde may diffuse across the membrane easily, membrane proteins may be the targets of adduction, disrupting membrane structure.[184] Depending on the target protein, exposure to aldehyde may induce cascading effects, such as escalated production of reactive oxygen species (ROS).[160] In the cellular model, exposure to HNE and MDA deactivated succinate dehydrogenase, disrupted the electron transport chain, and therefore promoted mitochondrial production of superoxide. The escalated oxidative stress hindered cell

viability.[181] For myocardium, such mitochondrial abnormalities further impacted ATP production and cardiac function.[185] The oxidative stress is also reflected *in vivo*. In pigs fed oxidized oil, the activities of key antioxidant enzymes, catalase (CAT), glutathione peroxidase (GPx), and superoxide dismutase (SOD) were significantly reduced in the small intestine epithelial cells.[100,101,186] Hepatic GPx, CAT, and SOD declined in rabbits fed oxidized vegetable oil.[187] However, pig-feeding trials reported varying results. In growing pigs, only serum GPx and hepatic CAT were depleted.[104] In finishing pigs, hepatic GPx, serum GPx, and CAT were unchanged.[188] Additionally, the ROS-elicited oxidative modification of lysine, proline, arginine, and threonine can further produce the protein carbonyls (PC), a direct indicator of oxidative stress.[189] HSO-feeding significantly increased serum PC groups in growing pigs.[104] But such incidence was absent in finishing and nursery pigs.[103,188] Additionally, aldehydes formed from lipid oxidation, such as HNE, may produce PC groups by Michael addition, a non-enzymatic adductation. This process is more prevalent than the direct oxidation of amino acids *in vitro*.[190]

1.2.6.3 Enzymatic metabolism of aldehydes and its consequences

The human body has aldehyde-metabolizing enzymes to mitigate the toxic effects, comprised of aldehyde oxidase (AOX), cytochrome P450 (CYP450) enzymes, aldo-keto reductases (AKRs), alcohol dehydrogenases (ADHs), short-chain dehydrogenase/reductases (SDRs), and aldehyde dehydrogenases (ALDHs). Subcellularly, these enzymes are vastly expressed in the mitochondria and cytosol of many organs, including gastrointestinal mucosa. They catalyze the redox conversion of aldehyde to less reactive compounds, such as acids and alcohols.[160] Their catalytic mechanisms are summarized in **Table 1.2**.

ALDH is a superfamily of enzymes, present in all subcellular locations. They are the main enzymes responsible for detoxifying aldehydes due to their high affinity and abundant cellular expression.[160] They are distributed in almost all subcellular organelles. To convert aldehydes to carboxylic acids, $NAD(P)^+$ is needed as a cofactor.[160] ALDH starts detoxifying dietary aldehydes in the gastric mucosa.[191] Hepatic activation of ALDH was identified in mice as a defensive mechanism in response to HSO feeding.[168] In recent swine-feeding projects, HSO depleted serum but not hepatic GPx.[103,188] The unchanged hepatic GPx was also observed in a rat model.[61] Yet, upregulation of GPx expression was reported in pigs fed oxidized rapeseed oil.[192]

Additionally, the redox imbalance was revealed by the increased *in-vivo* expression of *Nqo 1* and *HO1*. These two genes are regulated by nuclear factor erythroid 2-related factor 2 (Nrf2).[168] Activation of the Nrf2 signaling pathway was a response to the consumption of oxidized rapeseed oil.[192] As a transcription factor, Nrf2 plays an important role in the homeostasis of redox status. Some of its influences include the induction of antioxidant enzymes (GST, GPx, SOD).[193]

Table 1.2 Catalytic reactions of aldehyde-metabolizing enzymes in humans. Modified from Laskar and Younus, 2019.[160]

Enzyme	Catalytic mechanism	Subcellular location
AOX	$RCHO + O_2 + H_2O \rightarrow RCOOH + H_2O_2 + H^+$	Cytoplasm
CYP450	$RCHO + O_2 + NADPH + H^+ \rightarrow RCOOH + H_2O + NADP^+$	Endoplasmic reticulum
AKRs	$RCHO + NAD(P)H \rightarrow RCH_2OH + NAD(P)^+$	Cytoplasm
ADHs	$RCHO + NAD(P)H \rightarrow RCH_2OH + NAD(P)^+$	Cytoplasm
SDRs	$RCHO + NAD(P)H \rightarrow RCH_2OH + NAD(P)^+$	Microsome
ALDHs	$RCHO + NAD(P)^+ + H_2O \rightarrow RCOOH + NAD(P)H + H^+$	Cytoplasm, mitochondria, endoplasmic reticulum, and nucleus

Another important route to metabolize aldehydes is via glutathione S-transferases (GSTs) in the mercapturic acid (MA) pathway. They mainly metabolize alkenals and hydroxyalkenals. In rat hepatocytes, GST and ALDH account for the main metabolism of HNE, while ADH activity is very minor.[194-197] *In vivo*, the MA pathway starts with glutathione (GSH) conjugation with aldehyde in the hepatocytes. Taking HNE for example **(Figure 1.7)**, its β carbon is conjugated with the thiol group of GSH. GSH contains three structural moieties: cysteine, glutamate, and glycine. The glutamyl-glycine moiety is removed by γ-glutamyltranspeptidase (γ-GT) and dipeptidases (DP), forming the HNE-Cys thioether adduct. Then cysteine residue is further modified by acetyltransferase (AT), forming HNE-acetylcysteine, also known as MA adduct.[198-200] The acetylation enzyme, AT, is expressed in mainly in the liver and kidney of humans and rats.

Additionally, the MA pathway interacts with the redox enzymes, ALDH and AKR, forming a variety of MA adducts **(Figure 1.7)**. These adducts undergo further reaction and eventually become 4-hydroxynonenoic acid (HNA)-lactone-MA, HNA-MA, 1,4-dihydroxynonene(DHN), DHN-MA.[201,202] These urinary metabolites are used as marker for HNE.[171]

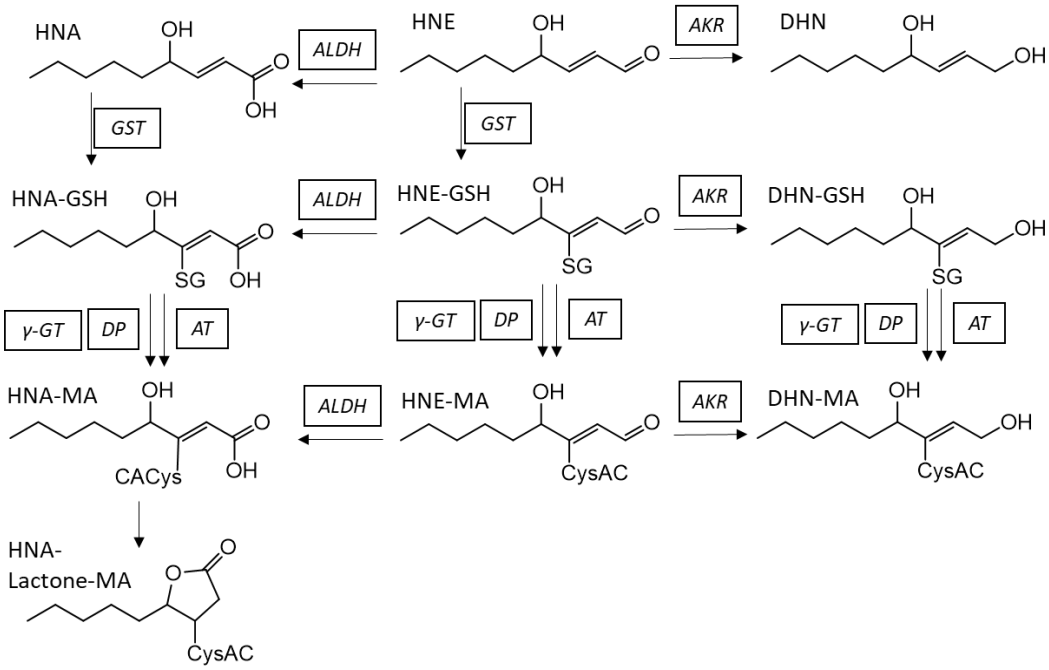

Figure 1.7 Mercapturic acid pathway for metabolizing HNE. Modified from Sidell et al., 2003[200] and Kuiper et al., 2008[203].

The distribution of these aldehyde-metabolizing enzymes is site-specific. GST, ADH, and ALDH are present in the stomach and intestines.[191] ADH4 is the main aldehyde-reducing in the ADH family, located dominantly in the epithelial cells of the villi.[204] In the human GI, ALDH has the strongest activity in jejunum (isoforms 1A1, 2, AND 3A1), and is higher than that of ADH.[205] In the liver, both phase I (ADH, ALDH, AKR, AOX, CYP450) and phase II (GST) enzymes are active. AOX is also expressed in the kidneys and lungs.[206] ALDH has an even broader distribution in the kidney, heart, lung, and brain. The isoform ALDH2 is the most abundant in the liver.[207] SDR are expressed in the kidney and brain besides the liver.[208]

Given the requirements of the detoxifying enzymes, substrates, and corresponding co-factors, consumption of aldehyde-rich oxidized oils can pose a challenge to the redox balance *in vivo*. In a mice-feeding trial, hepatic GSH and ascorbic acid were decreased by HSO feeding.[168] Aldehyde presumably contributed to this stress response[168], as the conjugation with GSH vis GST is a common detoxifying mechanism, as mentioned above. Moreover, in response to the consumption of rapeseed oil-induced oxidative stress, the activation of Nrf2 signaling pathway could promote the synthesis of reducing cofactors (NADPH, GSH) for the enzymatic detoxification of aldehydes.[193]

1.2.7 Current knowledge on the disposition of non-volatile lops from thermally oxidized oils

Thermally oxidized oils contain a variety of non-volatile LOPs besides aldehydes. Their composition, assessment approaches, disposition, transformation, and interactions with the GI are discussed in this section.

1.2.7.1 Composition of non-volatile LOPs

Aldehydes are the breakdown products of primary LOPs, the fatty acid hydroperoxides (FA-OOH). Along with aldehydes, the FA-OOH could degrade or decompose to ketones, single- and bi-carboxylic acids, hydroxy-, and epoxy-acids.[43] The free ketones and aldehydes are considered the volatile components of LOPs.

Other larger-molecule LOPs are generally non-volatile, including dimeric TG, oxidized TG (TG-OX), mono-, and di-acylglycerols (MG, DG). The TG-OX contains shorter-chain-, oxo-, hydroxy-, keto-, epoxy-fatty acyls, and free fatty acids. A specific type of TG-OX contains aldehyde groups in the fatty acyl chains, referred to as glycerol

core aldehyde (GCA). Examples of GCAs include 9-oxononanoic acid, 7-oxo-nonanoic acid, 8-oxooctanoic acid, 10-oxo-8-decenoic acid, and 11/13-oxo-9-octadecenoic acid.[209-212] Epoxy-GCAs were identified in corn and sunflower oils oxidized by metal oils. These GCAs are relatively stable after prolonged heating (24 – 60 hours) at frying temperature.[210] They are commonly formed via the homolytic β-scission of the hydroperoxides, simultaneous to the formation of volatile aldehydes. The aldehyde groups in GCAs can form the Schiff base with the amine group of the *p*-anisidine reagent. Consequentially, a positive correlation has been observed between total GCA and the AnV of frying rapeseed, sunflower, and cottonseed oils.[210]

All polar species mentioned above are reflected as total polar content (TPC). TPC concentration in heated oil positively correlates with heating time and temperature.[213] Currently, 25-27% TPC (by weight) is the maximum threshold of frying oils used in commercial establishments in European countries.[214] Oils with TPC above this limit are not deemed for re-use and need to be discarded. Typically, in an oil containing 25% TPC, TG-OX species take up only a small portion of 5.9-9.4% (weight).[215] Additional regulation on epoxy fatty acids was set as the maximum of 7 g/kg for cooking and frying oils.[216]

At frying temperature, even larger polymerized compounds, such as polymerized TG (PTAG), may also form.[70] Oils with higher degrees of unsaturation are more prone to forming PTAGs upon heating.[217] In European countries, the threshold for PTAG in cooking oil is set at 12-13%, yet 10% is recommended as the limit for replenishment.[217]

1.2.7.2 Approaches for assessing non-volatile LOPs

The challenge of analyzing non-volatile LOPs comes from their stability, size, and structural diversity. The TPC content in oil can be determined by size-exclusion chromatography, according to the AOCS method Cd 20-91.[218] However, such an approach is only an approximate analysis, as it does not reveal the identity of polar compounds and their concentrations. Chromatographic approaches, on the other hand, can provide more detailed information.

Oxidized TGs, including the GCA, epoxy, and hydroxy species, can be directly analyzed via reverse-phase LC coupled with MS.[211] The structure profiling of TG-OX species relied on two types of tandem MS/MS platforms: collision-induced dissociation (CID) and electron activated dissociation (EAD). The CID and EAD together elucidate the acyl chain identity. Then, EAD additionally reveals the fatty acyl chain identity at *sn*-2 position.[211] Even so, such findings were established based on high purity and authentic triglyceride standards. Oils, containing a mixture of versatile TG precursors, will add to the complexity of the structural analysis of TG-OX. Additional pre-column preparation is needed to separate and enrich the target TG-OXs for analysis, such as solid phase extraction.[219] Besides LC-MS, GC-MS has been widely used for profiling non-volatile LOPs.[209,210]

Nevertheless, interpretation of the chromatographic data for TG-OX is challenging as well. The heterogeneity of the data comes from the possible positions of unsaturation, oxidation, types of oxygenations, the diversity of triglyceride precursors, and the lack of a comprehensive database. The traditional manual interpretation approach is inefficient in

profiling the TG-OXs, especially those from oil or biological samples. Bioinformatic tools are being developed to fill in the gap and to facilitate the discovery of LOPs.[220]

The PTAG in the oxidized oil can be accessed and quantified via size-exclusion chromatography according to the official AOAC method 993.25-1996.[217]

1.2.7.3 Disposition of non-volatile LOPs in GI

Mouth and stomach

Lipid digestion starts in the mouth and is actioned by lingual lipase. Then, gastric lipase continues to de-esterify TGs and release DG and FFAs in the stomach.[221] Lipases can hydrolyze the TG-OX and dimeric TG usually, releasing the fatty acids from glycerol backbones.[222] However, polymerized TGs are resistant to such digestion and can pass to the large intestine.[222] In the gastric lumen, the non-enzymatic transformation of TG-OX for detoxification was observed. Hydroperoxides and hydroxy lipids, due to the presence of oxygen and a strong acidic environment, are decomposed to aldehydes and absorbed in the stomach (discussed in section 1.2.3). Hydroxy lipids can be uptaken by the stomach and rapidly utilized for energy as well, yielding CO_2.[50] The fate of epoxy lipids in the gastric lumen is less known. *In vitro* digestion of oxidized sunflower and rapeseed oils showed the transformation to diols.[223] But the quantity and reaction rate are unclear.[191] In addition to the above-mentioned luminal non-enzymatic transformations, gastric glutathione peroxide in the mucosa reduces hydroperoxides to water and lipid alcohols.[191,224]

Small intestine

Under normal conditions, in the small intestine, more than 95% of triglycerides are hydrolyzed to MG, FFA, and then uptaken.[225] The digestibility of the non-volatile LOPs remains inconclusive. Marques-Ruiz et al. reported comparable digestibility among non-oxidized, and oxidized-TGs from a study on oxidized trilinolein. But a less efficient hydrolysis of TG-OX was reported as well[226], potentially as a result of pancreatic lipase inhibition from TG dimers, polymers[222], and also hydroperoxides[227]. Epoxy-TG can also be hydrolyzed to release FFA, but at a slower rate than other TG-OX.[228]

In the transport of polar compounds in oxidized oils across the intestinal apical site, GSH is an important mediator.[191] The hydroperoxides that reach the intestine can be uptaken into enterocytes with sufficient presence of GSH and quickly reduced to alcohols by GPx. Hydroperoxides from normal dietary intake can be modified completely in the stomach. However, those from oxidized oils may overwhelm the gastric lumen's catalytic capacity and leak to the intestine.[50] In this case, the intestinal GSH-dependent uptake capacity may be saturated, accumulating hydroperoxide in the intestinal lumen.[229] In addition to GPx, GST is also an important enzyme in the intestine's defensive line. Mainly located in the mucosal coating of epithelial cells, GST conjugates polar compounds, specifically epoxides, and alcohols, to glutathione, preventing them from directly contacting the intestinal cells. The conjugates are then excreted via feces or urine. [229,230] Another less-known enzyme is acetyltransferase, which conjugates fatty alcohols to acetyl-CoA.[231]

The free fatty acids in the oxidized oil (or hydrolyzed from TGs) can be incorporated into lipoproteins and exported to lymph by enterocytes. The shorter-chain fatty acids

(C≤8), either from the free FFA in the oils, or hydrolyzed from TG-OX, can be directly transported to the liver.[191,232] However, the transport and disposition of other non-volatile LOPs from the intestine to systematic distribution is unclear.[191]

Large intestine

For healthy individuals under normal conditions, more than 95% of dietary lipids are digested and absorbed in the small intestine. Only a small proportion reaches the large intestine, except for dimeric and polymeric TGs.[226] But their presence throughout the entire GI tract is still noteworthy. By comparing diet and fecal excretions, Marques-Ruiz et al. reported a 50% and 90% fecal recovery of dimeric and polymerized TGs in rats dosed with labeled linoleic acid and oxidized olive oils.[233,234] Nonetheless, their metabolism by gut microbiome has not been thoroughly studied. On the other hand, the generic changes in gut microbiome induced by oxidized oil consumption are reviewed later in this chapter.

1.2.7.4 Metabolic fate of non-volatile LOPs

The disposition and metabolic fate of dietary non-volatile LOPs have not been systematically characterized. Nevertheless, as pointed out in a comprehensive review, it is consensus that the liver is the main organ for detoxification. Meanwhile, despite the absorption of non-volatile LOPs, they are mostly metabolized and transformed, without directly coming into contact with sensitive tissues.[191] Enzymes involved in metabolizing aldehydes are discussed in previous sections. One additional enzyme involved in metabolizing TG-OX in oxidized oils is epoxide hydrolase. In the liver, epoxide hydrolase adds a water molecule to epoxides, forming trans diols.[235] Human have two

isoforms, EH3 and EH4, specifically targeting fatty acid epoxides.[236] However, the conversion of epoxides to diols is not always protective and depends on the FA epoxide structure.[191] The detoxifying effect is applied to LCFA with epoxide in the middle. Nevertheless, for FAs longer than 18 carbons, their diols are more toxic.[237] The structure of epoxide species in oxidized oils have not been comprehensively studied. Therefore, their rates of digestion and metabolism will need further research.

1.2.8 Current knowledge on the interrupted nutrient metabolism associated with oxidized oil consumption

The health impacts of oxidized oil consumption have been evaluated in both humans and animals. In epidemiology studies, dietary intake of fried food was associated with elevated risks for cancer, cardiovascular disease, and metabolic syndrome. [161-163] In animal studies, consuming highly oxidized oil led to a series of biological implications, including depressed appetite, increased intestinal leakage, diarrhea, deterred growth performance, elevated liver and kidney weight, oxidative stress, and altered blood lipid panel.[100,103,104,167-169] Some established metabolic effects are discussed below.

1.2.8.1 Disruption on lipid metabolism

Oxidized oil consumption is known to activate hepatic peroxisome proliferator-activated receptor-alpha (PPAR-α).[168,238] Some LOPs in thermally oxidized oils are PPAR-α agonists, including cyclic and hydroxylated acids.[238] In a mice-feeding trial, 13-hydroxyoctadecadienoic acid (13-HODE), formed by oxidizing linoleic acid, was detected as a PPAR-α agonist in HSO. PPAR-α activation directly upregulated the β-oxidation of fatty acids in mitochondria, likely leading to reduced serum and hepatic

triglyceride (TAG).[168,239] Meanwhile, PPAR-α activation induced ω-oxidation of fatty acids, yielding medium-chain dicarboxylic acids.[240,241] Suberic acid and azelaic acid were detected in the urine of mice fed HSO.[168] Notably, for rodents, enzymes performing ω-oxidation are mostly distributed in the liver.[242] Peroxisome proliferation is associated with hepatic proliferation[243], which likely explained the increased liver weight in animals fed with heated oil.[103,168]

Oxidized oil may intervene in lipid metabolism via PPAR-γ activation, as observed in the cellular model.[244] PPAR-γ is a key regulator in adipogenesis, insulin sensitization, and glucose metabolism. Its activation in the liver alters energy metabolism homeostasis, favoring lipid storage.[245,246]

Cholesterol homeostasis may also be impacted by intake of oxidized oil to varying extents. In rats, the activation of sterol regulatory element-binding protein-2 (SREB-2), a transcription factor regulating cholesterol synthesis, was inhibited by intake of oxidized oil. Its target gene transcription for 3-hydroxy-3-methylglutaryl CoA (HMG-CoA) reductase and LDL receptor was reduced, lowering the serum and hepatic total cholesterol.[247,248] However, the cholesterol-lowering effect was absent in other animal trials.[249] Adverse trend was reported as well.[169]

1.2.8.2 Disruption on amino acid metabolism

In response to oxidized oil consumption, tryptophan-NAD^+ synthesis pathway was activated in mice and pigs.[130] This was a combined result of PPAR-α activation, oxidative stress, and inflammatory signaling. NAD^+ is a co-factor for ALDH to metabolize aldehyde[160] and for fatty acid β-oxidation[250]. It is also a precursor for NADPH, a cofactor

needed to regenerate GSH and combat oxidative stress. To supply the NAD^+, intracellular tryptophan was catabolized to synthesize NAD^+. Additionally, purine degradation was attenuated to preserve substrates for NAD^+.[168] In addition to tryptophan, threonine metabolism could be disrupted by oxidized oil consumption. In pigs fed oxidized corn oil, serum threonine increased while hepatic threonine decreased.[130] Such imbalance was induced by the inhibited threonine dehydratase (TDH), reflected by the decreased hepatic α-ketobutyrate, a downstream metabolite of threonine. As discussed by Guo et al., the lipidic aldehydes were likely the underlying cause for such a phenomenon by interfering with the Schiff base bound between TDH and its cofactor, pyridoxal-5'-phosphate. Though the physiological meaning of threonine preservation is unclear, together with the changes of GSH and tryptophan-NAD^+ pathway, the altered amino acid metabolism maybe protective for animals fed oxidized lipids.[130]

1.2.8.3 Impact on gut microbiome

The gut microbiome is actively involved in macro- and micronutrient metabolism.[251] However, current understanding of the interactions between the intestinal microbiome and oxidized oil consumption is very limited. Additionally, due to the complex compositional nature of oxidized oils, the impact and microbial metabolism in each class of LOPs are not fully understood. Therefore, most studies reported the generic changes in gut microbiome upon oxidized oil consumption. In rats gavaged with oxidized canola oil, their microbial diversity was reduced.[252] Similar results were observed in pigs, where HSO decreased microbial diversity, altered the composition of microbes, and suppressed short-chain fatty acid (SCFA) production.[100] In mice fed HSO, urinary metabolites

associated with microbial metabolism were detected. However, the associated metabolic pathway was not fully characterized.[168]

An inhibitory effect on butyrate was observed in hamsters fed oxidized corn oil[253], nursery pigs fed oxidized soybean oil[99,100], and rats chronically fed oxidized palm oil[254]. The abundance of butyrate-producing bacteria species also decreased, such as *Paraprevotella*, *Garnesiella,* and *Provotella* of the Bacteroidota phylum[100,252,253], *Parasutterella* of the Pseudomonadota phylum[253], and *Butyrivibrio* of the Bacillota phylum[254]. However, discrepancies have been reported. Oxidized perilla and sunflower oil did not impact the abundance of butyric acid, nor total SCFA in rats.[255] Meanwhile, oxidized oil feeding showed varying effects on propionic acid. A dramatic reduction by more than 50% was observed in hamsters fed oxidized corn oil.[253] Oxidized palm, canola, perilla, and sunflower oil did not alter rats' fecal propionic acid concentration.[254,255] In pig-feeding studies, the colonic propionic acid level remained comparable in the oxidized soybean oil group.[99,100] In general, acetic and valeric acids were not influenced by oxidized oil feedings.[99,100,252-255] One potential explanations for the varying result could be attributed to the varying oxidation status of the oils used in these studies. The oxidized corn[253], lard[253], and soybean oil[100] used in the above-mentioned animal studies had remarkably higher PV (33.15[253], 12.51[253], and 88.5[100] mEq peroxide/kg, respectively). During thermal processing of soybean oil, PV increased rapidly to >200 mEq peroxide/kg when heated from 22°C to 185°C within 1 hour, but then dropped and plateaued at about 50 mEq peroxide/kg with prolonged heating of 6 hours.[66] Additionally, these studies did not include *p*-anisidine value, or characterization of the lipidic content in the oils.

Therefore, the mechanistic role played by oxidized oil on gut microbiome remains unclear.

1.2.9 Current knowledge of the biomarker of dietary aldehydes

Understanding the level of exposure to targeted chemicals is crucial in characterizing their metabolic fates and physiological impacts. Several tools are available for measuring dietary intake of foods, beverages, and supplements in clinical practice, such as 24-hour recall, food records, food-frequency questionnaires, and dietary screeners.[256] However, these approaches heavily rely on self-reporting. Variations due to season, day-to-day changes, interview procedures, and questionnaire design can further affect the validity and reliability of these tools..[256] Additionally, the analysis of collected data from these dietary assessment tools depends on nutrient analysis software. One example of such software is the Nutrition Data System for Research (NDSR) developed by the University of Minnesota.[257] Other USDA-approved programs[258] and commercial software are available as well. The quantitative results of dietary analysis are limited by the databases these software rely on. For example, NDSR uses the University of Minnesota Nutrition Coordinating Center Food and Nutrient Database, whereas the USDA offers several publicly available nutrient databases, such as the Standard Reference (SR), the Food And Nutrient Database For Dietary Studies (FNDDS), and Dietary Supplement Ingredient Database (DSID). Consequently, the quantitative assessment of nutrients is limited by the availability of information in these databases.

However, lipidic aldehydes are not considered nutrients and are not reported in these databases, making the conventional methods ineffective for assessing dietary intake of these compounds. In this case, the aldehyde-associated biomarkers may provide an

alternative approach. In this context, aldehyde-associated biomarkers may provide an alternative approach. Studies have aimed to identify potential urinary biomarkers for dietary intake assessment of specific foods, food groups, dietary patterns, and supplements, as summarized in a systematic review.[259] Despite this, findings on urinary markers for reactive aldehydes are not comprehensively characterized.

For example, Lin et al. identified changes in urinary amino acids in mice dosed with 2,4-decadienal, including significantly decreased alanine, proline, valine, and glutamine levels. These amino acids showed better sensitivity in serum towards 2,4-decadienal dosing. [260] However, the metabolism of amino acids is complex and can be confounded by other pathophysiological conditions like nephro- and urolithiasis, making urinary amino acids less specific for aldehydes.[261] Despite this, urine samples are advantageous due to non-invasive collection procedures and easier accessibility. Furthermore, 24-hour urine samples can be collected to study the accumulation of markers of interest, whereas serum provides only a snapshot of the host metabolic status.

Urinary mercapturic acid conjugates (MACs) showed specificity towards the reactive aldehydes. For instance, the urinary 1,4-dihydroxynonane-mercaprutic acid (DHN-MA) has been identified and validated as a maker for exogenous HNE.[262,263] Additionally, various urinary MACs of HNE, octenal, and decadienal, along with their corresponding alcohol and acid species generated from endogenous metabolism, were identified in Fischer rats fed diets containing different oils with heme iron for catalyzing lipid peroxidation.[264] The MACs of HNE stem from the MA pathway for detoxifying the aldehydes, as mentioned previously in this chapter. Other HNE metabolites, including 9-hydroxy-nonanoic acid and thiomethyl and glucuronide conjugates, were detected in the

urine of rats dosed with HNE.[265] Yet, besides HNE, various reactive aldehydes are present in heated oils.[266] The presence of their corresponding urinary metabolites, and the potential efficacy for utilization as biomarkers still warrant further study.

Overall, investigating the urinary markers of aldehydes offers valuable insights into the body's exposure and metabolic response to these reactive compounds. The analysis of urinary markers provides a non-invasive method to assess dietary and environmental exposure. These markers can serve as reliable indicators of oxidative stress and metabolic disturbances, potentially linking aldehyde exposure to various health conditions. Understanding urinary markers also aids in identifying individuals at risk and developing preventive strategies. Ultimately, studies on aldehyde-responsive markers could contribute to better dietary guidelines, improved public health policies, and the development of therapeutic interventions to mitigate the adverse effects of aldehyde exposure.

1.3 CHEMOMETRICS, LIPIDOMICS, AND METABOLOMICS

Chemometrics refers to analytical chemistry workflow with a combination of mathematical and statistical analysis, emphasizing the investigation of causal relationships.[267] It is a powerful tool for investigating chemical changes in the system, providing quantitative and structural information on analyzed compounds. Frequently, an additional untargeted approach can be adopted to examine the unique markers associated with different samples or treatment groups. Lipidomics is a chemometric study focusing on fats, oils, and lipids on biological and food sample matrices.[268,269] Metabolomics is also a chemometric approach for studying the metabolites of biological systems. [194,195] Some technical instruments include LC, GC, NMR, and FTIR. LC and GC can be

coupled with different detectors, such as MS, flame ionization detector (FID), and UV detector. Their applications for studying oxidized oil and the associated metabolic effects are discussed below.

1.3.1 Chemometric and lipidomic investigation of oxidized oils

Chemometric and lipidomic approaches have extensive applications in studying edible oils. Luo et al. described a mass spectrometry-based method to identify the adulteration of olive oil with vegetable oil. The method was sensitive enough to identify vegetable oils mixed into olive oil by as low as 0.5% (*v/v*).[270] The lipidomic approach was applied to track the geographical origin of goat milk via analysis of their lipid composition. A total of 38 lipid compounds were suggested as good predictors.[271]

The lipidomic approach was also adopted to analyze oxidized oils. For the volatile LOPs, Wang et al. investigated the kinetics of aldehyde formation in soybean oils heated at frying temperature via an LC-MS-based approach.[66] GC-MS-based studies were conducted to examine the aldehyde produced from frying oil.[119] On the other hand, LC-MS is more powerful for detecting the larger non-volatile LOPs, mainly TG derivatives.[272]

However, the analysis of TG-OX is challenging. Firstly, different vegetables have varying fatty acid compositions, further complicating the TG composition.[211] Additionally, the oxidation status is easily impacted by temperature, heating time, and oxygen exposure, resulting in diverse TG-OX species. At the same time, the TG-OX species are not stable for enzymatic digestion, hydrolysis, and derivatization.[211] Last but not least, accurate identification and elucidation of the structure of TG-OX. For example, the location of unsaturation on each fatty acyl chain, and the position of each fatty acyl

chain on the glycerol backbone, are not always identified by LC-MS. Such complexity makes tracking the LOPs to their parent compound very difficult. Therefore, to simplify the target pool, some mechanistic studies are based on purified model lipids, such as triolein and trilinolein.[211,273,274]

In recent years, advancements in technical platforms illustrated a more detailed profile of non-volatile LOPs in heated vegetable oils. More than one hundred lipidic compounds were identified via an LC-MS-based lipidomic study, including DG, TG, TG-OX, and oxidized DG, with varying lengths of fatty acids and oxygenated groups.[211]

1.3.2 Metabolomic investigation of oxidized oil-induced metabolic effects

Compared to conventional targeted approaches, such as blood biochemistry analysis, metabolomics provides a more comprehensive coverage of the metabolites within the biological specimen. LC-MS-based metabolomics is an effective platform to examine complex metabolic interactions, especially the subtle changes in metabolites.[168] Through a combination of sample preparation, LC-MS analysis, and data analysis, a wide range of metabolites can be detected and profiled, including amino acids, fatty acids, lipids, and organic acids. In addition to targeted quantitative analysis, untargeted approaches characterize unknown metabolic changes induced by corresponding experimental designs. This untargeted approach is now commonly implanted for studying the interactions between diets and metabolic consequences and assessing dietary intake of foods of interest.[275-277]

To study the metabolic consequences of oxidized oil consumption, Wang et al. applied LC-MS based metabolomics platform. They revealed biological changes in the

mice fed heated soybean oil.[168] Yuan et al. revealed serum and hepatic metabolites in mice in response to the intake of oils fortified with polar compounds formed in frying palm oil.[278] Jamin et al. adopted an untargeted approach and profiled various urinary MACs from dietary intake of oxidized oils in rats.[264] Additional multivariate data analysis was conducted, which revealed and strengthened the specificity of these MACs towards the reactive aldehydes in oils of different fatty acid profiles.[264] In addition to biological specimens, the metabolomic approach can be applied to track the transformation of oxidized lipids during simulated gastrointestinal digestion.[279,280] The study on in-vivo luminal metabolome is currently limited to a handful of studies using LC-UV[50], GC-MS[71], LC-IR[71], and LC-MS[170]. A typical LC-MS-based metabolomics workflow for studying the impact of oxidized oils is illustrated in **Figure 1.8**.

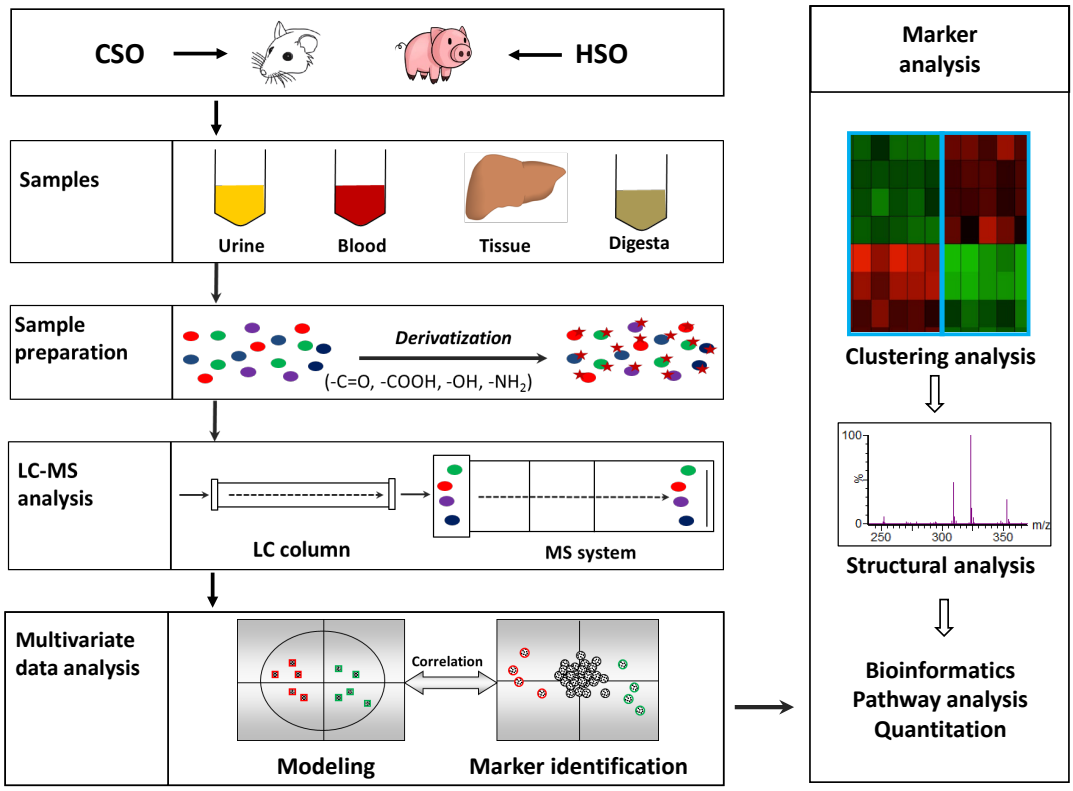

Figure 1.8 A typical LC-MS based workflow for studying the metabolic impacts of oxidized oils in animal models. Non-heated and heated oils are fed to animals, taking mice and pigs as an example. Then urine, blood, tissue, and digesta samples were collected, processed, and derivatized as needed for LC-MS analysis. The acquired LC-MS data further undergoes multivariate data analysis and modeling to identify the diet induced changes in the metabolome and the contributing markers. Further clustering analysis could be applied to further elucidate the correlations and shared patterns among the selected metabolites. Structural analysis, bioinformatics, pathway analysis, and quantitative analysis can be further applied to study the metabolites of interest. CSO, control soybean oil; HSO, heated soybean oil; LC, liquid chromatography; MS, mass spectrometry.

Chapter 2 Characterization of urinary *N*-acetyltaurine as a biomarker of hyperacetatemia in mice

Part of this chapter is modified from the publication:

Mao Q, Shi X, Ma Y, Lu Y, Chen C. Characterization of Urinary *N*-Acetyltaurine as a Biomarker of Hyperacetatemia in Mice. *Metabolites*. 2024; 14(6):322. https://doi.org/10.3390/metabo14060322

2.1 SUMMARY

Acetate is an important metabolite in metabolic fluxes. Its presence in biological entities originates from both exogenous inputs and endogenous metabolism. Because the change in blood acetate level has been associated with both beneficial and adverse health outcomes, blood acetate analysis has been used to monitor the systemic status of acetate turnover. The present study examined the use of urinary *N*-acetyltaurine (NAT) as a marker to reflect the hyperacetatemic status of mice from exogenous inputs and endogenous metabolism, including triacetin dosing, ethanol dosing, and streptozotocin-induced diabetes. The results showed that triacetin dosing increased serum acetate and urinary NAT but not other *N*-acetylated amino acids in urine. The co-occurrences of increased serum acetate and elevated urinary NAT were also observed in both ethanol dosing and streptozotocin-induced diabetes. Furthermore, the renal cortex was determined as an active site for NAT synthesis. Overall, urinary NAT behaved as an effective marker of hyperacetatemia in three experimental mouse models, warranting further investigation into its application in humans.

2.2 INTRODUCTION

Acetate is a ubiquitous metabolite in nature. Its presence inside the human body originates from both exogenous and endogenous sources.[281] Exogenously, acetate could be directly obtained via dietary intake of acetate-containing foods and beverages, such as apple cider vinegar[2] and fermented foods[282], or medical procedures, such as acetate supplementation and the infusion of acetate-containing buffers.[3] Alcohol intake is an indirect source of acetate in humans as acetate is the end product of the ethanol–acetaldehyde–acetate metabolic cascade in alcohol metabolism.[4] Endogenously, acetate is produced via multiple pathways. In the liver, acetate can stem from acetyl-CoA hydrolysis by cytoplasmic acylthioesterase-12 (ACOT12) to free coenzyme A for other metabolic activities.[5] For the cells under excessive nutritional supply, acetyl-CoA-independent metabolic activities of keto acid dehydrogenases are capable of converting pyruvate to acetate *de novo* through either thiamin- or reactive oxygen species (ROS)-dependent manners.[7] Acetate could also be released from the deacetylation reactions, such as from acetylated proteins.[9] In addition, gut microbiota produces acetate as a major fermentation product, which is then extensively absorbed and uptaken by the liver.[10]

The disposition and functions of acetate inside the body have been extensively investigated.[13] Acetate is transported into cells by both passive diffusion and monocarboxylate transporters-mediated facilitated diffusion.[12] Inside the cell, through the catalysis of acetyl-CoA synthetases[17], the direct usage of acetate is to produce acetyl-CoA, which is an essential intermediate in both catabolic and anabolic metabolism as well as the cofactor for the acetylation of proteins, nucleotides, and other amine-containing metabolites.[14] Meanwhile, acetate is a ligand of free fatty acid receptors 2

(FFAR2, also known as GPR43), which is a mediator for pancreatic β-cell function[21] and immune responses.[24] Acetate plays versatile roles in human health and disease through these metabolic and regulatory functions. In many cases, acetate is considered beneficial as the acetate from gut microbial fermentation of dietary fiber or from dietary supplementation, such as apple cider vinegar, has been shown to lower blood cholesterol, enhance insulin sensitivity, decrease body weight, expedite fatty acid oxidation, and reduce pro-inflammatory cytokines.[2,29-31,35] On the other hand, the associations of acetate with adverse health events have also been reported.[10] For example, increased plasma acetate levels after feeding rats with high-fat and high-calorie diets correlated with hyperinsulinemia, increased fat deposition, and weight gain.[37] Higher blood acetate level was associated with increased cancer risk[39], partially due to its usage as an energy source and a substrate for the lipogenesis and proliferation of cancer cells, especially the aggressive types.[20,38] Additionally, acetate, when used in the buffer of hemodialysis, has been implicated in the development of hypotension and hypoxemia through its vasodilatory effect.[40] Considering these double-edged effects of acetate, monitoring the status of circulating acetate levels carries clear values in both research and clinical applications. Currently, acetate levels are commonly monitored using blood samples as well as selected biological samples, such as the liver and fecal samples. Nonetheless, such biological specimens may not always be accessible due to invasive and inconvenient collection procedures. Hereby, we propose using urinary *N*-acetyltaurine (NAT) as a biomarker to reflect the systematic acetate level.

NAT was initially discovered as an ethanol metabolite in our mice ethanol-feeding study, in which the kidney was identified as an active organ conducting the

reaction between acetate and taurine to form NAT.[41] Subsequent studies confirmed NAT as an ethanol metabolite in human urine[283] and further showed that urinary NAT was increased by endurance exercises.[284,285] Considering the fact that acetate is the direct precursor of NAT and taurine is an abundant free amino acid, the potential utilization of urinary NAT as an alternative marker of hyperacetatemia from exogenous inputs or endogenous metabolism has been proposed[41] but not investigated. This study examined the correlations between serum acetate and urinary NAT in three animal models of hyperacetatemia, including direct acetate intake by triacetin administration, indirect input from ethanol feeding, and endogenous acetate formation under diabetes. In addition, the site of NAT synthesis in the kidney was examined by comparing the NAT synthesizing activity between the renal cortex and medulla samples *in vitro*.

2.3 MATERIALS AND METHODS

2.3.1 Chemicals and reagents

The chemicals and reagents used in sample preparation, LC–MS analysis, structural confirmation, and quantification are listed in **Table 2.1**. NAT was synthesized and authenticated in-house in a previous study.[41]

2.3.2 Animals, experimental design, and sample collection

Animal care and experimental procedures were approved by the University of Minnesota Institutional Animal Care and Use Committee (IACUC). Male C57BL/6 mice, 8–12-weeks old, were purchased from Charles River Lab (Wilmington, MA, USA). All mice were housed in the University of Minnesota animal facility at a constant temperature of 21 °C under a 12 h light–dark cycle, with *ad libitum* access to water and

feed. The mice were first acclimated to the normal chow for 7 days before corresponding dosing experiments. Blood samples were collected via submandibular bleeding and centrifuged at 3000 × *g* for 20 min to obtain serum samples. The 24-h urine samples were collected after housing individual mice in metabolic cages for 24 h. All samples were stored at −80 °C prior to the analysis.

2.3.2.1 Direct acetate intake through triacetin dosing

For triacetin feeding (IACUC protocol 2208-40322A, approved on 2 September 2022), two groups of male C57BL/6 mice were gavaged with 40% (*v*/*v* in water) glycerol at the dose of 2.52 g/kg body weight (n = 5) and triacetin at the dose of 5.8 g/kg body weight (n = 4), respectively. The selected dose of triacetin was known to increase the acetate level in mice brains within 1–2 h of oral gavage.[286] The selected dose of glycerol was equivalent to the molar quantity of the glycerol moiety in dosed triacetin. Serum samples were collected at 2 h after dosing. Urine samples were collected for 24 h after dosing.

2.3.2.2 Indirect acetate input from ethanol (EtOH) dosing.

For ethanol feeding (IACUC protocol 1211A24284, approved on 13 December 2012), two groups of male C57BL/6 mice were fed the control semi-solid dextrose diet (n = 4) and a modified semi-solid diet formulated based on the Lieber–DeCarli liquid ethanol diet (n = 8), respectively, for 15 days. The details on the preparation and feeding of semi-solid diets were described previously [41]. Ethanol concentration in the diet started at 2.2% (*v*/*v*), increased to 4.5% on day 4, and 6.7% on day 9. Urine and serum samples were collected on day 0 (D0) before feeding and day 15 (D15) of feeding, respectively.

2.3.2.3 Endogenous acetate input from streptozotocin (STZ) dosing.

Diabetes was induced by intraperitoneal injection of streptozotocin (STZ) at the dose of 180 mg/kg (IACUC protocol 1211A24284, approved on 13 December 2012). Two groups of male C57BL/6 mice (n = 4 per group) were dosed with STZ alone and STZ with 2% (*w*/*v*) taurine in drinking water, respectively. The selected dose of taurine supplementation has been reported to improve the glucose tolerance of Wistar rats under a high-fructose diet [287]. Individual mice were housed in metabolic cages with urine and serum samples collected on day 0 (D0) before STZ dosing and on day 6 (D6) of the treatment, respectively. The development of diabetes was confirmed by measuring blood glucose using a glucometer.

2.3.3 Sample preparation and chemical derivatization for LC-MS analysis

For quantifying urinary NAT, 100 μL of urine samples were quenched with 400 μL of 50% aqueous acetonitrile containing 5 μM sulfadimethoxine as the internal standard for protein precipitation. To analyze creatinine, 10 μL urine samples were diluted with 1,000 μL of 50% aqueous acetonitrile containing 5 μM sulfadimethoxine as the internal standard. These urine samples were centrifuged at 13,000 × *g* for 10 min, and their supernatants were submitted for LC–MS analysis. Serum samples were quenched with 2 volumes of acetonitrile containing 5 μM sulfadimethoxine as the internal standard, then centrifuged to acquire the supernatant.

For detecting and quantifying taurine, the serum and urine samples were derivatized by dansyl chloride (DC) prior to LC–MS analysis. In brief, 5 μL of quenched urine, serum, or taurine standard was mixed with 5 μL of 50 μM deuterated d_5-tryptophan

(internal standard), 50 µL of 10 mM sodium carbonate, and 100 µL of DC (3 mg/mL in acetone). The mixture was incubated at 60 °C for 15 min and then centrifuged at 13,000 × *g* for 10 min. Then, the supernatant was transferred to an HPLC vial for LC–MS analysis.

For detecting and quantifying acetate, the serum and urine samples were derivatized by 2-hydrazinoquinoline (HQ), following an established protocol [150]. In brief, 2 µL of quenched sample was mixed with 100 µL of freshly prepared acetonitrile solution containing 1 mM 2-2′-dipyridyl disulfide (DPDS), 1 mM triphenylphosphine (TPP), 1 mM HQ, and 20.8 µM deuterated d_4-acetate (internal standard). After incubation at 60 °C for 30 min, chilled on ice, the reaction was stopped by mixing with 100 µL of ice-cold water. After centrifuging at 13,000× *g* for 15 min, the supernatant was transferred to an HPLC vial for LC-MS analysis.

2.3.4 *In-vitro* incubation of renal tissues for NAT synthesis

To determine the site of NAT synthesis inside the kidney, cow kidneys were selected for sampling renal cortex and medulla tissues due to their large size. Fresh cow kidneys were obtained from grass-fed Angus beef cattle at the time of slaughtering. The kidney lobes were sliced perpendicular to their longitudinal axis to expose the medulla and cortex tissues. After the collection, the tissue samples were stored at −80 °C prior to the analysis. The tissue homogenates were prepared by homogenization in a buffer containing 320 mM sucrose, 50 mM phosphate buffered saline (PBS) solution, 1 mM EDTA, and protease inhibitor. The mixture was centrifugated at 600× *g* for 10 min to remove the nuclear pellet. The *in vitro* reaction was conducted by incubating the

homogenate with 20 mM taurine and 2.5 mM acetate in a phosphate-buffered saline solution at 37 °C for 30 min. The reaction was terminated by adding an equal volume of acetonitrile. The yield of NAT was quantified via the LC–MS analysis of the reaction mix.

2.3.5 LC-MS Analysis

An aliquot of 2 μL sample from the abovementioned preparation procedures was injected into a Waters Acquity Ultra-Performance Liquid Chromatography (UPLC) system (Milford, MA, USA) and separated in a column. The eluant from the LC was then introduced into a Waters Xevo-G2-S or Synapt-G2Si quadrupole time-of-flight mass spectrometer (QTOF-MS) for accurate mass measurement and ion counting. Nitrogen was used as both cone gas (50 L/h) and desolvation gas (600 L/h). The mass analyzer was calibrated to detect ions within the range *m/z* 50–1200 and was monitored by intermittent lock mass injection. The structures of interested metabolites were analyzed by tandem MS (MS/MS) fragmentation with a collision energy ramp of 10–50 eV. The column, mobile phases, mass detection mode, capillary and cone voltages, and lock mass used for different metabolites are included in **Table 2.2**.

Mass chromatograms and mass spectral data were acquired and processed by MassLynx^{TM} software V4.2 (Waters) in centroided format. Target compounds were quantified by accurate mass-based chromatograms. Standard curves of creatinine, NAT, *N*-acetyl-glutamate (NA-Glu), *N*-acetyl-glutamine (NA-Gln), *N*-acetyl-isoleucine (NA-Ile), *N*-acetyl-leucine (NA-Leu), *N*-acetyl-phenolalanine (NA-Phe), *N*-acetyl-tyrosine (NA-Tyr), and taurine (5 to 1,000 μm) were prepared. The concentration of target

compounds in the samples was determined by fitting the peak area (normalized by corresponding internal standards) with the standard curves via Quanlynx™ (Waters).

2.3.6 Untargeted multivariate data analysis

The LC–MS data were analyzed via MarkerLynx™ software V4.2 (Waters). The chromatographic and spectral data underwent centroiding, deisotoping, filtering, peak recognition, and integration. Then, a multivariate data matrix containing sample identity, ion identity (retention time and *m/z*), and ion abundance was generated and visualized via SIMCA™ software version 13.0 (Sartorius, Göttingen, Germany). The intensity of each single ion was normalized to the total ion counts, and the total ion intensity was set arbitrarily at 10,000. The processed data matrix was further transformed by Pareto scaling and then analyzed using principal components analysis (PCA). Major latent variables in the data matrix were described in a scores scatter plot of the multivariate model. The chemical identity of ions of interest was determined by accurate mass measurement, database search (HMDB www.hmdb.ca), and elemental composition analysis. The data matrix generated from MarkerLynx™ V4.2 (Waters) analysis was also log-transformed, Pareto scaled, and then processed by Metaboanalyst 6.0 (https://www.metaboanalyst.ca/) to construct the volcano plot.

2.3.7 Statistical Analysis

The concentrations or relative abundances of targeted metabolites were expressed as the mean ± standard deviation (SD). The statistical analysis was conducted by two-way ANOVA with Fisher's LSD tests on the rank-transformed data (RT-1, ranking of all

the data together) or non-paired *t*-test via Graphpad Prism 5™ (Dotmatics, Boston, MA, USA). The difference was considered significant with the p-value < 0.05.

2.4 RESULTS

2.4.1 Influences of triacetin dosing on urinary NAT and other urinary metabolites

Direct dosing of acetate was achieved by gavaging triacetin, a triglyceride with three units of acetate, to mice. The triacetin treatment increased serum acetate drastically and decreased serum taurine at 2 h of dosing compared to the glycerol control treatment **(Figure 2.1 A,B)**. In contrast, both acetate and taurine in the 24-h pooled urine were not affected by triacetin dosing **(Figure 2.1 C,D)**. Nevertheless, triacetin increased urinary NAT by more than six times **(Figure 2.1 E)**. To determine whether the observed increase of urinary NAT occurred to other acetylated amino acids, the concentrations of a group of *N*-acetyl amino acids (NAAAs) in urine were measured. The results showed that the concentrations of urinary *N*-acetyl-glutamate, *N*-acetyl-glutamine, *N*-acetyl-isoleucine, *N*-acetyl-leucine, *N*-acetyl-phenylalanine, and *N*-acetyl-tyrosine were comparable between the glycerol and triacetin groups **(Figure 2.1 F–K)**.

To further examine the uniqueness of NAT as a responsive urinary metabolite of hyperacetatemia, unsupervised multivariate modeling on the urinary metabolome was constructed using the data from both positive- and negative-mode MS analysis of urine samples. In the scores plot of the constructed PCA model, a clear separation of the glycerol control and triacetin treatment was observed **(Figure 2.1 L)**. NAT was reconfirmed as a urinary metabolite contributing to the differentiation of two feeding groups in a volcano plot **(Figure 2.1 M)**. Other urinary metabolites with greater fold

change (FC) and smaller *p*-values than NAT were further investigated for their structural identities by accurate mass-based elemental composition analysis, database search, and MSMS fragmentation **(Table 2.3)**. No more acetylated metabolites were identified among them, except one negative ion with *m/z* = 309.0815 because of the neutral loss of the acetyl group (the loss of 42 from *m/z* 309 → 267) in its MSMS spectrum. However, this metabolite was absent in the control urine, indicating its identity as a specific metabolite of triacetin, not an endogenous metabolite. Overall, NAT was the sole *N*-acetylated endogenous metabolite in the urine responsive to the triacetin treatment.

2.4.2 Influences of ethanol dosing on urinary NAT

Ethanol feeding was performed to achieve indirect input of acetate since acetate is the main intermediate in ethanol metabolism. The results showed that ethanol feeding increased serum acetate but did not affect serum taurine **(Figure 2.2 A,B)**. In the meantime, ethanol increased urinary NAT excretion **(Figure 2.2 C)**.

2.4.3 Influences of STZ-induced diabetes and taurine supplementation on urinary NAT

In addition to the exogenous acetate from triacetin and ethanol dosing, the effect of endogenous metabolism-derived acetate on urinary NAT was examined in the STZ-induced diabetes mouse model. The influence of taurine supplementation on serum acetate and urinary NAT was further examined by the joint treatments of STZ injection and 2% taurine in drinking water. The results showed that STZ effectively induced hyperglycemia **(Figure 2.3 A)** and increased serum acetate and urinary NAT **(Figure 2.3 B,D)** but did not affect serum taurine **(Figure 2.3 C)**. On the other hand, taurine

supplementation increased serum taurine **(Figure 2.3 C)** but did not affect STZ-elicited effects on serum acetate **(Figure 2.3 B)** and urinary NAT **(Figure 2.3 D)**.

2.4.4 Site of NAT synthesis site in the kidney

The kidney was previously identified as a more active organ than the liver and other organs/tissues for NAT synthesis in mice.[41] However, the site of NAT synthesis inside the mouse kidneys was not defined due to their small size. To address this question, bovine kidneys were used to harvest the renal cortex and medulla fractions. The results from the in vitro incubations showed that the NAT production from the cortex fraction was much greater than that of the medulla fraction **(Figure 2.4)**, indicating that the renal cortex is an active site for the NAT synthesis from taurine and acetate.

2.5 DISCUSSION

In this study, NAT was validated as a urinary metabolite marker of hyperacetatemia in three experimental mouse models, including direct dosing through triacetate, indirect input through ethanol metabolism, and endogenous production under diabetes **(Figure 2.5)**. The biochemical events underlying NAT synthesis, including the sources of acetate and the biochemical properties of the reaction between acetate and taurine, as well as the advantages and values of NAT as a biomarker of metabolic status and disorders, are discussed as follows.

2.5.1 Current knowledge of the biochemical properties of NAT synthesis

NAT is not the only *N*-acetylated amino acid (NAAA) in urine, but it was the only one responsive to triacetin-induced hyperacetatemia in this study **(Figure 2.1)**. The biosynthesis of NAAAs has been extensively studied since they have been widely

characterized as the urinary markers of metabolic disorders, such as inborn errors of metabolism[288], neurodegenerative diseases[289], and kidney disease[290]. The formation of the NAAAs from proteinogenic amino acids, such as *N*-acetylglutamate and *N*-acetylphenylalanine, is mainly through the acetylation of respective amino acids by the transferases using acetyl-CoA as the substrate.[291] In contrast, the formation of NAT by kidney homogenates in the current study was through the direct reaction of taurine and acetate **(Figure 2.4)**. This observation of direct taurine–acetate reaction is consistent with our previous investigation on the enzymatic kinetics of NAT synthesis, in which acetate was determined as a more favorite substrate for NAT synthesis than acetyl-CoA based on the facts that the taurine–acetate reaction had similar K_m value (affinity) but greater V_{max} value (capacity), in comparison with the taurine–acetyl-CoA reaction.[41] Together, the enzymatic analysis in our previous study and the incubations of renal fractions in the current study have defined the properties of the unknown enzyme responsible for NAT synthesis as a cytosolic metalloenzyme abundant in the kidney cortex that is capable of catalyzing the esterification reaction between taurine and acetate without the involvement of ATP and CoA.[41] Despite this knowledge, the exact identity of NAT synthase, its distribution, and its regulation remain to be determined.

In addition to acetate, taurine is a required substrate for NAT synthesis. Three known function- and distribution-related features of taurine are relevant to the NAT synthesis and the concentrations of its precursors in the three mouse models of hyperacetatemia in this study. Firstly, taurine, as a highly abundant free amino acid and an intracellular osmolyte, is actively synthesized inside the body. Its concentration in many mammalian organs and tissues, including the kidney, ranges between 5 and 50

mM[292], which is much greater, by 2–3 orders of magnitude, than its blood concentrations, including the ones observed in this study. Therefore, the observed changes in serum taurine, including the decrease from triacetin treatment or the increase from 2% taurine supplement in the STZ-induced diabetes model, might have limited influence on the availability of intracellular taurine for the enzymatic performance in NAT synthesis, which may further explain the lack of increase in urinary NAT after the joint treatment of STZ and taurine **(Figure 2.3 D)**. Secondarily, taurine turnover in the kidney is adjustable since increased urinary excretion and increased renal uptake were observed under taurine overloading and taurine deficiency, respectively.[293,294] This robust regulation can effectively maintain the systematic taurine pool, hence providing adequate taurine substrate for NAT synthesis. Lastly, taurine is known for its antioxidant and cytoprotective functions, contributing to its known activities against ethanol-induced liver injury[295] and STZ-induced diabetes in rodent models.[296] It will be interesting to investigate whether NAT, a direct derivative of taurine, shares these beneficial activities of taurine in future studies.

2.5.2 Urinary NAT as a marker of hyperacetatemia: a comparison with serum and urinary acetate

The three mouse models of hyperacetatemia in this study reflected the hyperacetatemic scenarios that could occur to humans through intentional acetate consumption, alcohol overdose, and diabetes. Many more events could also elevate serum acetate in humans and animals, such as vinegar consumption and supplementation, high-fat diet, endurance exercise, gut microbial fermentation on the fiber, as well as pathophysiological events.[37,284,285,297-299] Measuring blood acetate concentration can

definitely determine the status quo of acetate at the moment of sampling. However, it might not accurately reflect the overall status of acetate homeostasis since blood acetate concentration can change rapidly after acetate inputs. For example, post-prandial plasma acetate concentration in humans peaked at 30 min after breakfast and then decreased rapidly.[300] Additionally, the plasma concentration of acetate in human subjects after consuming 15 mL of apple cider vinegar peaked at 1 h and then returned to the baseline after 2 h of dosing.[297] Therefore, timely sampling or multiple samplings are needed to detect hyperacetatemia through blood acetate measurement. By contrast, urinary NAT has advantages for detecting hyperacetatemia based on the following considerations: (1) Urine is accumulative and covers a broader time window than blood; (2) for humans, urine collection is more compliant and less invasive than blood collection; and (3) detecting NAT is more convenient than detecting acetate, at least for the LC–MS analysis in the current study, where acetate detection required chemical derivatization, whereas NAT was directly detected.

As for urinary acetate, in contrast to the drastic increase of serum acetate, acetate in pooled urine samples from triacetin-treated mice did not increase. The lack of the change in urinary acetate, in this case, might be explained through acetate metabolism and renal functions in reabsorption. In the kidney, acetate is actively metabolized to bicarbonate, as shown by the usage of sodium acetate in dialysis, which leads to urine alkalinization instead of acidosis through the excretion of bicarbonate from acetate metabolism into urine due to compromised bicarbonate reabsorption function in the patients of renal diseases.[299,301] In addition, monocarboxylic acid transporters capable of acetate uptake are highly abundant in the renal proximal tubule, which may further

prevent unnecessary leakage of acetate into urine.[26,27] However, when this mechanism of metabolism and reabsorption was either overwhelmed by acetate dosing or compromised by renal injury, the elevations of urinary acetate were also observed[25,302], leading to the usage of urinary acetate in the diagnosis of urinary tract infection[303] and ischemia-reperfusion injury after kidney transplantation.[302] Therefore, under normal renal function, urinary NAT has an advantage over urinary acetate in sensitivity for detecting hyperacetatemia.

In addition to its presence in mouse urine, NAT as a constitutive molecule of human urine has been established.[283] The elevation of its levels in human urine and blood has also been observed after endurance exercises.[284,285] Based on the results from the current study, more investigations are needed to establish it as a marker of hyperacetatemia in humans and determine its value in the monitoring of exogenous acetate intake, such as vinegar supplementation, and the diagnosis of metabolic disorders.

2.5.3 Limitations

In addition to confirming the increases of urinary NAT in three mouse models of hyperacetatemia, our data analysis also revealed the limitations of the current study. Firstly, relatively small numbers of animals used in each model might contribute to the observed large variance among individual animals within the same treatment group, which is reflected by the high standard deviations in some measured values. Secondly, to explore the correlation between urinary NAT and serum acetate, their values in three models of hyperacetatemia were processed by linear regression, showing a significant correlation **(Figure 2.6 A)**. However, this correlation was mainly caused by the values

from the triacetin treatment since the exclusion of triacetin data made the correlation insignificant **(Figure 2.6 B)**. Such challenge of this correlation analysis can be partially attributed to the different properties between serum and urine because serum samples were collected at single time points while urine samples were accumulative. In future studies, a more reliable analysis of the correlation between urinary NAT and serum acetate may be achieved by measuring the dose–response of urinary NAT to different acetate inputs or by determining the area under the curve (AUC) of serum acetate during the period of urine collection for NAT analysis.

2.6 CONCLUSIONS

The current study examined the performance of urinary NAT as an indicator of elevated serum acetate in three mouse models of hyperacetatemia. Considering the importance of acetate in general metabolic fluxes and many pathophysiological events, the use of urinary NAT as a marker of hyperacetatemia could provide a convenient and effective venue for monitoring the status of acetate-related metabolism as well as for clinical diagnosis.

2.7 TABLES AND FIGURES

Table 2.1 Reagents and chemicals used in sample preparation and LC-MS analysis.

Chemical/Reagents	**Vendor**
Acetic acid, Acetone (LC-MS grade), Acetonitrile (LC-MS grade, ACN), Ammonium formate, Formic acid (LC-MS grade), Water (LC-MS grade)	Fisher Scientific (Houston, TX)
2-Hydrazinoquinoline (HQ), Triphenylphosphine (TPP)	Alfa Aesar (Ward Hill, MA)
N-acetyl-L-glutamine, Ammonium carbonate ($(NH_4)_2CO_3$), 2-2′-Dipyridyl disulfide (DPDS)	MP Biomedicals, LLC (Irvine, CA)
Creatinine, D_4-acetic acid, Dansyl chloride (DC), Leucine enkephalin, Sodium carbonate (Na_2CO_3),	Sigma-Aldrich (St. Louis, MO)
D_5-Tryptophan	Cambridge Isotope Laboratories (Tewksbury, MA)
Taurine	Thermo Fisher Scientific (Waltham, MA)
Acetyl-L-glutamic acid, Acetyl-L-isoleucine, Acetyl-L-leucine, Acetyl-L-phenylalanine, Acetyl-L-tyrosine	Chem-Impex International (Wood Dale, IL)
Ethanol (reagent alcohol)	Ricca Chemicals (Arlington, TX)

Table 2.2 LC-MS instrumental settings for data acquisition.

Target compounds	LC column and temperature	LC mobile phase	Lock mass and MS detection mode	Capillary and cone voltage	Source and desolvation temperature	Cone and desolvation gas flow	*Collision gas and energy ramp
Taurine (DC derivatization), and *N*-acetyl amino acids (except for NAT)	Waters BEH C18 (reverse phase), 40 °C	A: 0.1% formic acid in water B: 0.1% formic acid in ACN	Leucine enkephalin ($[M + H]^+$ = m/z 556.2771), Positive	0.2 kV, 40 V	120 °C, 350 °C	50 L/hr, 600 L/hr (N_2)	Argon, 10-50 eV
Acetic acid (HQ derivatization)	Waters BEH C18 (reverse phase), 40 °C	A: 2 mM NH_4OAc in water with 0.05% acetic acid B: 2 mM NH_4OAc in 95% ACN and 5% water with 0.05% acetic acid	Leucine enkephalin ($[M + H]^+$ = m/z 556.2771), Positive	0.2 kV, 40 V	120 °C, 350 °C	50 L/hr, 600 L/hr (N_2)	NA
NAT	Waters BEH C18 (reverse phase), 40 °C	A: 0.1% formic acid in water B: 0.1% formic acid in ACN	Leucine enkephalin ($[M - H]^-$ = m/z 554.2615), Negative	-0.2 kV, -40 V	120 °C, 350 °C	50 L/hr, 600 L/hr (N_2)	NA
Creatinine	Waters Amide (HILIC), 40 °C	A: 0.1% formic acid in water B: 0.1% formic acid in ACN	Leucine enkephalin ($[M + H]^+$ = m/z 556.2771), Positive	0.2 kV, 40 V	120 °C, 350 °C	50 L/hr, 600 L/hr (N_2)	NA

**Setting used for MSMS fragmentation analysis, if applicable*

Table 2.3 Information on selected triacetin-responsive urinary metabolites. Enlisted metabolites are selected from the volcano plot of the mouse urine metabolome with greater fold change (FC) and smaller *p*-values than NAT (Figure 1M). Accurate mass-based elemental composition analysis was performed to determine potential molecular formula.

Retention time (min)	Detected M/Z	Ion adduct	FC[#]	*p*-value	Potential molecular formula	Monoisotopic M/Z	Mass deviation (Δppm)
5.9152	240.232	$[M+H]^+$	7.7838	1.36E-06	$C_{15}H_{29}NO$^	239.2249	3
2.11	391.0629	$[M+H]^+$	7.763	2.73E-06	$C_{14}H_{10}N_6O_8$^	390.056	2
6.1748	459.4871	$[M+H]^+$	8.0529	5.46E-06	$C_{28}H_{62}N_2O_2$^	458.4811	4
2.1065	177.0741	$[M+H]^+$	8.188	5.58E-06	$C_7H_{12}O_5$^	176.0685	9
6.2401	485.1465	$[M-H]^-$	8.5178	5.75E-06	$C_{26}H_{22}N_4O_6$^	486.1539	2
2.1269	353.1073	$[M+H]^+$	8.4198	6.22E-06	$C_{23}H_{14}NO_3$^	352.0974	7
6.6641	515.5503	$[M+H]^+$	7.7516	7.91E-06	$C_{32}H_{70}N_2O_2$^	514.5437	3
2.1197	370.1341	$[M+H]^+$	9.7848	1.22E-05	$C_{14}H_{27}NO_6S_2$^	370.1353	3
1.0254	309.0815	$[M-H]^-$	8.6626	1.31E-05	$C_{11}H_{18}O_{10}$^	310.0907	5
3.1667	229.0163	$[M-H]^-$	8.7126	2.46E-05	$C_9H_{10}O_5S$^	230.0249	6
0.3157	166.0169	$[M-H]^-$	7.6126	9.07E-05	$C_4H_9NO_4S$*	167.0252	6

[#]FC, fold change, calculated by the relative abundance of metabolites in the triacetin group divided by that of the glycerol group;
^ Database seaech yielded no match with known urinary metabolites
**N-acetyltaurine, identity confirmed by comparison with authentic standard*

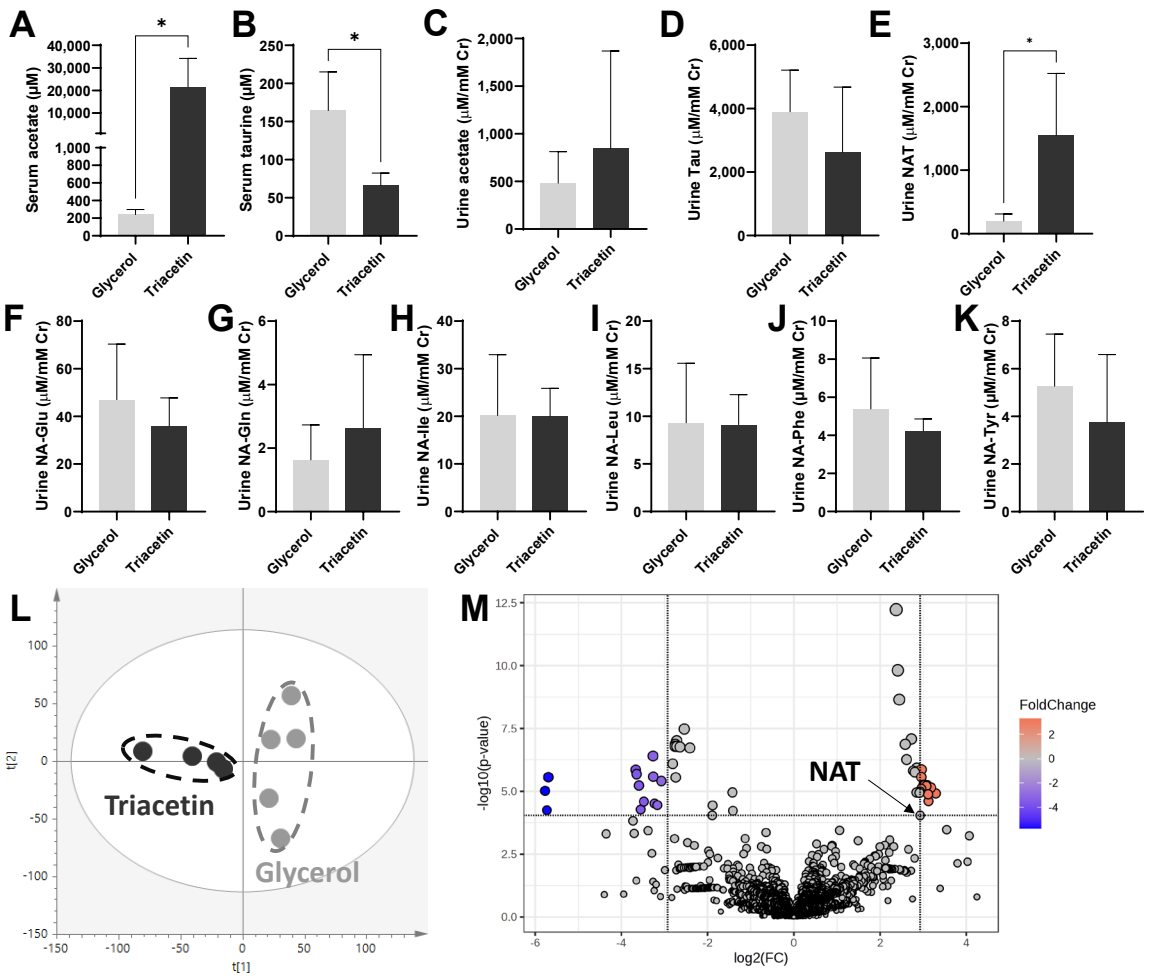

Figure 2.1 Concentrations of targeted serum and urine metabolites and the multivariate modeling of urine metabolome after triacetin dosing. Serum samples were collected 2 h post dosing. Urine samples were collected after housing each mouse individually in metabolic cages for 24 h post dosing (n = 5 in the glycerol group, n = 4 in the triacetin group). (A) serum acetate, (B) serum taurine, (C) urine acetate, (D) urine taurine, (E) urine NAT, (F) urine *N*-acetyl-glutamate (NA-Glu), (G) urine *N*-acetyl-glutamine (NA-Gln), (H) urine *N*-acetyl-isoleucine (NA-Ile), (I) urine *N*-acetyl-leucine (NA-Leu), (J) urine *N*-acetyl-phenolalanine (NA-Phe), (K) urine *N*-acetyl-tyrosine (NA-Tyr). * indicates p-value < 0.05 from non-paired t-test. (L) Scores plot of the PCA model on

combined positive- and negative-mode data on the urine metabolome, in which t[1] and t[2] stand for the principal components 1 and 2, respectively. (M) Volcano plot of the urinary metabolites contributing to the differentiation between the triacetin- and glycerol-dosing groups. The fold-change (FC) and p-value of individual metabolites are the ratios of triacetin vs. glycerol control and their statistical significances, respectively. The metabolites with a greater FC and more significant *p*-value (red colored) than NAT (marked) were selected for further analysis **(Table 2.3)**.

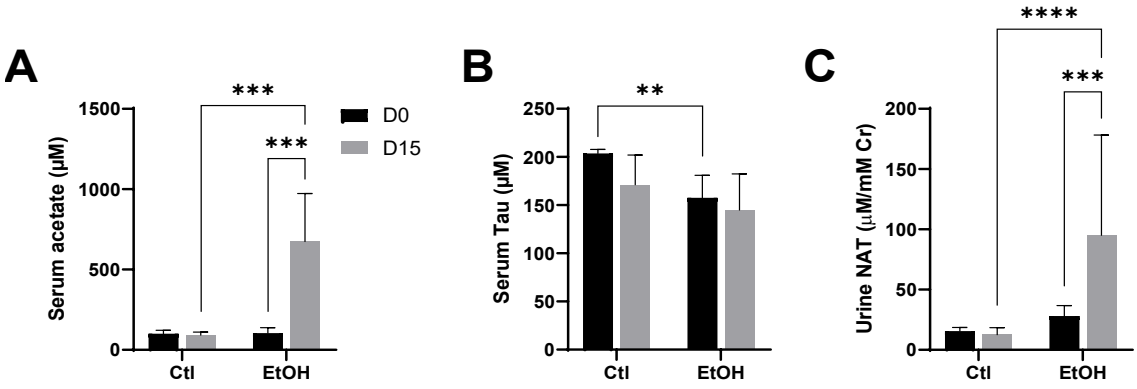

Figure 2.2 Serum acetate and taurine and urinary NAT after 15-day ethanol dosing. Serum and urine samples were collected from the control (Ctl) group (n = 4) and the ethanol (EtOH) feeding group (n = 8) on day 0 (D0) before feeding the semi-liquid diets and on day 15 (D15) of the feeding. (A) serum acetate, (B) serum taurine, (C) urine NAT. Two-way ANOVA tests were conducted on the rank-transformed data, followed by Fisher's LSD tests to examine the differences within the same treatment across days and between two treatments on the same day (** $p < 0.01$, *** $p < 0.001$, **** $p < 0.0001$).

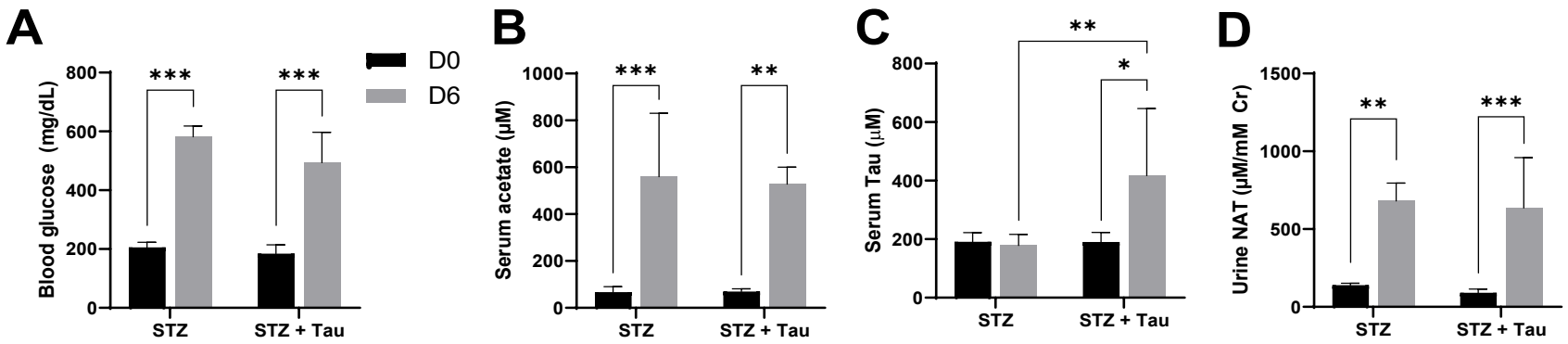

Figure 2.3 Blood glucose, serum acetate and taurine, and urinary NAT after STZ dosing and taurine supplementation. Serum and urine samples were collected from the STZ alone (STZ) treatment group (n = 4) and the SZT plus 2% (w/v) taurine in drinking water (STZ+Tau) treatment group on day 0 (D0) before STZ treatment and on day 15 (D15) after the treatment (n = 4 in each treatment group). (A) Blood glucose, (B) serum acetate, (C) serum taurine, (D) urinary NAT. Two-way ANOVA tests were conducted on the rank-transformed data, followed by Fisher's LSD tests to examine the differences within the same group across days and between the two groups on each day (* $p < 0.05$, ** $p < 0.01$, *** $p < 0.001$).

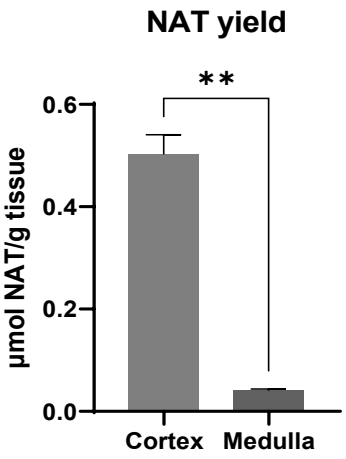

Figure 2.4 The yield of NAT synthesis from 30-min incubations of bovine renal cortex and medulla homogenates with acetate and taurine. ** indicates $p < 0.01$ from a non-paired t-test.

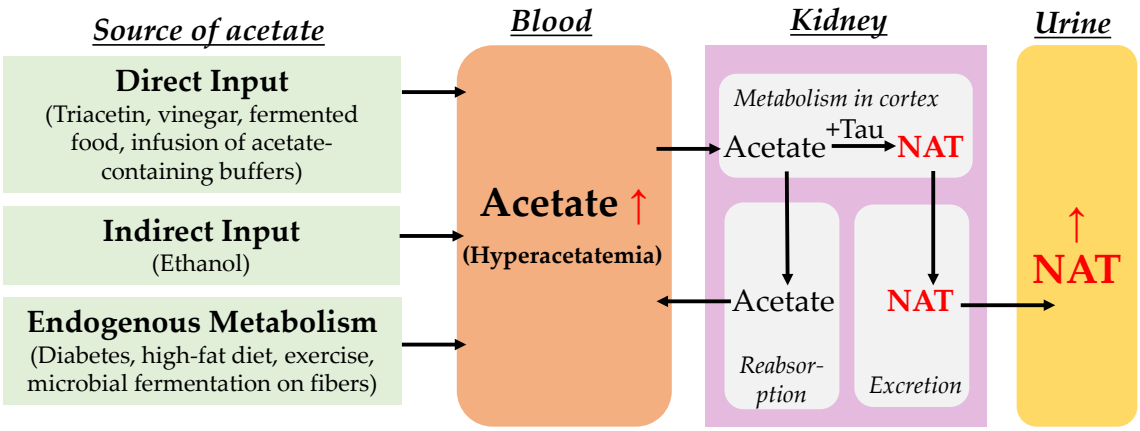

Figure 2.5 The sources of hyperacetatemia and the metabolic events leading to the increased urinary NAT. Blood acetate can be increased by diverse direct and indirect exogenous inputs as well as various endogenous metabolic events. In the kidney, after elevated acetate reacts with taurine to form NAT in the renal cortex, free acetate may undergo extensive reabsorption while NAT is readily excreted into urine, making urinary NAT, instead of urinary acetate, highly responsive to hyperacetatemia.

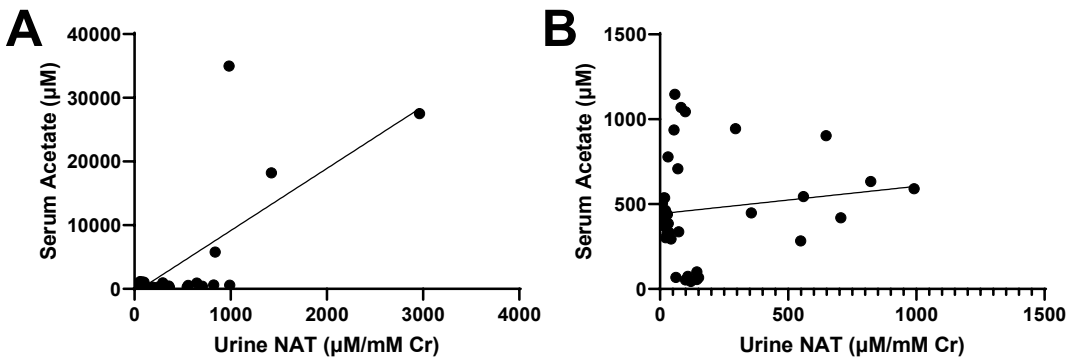

Figure 2.6 Correlation of urinary NAT and blood acetate levels in the animal models of hyperacetatemia. The linear regression was analyzed by GraphPad. A) The correlation in three animal models: Triacetin-dosing, EtOH-dosing, and STZ-dosing. R-square = 0.55, *p*-value of the slope < 0.0001. B) The correlation in two animal models: EtOH-dosing, and STZ-dosing. R-square = 0.02, *p*-value of the slope = 0.4.

Chapter 3 Metabolomic characterization of the effects of oxidized soybean oil on gastrointestinal lumen and its association with systemic metabolism in nursery pigs

3.1 SUMMARY

Consumption of fried foods by humans and feeding recycled cooking oils to animals introduces significant amounts of primary lipid oxidation products (LOPs), such as peroxidized fatty acids, and secondary LOPs, mainly lipidic aldehydes, into their gastrointestinal tracts (GIT). However, the metabolic fates of these LOPs and their interactions with dietary components in the GIT are not well understood. This study aims to delineate the metabolic changes induced by oxidized lipids in the GIT through a nursery pig feeding trial combined with comprehensive metabolomic and biochemical analyses.

Compared to a diet containing control soybean oil (CSO), the inclusion of 10% heated soybean oil (HSO) impaired the growth performance of nursery pigs and induced hepatocyte hypertrophy. Metabolomic analysis revealed substantial alterations in the gastrointestinal (GI) lumen due to HSO consumption, including decreased elastase activity, protein digestion in the small intestine, and disrupted bile acid and gut microbial metabolism. These functional changes in the GI lumen likely contributed to the observed growth impairment.

Lipidomic analysis of the oils, feeds, and luminal digesta showed significant transformations of dietary lipids in the GI lumen, potentially leading to *de-novo* aldehyde production. Notably, HSO feeding uniquely increased free caprylic acid levels in the GI lumen. This study suggests that caprylic acid could serve as a promising predictor for the oxidation status of heated oils and its impact on host health.

Furthermore, correlation analysis demonstrated that the GI caprylic acid level was significantly associated with post-absorption metabolites, including hepatic free amino acids, AMP, NAD^+, choline metabolites, serum free amino acids, and growth performance indices, suggesting the utilization of caprylic acid as a marker for oil oxidation and the oxidized-oil elicited metabolic changes. Additionally, the study highlighted the significant role of aldehydes in the adverse metabolic effects observed, with luminal aldehydes showing strong inverse correlations with growth performance and various metabolic markers. However, the precise contributions of pre-existing and *de-novo*-formed aldehydes to these metabolic disturbances remain unresolved and warrant further investigation.

Keywords: Lipid oxidation; aldehydes; metabolomics; lipidomics; luminal metabolome.

3.2 INTRODUCTION

Dietary fat is an essential macronutrient for humans and animals. Under thermal stress, oils undergo complex chemical changes, including oxidation, polymerization, and hydrolysis, forming a variety of lipid oxidation products (LOPs). The primary LOPs mainly consist of hydroperoxides (ROOH), which are unstable and reactive.[304,305] Primary LOPs further break down into secondary LOPs, including aldehydes, ketones, acids, and other small-molecule substances.[306] About 50% of the fat in the human diet is exposed to thermal treatment, such as frying and cooking.[90] Thermally stressed oils from commercial food production, mostly vegetable oils, are commonly rendered for animal feed production.[94] Meanwhile, lipid oxidation occurs commonly for feed-grade fats and oils, as a wide range of peroxide values (0.4 – 7.3 mEq/kg) have been observed in the survey on oil samples obtained from a local feed mill in the Midwest.[96] Therefore, thermally oxidized oils and fats are of great prevalence in the lipid intake of both production animals and humans.

Consumption of thermally oxidized oil is associated with adverse metabolic and health effects in animals and humans. Dietary intake of fried food has been associated with elevated risks for cancer, cardiovascular disease, and metabolic syndrome in humans.[161-163] In animals, consuming highly oxidized oil led to a series of biological implications, including depressed appetite, increased intestinal leakage, diarrhea, deterred growth performance, elevated liver and kidney weight, oxidative stress, and altered blood lipids.[100,103,104,167-169] Activation of the tryptophan-NAD^+ pathway with the dramatic decrease of circulating tryptophan was identified as a central response to heated soybean oil (HSO) feeding in animals.[168] Among the LOPs contributing to these adverse effects,

aldehydes were the most active.[168] As revealed in animal feeding studies, lipidic aldehydes, specifically C9-C11 unsaturated aldehydes, showed the strongest negative correlation to animal growth performance.[102]

The post-absorptive metabolism of the LOPs, especially lipidic aldehydes, has been extensively investigated. As highly lipophilic and electrophilic compounds, aldehydes are bioavailable and can form adducts with amino acids, proteins, and DNAs via a non-enzymatic mechanism, including both Schiff base and Michael addition, hence exerting toxic effects on host health.[45,173] On the other hand, the aldehyde-metabolizing enzymes, such as aldehyde dehydrogenase (ALDH) and aldo-keto reductase superfamily (AKR), convert aldehydes to less-reactive acids and alcohols, respectively.[160,168] Aldehydes can also be conjugated enzymatically to glutathione (GSH) via glutathione S-transferase (GST) in the liver and then excreted in the urine as mercapturic acid conjugates for detoxification.[198-200]

Despite the extensive knowledge of the post-absorption metabolism of aldehydes, the status of aldehydes in the lumen of gastrointestinal tract (GIT) was not well understood. Compared to the post-absorption organs and tissues, the GIT is directly exposed to dietary aldehydes upon consumption of thermally oxidized oils.[70] Current information on the interaction between aldehydes and other biochemical molecules in the lumen is limited to the observations that fatty acid hydroperoxides (e.g., linoleic acid hydroperoxide) can break down to aldehydes, such as hexanal, in the stomach[50,72]. Then, the formed aldehydes could proceed to the intestine, getting absorbed and transported to the liver.[50] Compared to these *de-novo*-formed aldehydes, aldehydes in oxidized oil are

more abundant in concentration and more diverse in structure. Understanding their disposition in the GIT may reveal more novel insights into the adverse health effects of oxidized oil consumption.

In addition to aldehydes, oxidized oils contain other non-volatile LOPs, including TG dimers, polymers, hydroxy-, epoxy-TG, and free fatty acids.[211,307,308] Except for the dimeric and polymeric TG species, most non-volatile LOPs can be digested and absorbed in the small intestine.[226] But their transformation in the GI lumen is not well understood. The hydroxy, epoxy-TG, fatty accids, and aldehydes are polar compounds in the oxidized oil, which have shown undesirable metabolic effects *in-vitro*[309] and *in-vivo*[310]. However, unlike aldehydes, the specific disposition and metabolic pathways of the non-volatile LOPs have not been fully characterized either.[191] Therefore, more research is warranted to better understand their associations and contributions to animal growth and health.[102]

In this study, we fed HSO to nursery pigs, and then investigated the changes in the luminal metabolome to obtain novel knowledge regarding the disposition of HSO, especially its lipidic aldehyde content in the GI lumen, and their interactions with digestive enzymes and metabolites, as well as their associations to the host metabolism.

3.3 MATERIALS AND METHODS

3.3.1 Chemicals

The chemicals and reagents used for sample preparation, LC-MS analysis, and quantification are included in **Table 3.1**.

3.3.2 Experimental design, animal management, and sample collection

3.3.2.1 Preparation of CSO and HSO oils

Control soybean oil (CSO) was heated at 187ºC for 42 hours with constant airflow at 30 L/min to obtain heated soybean oil (HSO). The peroxide value (PV) of the oils was analyzed via the standardized method AOCS Cd 8b-90. The *p*-anisidine value of the oils was analyzed via the standardized method AOCS Cd 18-90. The oxidized fatty acid level (OFA%) was analyzed by Barrow-Agee Laboratories (Memphis, TN).

3.3.2.2 Animal management and sample collection

All animal care and use procedures for this experiment were approved by the Institutional Animal Care and Use Committee at Iowa State University. A total of 60 weaning barrows were obtained from a commercial farm at 28 days of age, then transported to and housed at the Iowa State University Swine Nutrition Farm (Ames, IA). They were fed a common starter diet to acclimate and optimize feed intake. Then, piglets were randomly allotted into 10 pens (3 pigs/pen, initial average BW of 6.2 kg). Pigs were fed the corresponding experimental diet for 28 days and allowed *ad libitum* access to feed and water. On day 28, pigs and feed were weighed for calculation of average daily weight gain (ADG), average daily feed intake (ADFI), and weight gain: feed intake (G:F) ratio. At the end of the trial, one focal pig was chosen and sacrificed from each pen. Digesta from the stomach, duodenum, proximal jejunum, distal ileum, cecum, and proximal colon were collected from each pig for further metabolomics analysis. The whole liver sample was collected and weighed for the liver weight:body weight (LW:BW) ratio calculation.

All collected samples were flash-frozen in liquid nitrogen and stored at -80 ºC until further analysis.

3.3.3 LC-MS-based chemometrics and metabolomics

3.3.3.1 Sample preparation for LC-MS analysis

The oil content in the feed was extracted. For 1 gram of CSO and HSO feed samples, the oil content was extracted by two volumes of dichloromethane (v/w). To remove the water and insoluble contents, the extracts were then filtered through a column packed with anhydrous sodium sulfate. Then, the dichloromethane was evaporated under nitrogen. The extracts were weighed and stored at -80°C till further use. The original oils and their respective feed extracts were diluted by 100,000-fold in *n*-butanol containing 1 µg/mL tripentadecanoin (TG15:0) prior to LC-MS analysis.

For extracting the lipids in digesta, 50 mg digesta (stomach, jejunum, and colon only due to limited sample quantity) was weighed and mixed with 5 volumes of *n*-butanol containing 1 µg/mL tripentadecanoin (TG15:0) as internal standard. The mixture was sonicated in the ice bath for 30 min, vortexed for 30 min, and centrifuged 13,000 ×g for 15 min to obtain the supernatant. The extract from the stomach was further diluted 10-fold and then stored at -20°C for later use.

For extracting the aqueous phase, 50 mg of digesta sample was weighed and mixed with 10 volumes of 50% aqueous acetonitrile (ACN) containing 50 µM d_5-tryptophan, 2 µM sulfadimethoxine, 510 µM d_4-acetic acid, 5 µM ^{13}C-1-glycocholic acid, 10 µg/mL ^{13}C-1,2-palmitic acid, and 100 µM d_6-acetone as internal standard. The mixture was sonicated in the ice bath for 10 minutes. After centrifuging at 13,000 ×g for

15 min, the supernatant was acquired. All extracts were further diluted 10-fold and then stored at -20°C for later use.

Liver extracts were prepared based on the Bligh and Dyer method.[311] In brief, 100 mg frozen liver samples were mixed with and homogenized in 500 µL methanol containing 180 µM d_6-acetone, 90 µM d_5-tryptophan, 459 µM d_4-acetic acid, 36 µg/mL $^{13}C_2$-palmitic acid, 9 µM sulfadimethoxine, 9 µM glycyrrhetinic acid, and 20 µM tripentadecanoin (TG15:0) as internal standards. Then, 400 µL water and 500 µL chloroform were added into the mixture. After sonication in the ice bath for 1 min, the mixture was centrifuged at 1,3000 × g for 10 minutes for phase separation. The top layer was extracted as the aqueous phase and was stored at −80 °C before LC-MS analysis.

3.3.3.2 Chemical derivatization

For detecting and quantifying fatty acids, aldehydes, and metabolites containing carboxylic acid functional group, the oil, feed extract, and diluted digesta aqueous extract samples were derivatized with 2-hydrazinoquinoline (HQ), following a modified protocol.[150] In brief, 2 µL of aqueous extraction, oil, or feed extraction, was mixed with 100 µL of freshly prepared acetonitrile solution containing 1 mM 2-2′-dipyridyl disulfide (DPDS), 1 mM triphenylphosphine (TPP), 1 mM HQ. In fatty acid and aldehyde standards, the acetonitrile solution contained additional 90 µM d_6-acetone. The mixtures were incubated at 60 °C for 30 min, chilled on ice, and mixed with 100 µL of ice-cold water to stop the reaction. After centrifuging at 13000g for 15 min, the supernatant was transferred to an HPLC vial for LC-MS analysis.

For detecting and quantifying amino acids and metabolites containing amine functional group, the aqueous extraction of digesta was derivatized with dansyl chloride (DC) prior to LC-MS analysis. In short, 5 μL of digesta extraction was mixed with 5 μL of water, 50 μL of 10 mM sodium carbonate, and 100 μL of DC (3 mg/mL in acetone). For amino acid standard mixtures, 5 μL of 50 μM d_5-tryptophan (internal standard) was added instead of water. After incubation at 60°C for 15 min and centrifugation at 13,000 ×g for 10 min, the supernatant was obtained and transferred to an HPLC vial for LC-MS analysis.

3.3.3.3 LC-MS analysis

A 2 μL sample aliquot was injected into a Waters Acquity ultraperformance liquid chromatography (UPLC) system (Milford, MA) and separated in a BEH column. The eluant from LC was then introduced into a Waters Xevo-G2-S or Synapt-G2Si quadrupole time-of-flight mass spectrometer (QTOF-MS) for accurate mass measurement and ion counting. The mass analyzer was calibrated to detect ions within the range *m/z* 50 – 1200 and was monitored by intermittent injection of lock mass. The LC-MS instrumental settings used for different metabolites are included in **Table 3.2**. The acquired chromatograms were processed by MassLynx^{TM} V4.2 (Waters). The structures of interested metabolites were analyzed by tandem MS fragmentation with a collision energy ramp of 10-50 eV. For quantitative analysis, the individual peak areas of target compounds were calculated, scaled to the peak area of internal standards, and fitted into a calibration curve via Quanlynx^{TM} (Waters).

3.3.3.4 Untargeted multivariate data analysis and marker characterization

The MarkerLynx™ software V4.2 (Waters) was utilized to examine chromatographic and spectral data. This process involved constructing a data matrix incorporating sample identities, ion characteristics (specifically retention time and m/z values), and ion abundance. This matrix was derived through a series of steps, including centroiding, deisotoping, filtering, and recognizing and integrating peaks. Ion intensities were quantified by normalizing single ion counts (SIC) against the total ion counts (TIC) observed across the entire chromatogram. Subsequently, the refined data matrix was imported into SIMCA™ software (version 13.0, Umetrics, Kinnelon, NJ). The data underwent Pareto scaling transformation before undergoing principal components analysis (PCA). Each metabolite's relative abundance was determined by scaling the total ion intensity to a fixed value of 10,000. The primary latent variables within the data matrix were illustrated using a scores scatter plot derived from the multivariate model. Metabolic changes induced by HSO feeding were pinpointed by examining ions that significantly contributed to the principal components and the delineation of sample groups, as observed in the loadings scatter plot. Chemical identities were ascertained through a combination of accurate mass measurement, elemental composition analysis, database searches (including HMDB www.hmdb.ca and LIPID MAPS www.lipidmaps.org), fragmentation processes, and comparisons with authentic standards when feasible.

3.3.4 Analysis of trypsin and elastase activity

Elastase activity was assessed via a colorimetric assay with modification.[312] In brief, the digesta was extracted by x10 volume of 50 mM Tris-HCl buffer with 0.1%

Tween-20, pH 8. Then 100 µL of the extracted supernatant or prepared elastase standard solution was incubated at 37°C with 15 µL of 2 mg/mL *N*-succinyl-L-alanyl-L-alanyl-L-alanine-*p*-nitroanalide (Suc-AAA-*p*NA) and 85 µL of 50 mM Tris-HCl buffer, pH 8, followed by a 30-min kinetic reading at 410 nm. The absorbance change between 0-30 minutes was used to calculate the elastase enzyme activity. One elastase unit cleaves 1 mmol of Suc-AAA-*p*NA per minute at 37°C, pH 8.

Trypsin activity was assessed via a colorimetric assay with modification.[313] In short, 25 µL of extracted supernatant or prepared trypsin standard solution was incubated at 37°C with 15 µL of 4 mg/mL *N*-α-benzoyl-DL-arginine-p-nitroanilide (BAPA) and 160 µL of 50 mM Tris-HCl buffer, pH 8, containing 20 mM $CaCl_2$. The reaction mixture proceeded to a 30-min kinetic reading at 410 nm. One trypsin unit cleaves 1 mmol of BAPA per minute at 37°C, pH 8.

3.3.5 In vitro digestion of oils and feeds

The experimental procedures for simulated *in-vitro* gastric and intestinal digestion of oils and feeds were adopted from an established protocol for smaller volumes.[314] The procedure started with simulated gastric digestion by mixing 125 mg feed or 15 µL of oil with 500 µL of prepared simulated gastric fluid (SGF, prepared according to established protocol[314]) and heated at 37°C with constant shaking on a thermomixer. At the end of the 1-hour incubation, 100 µL sample was withdrawn and quenched with 2 volumes of acetonitrile. The remaining mixture was adjusted to pH 7 with 1 M sodium hydroxide, then proceeded to simulated intestinal digestion by adding 1 volume of simulated intestine fluid containing porcine pancreatin and bile extract (SIF, prepared according to

established protocol[314]). After 1 hour incubation at 37°C, 100 µL sample mixture was withdrawn and quenched by adding 2 volumes of acetonitrile. The quenched sample mixtures were centrifuged at 13,000 ×g for 15 min. Each digestion was conducted in 5 replicates. The acquired supernatant proceeded to chemical derivatization and LC-MS analysis to quantify aldehydes and fatty acids.

3.3.6 Analysis of protein carbonyls (PC) in feeds and digesta

Because the free lipidic aldehydes in the sample matrix could result in an overestimation of PC content[315], the feed samples were washed with hexane prior to 2,4-dinitrophenylhydrazine (DNPH) assay. In brief, 2 grams of feed was mixed with 6 mL hexane and vortexed for 5 minutes. Then, the mixture was centrifuged at 13,000 ×g for 10 minutes. The liquid was discarded. This washing process was repeated for 3 times. The remaining solid residues were air-dried under a hood at room temperature to allow for the evaporation of any leftover hexane. After drying, 250 mg feed was mixed with 5 mL water. A tissue homogenizer was used to maximize the protein extraction. After sonicating for 1 hour, the mixture was centrifuged at 5,000 ×g for 15 min. The obtained aqueous fraction was filtered through a 0.2 µm syringe filter. Then the filtered protein extraction solution proceeded to DNPH assay, based on an established protocol with modifications.[316]

For reacting with DNPH, 100 µL of 10 mM DNPH (dissolved in 2M HCl) was added to 500 µL protein extraction solution and incubated at room temperature for 1 hour. For blanking, 100 µL of 2 M HCl was added into protein extracts without DNPH. Then 0.6 mL of 20% trichloroacetic acid (TCA) was added into the mixture. After

chilling on ice for 20 min, the mixture was centrifuged at 13,000 ×g for 10 min. The aqueous fraction was then removed. To remove excessive DNPH, the precipitated pellet was washed with 500 μL of ethanol:ethyl acetate (*v:v*) for 3 times. After the last wash, the pellet was dried in a fume hood for 1 hour and resuspended in 500 μL of 6 M guanidine (dissolved in 20 mM PBS pH 6.5). The final solution was then transferred to a UV-compatible 96-well plate for measuring the absorbance at 366 nm by a Spectra Max 250 96-well plate reader (Molecular Devices 577, Sunnyvale, CA).

3.3.7 Thiobarbituric acid-reactive substance (TBARS) assay

Oil and serum samples were submitted to TBARS assay, following an established protocol with modifications.[317] The reaction solution contained 15% w/v trichloroacetic acid, 0.375% w/v 2-thiobarbituric acid, and 0.25 N hydrochloric acid. Then, in a 2-mL screw cap centrifuge tube, 20 μL of serum was mixed with 200 μL of the reagent solution. For oil samples, 5 μL of oils were mixed with 15 μL water and 200 μL of the reaction solution. Each type of oil was measured in 4 replicates. The mixture was incubated in boiling water (>95°C) for 30 minutes. After chilling on ice, the mixtures were centrifuged at 13,000 ×g for 15 min. Then the supernatants were transferred to a 96-well plate for spectrophotometer measurement of absorbance at 532 nm. Standards were prepared by mixing 1,1,3,3,-tetramethoxypropane in water with concentrations ranging from 2.5 – 500 μM.

3.3.8 Statistical analysis

The statistical analysis on the quantity of metabolites, the relative abundance of compounds, and enzyme activities were conducted by unpaired t-test to compare CSO

and HSO groups via GraphPad Prism version 10.0.1 (La Jolla, CA). The difference was considered significant with a *p*-value <0.05 and a trend with a *p*-value between 0.05 and 0.1.

Pearson's correlation analysis between small intestine elastase activity, bile acids, and free amino acids was performed by GraphPad Prism 10. The correlation analysis leading to the correlation heatmap was conducted by R using the associate and heat functions from the package 'microbiome' (https://github.com/microbiome/microbiome/blob/master/R/heat.R).

3.4 RESULTS

3.4.1 Oxidative status of oils and feeds

The oxidation status of CSO and HSO was first evaluated by proximal analysis, including thiobarbituric acid reactive substances (TBARS), peroxide value (PV), *p*-anisidine value (AnV), and oxidized fatty acid percentage (OFA%). HSO was notably oxidized, marked by the increased PV (CSO vs. HSO, 0.8 vs. 3.9, mEq/kg), AnV (CSO vs. HSO, 1.81 vs. 466), OFA% (CSO vs. HSO, 0.92% vs. 6.9%), and TBARS **(Figure 3.1 A)**. Following the increase of AnV and TBARS, the lipidic aldehydes in the HSO oil and the feed extract were quantified **(Figure 3.1 B and C)**. In HSO, the most abundant aldehyde was 2,4-decadienal (DDE), making up more than 50% of the total aldehyde pool, followed by HNE **(Figure 3.1 B)**. In the HSO feed extract, the aldehyde profile differed from the HSO, with hexanal as the highest concentration **(Figure 3.1 C)**. The DNPH assay further indicated a significantly higher PC level in the HSO feed than CSO feed **(Figure 3.1 D)**.

3.4.2 Influences of HSO on animal growth and physiology

Nursery pigs in the HSO group had lower weight gain and less feed intake compared to the CSO group **(Figure 3.2 A and B)**. The HSO group also had a lower weight gain: feed intake ratio (G:F, **Figure 3.2 C**). The liver weight: body weight (LW:BW, %) ratio was greater in the HSO group, indicating hepatic hypertrophy **(Figure 3.2 D)**.

3.4.3 Influence of HSO consumption on the luminal metabolome

3.4.3.1 Characterizing the fatty acids and lipidic aldehydes in the GI lumen

Given the presence of abundant aldehyde species in oils and feeds, the digesta was analyzed for fatty acids and aldehydes. Notably, in the digesta, the CSO and HSO had greater differences in the stomach (S), duodenum (D), and jejunum (J) **(Figure 3.3 A)**. Then, the magnitude of the differences became smaller in the ileum, cecum, and colon, yet still clearly separated **(Figure 3.3A)**. To identify the metabolites contributing to the differences between CSO and HSO digesta samples, the orthogonal partial least squares discriminant analysis (OPLS-DA) was conducted. In the S-plot of the OPLS-DA model **(Figure 3.3B)**, the markers in the upper right corner were increased by HSO treatment, whereas the ones in the lower left corner were decreased by HSO treatment (hence higher in CSO). Through comparison with authentic standards, some of these metabolites were identified as aldehydes and fatty acids (metabolites i_D – v_D, listed in **Table 3.3**).

The five listed metabolites belonged to two classes: lipidic aldehydes and fatty acids **(Table 3.3)**. Metabolites iv_D and v_D were identified as hexanal and nonanal **(Table**

3.3). Given the great abundance of aldehydes in HSO oil and feed, the distribution of other lipidic aldehydes in the GI lumen, in addition to hexanal and nonanal, was further quantified. Compared to oil and feed, the aldehyde profile underwent further transformation in the GI lumen. In both CSO and HSO groups, hexanal, pentanal, and nonanal were the top 3 species making up more than half of the total aldehyde pool in all the GI lumen locations **(Figure 3.3 C)**. Meanwhile, the HSO group showed significantly higher aldehyde concentration in the jejunum, with an increased trend in the duodenum, cecum, and colon, but lacked statistical significance in the stomach and ileum **(Figure 3.3 C).** Since aldehydes were substantially present in the GI lumen, the luminal PC content was further determined to investigate potential interactions between aldehydes and protein-derived metabolites. For the DNPH assay, only digestas from the stomach, jejunum, cecum, and colon were examined due to limited quantity. Interestingly, HSO feeding only elevated the PC content in the cecum and colon, but not in the stomach or jejunum **(Figure 3.3 D)**.

Metabolites i_D – iii_D were caprylic acid (CA), oleic acid (OA), and linoleic acid (LA). Their concentrations were further quantified **(Figure 3.3 E – G)**. HSO feeding significantly decreased the concentration of OA and LA in the stomach **(Figure 3.3 F and G)**. The colon LA was also decreased by HSO, but not in any other GI locations **(Figure 3.3 G)**. On the contrary, caprylic acid (CA), a medium-chain fatty acid, was elevated significantly throughout all GI segments by HSO feeding **(Figure 3.3 E)**. Despite its low abundance in the GI lumen compared to the C18 fatty acids, the CA in the HSO group increased by up to 5-fold more than the CSO group **(Figure 3.3 E)**.

3.4.3.2 Characterizing the triglyceride species in the GI lumen and oils

Free fatty acids in the GI lumen primarily originate from the digestion of dietary triglycerides. To determine the sources of caprylic acid, lipidomic analysis on oils and the butanol extract of digesta from the stomach, jejunum, and colon. The differences between CSO and HSO groups were visualized via the principal component analysis (PCA) of digesta samples. In the scores plot of the PCA models, site-specific separations of digesta samples were observed. HSO feeding induced a clear shift in the triglyceride profile in the stomach and colon, but not in the jejunum **(Figure 3.4 A)**. The gastric and colonic lipidome were further compared in separate models. In the PCA model of the gastric lipidome, the clustering and separation of samples were driven by the dietary groups **(Figure 3.4 B)**. In an S-plot of a corresponding OPLS-DA model comparing the differences between CSO and HSO groups, the markers contributing to the separation were selected for structural analysis (I_G – VII_G in **Figure 3.4 C**). Their structures were identified via database search, tandem MSMS, and elemental composition analysis as five triglycerides, labeled as TG1 – 5 **(Table 3.4)**. The identification of the ion VI_G (TG4) and MSMS fragmentation is illustrated in **Figure 3.4 D**. Two groups of triglycerides were identified: hydroxyl and caprylic-acid-containing TG (TG-CA) in the form of ammonia and sodium adducts were increased by HSO **(Table 3.4, Figure 3.4 E - I)**. Since the stomach is the first site of lipid digestion after the oral cavity. The triglycerides in both oils and feeds were examined by lipidomic analysis. The results showed the separation of CSO and HSO and their respective feeds in the PCA models **(Figure 3.5 A and 3.5 E)**. The same triglycerides containing hydroxy-fatty acids and caprylic acid were detected in the HSO group but were absent in the CSO group **(Figure 3.5 A-H)**.

The separation of CSO and HSO groups in the colon lipidome was confirmed by the PCA modeling **(Figure 3.6 A)**. The metabolites elevated in the HSO group were identified in the S-plot of an OPLS-DA model **(Figure 3.6 B)**. These metabolites were present in the HSO group, but largely absent in the CSO group **(Figure 3.6 C – K)**. Elemental composition analysis, preliminary tandem MSMS analysis, and database search indicated the potential identities as cholesterol and sterol-related species **(Table 3.5),** as exemplified by the MSMS spectrum shown in **Figure 3.6 L**.

Caprylic acid is not a constituent of soybean oil. To elucidate the connections between the free caprylic acid in the GIT and the detected caprylic acid-containing TGs in the oil and GIT, the oils and feed were subjected to *in-vitro* digestion, simulating the digestion in the stomach and small intestine. In the simulated gastric digestion, HSO feed, but not the oil, yielded free CA. In the simulated intestinal digestion, both HSO feed and oil increased the free CA **(Figure 3.7 A and B)**. The concentration of 2,4-decadienal, the most abundant aldehyde in HSO oil, was also increased by the simulated gastric and intestinal digestion of HSO and HSO feeds in the HSO group compared to the CSO group **(Figure 3.7 C and D)**.

3.4.4 Influences of HSO on the metabolic events inside the GI lumen

3.4.4.1 Influence of HSO consumption on the proteolytic function in the GIT

Protein digestion in the GIT is essential for supplying the essential amino acids for growth. The proteolytic activity in the GIT was hence investigated **(Figure 3.8)**.

The quantification of the free amino acids in the GI lumen showed that HSO significantly decreased the concentration of free amino acids (FAAs) in the small intestine, but lacked influence on the FAAs in the stomach and large intestine **(Figure 3.8 A)**. Examing of the relative abundance of lysine and methionine, two essential amino acids important for nursery pigs' growth, showed that HSO decreased lysine in the duodenum and cecum and methionine in the ileum and cecum **(Figure 3.8 B and C)**. Additionally, both dietary groups had comparable nitrogen content in the stomach and ileum (data not shown), and the HSO might negatively impact the proteolytic activities in the small intestine. To further validate this hypothesis, the activities of trypsin and elastase, two proteolytic enzymes in the small intestine, were determined using the digesta from the duodenum, jejunum, and ileum. The results showed that trypsin activity remained comparable between the two groups **(Figure 3.8 D)**, but the elastase activity was reduced **(Figure 3.8 E)**.

Effective digestion of protein is essential for the intake of essential amino acids for nursery pigs. The correlation analysis between the elastase activity and free amino acid level in the small intestine showed a significant positive correlation **(Figure 3.8 F)**. Soy isoflavones are known inhibitors of elastase.[318] Hence, the concentration of major soy isoflavones in the digesta was quantified, since the feed was formulated with soybean meal. However, the distribution of daidzin and genistin, and their respective aglycones, daidzein, and genistein, were comparable digesta of CSO and HSO groups (data not shown). To determine whether free aldehydes could contribute to the decrease in elastase activity, *in-vitro* co-incubations of porcine elastase was performed, showing that the

porcine elastase activity was not impacted by DDE or the stomach digesta from HSO group (data not shown).

3.4.4.2 Influence of HSO consumption on the bile acid metabolism

Besides facilitating the transportation and absorption of lipids in the small intestine and interacting with microbial metabolism in the large intestine, bile acids assist in the digestion of protein in the small intestine.[319] The bile acid concentrations from the duodenum to the colon were hence determined **(Figure 3.9 A)**. HSO feeding reduced the total bile acid level in the duodenum, jejunum, and cecum **(Figure 3.9 A).** The ratio of secondary to primary bile acid, which indicates the microbial transformation of primary to secondary bile acids, remained comparable between the two groups **(Figure 3.9 B)**. The Pearson's correlation analysis indicated a significant positive correlation between the total bile acid and amino acid levels in the small intestine **(Figure 3.9 C)**.

Bile acids are produced in the liver and stored in the gallbladder. To determine the cause of decreased bile acids in digesta, the concentrations of bile salts in the gallbladder were further quantified. The total bile salts in the gallbladder were decreased in the HSO group **(Figure 3.9 D)** due to the decrease of GHDCA, GCDCA, TCDCA, and TUDCA **(Figure 3.9 E)**.

3.4.4.3 Influence of HSO consumption on the gut microbial metabolism

Short-chain fatty acids (SCFA) are the hallmarks of gut microbial metabolism. The concentration of five SCFAs was quantified in the cecum and colon **(Figure 3.10)**. HSO decreased the concentration of propionic acid **(Figure 3.10 B),** butyric acid **(Figure 3.10 C),** and isovaleric acid **(Figure 3.10 E)**, but lacked impact on acetic acid **(Figure**

3.10 A) and valeric acid **(Figure 3.10 D)**. The total SCFA in the cecum and colon was also reduced by HSO feeding **(Figure 3.10 F)**.

3.4.5 Influence of HSO on the post-absorptive metabolism

As the potential consequences of HSO-elicited changes in the luminal metabolome, changes in the hepatic metabolome were investigated. The analysis of the aqueous fraction of the liver extract showed a clear separation between the CSO and HSO groups in the scores plot of a PCA model **(Figure 3.11 A)**. The markers contributing to the separation of CSO and HSO groups were further identified from an S-plot of an OPLS-DA model **(Figure 3.11 B)**. In addition, as the key antioxidants, the concentration of hepatic glutathiones was quantified. Notably, the reduced glutathione (GSH), oxidized glutathione (GSSG), and GSH/GSSG ratio were comparable between the two groups **(Figure 3.11 C – E)**. HSO feeding decreased the concentrations of choline, phosphocholine (PhosC), and glycerophosphocholine (GPC) **(Figure 3.11 F – H)**, but increased the concentrations of NAD^+ and adenosine monophosphate (AMP) **(Figure 3.11 I and J)**.

Because the proteolytic activity in the GI lumen was negatively impacted by HSO feeding **(Figure 3.8)**, the potential influence on the post-absorption amino acid homeostasis was investigated by quantifying the free amino acids (FAAs) in the liver, serum, and muscle **(Table 3.6)**. HSO reduced the concentrations of alanine, valine, proline, and tryptophan concentrations in the liver, but decreased their concentrations in the serum and muscle. The liver and serum also exhibited opposite trends in the concentrations of phenylalanine, asparagine, aspartate, arginine, and total amino acids.

The correlations of HSO feeding induced substantial changes in the digesta with impaired growth performance, and the hepatic metabolome of nursery pigs was analyzed. The Pearson's correlation coefficient was calculated and visualized in heatmaps **(Figure 3.12)**. The correlation between the growth performance indices and the luminal metabolites could be categorized into two major categories: A1 and A2 **(Figure 3.12 A)**. The metabolites in the A1 cluster showed significant positive correlations with ADFI, ADG, and G:F ratio **(Figure 3.12 A)**, including duodenum elastase activity, gastric oleic and linoleic acids, total free amino acids in the small intestine, and the cecum SCFAs. At the same time, significant negative correlations were identified with gastric oxidized triglycerides, jejunum, and colon aldehydes, as well as the caprylic acid in the entire GI lumen.

The correlation analysis between the luminal metabolites and the post-absorption metabolites **(Figure 3.12 B)** showed that luminal aldehyde, caprylic acid, TG-OH, and TG-CA positively were correlated with hepatic FAA, AMP, and NAD^+, and negatively correlated with choline metabolites and serum FAA. The B2 group metabolites, including the SCFAs, bile acids, and C18 fatty acids in the stomach, exhibited trends opposite to those of the B1 group. The B3 group metabolites and markers, which are associated with the proteolytic activity in the small intestine, overall lacked significant correlation with post-absorption metabolites.

3.5 DISCUSSION

To our knowledge, this is the first attempt to characterize and track the fates of lipidic aldehydes and their metabolic impacts in the luminal metabolome after feeding fed

thermally oxidized oil, as summarized in **Figure 3.13**. The GIT is the first line of contact with the HSO and the dietary aldehydes. The intake of lipidic aldehydes from HSO was considered a significant contributor to HSO-induced adverse metabolic events in animals.[168] However, the distribution of aldehydes and their interaction with other nutrients and functional metabolites in the GI lumen has not been fully characterized. In the current feeding trial, the HSO feeding introduced a substantial quantity of lipidic aldehydes into the GIT **(Figure 3.3)**, compromised intestinal protein digestion **(Figure 3.8)** and animal growth **(Figure 3.2)**. Additionally, the *de-novo* formation of aldehydes occurred in the GI lumen **(Figure 3.13)** from the decomposition of pre-existing and newly formed oxidized lipids. The lipidomic analysis additionally revealed caprylic acid and the caprylic acid containing TGs as potential and potent indicators that can connect the oil's oxidation status to animal health. The influence and contribution of HSO feeding to nutrient digestion, metabolism, and host health are discussed below.

3.5.1 The lipidic aldehyde profile exhibited a significant shift when comparing oil to feed extract

Aldehydes are secondary lipid oxidation products, and exhibited significant and inverse correlation with the growth performance of production animals fed thermally oxidized oils.[102] The TBARS assay and the LC-MS analysis confirmed the substantial amount of aldehydic content in HSO **(Figure 3.1 A and B)**. The profile of lipid aldehydes underwent a notable shift from oil to feed **(Figure 3.1 C)**. In HSO, the most abundant species was 2,4-decadienal (DDE), followed by 4-hydroxynonenal (HNE). This finding was consistent with a previous report from our lab.[66] DDE and HNE are the oxidative products of linoleic acid, accounting for over half of the fatty acid pool of

soybean oil.[320] However, in the feed, hexanal was the most abundant species, comprising more than half of the free aldehyde pool **(Figure 3.1 C)**, with DDE only accounted for 13% in the feed (data modified from **Figure 3.1 C**).

One plausible explanation for the shift in the aldehyde profile is the continuous degradation of DDE. During thermal oxidation, LA is first oxidized to its hydroperoxides (LA-OOH)[107], which further decomposes to hexanal (15%), and DDE (14%).[321] As a highly reactive α,β-unsaturated aldehyde, DDE can further decompose to hexanal[322], since an exponential decrease of DDE and increased hexanal co-occurred in oils continuously heated at 200 °C were observed.[124] Therefore, the thermal processing in the production of swine feeds might potentially promote the transformation of DDE to hexanal. Besides DDE, hexanal could derive from the thermal degradation of 2-octenal[124], a C8 aldehyde that was decreased from 4.5% in HSO to 0.7% in HSO feed.

The change of the aldehyde profile in the feed would also be attributed to the reactivity of aldehyde towards amino acids. Lipidic α,β-unsaturated aldehydes can form carbonyl adducts with amino acids.[45,173] In the present study, the HSO feed had higher PC levels than the CSO feed **(Figure 3.1 D)**, indicating the adduct formation in the feed matrix. Since hexanal, a saturated aldehyde, is less reactive than DDE, an α,β-unsaturated aldehyde, it is likely that more hexanal remained in the feed **(Figure 3.1 C)**.

3.5.2 De-novo formation of aldehydes in the GI lumen

Compared to the oil and feed extract, the lipidic aldehyde composition in the GIT underwent more changes. The hexanal remained as the most abundant aldehyde in the GI lumen **(Figure 3.3 C)**. Together with nonanal and pentanal, these three species made up

more than 75% of the total aldehyde pool in the digesta of the HSO group **(Figure 3.3 C)**. These three aldehydes were also detected at ample concentrations in the GIT of the CSO group **(Figure 3.3 C)**. Since comparable PC values were observed between the two feeding groups in the gastric and jejunal digesta **(Figure 3.3 D)**, the changes in the aldehyde profile in the GI lumen could be attributed to the *de-novo* formation.

The potential precursors for the *de-novo* formation of aldehydes are the oxidized triglycerides (TG-OXs) in the HSO, a constituent in thermally oxidized vegetable oils.[280,323] These TG-OX species contain one or more oxygenated functional groups, including epoxyl, hydroxyl, hydroperoxyl, and ketone groups.[280,323] In the present study, hydroxylated triglyceride (TG-OH) was detected in the HSO, HSO feed **(Figure 3.5)**, and gastric digesta **(Figure 3.4)**. TG-OHs can further decompose to secondary LOPs, such as aldehydes, in heated oils.[280] Furthermore, the *in-vivo* study showed that the hydroxylated linoleic acid (LA-OH) could decompose and produce hexanal in the stomach of rats dosed with LA-OH.[50]

Another potential precursors for the *de-novo* formation of aldehydes are the aldehyde-containing TGs in thermally oxidized oils.[280] These species are also known as the glycerol-core aldehydes (GCAs). However, the current analysis of the oils did not detect their presence. Further modification and optimization of the chromatographic workflow might be needed to fully characterize the TG-OXs in the HSO, feed, and digesta.

Besides the pre-existence in the HSO, the precursors for the *de-novo* formation of aldehydes could be produced locally.[69] The highly acidic environment and availability of

oxygen in the stomach can promote lipid peroxidation.[68] Linoleic acid could be oxidized to LA-OOH in the stomach[6,25,26], which can be reduced to hydroxide through a glutathione-dependent pathway in the gastric mucosa.[224] Additionally, two studies by Kanazawa et al. demonstrated the enzymatic-independent decomposition of ingested TG-OXs to aldehydes in the stomach.[50,71] The orally dosed LA-OOH was found to transform into hydroxides and epoxyketones in the stomach.[50] Hence, the *de-novo* formation of TG-OOH could further contribute to the observed TG-OH pool in the stomach. These observations may also explain the presence of aldehydes in the digesta of CSO group pigs **(Figure 3.3 C)**. Nevertheless, more studies are needed to examine the underlying events behind the *de-novo* formation of aldehyde in the GIT.

3.5.3 Caprylic acid as a predictor for the oxidation status of heated oil

The oxidation status of heated oils is typically assessed by PV, TBARS, *p*-anisidine values, etc. Yet, these indices have their own limitations due to their chemical natures and may not accurately reflect the quality of extensively oxidized oils.[102] For example, free aldehydes are reactive and volatile, making them susceptible to further degradation during processing[124], as shown by the increase of hexanal levels in fried foods stored at room temperature.[324] Similarly, concerns have been raised on the reliability of *p*-anisidine value in the prediction of feeding heated oil to production animals.[130] This study identified caprylic acid (C8:0) as an alternative predictor for oil quality and animal growth.

Caprylic acid, a saturated medium-chain fatty acid, is not a main constituent of soybean oil.[325] Therefore, the caprylic-acid-containing triglycerides (TG-CA) should be

considered as LOPs, as they were detected in the oil, feed extract, and digesta of the HSO group, but not the CSO group **(Figure 3.4 and 3.5**). Interestingly, free caprylic acid concentrations were consistently higher across all GI locations in the HSO group. **(Figure 3.3 E)**. Meanwhile, medium-chain fatty acids (MCFA) like caprylic acid are generally absorbed faster than long-chain fatty acids due to their direct incorporation into the portal circulation..[326] Additionally, the ratio of CA to DDE in the GIT remained comparable between CSO and HSO groups (data not shown). Therefore, the caprylic acid detected in the GIT likely resulted from the continuous hydrolysis of TG-CA species originating from the HSO **(Figure 3.3 E)**.

Structurally, caprylic acid is a known degradation product of the 9-hydroperoxides of oxidized fatty acids, including OA, LA, and LnA.[327,328] The decomposition of the 9-hydroperoxide of LA additionally yields a 2,4-decadienal simultaneously.[328] This is consistent with the findings from the *in-vitro* digestion of oils and feeds, which showed similar distribution patterns of caprylic acid and DDE **(Figure 3.7)**.

Compared to highly volatile and reactive aldehydes, caprylic acid is more stable and potentially a more reliable quality marker than *p*-anisidine value, especially for extensively oxidized oils. The concentration of caprylic acid in the heated soybean oil showed significant positive correlations with the non-volatile LOPs, including the total polar content, polymerized TG, oxidized TZ, epoxy, keto, and hydroxy acids.[213] The co-occurrence of the caprylic acid to unsaturated fatty acid ratio and the increased oxidation of soybean oils have also been observed.[329] Established methods for profiling fatty acids

in oils, such as gas chromatography after derivatization to fatty acid methyl esters, make it feasible to quantify caprylic acid in oxidized oils.[325] Furthermore, the application of caprylic acid as an oxidation indicator could extend to other oils, as it is not a natural fatty acid in many vegetable oils.[325] However, additional heated oil samples and animal feeding trials are necessary to validate the correlation between caprylic acid concentrations, oil oxidation status, and animal growth performance.

3.5.4 HSO consumption interfered with the proteolytic activity in the GI lumen

Proteolytic enzymes are crucial for digesting dietary proteins into peptides and amino acids in the gastrointestinal tract (GIT) of pigs. These enzymes, secreted by the pancreas as inactive proenzymes, play an essential role in the growth of young weaning piglets. Trypsin is activated from trypsinogen by enteropeptidase and subsequently activates elastase from proelastase.[330] The adequate secretion of these pancreatic enzymes plays an important role in pigs' growth, especially for the young weaning piglets.[331] Supplementation of the pancreatic enzymes in the diet has been shown to enhance growth performance[332], whereas enzyme insufficiency can impair nutrient utilization and growth.[333]

Pancreatic trypsin and elastase are both serine proteases, containing serine in their catalytic triads.[334] To initiate the proteolytic process, serine functions as a nucleophile, activating the carbonyl site of the peptidyl substrates and forming a high-energy transitional state tetrahedral intermediate that facilitates substrate cleavage.[334] Due to the nucleophilic nature, serine may bond with aldehydes, which are electrophilic. The formed analog tetrahedral intermediate blocks the active site from interacting with the substrates,

hence inhibiting enzyme activities. Some peptidyl aldehydes function as serine protease inhibitors based on such principles, such as leupeptin.[335] Since HSO feeding decreased elastase activity in the small intestine, we explored the potential contribution of aldehydes in this observation. However, co-incubation of elastase with DDE, the predominant aldehyde in HSO, did not reveal any inhibitory effects (data not shown). Trypsin activity also remained unaffected by DDE. Therefore, the role of aldehydes in inhibiting trypsin or elastase activity in the GIT remains inconclusive.

Elastase is a marker of pancreatic health due to its resistance to intestinal and bacterial degradation.[336] Low fecal elastase levels (<200 μg/g stool) are indicative of exocrine pancreatic insufficiency (EPI) in humans.[337] Although fecal samples were not collected from the pigs in the current feeding trial, the absence of differences in free fatty acid levels in the jejunum between CSO and HSO groups suggested normal lipolytic and pancreatic exocrine function **(Figure 3.3 F and G)**. Additionally, soybean isoflavones, known inhibitors of trypsin activity, did not differ between dietary groups, nor did they impact trypsin or elastase activity in co-incubation studies (data not shown). The cause and the molecular mechanism of the inhibitory effect on proteolytic enzymes need more study.

In the small intestine, the elastase activity showed a significant correlation with total free amino acid (FAA) concentration **(Figure 3.8 F)**, indicating that decreased elastase activity contributed to reduced FAA levels in the small intestine of HSO-fed pigs **(Figure 3.8 A)**. Another plausible contributing factor was the reduced total bile acids in the small intestine **(Figure 3.9 A)**, where it showed a positive correlation with total free

amino acids **(Figure 3.9 C)**. The primary function of bile acid is to promote lipid digestion and absorption. A less-known function of bile acid is to aid in protein digestion.[319,338] *In-vitro*, bile acids facilitate the protein unfolding and expedite the hydrolysis of proteins by pancreatic proteases.[319,339] Yet the *in-vivo* molecular mechanism is not fully understood. In the current study, the combined reduction in elastase activity and bile acids likely impaired dietary protein digestion, potentially contributing to the decreased growth performance observed in HSO-fed pigs.

Protein is essential to the growth and health of nursery pigs. The decreased intestinal proteolytic activity may further explain the decreased ADG and G:F ratio in the current trial **(Figure 3.3)**. Decreased nutrient digestibility was observed in animals consuming oxidized oil.[101,340] In a meta-analysis, decreased G:F was observed in 17 out of the total 65 studies examined, but 48 out of 65 studies observed no difference.[105] The underlying biochemical mechanisms contributing to the variations in the G:F of animals, therefore, need more investigation.[103]

3.5.5 Bile acid and choline metabolism were affected by HSO feeding

Overall, HSO feeding decreased the total bile acid concentration in the duodenum, jejunum, and cecum **(Figure 3.9 A)**. As discussed above, in the small intestine, bile acid concentration likely affected the amino acid digestion **(Figure 3.9 C)**; whereas in the lower GI, the microbial metabolism of bile acid was indifferent between the two groups **(Figure 3.9 B)**.

For pigs, bile acids are synthesized in the liver, starting from the hydroxylation of cholesterol by cholesterol 7α-hydroxylase (CYP7A1), the rate-limiting step in the bile

acid biosynthesis pathway.[341] CYP7A1 activity is transcriptionally regulated by the farnesoid X receptor (FXR), which, upon activation, inhibits hepatic bile acid uptake and promotes bile acid efflux into the gallbladder.[342,343] FXR upregulation in the HSO group likely reduced hepatic bile acid synthesis, resulting in decreased bile salts in the gallbladder **(Figure 3.9D)** and lower bile acid levels in the GI lumen **(Figure 3.9A)**.

FXR activation also upregulates PPARα, promoting fatty acid β-oxidation.[344] But in a previous study, the PPARα was thought to be activated by binding with dietary oxidized fatty acids, which are known PPAR ligands.[168] Such a shift in fatty acid metabolism was considered a contributor to the decreased serum total triglyceride and has been reported in animals consuming oxidized lipids.[168,345] PPARα activation additionally down-regulates the transporters responsible for hepatic BA uptake and efflux.[346] Therefore, the reduction of BA in the GI lumen and gallbladder could be a joined effect from the FXR and PPARα activation. Nevertheless, the interplay between bile acid metabolism, FXR activation, and the host metabolism in the current study warrants further study.

The reduction in available bile acid in the GIT was likely connected to the reduced total bile salts in the gallbladder **(Figure 3.9 D)**. The gallbladder bile acid pool was attributed mostly to the decreased GHDCA, GCDCA, TCDCA, and TUDCA **(Figure 3.9 E)**. GHDCA is a member of the hyocholic acid (HCA) family. The HCA species are of health benefits, known for their association with resistance to type 2 diabetes.[347] Consumption of oxidized oil is known to impair glucose metabolism and increase insulin resistance.[348,349] In the current study, Although glucose homeostasis was not investigated, other HCA species (HCA and HDCA) were reduced in the GI lumen

(Figure 3.9 A). Meanwhile, the proportion of GHDCA, on the contrary, increased in the HSO group (data modified from **Figure 3.9 E**). However, the proportion of GHDCA in the GI lumen was indifferent (data modified from **Figure 3.9 A**). Such findings suggest that the GHDCA reduction was more likely attributed to the decrease of the total bile acids. Nevertheless, the connections between HSO-induced alteration in the HCA species and glucose homeostasis warrant further study.

T/G-CDCA are produced from deoxy-HCA (DHCA), an intermediate in the hepatic BA synthesis pathway.[350] DCHA can be produced from several different routes of cholesterol hydroxylation, via CYP7A1, sterol 27-hydroxylase (CYP27A1), sterol 25-hydroxylase, and sterol 24-hydroxylase (CYP46A1).[350] The proportion of T/G-CDCA in the gallbladder decreased in the HSO group (data modified from Figure 3.9 E), suggesting their decrease was likely attributed to the reduction in total BA availability and their synthesis or downstream metabolic pathways. TUDCA, an FXR antagonist[347] and a therapeutic agent for treating cholestatic liver disease[351], is synthesized from conjugating taurine to UDCA. In the duodenum and cecum, the concentration of UDCA was reduced in the HSO group **(Figure 3.9 A)**. In the liver, taurine concentration was decreased in the HSO group **(Table 3.6)**. Although serum methionine, a taurine precursor, was decreased, liver methionine levels were unaffected **(Table 3.6)**. Comparable hepatic glutathione (GSH) and its oxidized product (GSSG) between groups indicated that the taurine synthesis pathway was maintained **(Figure 3.11)**. Study on animal model of endogenous taurine synthesizing ability had reported that depletion of dietary taurine decreased the ratio of taurine-conjugated BAs significantly while increased that of unconjugated species.[352] However, the ratio of taurine-conjugated to

total bile acids in the gallbladder and GI lumen was unchanged, suggesting that HSO feeding influenced systemic methionine homeostasis to sustain hepatic taurine production (data modified from **Figure 3.9**). Further study is needed to elucidate these mechanisms and their metabolic consequences.

Microbial metabolism is another important component of bile acid metabolism. In the current study, the secondary to primary BA ratio was comparable throughout the GIT **(Figure 3.9 B)**. However, the observed reduction in luminal and gallbladder bile acids may correlate with gut microbiome changes beyond secondary bile acid synthesis. Unique metabolites enriched in the HSO group **(Figure 3.6, Table 3.5)** likely represent bile acid-fatty acid (BA-FA) conjugates. The most known BA-FA conjugates are synthetic pharmacological agents with cholesterol-lowering, triglyceride-lowering, and gallstone-preventing effects.[353,354] In the stools of health subjects, the BA-FA conjugates were detected and identified as predominantly C16- and C18-FA-linked isodeoxycholic acid and isolithocholic acids. Moreover, these compounds were absent in the bile, serum, and urine, hence suggesting a gut microbial origin.[355] Yeast lipase had been shown to esterify C12-16 FA to BAs.[356] However, their *in-vivo* biosynthesis schemes and contribution to host metabolism have not been fully elucidated, but they might contribute to the decreased luminal bile acids in the HSO group.

Correlation analysis revealed a significant positive relationship between jejunal bile acids and hepatic choline levels **(Figure 3.12 B)**. Choline and phosphocholine are precursors for phosphatidylcholine, a crucial component of cell membranes and lipoproteins. Phosphatidylcholine is essential for hepatic very low-density lipoprotein

(VLDL) production, which transports triglycerides and cholesterol esters.[357] Choline deficiency can lead to non-alcoholic fatty liver disease by impairing triglyceride export via VLDL.[358] Additionally, phosphatidylcholine could comprise up to 40% of the organic content in bile.[359] Consumption of oxidized oil had varying impacts on VLDL cholesterol, with both increased trend[360,361] and indifference[169] reported. In addition, increased serum total cholesterol (TC), HDL-cholesterol (HDL-C)[169], and LDL-cholesterol (LDL-C)[345] have been observed as well, which could be atherogenic.[345] As oxidized oil consumption has shown to reduce hepatic triglyceride concentration[168], the decrease of hepatic choline in the current study hence likely disrupted cholesterol homeostatis.

Considering the findings from the present study, HSO consumption likely disrupted the choline, cholesterol, and bile acid homeostasis. More investigation is needed to reveal the underlying mechanism and its influence on host health.

3.5.6 Gut microbial metabolism was affected by HSO

Microbial dysbiosis was associated with undesirable health effects, such as redox imbalance, intestinal barrier impairment, and inflammation.[100] Consumption of thermally processed oils and fats has been shown to influence animals' gut microbiota.[99,100,252-255] However, the molecular mechanism of oxidized oil exerted microbial dysbiosis has not been fully elucidated. Short-chain fatty acids (SCFA) are characteristic metabolites of gut microbial metabolism. In the current trial, the HSO feeding selectively decreased the production of propionic acid and butyric acid **(Figure 3.10 B and C)**.

Inhibitory effects on butyrate were observed in hamsters fed oxidized corn oil[253], nursery pigs fed oxidized soybean oil[99,100], and rats chronically fed oxidized palm oil[254]. These studies also reported reduced abundance of butyrate-producing bacteria species, such as *Paraprevotella*, *Garnesiella,* and *Provotella* of the Bacteroidota phylum[100,252,253], *Parasutterella* of the Pseudomonadota phylum[253], and *Butyrivibrio* of the Bacillota phylum[254]. Nonetheless, discrepancies exist. For instance, For instance, oxidized perilla and sunflower oil did not affect butyric acid or total SCFA levels in rats.[255] Additionally, the impact of oxidized oil feeding on propionic acid varied: a dramatic reduction by more than 50% was observed in hamsters fed oxidized corn oil.[253] Oxidized palm, canola, perilla, and sunflower oil did not alter the fecal propionic acid concentration of rats.[254,255] In pig-feeding studies, the colonic propionic acid level remained comparable in the oxidized soybean oil group.[99,100] In general, acetic and valeric acid were not influenced by oxidized oil feedings.[99,100,252-255]

The varying results could be due to differences in the oxidation status of the oils used. The peroxide values of the oxidized corn[253], lard[253], and soybean oil[100] used in above mentioned animal studies were significantly higher (33.15[253], 12.51[253], and 88.5 mEq peroxide/kg respectively than the HSO in the current trial (3.9 meq). During thermal processing of soybean oil, PV increased rapidly to >200 mEq peroxide/kg when heated from 22°C to 185°C within 1 hour, but then dropped and plateaued at about 50 mEq peroxide/kg with prolonged heating of 6 hours.[66] Furthermore, these studies did not account for *p*-Anisidine values or lipidic aldehyde content, leaving the mechanism of oxidized oil effects on the gut microbiome inconclusive.

Our data showed that HSO feeding significantly increased free aldehydes, protein carbonylation, and caprylic acid levels in the colon **(Figure 3.3 C, D, E)**. Hexanal and caprylic acid are potential modulators of the gut microbiome. Total free aldehyde concentration showed a significant inverse correlation with total SCFA concentration in the colon (data not shown, *p*-value = 0.007). Additionally, colonic PC level showed a trend to correlate with total SCFA (data not shown, *p*-value = 0.06). Hexanal, one of the most abundant aldehydes in the HSO group **(Figure 3.3 C)**, negatively correlated with colonic SCFA (data not shown, *p*-value = 0.01). As a natural flavor compound in fruits and vegetables, hexanal has antimicrobial activity and protects food against spoilage.[362] *In-vitro*, it exerts a bactericidal effect by altering the fatty acid composition of the cytoplasmic membrane[362], and hence increasing the membrane permeability.[363] This suggests that hexanal selectively inhibits gut microbiota, contributing to decreased SCFA and microbial dysbiosis. The *in-vivo* mechanisms, however, require further study.

Caprylic acid, known for its antimicrobial properties[364], was another potential modulator. Unfortunately, its concentration in oxidized oils was not reported in the aforementioned animal studies. Meanwhile, colonic caprylic acid did not show significant correlation with total SCFA (data not shown, *p*-value > 0.1), indicating that the impact of caprylic acid concentration on microbial metabolism needs further validation.

3.5.7 Post-absorptive amino acid homeostasis was substantially altered by HSO feeding

In the post-absorption system, the amino acid homeostasis between the liver and serum was significantly skewed, with an apparent increase of most FAAs in the liver, and a decrease in the serum **(Figure 3.13, Table 3.6)**.

The decreased serum tryptophan and increased liver NAD^+ **(Table 3.6, Figure 3.11)** can be explained by the heightened need for NAD^+ synthesis in animals fed oxidized oils, which is a known hallmark in animals fed oxidized oils.[130,168] Yet, interestingly, the hepatic tryptophan increased **(Table 3.6)**, contrary to other studies where it was unaffected by oxidized oil consumption.[130] Such variation could be due to differences in oil quality and the extent of oxidation. The HSO oil in the current study had a dramatically increased AnV, exceeding the reported AnV of 138 in the oxidized corn oil used by Guo et al.[130] This severe oxidation likely impaired growth **(Figure 3.2 A-C),** suggesting a heightened need for tryptophan catabolism for NAD^+ production and hence requiring for more tryptophan in the liver. Yet, the changes in hepatic tryptophan transportation were not examined in the present trial.

Besides tryptophan, oxidized oil consumption could influence the metabolism of other amino acids.[130,168] Similar trends were observed in this trial, including decreased serum alanine and glutamate, and increased hepatic proline, citrulline, and histidine **(Table 3.6)**. As discussed by Guo et al., Guo et al. suggested that the decrease of serum alanine and glutamate could result from PPARα activation, which represses glucose utilization and glycolysis.[130] In contrast to the findings by Guo et al., in the current trial,

liver alanine was increased, whereas glutamate was indifferent, warranting for more investigation into the molecular mechanisms.

The increased hepatic proline, a proteogenic amino acid, was thought to be associated with tryptophan-NAD^+ pathway activation, as the NAD^+ feeds into NADPH, a key cofactor for proline biosynthesis[168] The metabolism of citrulline is tied with arginine and ornithine in the urea cycle.[365] In this study, the HSO group had higher hepatic citrulline and ornithine but lower arginine concentrations than the CSO group **(Table 3.6)**. This could indicate an expedited urea cycle in the HSO group, where arginine was metabolized by arginase (*ARG*) to urea and ornithine, which is then converted to citrulline by ornithine transcarboxylase (*OTC*).[366] However, the enzyme activity and its implications for host health need further exploration. Elevated serum citrulline levels are associated with muscle mass loss in aging populations.[367] Given the impaired protein digestion and growth in the HSO group, it is plausible that muscle loss was increased compared to the CSO group, but this requires further investigation.

In addition to the above-mentioned events, the hepatic PPARα activation likely contributed to the increased hepatic FAAs and decreased serum FAAs. The hepatic PPARα extensively influences amino acid metabolism, down-regulating hepatic amino acid catabolism, such as transamination and deamination.[368] The peroxisome contains many enzymes carrying out diverse biological activities.[369] PPARα activation, associated with peroxisome proliferation, potentially increases the need for protein synthesis and enzyme production in the liver to handle HSO-induced metabolic challenges, resulting in increased FAAs in the liver.

3.5.8 Correlation of luminal to animal growth and post-absorptive metabolism

The GIT plays an essential role in the digestion and absorption of nutrients needed for animal health and growth. Considering the drastic influence on the growth of HSO-fed pigs, correlation analysis was conducted to investigate the potential contribution of changes in the luminal metabolome to host health. In the correlation coefficient heatmaps **(Figure 3.12)**, the C8:0 concentration in the GIT exhibited a substantial correlation with the growth performance and the post-absorptive metabolites.

As discussed above, caprylic acid can potentially reflect the oils' oxidation status. It showed significant positive correlations with hepatic free amino acids, AMP, and NAD^+, and negative correlations with choline metabolites, serum free amino acids, ADG, and G:F ratio. Hence, dietary caprylic acid is not only indicative of oil oxidation status but also shows potential associations with post-absorptive metabolism and overall host health. These findings support the proposed utilization of caprylic acid as a predictor for oil oxidation status in animals fed oxidized oil. Additionally, the TG-CA, and TG-OH in the stomach showed a similar pattern to the caprylic acid, further emphasizing the interconnections among these lipid oxidation products and their association with host health. Moreover, the luminal caprylic acid was the only luminal metabolite that showed a significant and negative correlation to the hepatic GPC **(Figure 3.12 B)**.

Aldehydes were previously thought as the major contributor to the adverse metabolic effects in animals fed oxidized oils, and this is supported by the findings from the current study. The luminal aldehydes showed significant inverse correlations to the growth performance indices and hepatic AMP and NAD^+, as well as a negative

correlation to serum FAAs **(Figure 3.12 B)**. However, the extent to which pre-existing and de-novo formed aldehydes contributed to the HSO-elicited impacts on host health remains unresolved.

Meanwhile, as expected, the amino acid concentrations in the small intestine had robust correlations with animal growth, including ADG and G:F ratio **(Figure 3.12)**. One potential interpretation is that HSO feeding reduced feed conversion efficiency in nursery pigs and adversely affected protein digestion. About 65 – 76% of production cost is spent on feeds. The impaired feed conversion efficiency potentially poses a significant challenge to the production animal industry.[370] Therefore, identifying a more reliable and accurate quality indicator of oxidized oil could potentially benefit the industry.

3.6 CONCLUSION

In conclusion, the study demonstrated that HSO significantly impair the growth performance of nursery pigs. Analysis of the luminal metabolism revealed HSO-elicited alterations in the GI, including reduced digestion of amino acids, reduced bile acid concentration, and shifts in gut microbial metabolism. These changes were closely correlated with animal growth and systematic metabolism. Further examination of the hepatic metabolome suggested substantial changes in cholesterol and amino acid homeostasis. Additionally, correlation analysis identified dietary caprylic acid as a promising marker for predicting the oxidation status of oils and associated animal growth performance. However, the precise role of aldehydes in these metabolic disturbances remains unresolved. Further research is required to elucidate the mechanisms behind the *de-novo* aldehyde formation and to distinguish their effects from pre-existing dietary

aldehydes in HSO. Understanding these processes will be crucial for developing strategies to mitigate the adverse effects of oxidized oils on animal health and growth.

Acknowledgment: This research was supported, in part, by the NIFA project MIN-18-125.

3.7 TABLES AND FIGURES

Table 3.1 Reagents and chemicals used for sample preparation, LC-MS analysis, quantification, and biochemical assays.

Chemical/Reagents	Vendor
Acetone (LC-MS grade), Acetonitrile (LC-MS grade, ACN), Ammonium formate, Calcium chloride ($CaCl_2$), Dichloromethane (GC grade), Formic acid (LC-MS grade), Isopropanol (LC-MS grade), Methanol (LC-MS grade), *n*-Butanol (HPLC grade), Sodium chloride (NaCl), Sodium sulfate (anhydrous), Water (LC-MS grade)	Fisher Scientific (Houston, TX)
2-Hydrazinoquinoline (HQ), Triphenylphosphine (TPP), *p*-Anisidine,	Alfa Aesar (Ward Hill, MA)
Ammonium carbonate ($(NH_4)_2CO_3$), 2-2′-Dipyridyl disulfide (DPDS), Sodium hydroxide (NaOH)	MP Biomedicals, LLC (Irvine, CA)
D_4-acetic acid, Amino acid standards, Dansyl chloride (DC), Dimethyl sulfoxide (DMSO), Leucine enkephalin, Magnesium chloride ($MgCl_2$), Potassium chloride (KCl), Potassium phosphate monobasic (KH_2PO_4), Reserpine, Sodium bicarbonate ($NaHCO_3$), Sodium carbonate (Na_2CO_3), Sodium dodecyl sulfate (SDS), 2-Thiobarbituric acid, Trypsin (porcine pancreas), Tween 20	Sigma-Aldrich (St. Louis, MO)
2,4-Dinitrophenylhydrazine (DNPH), *N*-Hexane, Hydrochloric acid (HCl),	Honeywell (Charlotte, NC)
D_5-Tryptophan	Cambridge Isotope Laboratories (Tewksbury, MA)
D_6-acetone, Elastase (porcine pancreas), 1,1,3,3-Tetramethoxypropane, Trichloroacetic acid, BCA assay kit	Thermo Fisher Scientific (Waltham, MA)
N-Benzol-*DL*-arginine-4-nitroanilide hydrochloride (BAPA)	Chem Impex (Wood Dale, IL)
N-succinyl-L-alanyl-L-alanyl-L-alanine-*p*-nitroanalide (Suc-AAA-*p*NA)	Vivitide (Korea)
Tris base	Amresco (Solon, OH)
Ethanol (reagent alcohol)	Ricca Chemicals (Arlington, TX)
Ethyl acetate	Mallinckrodt Chemicals (Ireland)
Guanidine hydrochloride, Isooctane	TCI (Japan)
^{13}C-1,2-palmitic acid	CDN Isotopes (Canada)

Table 3.2 LC-MS instrumental settings for data acquisition.

Target compounds	LC column and temperature	LC mobile phase	Lock mass and MS detection mode	Capillary and cone voltage	Source and desolvation temperature	Cone and desolvation gas flow	Collision gas and energy ramp
Amino acids (DC derivatization)	Waters BEH C18, 40 °C	A: 0.1% formic acid in water B: 0.1% formic acid in ACN	Leucine enkephalin ($[M + H]^+$ = *m/z* 556.2771), Positive	0.2 kV, 40 V	120 °C, 350 °C	50 L/hr, 600 L/hr (N_2)	Argon, 10-50 eV
Fatty acids, aldehydes (HQ derivatization)	Waters BEH C18, 40 °C	A: 2 mM NH_4OAc in water with 0.05% acetic acid B: 2 mM NH4OAc in 95% ACN and 5% H_2O with 0.05% acetic acid	Leucine enkephalin ($[M + H]^+$ = *m/z* 556.2771), Positive	0.2 kV, 40 V	120 °C, 350 °C	50 L/hr, 600 L/hr (N_2)	Argon , 10-50 eV
Triglycerides	Waters BEH C8, 60 °C	A: 40% MeOH in water, with 0.1% formic acid, 10 mM ammonium formate B: 100% MeOH, with 0.1% formic acid, 10 mM ammonium formate	Reserpine ($[M + H]^+$ = *m/z* 609.2812), Positive	0.2 kV, 40 V	120 °C, 500 °C	40 L/hr, 600 L/hr (N_2)	Argon , 10-50 eV
Hepatic hydrophilic metabolites	Waters Amide, 40 °C	A: 0.1% formic acid in water B: 0.1% formic acid in ACN	Leucine enkephalin ($[M + H]^+$ = m/z 556.2771), Positive; or Leucine enkephalin ($[M - H]^-$ = m/z 554.2615), Negative	0.2 kV, 40 V	120 °C, 350 °C	50 L/hr, 600 L/hr (N_2)	Argon, 10-50 eV

Table 3.3 Identification of HSO-induced changes in the luminal metabolome from an S-plot of an OPLS-DA model, based on data from HQ derivatization and LCMS analysis.

	Compound name	RT (min)	Detected *m/z*	Monoisotopic *m/z*	Molecular formula (with HQ adduct)	Molecular formula (without HQ adduct)	Mass deviation (Δppm)
i_D	Caprylic acid (C8:0)	6.2	286.19	286.1919	$C_{17}H_{23}N_3O^+$	$C_8H_{16}O_2$	-6.64
ii_D	Oleic acid (C18:1)	8.51	424.3332	424.3328	$C_{27}H_{41}N_3O^+$	$C_{18}H_{34}O_2$	0.94
iii_D	Linoleic acid (C18:2)	8.21	422.318	422.3171	$C_{27}H_{39}N_3O^+$	$C_{18}H_{32}O_2$	2.13
iv_D	Hexanal	6.05	242.1666	242.1657	$C_{15}H_{19}N_3^+$	$C_6H_{12}O$	3.72
v_D	Nonanal	6.82	284.2128	284.2127	$C_{18}H_{25}N_3^+$	$C_9H_{18}O$	0.35

Table 3.4 Identification of the markers associated with HSO oil intake in the gastric lipidome.

Ion label	TG label	RT	Detected m/z	Detected ion adduct	Accurate m/z	Putative identity	Putative structure	Molecular formula	Mass deviation (ΔPPM)	Major fragments
I_G	**TG1**	6.53	914.7825	$[M+NH_4]^+$	914.7813	TG 54:5;O	TG(18:1/18:2/18:2-OH)	$C_{57}H_{100}O_7$	1	897, 879, 617, 601
II_G	**TG2**	6.22	912.7665	$[M+NH_4]^+$	912.7656	TG 54:6;O	TG(18:2/18:2/18:2-OH)	$C_{57}H_{98}O_7$	1	895, 877, 615, 599
V_G	**TG3**	6.22	764.6794	$[M+NH_4]^+$	764.6768	TG-44:2	TG(8:0/18:1/18:1)	$C_{47}H_{86}O_6$	3	747, 603, 465
III_G	**TG4**	5.89	767.62	$[M+Na]^+$	767.6166	TG-44:3	TG(8:0/18:1/18:2)	$C_{47}H_{84}O_6$	4	623, 601, 487, 484, 465, 463
VI_G	**TG4**	5.89	762.6617	$[M+NH_4]^+$	762.6612	TG-44:3	TG(8:0/18:1/18:2)	$C_{47}H_{84}O_6$	0.6	745, 601, 465, 463
IV_G	**TG5**	5.52	765.6035	$[M+Na]^+$	765.6009	TG-44:5	TG(8:0/18:2/18:2)	$C_{47}H_{82}O_6$	3	621, 599, 485, 463
VII_G	**TG5**	5.52	760.6461	$[M+NH_4]^+$	760.6455	TG-44:4	TG(8:0/18:2/18:2)	$C_{47}H_{82}O_6$	0.8	743, 599, 463

Table 3.5 Putative identification of the markers associated with HSO oil intake in the colon lipidome.

	Retention time (min)	Detected m/z	Putative molecular formula	Adduct form	Putative adduct m/z	Mass deviation (Δ ppm)	Identity	Major fragments
Ic	3.55	473.3988	$C_{31}H_{52}O_3$	$[M+H]^+$	473.3989	-0.21	α-tocopherol acetate	165, 207*
IIc	2.85	575.4672	$C_{36}H_{62}O_5$	$[M+H]^+$	575.467	0.35	Sterol specie	
IIIc	3.24	576.4984	$C_{36}H_{65}NO_4$	$[M+NH_4]^+$	576.4986	-0.35	Unresolved	
IVc	3.89	613.519	$C_{40}H_{68}O_4$	$[M+H]^+$	613.5196	-0.98	Sterol specie	
Vc	2.6	615.4593	$C_{38}H_{62}O_6$	$[M+H]^+$	615.4619	-4.22	Unresolved	
VIc	4.01	615.5324	$C_{35}H_{70}N_2O_6$	$[M+H]^+$	615.5312	1.95	Sterol specie	
VIIc	3.24	629.5142	$C_{40}H_{68}O_5$	$[M+H]^+$	629.514	0.32	Sterol specie	
VIIIc	3.38	631.5295	$C_{40}H_{70}O_5$	$[M+H]^+$	631.5296	-0.16	Sterol specie	
IXc	4	632.5612	$C_{40}H_{73}NO_4$	$[M+NH_4]^+$	632.5612	0.00	Sterol specie	

**Compared with the MS/MS spectra from HMDB*

Table 3.6 Free amino acids in liver, serum, and muscle. (* P<0.05, ** P<0.01*** P<0.001, N.S., not significant, from unpaired t-test between CSO and HSO dietary treatments)

	Liver (nmol/g tissue)			Serum (μM)			Muscle (nmol/g tissue)		
Amino Acids	**CSO**	**HSO**	***P*-value**	**CSO**	**HSO**	***P*-value**	**CSO**	**HSO**	***P*-value**
Alanine	2,903.40±368.84	3,308.80±459.04	*	251.94±51.86	155.07±36.32	***	3,242.52±1,444.83	1,569.69±584.74	**
Glycine	7,554.19±553.56	7,686.90±862.07	N.S.	746.22±207.21	590.73±142.91	N.S.	14,643.54±2,495.62	11,618.91±1,373.60	**
Taurine	3,129.87±1,221.58	1,803.30±844.94	*	90.60±39.97	63.66±25.06	N.S.	3,194.28±558.95	2,823.66±964.96	N.S.
Phenylalanine	783.25±103.10	1,069.30±162.83	**	68.31±12.05	57.48±8.60	*	110.79±28.75	120.69±20.18	N.S.
Methionine	429.95±83.06	476.90±117.47	N.S.	35.64±13.47	21.90±5.68	*	ND	ND	NA
Glutamate	9,129.35±1,116.26	10,081.30±1,427.54	N.S.	204.84±75.65	101.04±36.29	**	2,074.59±589.77	1,870.29±562.44	N.S.
Serine	3,370.17±405.14	5,750.90±1,158.57	***	93.63±23.89	79.02±18.96	N.S.	439.65±91.07	643.77±235.92	*
Valine	1,630.64±174.51	2,086.70±357.84	**	155.52±24.02	112.47±30.78	**	382.68±61.76	300.60±95.35	*
Threonine	1,742.40±262.73	1,995.90±226.06	*	164.97±51.29	123.93±55.60	N.S.	1,010.61±423.41	657.45±330.78	N.S.
Iso/Leucine	1,616.24±227.58	1,891.90±382.64	N.S.	99.09±15.86	73.23±16.24	**	220.68±44.36	161.82±52.97	*
Asparagine	4,229.92±531.12	4,894.30±685.60	*	143.64±36.31	99.51±34.64	*	1,114.47±374.36	1,053.63±249.70	N.S.
Aspartate	2,026.72±405.57	3,116.30±762.28	**	16.50±6.64	8.82±2.40	**	229.59±50.56	237.33±27.30	N.S.
Proline	1,638.41±186.01	1,962.00±335.01	*	243.42±52.99	172.62±37.93	**	1,912.95±519.91	1,249.29±569.22	*
Tyrosine	2,651.40±313.06	2,544.90±386.13	N.S.	87.42±21.08	68.70±18.20	*	164.79±84.95	136.08±76.79	N.S.
Citruline	27.49±10.67	49.40±18.37	**	36.93±10.20	39.09±9.26	N.S.	251.37±105.70	385.92±87.28	**
Arginine	890.43±170.98	706.10±187.34	*	87.15±21.22	65.76±20.55	*	984.78±315.82	981.45±311.55	N.S.
Lysine	1,863.25±234.60	2,202.80±457.46	N.S.	78.30±23.86	45.24±23.38	**	510.30±295.72	389.97±222.46	N.S.
Histidine	452.62±114.95	695.20±98.80	***	23.85±8.77	20.07±4.63	N.S.	29.88±17.18	50.49±17.61	*
Tryptophan	103.66±8.03	127.30±23.72	*	24.51±7.35	12.42±4.63	**	10.08±3.59	6.39±4.68	*
γ-Aminobutyric acid	13.99±4.25	14.40±3.40	N.S.	0.11±0.16	0.09±0.15	N.S.	20.52±9.92	14.04±5.91	N.S.
Ornithine	607.91±149.34	1,248.50±243.43	***	47.25±12.59	42.24±16.09	N.S.	1,363.41±536.53	1,336.59±538.71	N.S.
Glutamine	7,007.48±1,077.83	8,646.70±2,843.15	N.S.	478.44±191.67	329.31±55.90	*	11,905.56±3,475.31	14,426.28±5,947.92	N.S.
Total	53,802.74±3,568.38	62,359.80±5,780.97	**	3,178.26±644.21	2,282.37±385.24	**	43,817.04±6,940.54	40,034.97±6,797.68	N.S.

Table 3.7 Identification of functional hepatic metabolites influenced by HSO feeding. Identities confirmed by comparison with authentic standards.

RT	Detected m/z	Adduct form	Identity	Molecular formula	Monoisotopic m/z	Mass deviation (Δ ppm)
4.0862	308.0913	$[M+H]^+$	GSH	$C_{10}H_{18}N_3O_6S^+$	308.0916	-1.0
6.2725	613.1581	$[M+H]^+$	GSSG	$C_{20}H_{33}N_6O_{12}S_2^+$	613.1598	-2.8
4.1681	104.1076	$[M+H]^+$	Choline	$C_5H_{14}NO^+$	104.1075	1.0
4.1607	184.0738	$[M+H]^+$	Phosphocholine (PC)	$C_5H_{15}NO_4P^+$	184.0739	-0.5
4.1643	258.1108	$[M+H]^+$	Glycerophosphocholine (GPC)	$C_8H_{21}NO_6P^+$	258.1106	0.8
5.8831	664.1156	$[M+H]^+$	NAD^+	$C_{21}H_{28}N_7O_{14}P_2^+$	664.1169	-2.0
4.8025	348.0711	$[M+H]^+$	AMP	$C_{10}H_{15}N_5O_7P^+$	348.0709	0.6

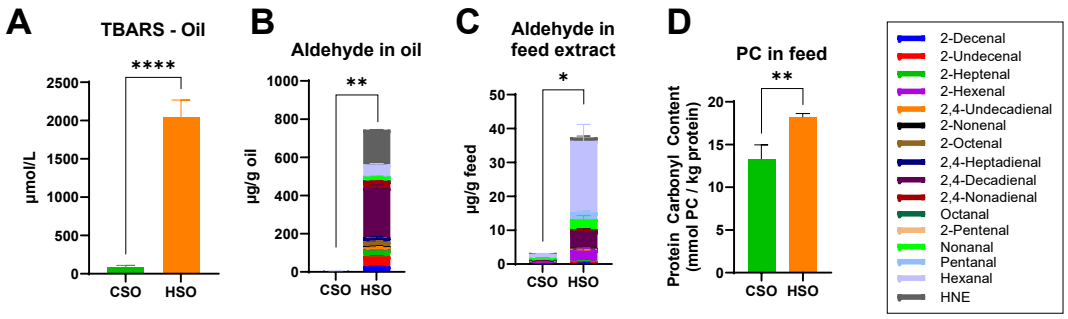

Figure 3.1 Characterization of heating-induced changes in the aldehyde content of oils and the feeds. A) TBARS values of the oils. B) The concentration of free aldehydes in the oils. C) The concentration of free aldehydes in the feeds. D) The protein carbonyl (PC) content in the feed. (n = 5, * P<0.05, ** P<0.01, **** P<0.0001, from unpaired t-test between CSO and HSO.)

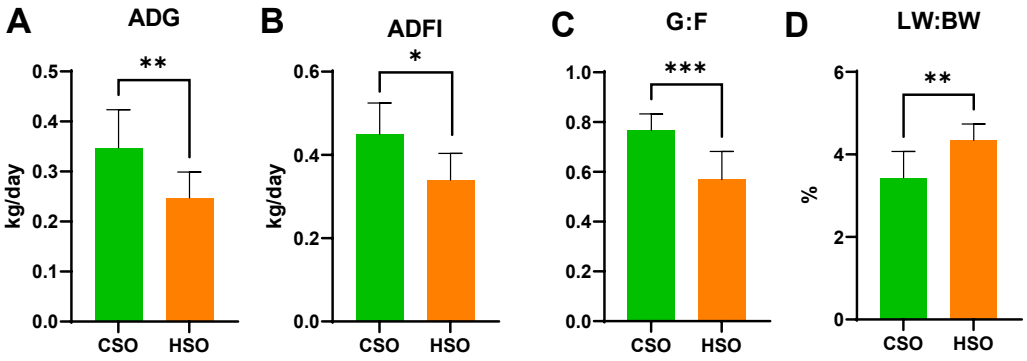

Figure 3.2 Growth performance of nursery pigs fed with CSO and HSO feeds (n = 10 for each group). A) Average daily weight gain (ADG). B) Average daily feed intake (ADFI). C) G:F ratio. D) Liver weight (LW):body weight (BW) ratio (%). (* $P<0.05$, ** $P<0.01$, *** $P<0.001$, from unpaired t-test between CSO and HSO)

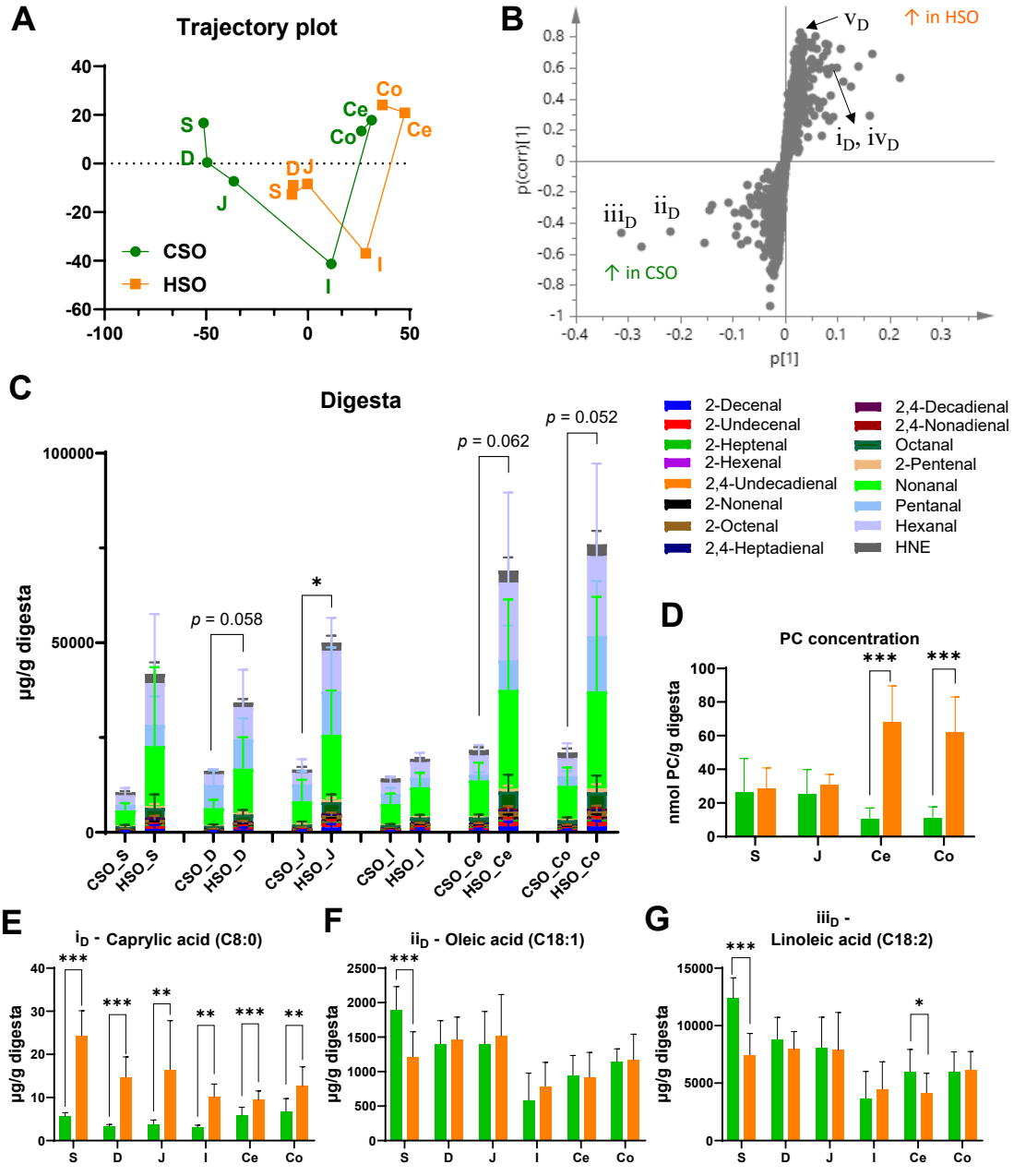

Figure 3.3 Characterization of the fatty acids and lipidic aldehydes in the GI lumen after CSO and HSO feeding (6-10 samples for each GI segment). A) The trajectory plot of the distribution of digestas from different GI locations. The coordinates are calculated as the average of the samples in respective groups from the scores plot of a PCA model. Data

acquired from LC-MS analysis of HQ derivatized digesta samples. S. stomach; D, duodenum; J. jejunum; I, ileum; Ce, cecum; Co, colon. B) Loadings plot of the OPLS-DA model of digesta samples, comparing the difference of all GI locations between CSO and HSO groups. Markers in the upper right corners had higher abundance in HSO group, whereas the ones in the lower left corners had higher abundance in CSO group. Markers labeled i_D - v_D were identified and listed in **Table 3.3**. C) Free aldehyde content in the GI lumen was detected and quantified by LC-MS based analysis. D) PC concentration in the digesta, determined by the DNPH assay (only digesta samples from S, J, Ce and Co were sufficient to supply DNPH assay). Quantification of E) CA, F) OA, and G) LA in the GI lumen. (* $P<0.05$, ** $P<0.01$, *** $P<0.001$, from unpaired t-test between CSO and HSO dietary treatments in each GI segment).

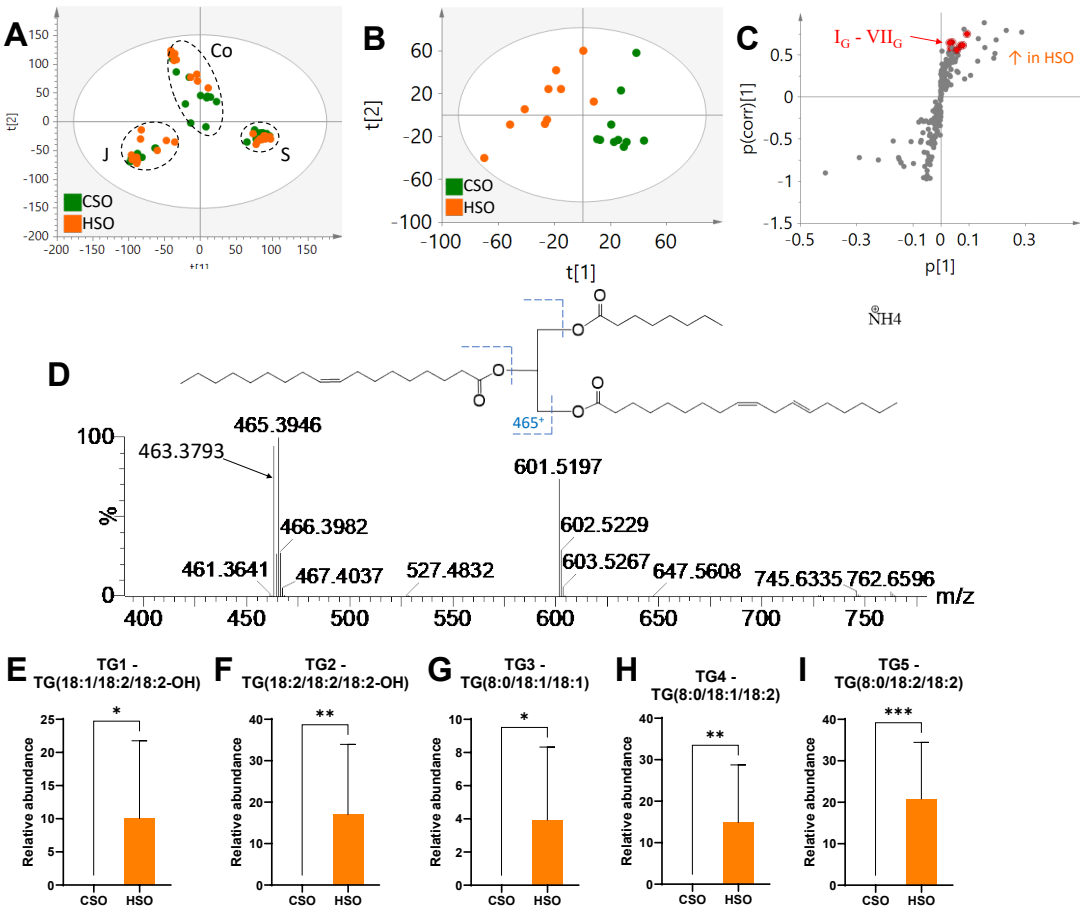

Figure 3.4 Modeling and characterization of the digesta lipidome from CSO and HSO feeding (butanol extraction) (n = 9-10 for each group). A) The scores plots of a PLS-DA model on the analysis of the triglyceride profiles of stomach (S), jejunum (J), and colon (Co) digesta (butanol extract). B) The scores plots of a PCA model on the triglyceride profiles of stomach (S). C) The S-plot of an OPLS-DA model on the butanol extract of stomach digesta. Compounds I_G - VII_G (labeled in red) were HSO-responsive markers and only detected in HSO group. These markers were identified as 5 TG species, listed in **Table 3.4**. D) Frgmentation pattern of ion $[M+NH_4]^+$=762.6617. The fatty acid composition was determined by the neutral loss from the parent ion to the daughter ion.

E-I) The relative abundance of TG1-TG5 in gastric digesta (corresponding to ions I_G - VII_G listed in **Table 3.4**). (* P<0.05, ** P<0.01, *** P<0.001 from unpaired t-test between CSO and HSO groups).

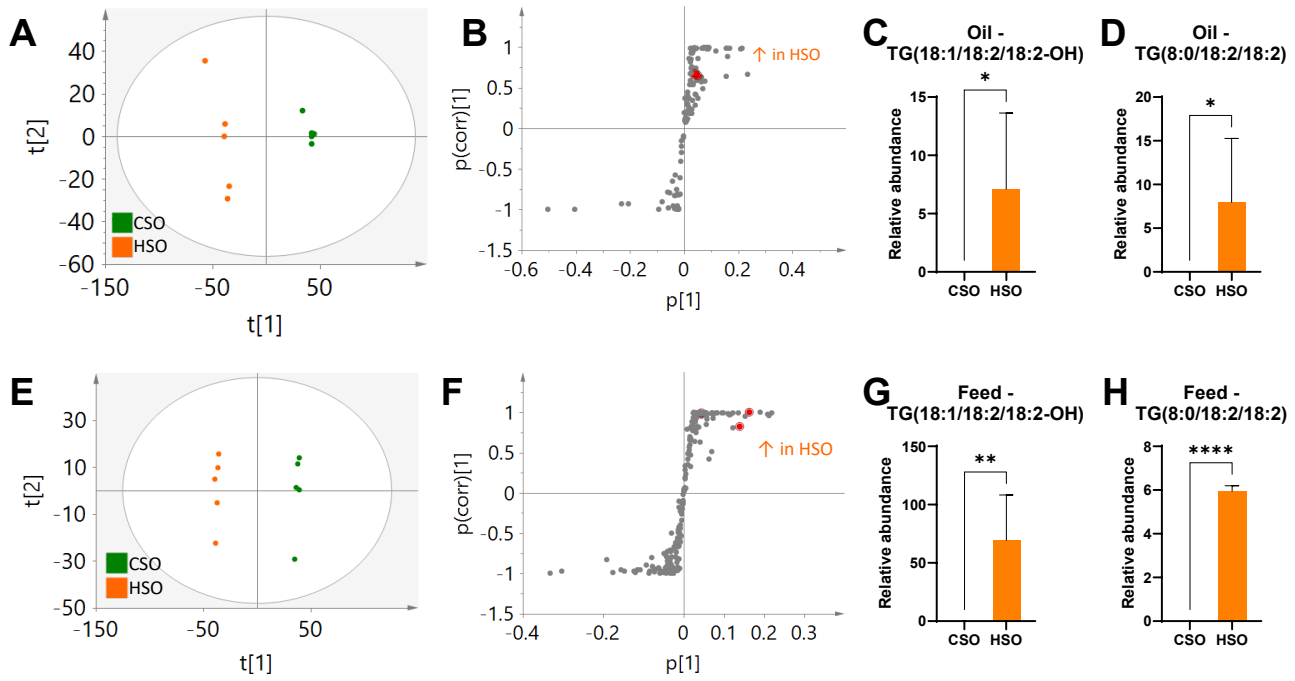

Figure 3.5 Modeling and characterization of the lipidome of oils and the feeds (n = 5 for each group). A) The scores plots of the a PCA model on CSO and HSO. B) The S-plot of an OPLS-DA model on CSO and HSO. TG1 and TG5 are labeled in red. C) Relative abundance of TG1, TG(18:1/18:2/18:2-OH), in oil. D) Relative abundance of TG5, TG(8:0/18:2/18:2), in oil. E) The scores plots of a PCA model on the lipid extracts of CSO and HSO feeds. F) The S-plot of an OPLS-DA model on the lipid extracts of CSO and HSO feeds. TG1 and TG5 are labeled in red. G) Relative abundance of TG1, TG(18:1/18:2/18:2-OH), in feed extract. H) Relative

abundance of TG5, TG(8:0/18:2/18:2), in feed extract. (* $P<0.05$, ** $P<0.01$, **** $P<0.0001$ from unpaired t-test between CSO and HSO groups).

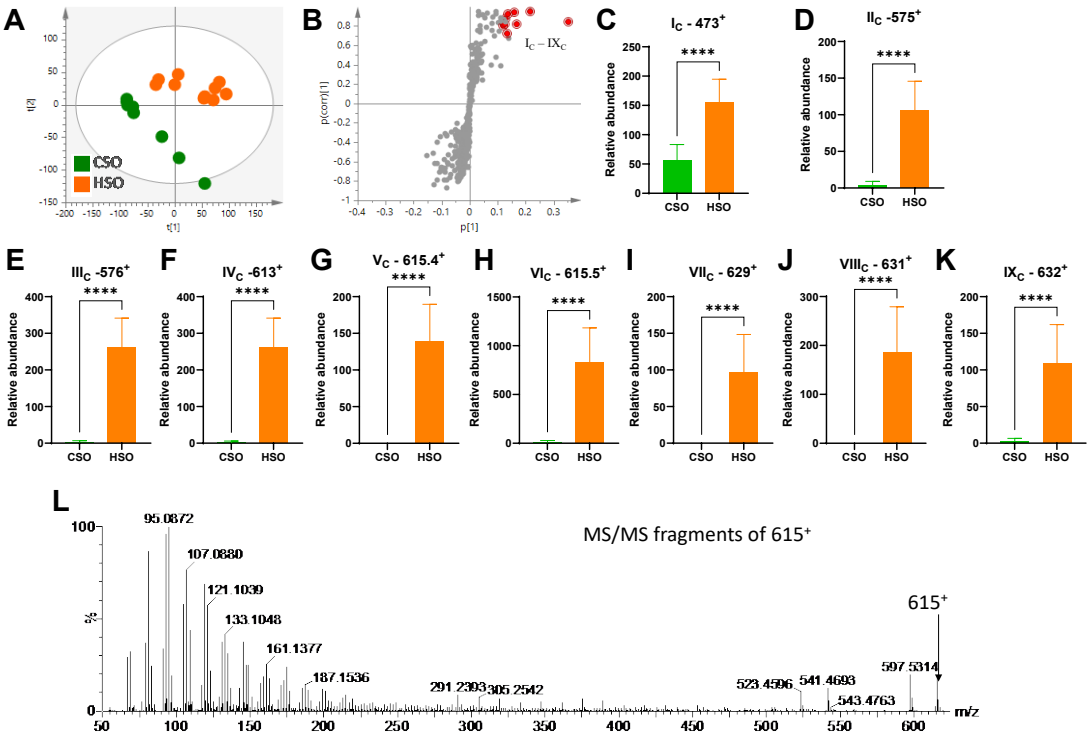

Figure 3.6 Modeling and characterization of of the lipidome (butanol extraction) of digestas from colon (n = 9-10 for each group; Other digesta had limited quantity and was unavailable for butanol extraction). A) The scores plots of a PCA model on the triglyceride profiles of colon digesta. B) The S-plot of an OPLS-DA model on the lipidome of colon digesta. The putative identification of $I_C - IX_C$ (labeled in red) are listed in **Table 3.5**. The relative abundance of selected $I_C - IX_C$ are shown in C-K). L) MS/MS fragments of the VI_C - 615$^+$ ion. (**** P<0.0001 from unpaired t-test between CSO and HSO dietary treatments)

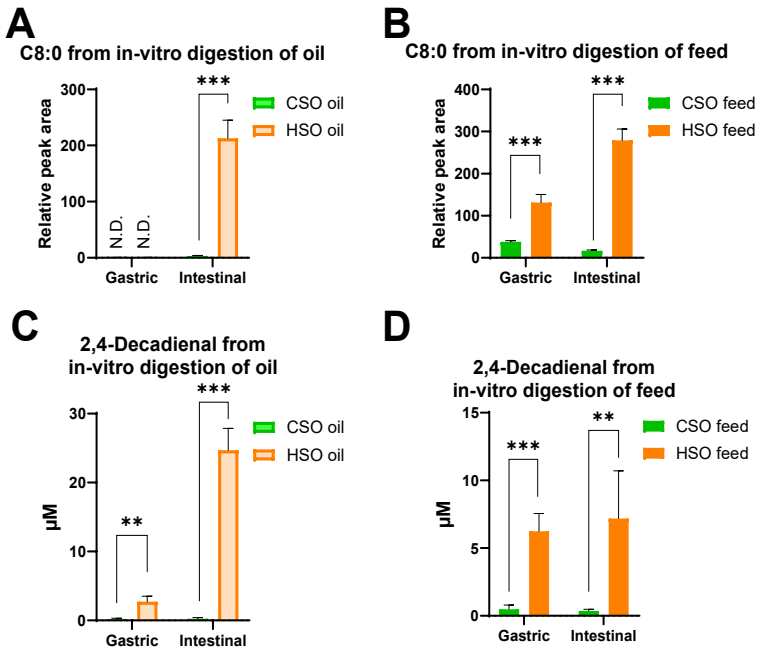

Figure 3.7 In-vitro digestion of oils and feeds. (n = 5). The relative abundance of caprylic acid from the incubation of A) oils and B) feeds. The concentrations of 2,4-decadienal in the digestion fluid from the incubation of C) oils and B) feeds were. (** $P<0.01$, *** $P<0.001$ from unpaired t-test between CSO and HSO groups)

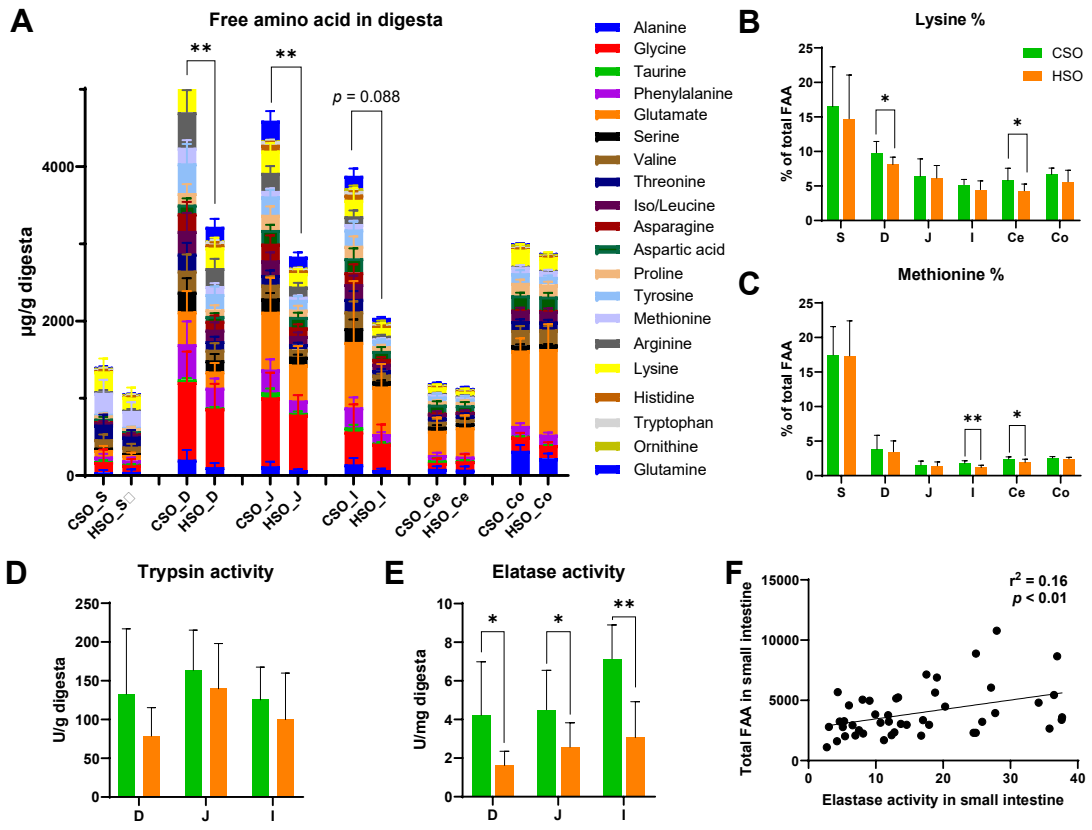

Figure 3.8 Characterization of the proteolytic activity in the GI lumen. A) Free amino acid levels in the stomach, jejunum, and colon were quantified by LC-MS-based analysis (n = 9-10 for each group; some samples had limited quantity and were unavailable for enzyme assays). The percentage of B) lysine, C) methionine, in the total free amino acid pool in the GI. D) Trypsin activity and E) elastase activity in jejunum determined by colorimetric assays. (Green bars: CSO; Orange bars: HSO. * P<0.05, ** P<0.01, from unpaired t-test between CSO and HSO groups). F) Pearson's correlation between the elastase activity and jejunal total free amino acid.

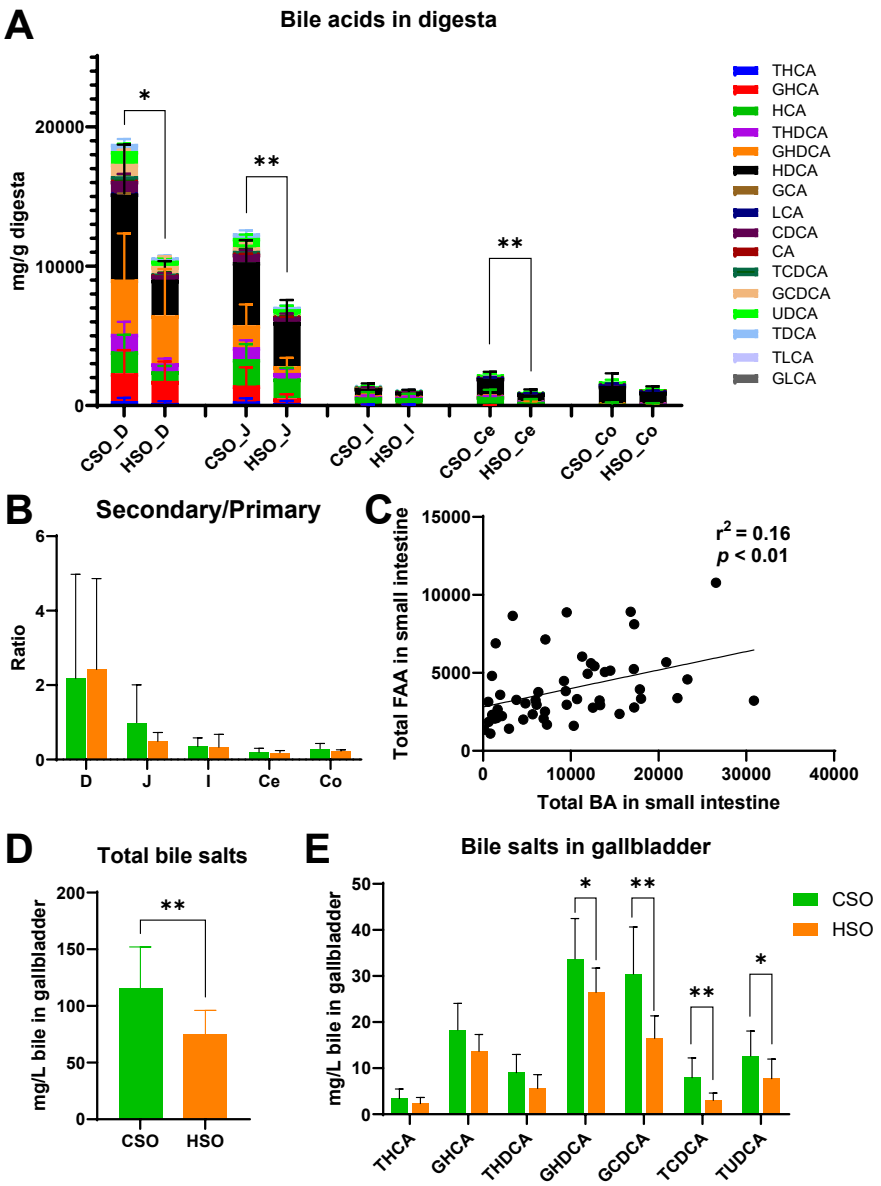

Figure 3.9 Influence of HSO on the bile acids in digesta and gallbladder bile. A) Concentration of total bile acid in digesta (n = 5-10 for each group). B) The ratio of secondary to primary bile acids in digesta. C) Pearson's correlation between the total bile

acid concentration to the total free amino acid concentration in the small intestine. D) Concentration of total bile salts in gallbladder. E) Concentration of individual bile acids in the gallbladder bile. (* $P<0.05$, ** $P<0.01$ from unpaired t-test between CSO and HSO groups). THCA, taurohyocholic acid; GHCA, glycohyocholic acid; HCA, hyocholic acid; THDCA, taurohyodeoxycholic acid; GHDCA, glycohyodeoxycholic acid; HDCA, hyodeoxycholic acid; GCA, glycocholic acid; LCA, lithocholic acid; CDCA, chenodeoxycholic acid; CA, cholic acid; TCDCA, taurochenodeoxycholic acid; GCDCA, glycochenodeoxycholic acid; UDCA, ursodeoxycholic acid; TDCA, taurodeoxycholic acid; TLCA, taurolithocholic acid; GLCA, glycolithocholic acid; TUDCA, tauroursodeoxycholic acid.

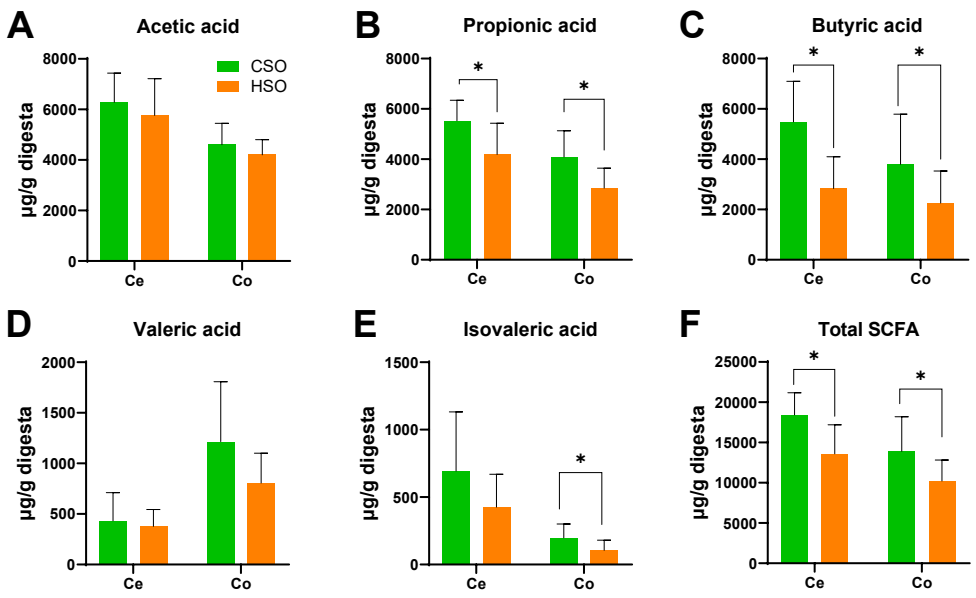

Figure 3.10 Short chain fatty acids (SCFA) in the cecum and colon. (n = 10 for each group). Concentrations of A) acetic acid, B) propionic acid, C) butyric acid, D) valeric acid, E) isovaleric acid, and F) total SCFA. (* $P<0.05$, from unpaired t-test between CSO and HSO groups).

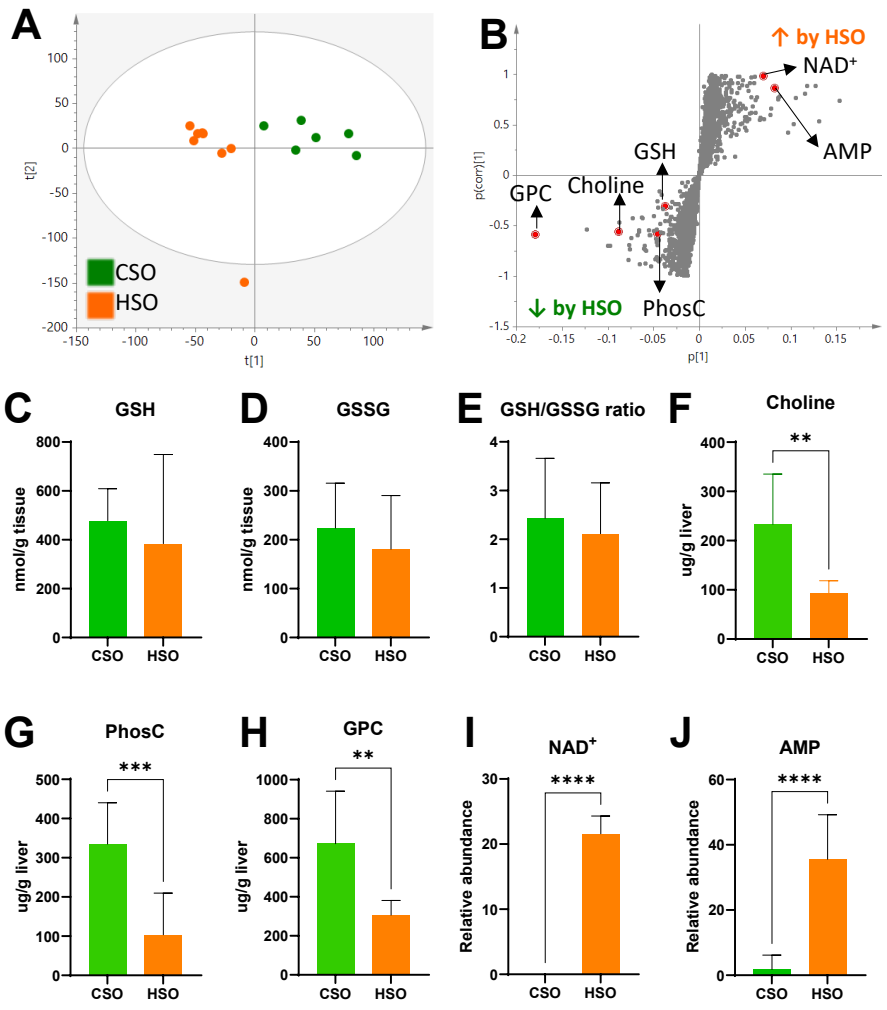

Figure 3.11 Influence of HSO on the hepatic metabolome. A) The scores plot of a PCA model constructed based on the LC-MS data acquired from the analysis of the polar fraction of the liver extracts. B) The S-plot of an OPLS-DA model comparing the hepatic metabolome of CSO and HSO groups. C) Concentration of glutathione (GSH). D) Concentration of oxidized glutathione (GSSG). E) GSH/GSSG ratio. F) Concentration of choline. G) Concentration of phosphocholine (PhosC). H) Concentration of glycerophosphocholine (GPC). I) Relative abundance of NAD^+. The ion intensity of NAD^+ in the CSO groups was below the quantitation limit and hence annotated as zero.

J) relative abundance of adenosine monophosphate (AMP). (** $P<0.01$, *** $P<0.001$, **** $P<0.0001$ from unpaired t-test between CSO and HSO groups). The identification of these markers are listed in **Table 3.7**.

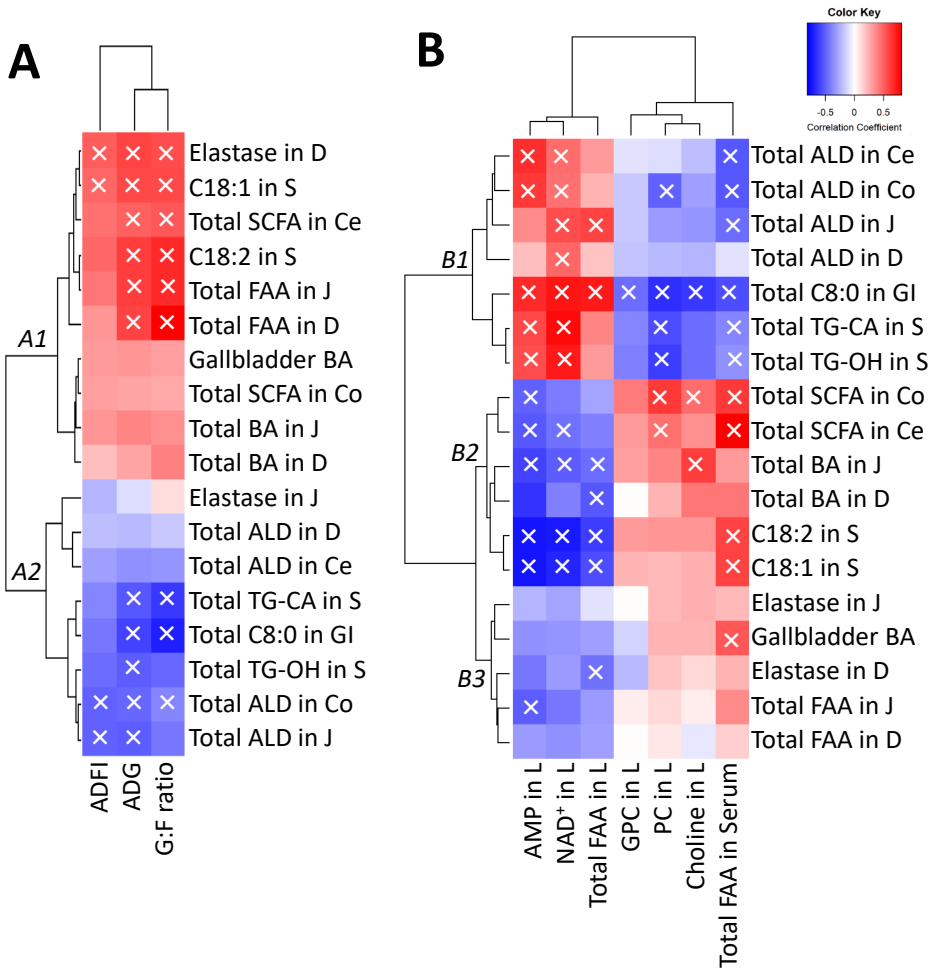

Figure 3.12 Heatmap of Pearson's correlation coefficient between the pigs' growth performance indices, hepatic metabolites (affected by HSO feeding), and key functional metabolites in the GI lumen. A) Correlation between the growth performance indices and the functional metabolites in GIT. Based on the dendrogram and the cluster analysis, the GI metabolites are clustered into two groups: A1 and A2. B) Correlation between the hepatic and serum metabolites and GI functional metabolites. Based on the dendrogram and the cluster analysis, the GI metabolites are clustered into three groups: B1, B2, and B3. Significant correlations (non-adjusted $p < 0.05$) are marked with ×. ALD, aldehyde;

FAA, free amino acids; BA, bile acids; SCFA, short-chain fatty acids; S, stomach; J, jejunum; Co, colon; GIT, gastrointestinal tract; L, liver.

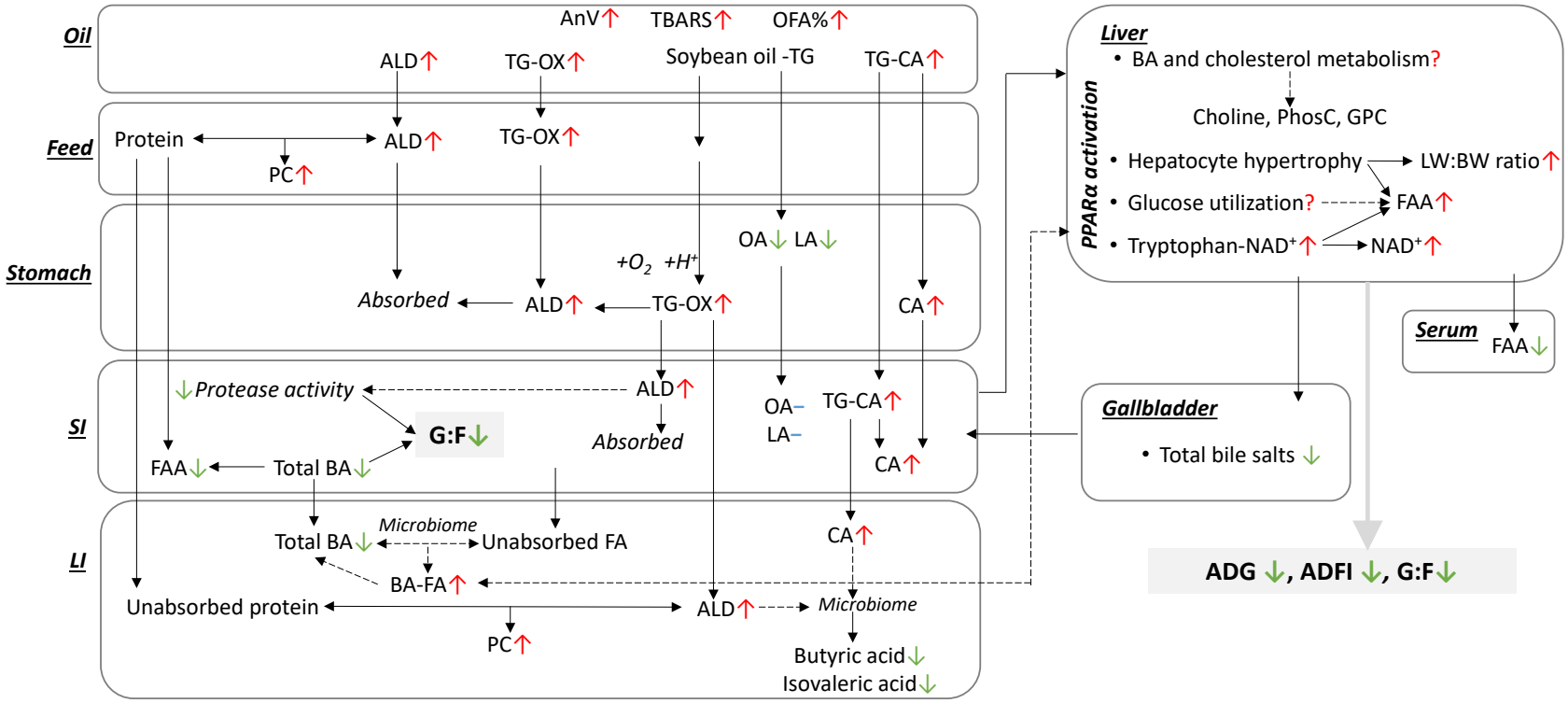

Figure 3.13 Summary of HSO induced changes in the GI metabolome and post-absorptive metabolism in pigs fed HSO. SI, small intestine; LI, large intestine; AnV, p-anisidine value; OFA, oxidized fatty acids; ALD, aldehyde; TG-OX, oxidized triglycerides; TG-CA, caprylic acid-containing triglyceride; OA, oleic acid; LA, linoleic acid; CA, caprlic acid; BA, bile acid; PC, protein carbonyl;

BA-FA, bile acid-fatty acid conjugates; FA, fatty acids; LW:BW, liver weight:body weight; FAA, free amino acids. Dashed lines indicate a potential pathway or interaction between metabolites.

Chapter 4 Influence of aldehyde abatement on heated soybean oil-elicited metabolic changes in mice

4.1 SUMMARY

Heated cooking oils are a constitutive component of contemporary human diets and a common ingredient in animal feed. Aldehydes, the most reactive lipid oxidation products (LOPs) in heated oils, are widely considered contributors to the adverse health effects of heated oil consumption. However, the specific contribution of aldehydes to these adverse metabolic effects remains undefined. This study adopted a novel silica-based approach to remove most free aldehydes from heated soybean oil (HSO). Young mice were then fed four diets containing control and heated soybean oils with varying aldehyde concentrations.

Lipidomic analysis of the oils revealed that silica treatment reduced free aldehydes by 80% in the HSO but did not impact identified oxidized triglycerides and caprylic-acid-containing triglycerides. Despite reducing free aldehydes, silica treatment did not completely mitigate the adverse metabolic effects associated with HSO consumption, indicating the presence of other reactive compounds contributing to these effects, such as the non-volatile oxidized triglycerides. The mice's growth performance did not differ significantly among the four dietary groups. However, the liver weight to body weight (LW:BW) ratio was higher in both HSO and HSO-Si groups, indicating hepatocyte hypertrophy. Subsequent metabolomic analysis of the luminal metabolome of the gastrointestinal tract (GIT) revealed changes in the digestion and metabolism of amino acids and bile acids. Further analysis on the liver and serum suggested that the activation of tryptophan-NAD^+ pathway and PPARα, and oxidative stress were primarily driven by LOPs other than the free aldehydes in HSO.

Novel urinary metabolites potentially associated with the free aldehydes in the HSO were identified via the metabolomic analysis of the urines, which likely formed *de novo* in the GI lumen. Additional *in-vitro* assays further revealed their identities as acetylated adduct of 2,4-decadienal and lysine, but the exact structure and synthetic pathways still warrant more study.

Overall, the findings from this study highlighted the complexity of LOPs in HSO and underscored the need for further analysis of their compositions and impacts on host health. The urinary marker might serve as a biomarker for the metabolic processing of free lipidic aldehydes, reflecting the dietary intake of heated oils.

Keywords: Lipid oxidation; aldehydes; metabolomics; lipidomics; biomarker.

4.2 INTRODUCTION

Fats and lipids are essential macronutrients. American's Dietary Guideline recommends allocating 20-35% of daily calorie intake from fats and lipids. Approximately half of the fats and lipids consumed daily are thermally processed, such as by frying.[90] Fried food is commonly consumed. The study on the Million Veteran Program revealed that 32% and 17% of the cohort consume fried foods 1-3 and 4-6 times weekly.[371]

For humans, fried food consumption is known to be associated with elevated risk for chronic diseases, such as type 2 diabetes and coronary heart disease. [161-163,371] In animals, using thermally oxidized oil as a feed ingredient has been linked to a series of biological implications, including depressed appetite, increased intestinal leakage, diarrhea, deterred growth performance, elevated liver and kidney weight, oxidative stress, and altered blood lipid panel.[100,103,104,167-169] Studies on the underlying metabolic changes revealed a series of changes in amino acid metabolism induced by heated oils, hallmarked by the activation of the tryptophan-NAD^+ pathway, altered glutathione homeostasis, and decreased threonine catabolism.[130,168] Some of these metabolic responses carry protective effects, while others are damaging. The balance between these events may determine the consequences of heated oil exposures, as reflected by the inconsistent effects on animal growth in feeding trials.[105]

The undesirable metabolic changes are generally considered to be contributed by the wide range of lipid oxidation products (LOPs) generated from the oxidation, decomposition, and polymerization of triglycerides. Recent studies reported that lipidic

aldehydes, a class of secondary LOPs, especially the C9-C11 unsaturated species, showed strong inverse correlations with animal growth, as observed in pig and poultry feeding experiments.[102] Aldehydes are known reactive molecules, capable of reacting with large biological molecules, proteins, and DNAs.[182,184] However, the contribution of aldehydes to the observed adverse metabolic changes remains undefined, because the heated oils used for feeding were confounded by the presence of other LOPs, which have not been comprehensively profiled. Additionally, the study on the luminal metabolome of pigs fed HSO (Chapter 3) further revealed the *de-novo* formation of aldehydes. The contribution of pre-existing and *de-novo*-formed aldehydes to the host metabolism and health has not been clearly defined.

Given the current knowledge gap, a mouse feeding trial was conducted to distinguish the contribution of free lipidic aldehydes to the HSO-induced metabolic effects. Mice feeds were formulated with oils containing varying concentrations of lipidic aldehydes. The aldehyde-responsive markers were identified and characterized by the LC-MS-based metabolomics.

4.3 METHODS

4.3.1 Preparation of oils and mouse feed

Control soybean oil (CSO) was purchased from a local grocery store. The HSO was prepared using a previously established method.[66] In brief, 300 mL of soybean oil was placed into a 500 mL round-bottom glass flask, and then heated in an electric heating mantle with bubbling air (50 mL/min). The temperature ramped up slowly from room

temperature to (22 °C) to 185 °C in 1 hour and was held at 185 °C for an additional 6 hours. The HSO was let cool down to room temperature for mouse feed preparation.

To achieve abatement of free aldehydes from HSO, silica beads (SiliaBond Piperazine, Silicycle, Canada) were mixed with HSO at 1:5 ratio (w/v). The silica beads contain a functionalized piperazine group attached to the silica base, which can interact with aldehydes. The scheme of reaction is illustrated in **Appendix Figure A1**. The mixture was incubated at room temperature (22 °C) for 6 hours. After centrifugation at 3,000 × g for 30 min, the oil on the top layer was carefully transferred into a 50 mL centrifuge tube without stirring the silica on the bottom. The acquired silica-processed HSO (HSO-Si) was stored at 4 °C till further use. In addition, silica-processed CSO (CSO-Si) was prepared using the same approach to monitor the potential confounding effects of silica-based treatment.

Mice feed was formulated as the AIN-93G diet.[372] Oils were incorporated at 7% (w/w) into the respective diets. The formed pellets were dried in a dehydrator at 45 °C (115 °F) for 24 hours.

4.3.2 Animal treatment and sample collection

Animal care and experimental procedures were approved by the University of Minnesota Institutional Animal Care and Use Committee (IACUC) (protocol number 2109-39393A, approved on September 17, 2021). Female C57BL/6 mice (total n=16), 8-9 week-old, were purchased from Charles River Lab (Wilmington, MA). All mice were housed in the University of Minnesota animal facility at a constant temperature of 21 °C under a 12 h light-dark cycle, with ad libitum access to water and feed. Mice were first

acclimated to the control AIN-93G diet (same as CSO diet) for 7 days, then randomly assigned to 4 feeding groups (4 mice/group): CSO, HSO, CSO-Si, HSO-Si. Then the mice were fed experimental diets for 28 days. Feed intake and body weight were monitored and measured twice per week. On the last day of the feeding, mice were weighed, transferred to, and housed individually in a metabolic cage for 24 hours. Fecal samples and 24-hour urine samples were collected. Then blood samples were collected by submandibular bleeding and centrifuged at 2,000 × g for 10 minutes to obtain serum. Mice were then euthanized by carbon dioxide and dissected for collection of ileal and cecum digesta, whole liver, and whole kidney samples. The liver samples were weighed prior to flash frozen in liquid nitrogen. All samples were stored at −80 °C till further use.

In a separate trial, male mice (n = 4 for control and gavage, respectively) were fed the AIN-93G diet and then gavaged with 2,4-decadienal (20 mg/mL in CSO). Then 24-hour urine samples were collected after housing each mouse individually in metabolic cages.

4.3.3 Lipidomics and metabolomics

4.3.3.1 Sample preparation for LC-MS analysis

The reagents and chemicals used for sample preparation and LC-MS analysis are listed in **Table 4.1**. Oils and the lipid phase of feed extracts were diluted by 100,000 in *n*-butanol containing 1 μg/mL tripentadecanoin (TG15:0) as an internal standard prior to LC-MS analysis. The lipid phase of the feed extract was prepared based on a previously described procedure.[66] In brief, the dried pellets were grounded and mixed with two volumes of dichloromethane (w:v). The mixture passed through a column packed with

anhydrous sodium disulfate for removing water and insoluble residuals. Then the dichloromethane was evaporated under nitrogen. The aqueous phase of the feed extract was prepared by mixing the grounded pellets with 5 volumes of 50% aqueous acetonitrile containing 2 μM sulfadimethoxine. The supernatant was acquired after vortexing, sonicating, and centrifugation at 13,000 ×g for 10 min. All the extracts were then stored at -80°C till further use.

Urine samples were mixed with 5 volumes of 50% aqueous acetonitrile containing 2 μM sulfadimethoxine and centrifuged at 13,000 × g for 10 min to remove proteins and insoluble substances. Fecal and digesta samples were mixed with 50% aqueous acetonitrile (1:10, w/v) containing 50 μM d_5-tryptophan, 2 μM sulfadimethoxine, 510 μM d_4-acetic acid, 5 μM ^{13}C-1-glycocholic acid, 10 μg/mL ^{13}C-1,2-palmitic acid, and 100 μM d_6-acetone as internal standard. The mixture was sonicated for 10 minutes. After centrifuging at 13,000 ×g for 15 min, the supernatant was extracted. Serum samples were mixed with 2 volumes of acetonitrile, then centrifuged for 13,000 ×g for 10 min to obtain the supernatant.

Liver and kidney extracts were prepared based on the Bligh and Dyer method.[311] In brief, 100 mg frozen liver samples, or one whole kidney, were mixed with and homogenized in 500 μL methanol containing 180 μM d_6-acetone, 90 μM d_5-tryptophan, 459 μM d_4-acetic acid, 36 μg/mL ^{13}C-1,2-palmitic acid, 9 μM sulfadimethoxine, 9 μM glycyrrhetinic acid, and 20 μM tripentadecanoin (TG15:0) as internal standards. Then, 400 μL water and 500 μL chloroform were added into the mixture. After sonication in an ice bath for 1 min, the mixture was centrifuged at 13,000 × g for 10 minutes for phase

separation. The top layer was extracted as the aqueous phase. All samples were stored at −80 °C for further analysis.

4.3.3.2 Chemical derivatization

For detecting and quantifying fatty acids, aldehydes, and metabolites containing a carboxylic acid functional group, the oils, digesta extract, and the aqueous extract of liver and kidney, urine, and serum samples were derivatized with 2-hydrazinoquinoline (HQ), following a modified protocol.[150] In brief, 2 µL of aqueous sample was mixed with 100 µL of freshly prepared acetonitrile solution containing 1 mM 2-2′-dipyridyl disulfide (DPDS), 1 mM triphenylphosphine (TPP), 1 mM HQ. In fatty acid and aldehyde standards, the acetonitrile solution contained additional 90 µM *d*--acetone. The mixtures were incubated at 60 °C for 30 min, chilled on ice, and mixed with 100 µL of ice-cold water to stop the reaction. After centrifuging at 13,000 × g for 15 min, the supernatant was transferred to an HPLC vial for LC-MS analysis.

For amino acid quantification, the serum and the aqueous extraction of liver proceeded to dansyl chloride (DC) derivatization prior to LC-MS analysis. Briefly, 5 µL of sample was mixed with 5 µL of water, 50 µL of 10 mM sodium carbonate, and 100 µL of DC (3 mg/mL in acetone). In the amino acid standard mixture, 5 µL of 50 µM d_5-tryptophan (internal standard) was added instead of water. After incubation at 60°C for 15 min and centrifugation at 13,000 ×g for 10 min, the supernatant was transferred to a HPLC vial for LC-MS analysis.

4.3.3.3 LC-MS analysis

An aliquot of 2 μL sample was injected into a Waters Acquity ultraperformance liquid chromatography (UPLC) system (Milford, MA) and separated in a BEH column. The eluant from LC was then introduced into a Waters Xevo-G2-S or Synapt-G2Si quadrupole time-of-flight mass spectrometer (QTOF-MS) for accurate mass measurement and ion counting. Nitrogen was used as both cone gas (50 L/h) and desolvation gas (600 L/h). The mass analyzer was calibrated for detecting ions within the range *m/z* 50 – 1200 and monitored by intermittent injection of lock mass. The column, mobile phases, mass detection mode, and lock mass used for different metabolites are included in **Table 4.2**. The acquired chromatograms were processed by MassLynx^{TM} V4.2 (Waters). The structures of interested metabolites were analyzed by tandem MS fragmentation. For quantitative analysis, the individual peak areas of target compounds were calculated, scaled to the peak area of internal standards, and fitted into a calibration curve via Quanlynx^{TM} (Waters).

4.3.3.4 Untargeted multivariate data analysis and marker characterization

After processing by MarkerLynx^{TM} software (Waters), a multivariate data matrix is produced based on the chromatographic and spectral data via centroiding, deisotoping, filtering, peak recognition, and integration. The matrix contains sample identity, ion's retention time and *m/z*, and ion abundance. The intensity of each ion was calculated by normalizing the single ion counts (SIC) versus the total ion count (TIC). After Pareto scaling, principal component analysis (PCA) was conducted by importing the data matrix into SIMCA^{TM} software version 13.0 (Sartorius, Göttingen, Germany). The total ion intensity was artificially set as 10,000, which was then used to determine each

metabolite's relative abundance. Major latent variables in the data matrix were described in a scores scatter plot of multivariate model. The compounds influenced by feeding were identified by analyzing ions contributing to the principal components and to the separation of sample groups in the loadings scatter plot. The chemical identity was determined by accurate mass measurement, elemental composition analysis, database search (HMDB www.hmdb.ca; LIPID MAPS www.lipidmaps.org/), MSMS fragmentation, and comparison with authentic standards if possible.

4.3.4 *p*-Anisidine value (AnV) measurement

The *p*-Anisidine was measured according to the Official Method Cd 18–90 from the American Oil Chemists Society (AOCS).[373] Briefly, 0.1 g of oil sample was mixed with 5 mL of isooctane, followed by 30-min vertexing and 10-min centrifugation at 18,000× *g*, and the supernatant was collected for the AnV analysis according to the official method. HSO oil was mixed with 30 mL of isooctane instead for accurate absorbance measurement.

4.3.5 Thiobarbituric acid-reactive substance (TBARS) assay

Oils were submitted to TBARS assay. The reagent solution was prepared to contain 15% w/v trichloroacetic acid, 0.375% w/v 2-thiobarbituric acid, and 0.25 N hydrochloric acid. Then, in a 2-mL screw cap centrifuge tube, 20 µL of serum was mixed with 200 µL of the reagent solution. For oil samples, 5 µL of oils were mixed with 15 µL of water and 200 µL of the reagent solution. The mixture was incubated in boiling water (>95°C) for 30 minutes. After chilling on ice, the mixtures were centrifuged at 13,000 ×g for 15 min. Then the supernatants were transferred to a 96-well plate for

spectrophotometric measurement of absorbance at 532 nm. Standards were prepared by mixing 1,1,3,3,-tetramethoxypropane in water with concentrations ranging from 2.5 – 500 μM.

4.3.6 Coincubation of lysine and 2,4-decadienal

Lysine, d_8-lysine (CAS No: 344298-93-7, lysine-3,3,4,4,5,5,6,6-D8), ^{15}N-lysine (CAS No: 204451-50-3, lysine-2-^{15}N), *N*α-acetyl-lysine and *N*ε-acetyl-lysine were incubated with 2,4-decadienal respectively for elucidating the structure of the urinary marker. Briefly, 100 μL of lysine, isotopes, or acetyl-lysine (1 mM in water) was mixed with 740 μL water, 60 μL of sodium carbonate (10 mM in water), and 100 μL of 2,4-decadienal (20 mM in ethanol). The mixture was then incubated at 45 °C for 15 min to expedite adduct formation. Then, the mixture was submitted to LC-MS/MS analysis.

4.3.7 Statistical analysis

The statistical analysis on the concentration, relative abundance of metabolites, and results of biochemical assays were conducted by two-way ANOVA via R (HSO × Silica) and GraphPad Prism 10 (Boston, MA). Significant main effects and interactions were considered when the p-value < 0.05. The analytes of interests were further analyzed by Fisher's LSD tests to examine the different between groups. The groups annotated with different letters indicated significance when the p-value <0.05.

4.4 RESULTS

4.4.1 Evaluating the oxidative status of oils and feed extracts

Heating is known to change the chemical properties of oils extensively. According to the *p*-Anisidine (AnV) and TBARS values of the four oils, heating induced

the formation of aldehydic compounds in the heated oils, compared to the non-heated ones **(Figure 4.1 A and B)**. Further LC-MS analysis also confirmed the formation of aldehydes in the HSO **(Figure 4.1 C)**. After silica treatment, the AnV and TBARS value of HSO-Si decreased by about 50% **(Figure 4.1 A and B)**. Meanwhile, the LC-MS analysis revealed a reduction of total free aldehydes by 80% after silica treatment in the HSO-Si **(Figure 4.1 C)**. The abatement rate was higher for 2-alkenals and 2,4-dienals, exceeding 90%, but was lower for saturated alkanals, below 70%. These species were also the primary contributors to the separation and clustering of the four oils in a PCA model **(Figure 4.1 E and F)**. Their *m/z*, molecular formula, detected ion adduct form, and mass deviation are listed in **Table 4.3**, with identities confirmed by comparison with authentic standards. On the other hand, an abundant quantity of aldehydes was detected in the feed extract **(Figure 4.1 D)**, but the composition differed from the oils **(Figure 4.1 C)**. The reduction of total free aldehydes was reflected in the HSO-Si feed, but to a much smaller extent than the respective oils **(Figure 4.1 D)**.

The lipidomic analysis compared the CSO and HSO for their triglyceride profiles. The major triglyceride species in the soybean oils eluted between 6 and 8 min were identified. The analysis of the oils' chromatograms revealed that the concentration of TGs rich in polyunsaturated fatty acids (PUFA) was more sensitive to heating and was lowered in the HSO oil. Meanwhile, the main TG profile in the oils remained comparable after silica treatment **(Figure 4.2 A)**. The PCA modeling revealed that the main difference in the oils was driven by the chemical changes induced by heating, which was more predominant than the Si treatment **(Figure 4.2 B).** In the S-plot of an OPLS-DA model, the lipid species contributing to the separation were examined **(Figure 4.2 C)**.

The oxidized triglycerides (TG-OXs), including the species that were additionally oxygenated **(Figure 4.2 D and E)** and that contained a caprylic acyl chain (TG-CAs) **(Figure 4.2 F and G)** were significantly increased in HSO and HSO-Si while minimally impacted by silica abatement. The identification of these triglycerides are listed in **Table 4.4**.

4.4.2 Animal health and growth

4.4.2.1 Influence in the distribution of free amino acids in the GI

Based on the analysis of the pig luminal digesta in the Chapter 3, the digestion of proteins was expected to be altered by HSO feeding. Via targeted LC-MS analysis, the composition of free amino acid pool in ileum and cecum digesta, and feces was determined **(Table 4.5 – 4.7)**. To minimize the confounding effect of the varying volume of digesta and feces collected, the amino acid composition is presented and compared as a percentage of the total amino acid pool. HSO and HSO-Si feeding significantly increased the proportion of lysine in the ileal digesta and feces **(Table 4.5 and Table 4.7)**, but decreased that of lysine in the cecal digesta **(Table 4.6)**. Silica abatement lacked the efficacy to affect the percentage of free lysine. Instead, consumption of CSO-Si and HSO-Si appeared to increase the lysine excretion in feces **(Table 4.7)**. Such fluctuation was largely contributed by the fact that the fecal samples were collected over a 24-hour window. Additionally, unlike serum samples, fecal pellets were not homogenous.

4.4.2.2 Influence on the bile acid and microbial metabolism

The bile acids in the gallbladder, ileal and cecal digesta, and feces were quantified and presented as the proportion of the total bile acid (BA) pool **(Table 4.8 – 4.11)**. In the

gallbladder and ileum, HSO and HSO-Si intake raised the proportion of taurocholic acid (TCA) **(Table 4.8 - 4.9)**. Whereas in the cecum and feces, the percentage of deoxycholic acid (DCA) increased, and that of lithocholic acid (LCA) decreased, neither of which was ameliorated by HSO-Si **(Table 4.10 – 4.11)**. Meanwhile, the secondary to primary bile acid (and the conjugated primary BA) ratio was determined for cecum and feces, calculated by the proportion of DCA+LCA+UDCA+MDCA / TMCA+TCA+MCA+CA. Notably, the consumption of heated oils had a main effect on increasing this ratio in the cecal digesta and feces. It was ameliorated by the silica processing in the feces only **(Table 4.10 – 4.11).**

In the cecum, as the hallmark of microbial activity, the concentration of short-chain fatty acids (SCFAs) was determined **(Figure 4.3)**. HSO feeding increased the levels of all four SCFAs, and was reduced to a level comparable to CSO group in the HSO-Si group **(Figure 4.3)**.

4.4.2.3 Influence on animal growth and key functional metabolites in the liver and serum

Heated oil consumption has been shown to influence the growth performance, hepatic redox status, and serum amino acid profile in animals.[168] In the current study, even though the average daily weight gain (ADG) was comparable across the four groups, the liver weight to body weight ratio (LW:BW) was elevated in both HSO and HSO-Si groups **(Figure 4.4 A and B)**. The hepatic glutathione status was evaluated to assess the changes in antioxidant activity. Consumption of heated oils, regardless of aldehyde abatement, increased hepatic reduced glutathione (GSH) and GSH:glutathione

disulfide (GSH/GSSG) ratio but lacked the main effect on the GSSG level in the HSO and HSO-Si groups **(Figure 4.4 D)**.

The concentrations of serum and liver amino acids were quantified **(Table 4.12 – 4.13)**. The serum tryptophan and lysine were decreased in HSO and HSO-Si groups, and were not reversed by aldehyde abatement **(Table 4.12)**. In the liver, the HSO feeding only had main effects on histidine and taurine, but lacked impact on tryptophan **(Table 4.13)**.

Considering the lack of impact of HSO-Si feeding compared to the HSO feeding on the growth, hepatic amino acid, and glutathiones, the feeding-induced changes in the systematic metabolism were not investigated. Instead, further analysis was devoted to the urinary metabolome to identify potential aldehyde-responsive markers.

4.4.3 Characterizing the changes in the urine metabolome

4.4.3.1 Markers associated with HSO intake

The metabolites contributing to the discrimination between CSO, CSO-Si, HSO, and HSO-Si samples in the urine metabolome model were subjected to further characterization. To start, the influence of HSO feeding, regardless of silica processing, was examined in a PCA model **(Figure 4.5 A)**. Notably, the primary contributor to the separation along the principal component 1 (x-axis) was whether the oil had undergone a heating process **(Figure 4.5 A)**. Subsequently, the S-plot of an OPLS-DA model showed the urinary metabolites that were impacted by both HSO and HSO-Si (CSO and CSO-Si vs HSO and HSO-Si), with the metabolites that were more abundant in HSO and HSO-Si labeled **(Figure 4.5 B)**. HSO-responsive urinary metabolites were previously identified in

mice fed HSO.[168] The di-carboxylic acid, hydroxyalkenoic acids, and glycine conjugates of hydroxyalkenoic acids were examined in the current study. Two hydroxyalkenoic acids, with the molecular formula of $C_nH_{2n-2}O_3$, were identified. The other two were putatively determined di-carboxylic acids, with the formula of $C_nH_{2n-2}O_4$. Their identity and relative abundance in the urine samples are shown in **Table 4.14** and **Figure 4.5 C – F and L**. These HSO-responsive metabolites had very low relative abundance in CSO and CSO-Si groups. At the same time, HSO-Si did not mitigate their abundance, compared to the HSO **(Figure 4.5 C – F and L)**.

Five potential exposure markers were identified **(Figure 4.5 B, G–K; Table 4.14)**. Their absence in the CSO and CSO-Si groups, along with the increase in the HSO and HSO-Si groups, suggest their potential association with HSO exposure. Following structural analysis, metabolites i_U - v_U displayed two neutral losses of 18 Da. Meanwhile, elemental composition analysis indicated that i_U and ii_U shared a formula of $C_nH_{2n-2}O_2$. Database search suggested their identity as octenoic and nonenoic acids. Authentic standards of 2- and 3-octenoic acid were then submitted to HQ derivatization. However, their retention time was 6.07 min, distinct from the urinary marker i_U. Hence, metabolites i_U and ii_U are unlikely carboxylic acids. Instead, they potentially consist of an aliphatic carbon-hydrogen chain with hydroxy groups and two degrees of unsaturation. In addition to i_U and ii_U, iii_U had a molecular formula of $C_nH_{2n-6}O_5$, whereas iv_U and v_U shared a molecular formula of $C_nH_{2n-4}O_4$. Furthermore, metabolites i_U-v_U were not detected in the feed extracts, suggesting an endogenous origin.

Then, the urine of mice gavaged with 2,4-decadienal was analyzed for the targeted examination of these metabolites. Despite the detection of some of the metabolites in the list **(Table 4.14)**, their relative abundance was not changed by additional 2,4-decadienal intake (data not shown).

4.4.3.2 Markers associated with lipidic aldehyde intake

Compounds contributing to the separation of HSO from HSO-Si in this PLS-DA model in the direction of PC2 (y-axis) **(Figure 4.6 A)** were further studied **(Figure 4.6 B)** to elucidate the influence of aldehyde abatement on the mice urinary metabolome. Notably, four metabolites shared similar distribution patterns, showing a unique increase in the HSO feeding group only and near absence in the CSO and CSO-Si groups **(Figure 4.6 C-F)**.

To determine the origin of these four ions, the aqueous phase of diet extract, digesta, as well as the aqueous extract of liver and kidney were examined. Remarkably, these ions were not detected in the aqueous extract of feed, liver, and kidney **(Table 4.15)**. Further analysis revealed that two ions, with *m/z* of 321^+ and 319^+ **(I_u and II_u in Figure 4.6 and Table 4.15)**, were detected in the ileal and cecal digesta, and feces of HSO group. Notably, the relative abundance of the 321^+ ion in the HSO group gradually increased from ileal digesta to feces, and was significantly reduced in the HSO-Si group **(Figure 4.6 G-I)**, proving their responsiveness to the presence of free aldehydes in the oil. Upon tandem MS/MS analysis, the 321^+ and 319^+ ions displayed similar fragments and were further analyzed to determine their putative molecular formula and structure**.**

After elemental composition analysis and isotope modeling, the molecular formula of parent ions and their fragments were determined, as shown in **Table 4.16.** Both parent ions, 321^+ and 319^+, shared two fragments with *m/z* of 130^+ and 84^+. The 130^+ fragment showed a molecular formula of $C_6H_{12}NO_2^+$, consistent with pipecolic acid, a lysine oxidation product. Additionally, the parent ions exhibited a shared neutral loss of 42 Da, consistent with the neutral loss of an acetyl group. Therefore, it can be reasonably inferred that 321^+ and 319^+ shared highly similar structural moieties, potentially comprising an acetyl group, lysine-based moiety, and a 10-carbon moiety.

To better understand the identity of these two markers, lysine, and its two isotope forms were incubated with 2,4-decadienal (DDE), a 10-carbon α,β-unsaturated aldehyde, and the most abundant aldehyde in HSO. The results revealed that lysine coincubated with 2,4-decadienal generated two distinct adducts, characterized by *m/z* of 281^+ and 279^+, which shared a fragment of 84^+. Subsequent experiments showed that the 84^+ fragment had a *m/z* shift of 8 and 1 Da, respectively, when incubating d_8-lysine and ^{15}N-lysine with 2,4-decadienal, which confirmed its origin from lysine **(Table 4.16)**. Moreover, the 279^+ ion had a fragment of 150^+, which did not exhibit any *m/z* shift when lysine isotopes were introduced. Consequently, it was established that the 10-carbon fragment was derived from 2,4-decadienal.

In another experiment, *N*α-acetyl-lysine was incubated with 2,4-decadienal, which resulted in the formation of an ion with *m/z* of 321^+ that displayed an identical fragmentation pattern to the 321^+ ion found in urine **(Table 4.16)**. Notably, it was intriguing that the synthetic and urinary 321^+ displayed distinct retention times with 0.5

min apart. The difference in retention time was further confirmed by spiking mice urine with the reaction solution from *N*α-acetyl-lysine and 2,4-decadienal coincubation. The synthetic 321^+ and the urinary 321^+ again exhibited two distinct peaks of the same *m/z* (data not shown), with the synthetic counterpart eluted 0.5 min later than the urinary metabolite. At the same time, when incubating 2,4-decadienal with *N*ε-acetyl-lysine, an adduct with *m/z* of 321^+ was formed but had a significantly lower yield than incubating with the *N*α form (data not shown). In a separate animal feeding trial, mice were kept on the AIN-93G diet and gavaged with 2,4-decadienal. A urinary metabolite with *m/z* of 321^+ was detected in the dosed mice but not in the non-gavaged control. Subsequent analysis revealed a fragmentation pattern identical to the previously detected urinary and synthetic 321^+ ions. However, this metabolite displayed a retention time approximately 0.5 min later than the urinary 321^+ ion from mice fed HSO diet. Hence, it is reasonable to conclude that the urinary 321^+ ion of HSO-fed mice in the current feeding trial likely EXISTED IN AN ISOMERIC FORM TO FROM ITS SYNTHETIC COUNTERPARTS.

4.5 DISCUSSION

The current study aimed to identify the metabolic events associated with the free aldehydes through feeding HSO and HSO-Si to young mice, which had most of the free aldehydes removed. Through the metabolomic analysis of the digesta, feces, liver, kidney, serum, gallbladder, and urine, a series of metabolic changes associated with heated oil consumption were identified, including the PPARα activation, aldehyde detoxification activity, oxidative stress, tryptophan-NAD^+ pathway activation, and bile acid metabolism **(Figure 4.7)**. A novel urinary metabolite with *m/z* = 321^+ was identified as a free-aldehyde-responsive marker, likely derived from the interaction between free

lysine, 2,4-decadienal, and microbial metabolism within the gastrointestinal (GI) lumen **(Figure 4.7)**. The detailed metabolic pathways responsible for the events described above and the investigation of the urinary markers' structure are discussed below.

4.5.1 Influences of silica-based aldehyde abatement on the chemical composition of HSO

Based on the current findings, Si-PPZ was an effective adsorbing agent for lowering the free aldehyde concentration in HSO by over 80% **(Figure 4.1 C)**. However, this substantial decrease was not fully reflected in the proximate analyses. From the *p*-anisidine and TBARS values, the application of Si-PPZ removed the total aldehydic content by 56% and 60%, respectively **(Figure 4.1 B and A)**. The disparities among LC-MS, *p*-anisidine analysis, and TBARS analysis were primarily due to their different chemical natures.

LC-MS analysis, known for its high specificity and accuracy, quantified individual free lipidic aldehydes in heated soybean oil. This method, developed and validated to investigate the kinetics of aldehyde formation in heated soybean oil[66], is advantageous for quantitative aldehyde analysis. Conversely, *p*-anisidine (AnV) and TBARS are proximate approaches commonly used for assessing secondary LOPs.

The primary amine in the *p*-anisidine reagent forms a Schiff base with the carbonyl or aldehyde group in 2-alkenals and 2,4-dienals, and the AnV value of oxidized oils showed a strong inverse correlation with animal growth.[102] However, one limitation of the AnV assay is its higher colorimetric absorbance for products formed from unsaturated aldehydes than from saturated alkanals.[131] In the current study, the LC-MS

quantitative analysis revealed that Si-PPZ adsorbs unsaturated aldehydes more effectively than saturated alkanals **(Figure 4.1 C)**. Therefore, the incomplete reflection of total aldehyde reduction in the AnV values suggests that aldehydic species remain in the heated oil in forms other than free aldehydes. Meanwhile, TBARS assay displayed a similar reduction trend to AnV **(Figure 4.1 A)**. TBARS is commonly used for detecting malondialdehyde (MDA). Principally, each MDA molecule can react with 2 TBA molecules where each MDA molecule reacts with two TBA molecules to give a red chromophore absorbable at 532 nm.[374] Thus, the AnV and TBARS results confirm the presence of compounds containing additional carbonyl and aldehydic groups in the heated oils, even after silica treatment.

One potential example of such compounds is 9-oxononanoic acid generated from the homolytic β-scission of the hydroperoxide of oleic, linoleic, and linolenic acid.[107,210] The terminal carbonyl group can form a Schiff base with primary amines, AnV reagent included. Significant correlations between total glycerol core aldehyde (GCA) content and the AnV of frying rapeseed, sunflower, and cottonseed oils have been observed[210], and the free form of 9-oxononanoic acid can be detected in oxidized oils.[323,375] However, unlike aldehydes, 9-oxononanoic acid was not a major contributor to the compositional differences between heated and control soybean oil, revealed by a kinetic study of oil oxidation at frying temperature.[66] In the current study, multivariate data analysis identified lipidic aldehydes as more dominant markers separating the heated and non-heated oils **(Figure 4.1 E and F**). Nevertheless, 9-oxononanoic acid may exist as a glycerol core aldehyde (GCA), and remain bonded to the glycerol backbone.[210] Similar elevated GCAs were observed in heated oils, including those containing 7-oxo-nonanoic

acid, 8-oxooctanoic acid, 10-oxo-8-decenoic acid, and 11/13-oxo-9-octadecenoic acid.[209-212] These GCAs are fairly stable after prolonged heating (24 – 60 hours) at frying temperature.[210] It is reasonable to conclude that the GCAs were likely present in the HSO and HSO-Si, but were not identified via the lipidomic analysis of the oils.

Despite the extensive alteration in the chemical profile of the aldehydic LOPs, Si-PPZ exerted minimal impact on the major triglyceride species in the oils **(Figure 4.2 A)**. Triglycerides with higher degrees of unsaturation were more sensitive to heating, showing a significant reduction in their abundance **(Figure 4.2 A**), consistent with previous findings in heated soybean oil.[168] Additionally, the untargeted lipidomic analysis showed that heating decreased the triglycerides containing unsaturated fatty acids and led to the formation of additionally oxygenated TG (TG-OX) and triglycerides containing a caprylic acyl chain (TG-CA) **(Figure 4.2 D- G, Table 4.3)**, which were not removed by Si-PPZ. Profiling oxidized triglycerides, including GCAs, might be necessary to provide a more comprehensive evaluation of the oxidation status of oils.

4.5.2 Influences and significance of aldehyde abatement on animal growth

Growth performance was found to be hindered in animals consuming thermally oxidized oils, as evidenced by studies in pigs[105], poultry[102,105], and mice.[168] However, inconsistencies have been noted, with some animals showing tolerance and comparable growth to control groups.[105,130] The AnV level and the concentration of C9-C11 unsaturated aldehydes were identified as effective predictors of animal growth.[102] Furthermore, Guo et al. suggested an AnV threshold of 172, below which oils did not

adversely impact growth, possibly due to protective amino acid metabolism, though exceptions exist.[105,130]

In the current trial, the HSO utilized had an AnV of around 200, which is above the suggested threshold of 172, yet the average daily gain (ADG) of mice in the HSO group did not differ from the CSO group **(Figure 4.4 A)**. This discrepancy is potentially associated with the differing levels of oil oxidation. Comparing the oxidation status of oils used in different studies is challenging due to varying quality indicators and the limitations of their chemical natures. Xu et al. assessed oxidized oils with AnV maxing at 134 and total GCA maxing at 0.24 mg/g oil[210], while other studies reported heated oils with AnV about 45 accumulated approximately 0.21 mg/g oil of GCAs.[209] The HSO used in the current study had an AnV around 200, and the total free aldehydes were approximately 500 μg/g oil (equivalent to 0.5 mg/kg oil) **(Figure 4.1 B and C)**. AnV has been shown to positively correlate with the concentration of 4-hydroxynonenal (HNE) in the oxidized oils.[376] But its correlation with GCA has not been comprehensively characterized. Therefore, the applicability of the suggested cutoff of AnV at 172 as a tolerance threshold for predicting animal growth needs further investigation.

As indicated by the AnV value of the HSO-Si oil used in the current study, the aldehydic species other than the free aldehydes in the HSO impacted animal health (**Figure 4.1B, Figure 4.4**). Identifying and analyzing these compounds, such as GCAs, is challenging, requiring advanced analytical techniques and robust databases. Lipidomic studies used high-purity triglyceride standards like triolein and trilinolein[211], which could only reflect TG oxidations to a limited extent due to diverse lipid profiles in dietary oils.

Alternatively, thin-layer chromatography (TLC) can be applied to separate and analyze GCAs via GC-MS but requires extensive pre-column sample treatment.[209,210,377]

Furthermore, the toxicity of GCAs has not yet been thoroughly studied. According to the Safety Data Sheet, 9-oxononanoic acid is not classified in the Globally Harmonized System and has no known information on its toxicity or carcinogenicity. However, the aldehyde functional group still enables interaction with biological molecules, as shown in an *in-vitro* study.[378] As a result, comprehensive profiling of GCAs and polar contents of oils showing high AnV is needed to better understand the effects of oxidized oil consumption on metabolism.

4.5.3 Influence and significance of aldehyde-independent metabolic effects

4.5.3.1 Activation of tryptophan-NAD+ pathway, and PPARα

Tryptophan, an essential amino acid, is crucial in various physiological functions. In humans, approximately 30% of the tryptophan pool is allocated for protein synthesis, while a mere 1% contributes to serotonin synthesis. Significantly, over 66% of non-proteogenic tryptophan (more than 95% of its non-protein usage) is utilized in the tryptophan-NAD^+ pathway to synthesize NAD^+.[379,380] The upregulation of this pathway was considered a central metabolic response to HSO consumption, hallmarked by the decrease of serum tryptophan.[168] This phenomenon stems from a confluence of factors, including upregulated PPARα activation, a response to metabolic stress, and aldehyde detoxification, with NAD^+ serving as a cofactor for the enzymes involved.[168]

In the current experiment, HSO-induced tryptophan-NAD^+ activation was evidenced by the decreased serum tryptophan **(Table 4.12)** and a trend towards increase

of hepatic tryptophan (p=0.08, **Table 4.13**), consistent with previous reports on animals fed oxidized corn and soybean oil.[130,168] Notably, the change in serum tryptophan persisted even with dietary aldehyde abatement, as evidenced by the lack of main effect from Silica processing on the serum tryptophan **(Table 4.12)**.

A plausible explanation for the lack of improvement in serum tryptophan could result from the activation of peroxisome proliferator-activated receptor (PPAR). The subtype PPARα is expressed in organs involved in active fatty acid β-oxidation, particularly in the liver.[381] Consumption of heated oil reportedly upregulated the PPAR target genes involved in hepatic lipid transport and catabolism.[168,239,382] Physiologically, this activation manifests as peroxisome proliferation and hepatomegaly, observed as an increased liver weight to body weight (LW:BW) ratio in animals fed HSO.[9] This condition remained unaltered in the HSO-Si group **(Figure 4.4 B)**. Metabolically, the upregulation of PPARα was indicated by changes in urinary suberic and azelaic acid levels **(Figure 4.5 E and F)**, which likely resulted from the peroxisomal ω-oxidation of fatty acids due to PPARα upregulation. Under normal conditions, ω-oxidation of fatty acids is a minor catabolic pathway, compared to β-oxidation. Thus, the urinary dicarboxylic acids are suggested as convenient markers for PPARα activity and peroxisomal fatty acid oxidation.[168] The relative abundance of these medium-chain dicarboxylic acids increased significantly in both HSO and HSO-Si groups, unaffected by aldehyde abatement **(Figure 4.5 E and F)**. As a result, the PPARα upregulation was likely attributed by compounds in the HSO other than the free aldehydes.

Animal feeding studies have confirmed that oxidized fatty acids (OFAs), such as hydroxy- and cyclic-fatty acids, are more potent ligands of PPARα than unoxidized ones.[238,383,384] OFAs and OFA-containing triglycerides are common and abundant compounds in thermally oxidized oils.[211] The current study identified triglycerides containing OFAs and increased in HSO oil **(Figure 4.2 D and E)**. Based on the statistical analysis, silica treatment appeared to adsorb and lower the abundance of OFA-containing triglycerides **(Figure 4.2 D and E)**. However, compared to the dramatic extent to which free aldehydes were decreased **(Figure 4.1 C)**, the reduction of OFA-containing triglycerides was much milder, reasonably lacking potency in reversing the physiological response of PPARα.

Besides PPARα, aldehyde-metabolizing enzymes, such as aldehyde dehydrogenases (ALDHs), also require $NAD(P)^+$ as a cofactor.[168] The upregulation of aldehyde detoxification activity was evidenced by the increased urinary hydroxyalkenoic acids and their glycine conjugate in HSO and HSO-Si groups **(Figure 4.5)**, which likely derived from the oxidation of their respective hydroxyalkenals by ALDH.[168] Considering the significant reduction of total free aldehydes in the oils and the absence of reduction urinary hydroxyalkenoic acids in the HSO-Si group, it is reasonable to assume the presence of aldehyde-containing compounds in the HSO and HSO-Si other than free aldehydes. This hypothesis again aligned with the changes in the TBARS and AnV values of oils **(Figure 4.1 A and B)**, strengthening the need for comprehensive characterization of the triglycerides in the oxidized oils.

4.5.3.2 Stress response

Consumption of oxidized oils has been previously linked to exacerbated oxidative stress in animal models.[103,104,130,167,168] In the current trial, evidence of oxidative stress included elevated hepatic glutathione (GSH) levels and an increased GSH/GSSG ratio in both HSO and HSO-Si groups **(Figure 4.4 C and E)**, suggesting an overall shift towards a more reduced state within the hepatic environment. Nonetheless, the dynamic interplay between oxidants and antioxidants in response to oxidized oil intake appears complex.

Previous studies have reported varying effects of oxidized oil consumption on hepatic GSH levels. In a previous mice feeding trial, HSO consumption resulted in a decrease in hepatic GSH concentrations.[168] The discrepancy might be attributed to differences in aldehyde concentrations - the previous trial's HSO had approximately 800 mg/L total aldehydes (AnV and GSH/GSSG ratio not reported)[168], significantly higher than the HSO in the current study **(Figure 4.1 C)**. In that trial, the high aldehyde concentrations likely overwhelmed the antioxidant capacity, preventing the effective regeneration of GSH from GSSG. Conversely, in the current study, the mice likely retained the effective GSSG to GSH turnover. Regenerating GSH from GSSG, the enzyme glutathione reductase needs NADPH as electron donor, which is a direct phosphorylation product of NAD^+.[385] Therefore, the tryptophan was probably further consumed to fulfill the intensified need of NAD^+, which partially explained the lack of changes in serum tryptophan in the HSO-Si compared to HSO **(Table 4.12)**.

The variability in reports of glutathione levels complicates comparisons across studies. The GSH and GSH/GSSG ratio reduction were observed in mice chronically fed

used palm oil (oxidation status not reported), accompanied by liver injury.[386] Weaning piglets fed oxidized linseed oils (peroxide value 225 mEq O_2/kg oil) showed decreased hepatic GSH and unchanged GSSG.[387] Rats consuming thermally processed sunflower oils (peroxides concentration = 157.1 and 133.6 mM/kg oil) also exhibited lowered hepatic GSH levels, though the GSH/GSSG ratio was not reported.[388] Increased hepatic glutathione reductase activity was noted in another trial with oxidized sunflower oils (peroxide value = 262 mmol/kg oil), but without measuring GSH concentration.[389] Another rat-feeding trial showed reduced liver GSH and comparable glutathione reductase activity after feeding thermally oxidized coconut and mustard oils (AnV elevated, at 0.685 and 4.320, respectively).[390] These studies employed different measures of oil oxidation status and did not consistently report free aldehyde concentrations, complicating direct comparisons of dose-dependent effects on hepatic glutathione

Despite the significant reduction in free aldehydes in HSO-Si, oxidative stress persisted, as indicated by the GSH levels and GSH/GSSG ratio in the HSO-Si group **(Figure 4.4 C and E)**. Lipid peroxidation products, particularly lipidic aldehydes, are key contributors to redox imbalance and GSH depletion in the context of oxidized oil consumption.[130,168] GSH is used not only in neutralizing free radicals from lipidic hydroperoxides but also in detoxifying aldehydes via the mercapturic acid pathway.[200,203] Although silica treatment reduced free aldehydes, the presence of glycerol core aldehydes (GCAs) and other lipid oxidation products may still require detoxification, increasing the need for GSH **(Figure 4.4 C and E)**.

The persistence of oxidative stress despite aldehyde abatement suggests the involvement of other electrophilic aldehyde-containing compounds in HSO and HSO-Si. The metabolic fate of GCAs remains unclear, underscoring the need for further investigation into the roles of lipid oxidation products beyond free aldehydes. Comprehensive characterization of these compounds might be beneficial for better understanding their impact on oxidative stress and hepatic glutathione metabolism.

4.5.3.3 Luminal metabolome and functional metabolites

As discussed in the previous chapter, heated oil consumption extensively changed the luminal metabolome of pigs. Due to the significantly smaller size of the mice GI tract, digesta collection was limited to the ileum and cecum, with feces collected as the terminal point of the GI metabolome.

In contrast to the pigs, the proportion of lysine in the total free amino acid pool was elevated in heated oil groups and remained unaffected in the Si-processed groups in the ileum and cecum **(Table 4.5 and Table 4.6)**. Cocurrently, the fecal elimination of lysine was elevated by HSO, and even further increased by HSO-Si **(Table 4.7)**. Additionally, the free lysine in the serum **(Table 4.12)** was decreased in the HSO and HSO-Si groups. These findings suggest that HSO consumption likely impacted protein digestion and absorption, as implicated in the previous chapter. However, in the pig study, lysine in the intestinal lumen decreased with HSO feeding, contrasting with the increased ileal and fecal lysine observed in the current mice study **(Table 4.5 and Table 4.7)**. Lysine uptake in the intestine occurs via the system B0 neutral amino acid transporter B^0AT1 (SLC6A19), whose binding site consists of cysteine, phenylalanine,

leucine, asparagine, and serine. [391,392] The sulfhydryl group in cysteine[393], and terminal amine group in asparagine are potential targets for non-enzymatic interaction with aldehydes. It is plausible that luminal aldehydes affected this amino acid transporter, though direct evidence of such inhibition has not been clearly established. Digestive enzyme activities were not determined due to the limited quantity of mice digesta samples. Investigating the influence of HSO and HSO-Si on protein digestibility would be meaningful.

Interestingly, besides lysine, the distribution of other free amino acids in the feces was changed extensively by the feedings, showing the main effects of both oil oxidation and silica treatment **(Table 4.7)**. The gut microbiome can catabolize, utilize, ferment, and even synthesize amino acids[394], indicating that variations of free amino acids from cecal digesta to feces potentially reflect altered gut microbial metabolism. The underlying mechanism and association with host metabolism warrant further study.

In addition to the amino acids, the bile acid profile in the luminal metabolome was affected by HSO feeding. In the gallbladder, HSO intake exerted a main effect and decreased the proportion of TCDCA, MCA, TUDCA, while increased that of TCA. **(Table 4.8)**, indicating an extensive alteration in the non- and conjugated primary bile acids. Interestingly, the taurine was not affected in the serum **(Table 4.12)** and was increased in the liver **(Table 4.13)**, suggesting the adequate supply of taurine for primary bile acid conjugation. In the cecum and feces, the proportion of DCA stood out and showed a dramatic increase and was indifferent in HSO and HSO-Si groups, though its precursor, CA[395], was unaffected by the feedings **(Table 4.10 and Table 4.11)**. DCA is a

secondary bile acid, produced via the microbial metabolism of CA[396] and has been associated with increased cardiac output and blood pressure in rats.[397] The increase of fecal DCA was considered to have a promoting effect on colorectal tumor[398], intestinal inflammation[399], and intestinal barrier dysfunction.[400] Dietary intake significantly modulates DCA metabolism. As observed in a human study, the DCA was increased by 2- to 10-fold after consumption of an animal-based diet rich in meat, dairy, and eggs.[401] High-fat diet and high-protein intake could also increase fecal[402] and serum[403] DCA, respectively. However, due to the lack of response to aldehyde abatement in HSO-Si group, the implication of the increased DCA percentage in the cecum and fecal BA pool was not further investigated.

4.5.4 Influence and significance of aldehyde-dependent metabolic effects

4.5.4.1 Novel urinary biomarker identification

Lipidic aldehydes, such as 2,4-decadienal and 4-hydroxynonenal (HNE), are reactive compounds with potential toxicity, known to interact with key biological molecules including DNA and proteins.[45,173,175,404] These aldehydes have shown strong inverse correlations with animal growth.[102] In the current experiment, two novel urinary exposure markers were identified, annotated as 321^+ and 319^+ ion. Based on the MSMS fragmentation pattern and comparison with synthetic lysine-DDE adducts, the structural moieties of the two markers were putatively determined **(Table 4.16)**. Given their distribution in the GI tract and response to the HSO-Si feeding, it is reasonable to presume their origin from microbial-catalyzed acetylation on the 2,4-decadienal-lysine adduct.

Lysine, an essential amino acid for growing mice, contains a unique primary amine group on the side chain (*N*ε), which is reactive towards aldehydes via forming Schiff-base and Michael-type adducts.[45,173,175,404] Both ε and α positions can form adducts, with higher activity at the ε end.[404] Many reported adducts showed fragments of 84^+ and 130^+ from the lysine moiety[404], which aligned with the fragmentation pattern of the urinary 321^+ and 319^+ ions in the current study. Additionally, Although both Schiff-base and Michael-type lysine-DDE adducts can form, the Schiff-base is preferred by basic amino acid residues.[405] For instance, a typical *N*α-acetyl-lysine-DDE Schiff-type adduct has a *m/z* of 323^+ **(Figure 4.8 A)**, which was synthesized from coincubating *N*α-acetyl-lysine with DDE. An oxidized form with *m/z* of 321^+ was detected from the same incubation experiment **(Figure 4.8 B, Table 4.16)**, containing a pipecolic acid moiety and displaying the same fragmentation pattern as the urinary 321^+. However, the urinary 321^+ had an earlier retention time, possibly due to the rearrangement of the decadienal moiety **(Figure 4.8 C)**.

DDE, known for its reactivity with amino acids, can rearrange and form pyridine structures.[406-408] For example, the formation of 2-pentylpyridine in the reaction between DDE and phenylalanine was documented.[408] This process is also sensitive to pH, showing the highest yield in a neutral environment.[409] Additionally, a pyridine-type structure was observed in DDE-modified proteins, but was detected as a dimeric DDE adduct.[410] Similarly, a compound containing a butyl pyridine structure was formed from hexenal reaction with ammonia.[411] These pyridine-type adducts were mostly observed *in-vitro*, such as soybean protein isolates[409], or in reactions of authentic standards.[408,411] The typical pH in the small and large intestines ranges between 6-7.5, which is relatively

neutral. Therefore, the formation of a lysine-DDE adduct containing a pyridine structure in the GI tract appears feasible. Our *in-vitro* study also confirmed that the *N*α-acetyl-lysine rearranged to an acetylated pipecolic acid without enzymatic facilitation **(Table 4.16)**. This finding aligns with studies reporting the presence of 2-pentylpyridines in foods, as a result of Maillard reaction between amino acids and oxidized lipids.[322] However, neither the free form of 2-pentylpyridine, nor lysine-DDE adducts (*m/z* = 279^+ or 281^+) were detected in the aqueous extract of the feed extracts or digesta, warranting further study into the interactions of amino acid-aldehyde adducts in the GI lumen.

The presence of an acetyl group in the 321^+ metabolite raises questions about its origin. While aldehydes can interact with amino acids non-enzymatically, acetylation typically involves enzymes such as acetyltransferase. Lysine acetylation is a common post-translational modification in both pro- and eukaryotes, usually occurring on the ε-position of protein-bound lysine. However, the gut microbiome can produce *N*α-acetyl-lysine, which antagonizes SCFA production.[412] Moreover, the *N*α-acetyl-ε-(2-propenal)lysine (APL) was identified as a urinary marker for malondialdehyde.[413] Its urinary excretion increased in rats fed oxidized cod liver oil and decreased in those fed hydrogenated coconut oil, a highly saturated oil. McGirr et al. suggested that this urinary metabolite could result from the pre-existing APL in the MDA-albumin complex, or *in-vivo* formation, given the detection of APL in the urine of mice fed only the sodium MDA salt.[413] However, the detailed pathway leading to APL formation remains to be fully characterized.

Based on the detection sites and the increasing relative abundance from the ileum to feces **(Table 4.15, Figure 4.6)**, we propose a potential pathway for the *de-novo* formation of 321^+ **(Figure 4.9)**. This cascade initiates with DDE **(Figure 4.9 A)** oxidation, producing an epoxide, 4,5-epoxy-2-decenal **(Figure 4.9 B).** Such transformation was observed in the thermal oxidation of linoleic acid, as an oxidation product of 2,4-decadienal[414], and the autooxidation of arachidonic acid.[415] At the same time, free lysine **(Figure 4.9 C)**, becoming available in the stomach as protein hydrolysis begins, reacts with the aldehyde group of 4,5-epoxy-2-decenal at the active ε-position, yielding a hydroxy-DDE-lysine **(Figure 4.9 D)**. This intermediate is hypothesized to undergo further rearrangement, forming a pyridine structure *de novo* **(Figure 4.9 E)**. Eventually, the gut microbiome in the large intestine carries out the α-acetylation of lysine and yields the 321^+ metabolite **(Figure 4.9 F)**.

Considering the similarities in MSMS fragmentation patterns as detailed in **Table 4.4**, it is reasonable to presume 319^+ as an oxidation product of the 321^+ metabolite. This hypothesis was additionally supported by the *m/z* shift of fragments **(Table 4.16)**, suggesting the additional oxidation site on the DDE arm. However, in our attempts to synthesize the 321^+ metabolite, coincubation of *N*-acetyl-lysines with DDE failed to produce ions with *m/z* of 319^+. Alternatively, a potential origin of this compound is the decatrienal, produced from oxidized linolenic acid (LNA).[416] Soybean oil contains about 8% linolenic acid[320], which provides the viable precursor for decatrienal. However, decatrienal is not a dominant species in the aldehyde pool of HSO[266], requiring further studies to elucidate the origin and formation pathway of 319^+.

Previous animal studies revealed that DDE is quickly detoxified in the liver, transforming to a carboxylic acid, alcohol, or GSH-conjugate, which are further metabolized and excreted as 2,4-decenoic acid and cysteine-conjugated 2,4-decadienol, serving as urinary biomarkers for mice gavaged with DDE.[417] The difference in urinary biomarkers was unlikely attributed to the varying DDE dosages. In our current study, mice fed the HSO diet had an average daily feed intake of 2.4g (data not shown), equivalent to 39 mg DDE for a 20 g mouse. Mice were also gavaged with 20 mg/mL DDE-containing oil, equivalent to 20 mg DDE for a 20g mouse. Pan et al. adopted a range of doses of DDE, including 0.5, 1, and 2mg DDE /g body weight.[417] The highest dose was equivalent to 40 mg DDE for a 20-g mouse, comparable to the dosing of DDE in the current aldehyde abatement feeding study. Therefore, the chemical nature and potential dose-dependent response of the 321^+ and 319^+ markers still warrant more investigation.

4.5.4.2 Gut microbial metabolism

The gut microbial metabolism showed responses to aldehyde abatement via two aspects. The first aspect was the increased secondary to primary BA ratio in HSO groups in the cecal digesta and feces **(Table 4.10 and 4.11)**. Interestingly, in the feces, this trend was relieved by HSO-Si **(Table 4.11**), suggesting the potential association with free aldehydes in the oils. Given the known association between gut microbial metabolism on bile acid and host health[418], it will be interesting to investigate the aldehyde-specific influence on the gut microbiome.

The second aspect was implicated by observing cecal short-chain fatty acids **(Figure 4.3)**. It is intriguing that all four SCFAs were elevated by HSO and then ameliorated by HSO-Si **(Figure 4.3)**. Such a trend contrasts with the findings from other feeding studies in which animals were fed oxidized oils and experienced decreased butyrate[99,100,253,254], or indifferent butyrate[255], propionate[254,255], acetate, and valerate[99,100,252-255]. The potential reasons for the discrepancies were discussed in the previous chapter. Meanwhile, the molecular mechanisms of oxidized lipid's influence on the microbiome remain an area to further study.

4.6 CONCLUSION

Overall, the current study adopted a novel approach to remove the free aldehydes in the HSO via silica treatment to identify potential aldehyde-dependent events among the HSO-elicited metabolic changes. Despite the effective reduction of total aldehyde content, the AnV and TBARS values suggested the potential presence of other aldehyde-containing compounds, such as GCAs. However, more lipidomic analysis would be needed to characterize the oxidized lipid species in the HSO comprehensively. Even though the growth performances of HSO and HSO-Si groups were comparable to the control groups, characterization of the urinary metabolome revealed novel urinary metabolites potentially related to the metabolism of 2,4-decadienal and lysine. To our knowledge, the current study is the first to report the detection of a urinary metabolite featuring a DDE and acetyl-lysine moiety. Nonetheless, the structure and biosynthesis pathway of the identified markers still warrants additional investigation.

4.7 TABLES AND FIGURES

Table 4.1 Reagents and chemicals used for sample preparation, LC-MS analysis, quantification, and biochemical assays.

Chemical/Reagents	Vendor
Acetone (LC-MS grade), Acetonitrile (LC-MS grade, ACN), Ammonium formate, Dichloromethane (GC grade), Formic acid (LC-MS grade), Isopropanol (LC-MS grade), Methanol (LC-MS grade), *n*-Butanol (HPLC grade), Sodium chloride (NaCl), Sodium sulfate (anhydrous), Water (LC-MS grade)	Fisher Scientific (Houston, TX)
2-Hydrazinoquinoline (HQ), Triphenylphosphine (TPP), *p*-Anisidine,	Alfa Aesar (Ward Hill, MA)
Ammonium carbonate ($(NH_4)_2CO_3$), 2-2′-Dipyridyl disulfide (DPDS), Sodium hydroxide (NaOH), *N*ε-acetyl-lysine	MP Biomedicals, LLC (Irvine, CA)
D_4-acetic acid, Amino acid standards, Dansyl chloride (DC), Dimethyl sulfoxide (DMSO), Leucine enkephalin, Magnesium chloride ($MgCl_2$), Potassium chloride (KCl), Potassium phosphate monobasic (KH_2PO_4), Reserpine, Sodium bicarbonate ($NaHCO_3$), Sodium carbonate (Na_2CO_3), 2-Thiobarbituric acid, ^{15}N-lysine (lysine-2-^{15}N), Bile acid standards, Glycocholic acid-$^{13}C_1$	Sigma-Aldrich (St. Louis, MO)
2,4-Dinitrophenylhydrazine (DNPH), *N*-Hexane	Honeywell (Charlotte, NC)
D_5-Tryptophan	Cambridge Isotope Laboratories (Tewksbury, MA)
D_6-acetone, Trichloroacetic acid, BCA assay kit	Thermo Fisher Scientific (Waltham, MA)
Ethanol (reagent alcohol)	Ricca Chemicals (Arlington, TX)
Ethyl acetate	Mallinckrodt Chemicals (Ireland)
Guanidine hydrochloride, Isooctane	TCI (Japan)
^{13}C-1,2-palmitic acid, d_8-lysine (lysine-3,3,4,4,5,5,6,6-D8)	CDN Isotopes (Canada)
Nα-acetyl-lysine	Chem-Impex International (Wood Dale, IL)
Aldehyde standards	Bedoukian Research (Danbury, CT)

Table 4.2 LC-MS instrumental settings for data acquisition.

Target compounds	LC column and temperature	LC mobile phase	Lock mass and MS detection mode	Capillary and cone voltage	Source and desolvation temperature	Cone and desolvation gas flow	Collision gas and energy ramp
Amino acids (DC derivatization), and urine samples (non-derivatized)	Waters BEH C18, 40 °C	A: 0.1% formic acid in water B: 0.1% formic acid in ACN	Leucine enkephalin ($[M + H]^+$ = *m/z* 556.2771), Positive	0.2 kV, 40 V	120 °C, 350 °C	50 L/hr, 600 L/hr (N_2)	Argon, 10-50 eV
Fatty acids, aldehydes (HQ derivatization)	Waters BEH C18, 40 °C	A: 2 mM NH_4OAc in water with 0.05% acetic acid B: 2 mM NH4OAc in 95% ACN and 5% H_2O with 0.05% acetic acid	Leucine enkephalin ($[M + H]^+$ = *m/z* 556.2771), Positive	0.2 kV, 40 V	120 °C, 350 °C	50 L/hr, 600 L/hr (N_2)	Argon , 10-50 eV
Triglycerides	Waters BEH C8, 60 °C	A: 40% MeOH in water, with 0.1% formic acid, 10 mM ammonium formate B: 100% MeOH, with 0.1% formic acid, 10 mM ammonium formate	Reserpine ($[M + H]^+$ = *m/z* 609.2812), Positive	0.2 kV, 40 V	120 °C, 500 °C	40 L/hr, 600 L/hr (N_2)	Argon , 10-50 eV
Bile acids	Waters BEH C18, 40 °C	A: 10 mM NH_4OAc, pH 9, in water B: 95% ACN with 5% A	Leucine enkephalin ($[M - H]^-$ = *m/z* 554.2615), Negative	0.2 kV, 40 V	120 °C, 350 °C	50 L/hr, 600 L/hr (N_2)	Argon, 10-50 eV

Table 4.3 Identification of aldehydes in heated soybean oils.

	Molecular formula	Detected ion	Detected molecular formula	Detected *m/z*	Monoisotopic mass of detected ion	Mass deviation (Δ ppm)
2-Heptenal	$C_7H_{12}O$	$[M+HQ]^+$	$C_{16}H_{20}N_3$	254.1663	254.1657	2.36
2,4-Heptadienal	$C_7H_{10}O$	$[M+HQ]^+$	$C_{16}H_{18}N_3$	252.1506	252.1501	1.98
2-Octenal	$C_8H_{14}O$	$[M+HQ]^+$	$C_{17}H_{22}N_3$	268.1817	268.1814	1.12
2,4-Nonadienal	$C_9H_{14}O$	$[M+HQ]^+$	$C_{18}H_{22}N_3$	280.1814	280.1814	0.00
2,4-Decadienal	$C_{10}H_{16}O$	$[M+HQ]^+$	$C_{19}H_{24}N_3$	294.1971	294.1970	0.27
2-Decenal	$C_{10}H_{18}O$	$[M+HQ]^+$	$C_{19}H_{26}N_3$	296.2123	296.2127	-1.35
4-HNE	$C_9H_{16}O_2$	$[M+HQ]^+$	$C_{18}H_{24}N_3O$	298.1916	298.1919	-1.13
2-Undecenal	$C_{11}H_{20}O$	$[M+HQ]^+$	$C_{20}H_{28}N_3$	310.2284	310.2283	0.25

Table 4.4 Identification of triglyceride species from soybean oils.

	TG species	Molecular formula	Detected ion	Detected molecular formula	Detected *m/z*	Monoisotopic mass of detected ion	Mass deviation (Δ ppm)	Major fragments
I_o	TG(18:2/18:2/18:3)	$C_{57}H_{96}O_6$	$[M+NH_4]^+$	$C_{57}H_{100}NO_6^+$	894.7554	894.7551	0.34	595, 597, 599, 877
II_o	Tripentadecanoin*	$C_{48}H_{92}O_6$	$[M+NH_4]^+$	$C_{48}H_{96}NO_6^+$	782.7222	782.7238	-2.04	523
III_o	TG(18:2/18:2/18:2)	$C_{57}H_{98}O_6$	$[M+NH_4]^+$	$C_{57}H_{102}NO_6^+$	896.7714	896.7707	0.78	599, 879
IV_o	TG(16:0/18:2/18:2)	$C_{55}H_{98}O_6$	$[M+NH_4]^+$	$C_{55}H_{102}NO_6^+$	872.7702	872.7707	-0.57	575, 599, 855
V_o	TG(18:1/18:2/18:2)	$C_{57}H_{100}O_6$	$[M+NH_4]^+$	$C_{57}H_{104}NO_6^+$	898.7886	898.7863	2.56	599, 601, 881
VI_o	TG(16:0/18:1/18:2)	$C_{55}H_{100}O_6$	$[M+NH_4]^+$	$C_{55}H_{104}NO_6^+$	874.7859	874.7863	-0.46	575, 577, 601, 857
VII_o	TG(18:1/18:1/18:2)	$C_{57}H_{102}O_6$	$[M+NH_4]^+$	$C_{57}H_{106}NO_6^+$	900.8015	900.8020	-0.56	599, 604, 603, 883
$VIII_o$	TG(16:0/18:1/18:1)	$C_{55}H_{102}O_6$	$[M+NH_4]^+$	$C_{55}H_{106}NO_6^+$	876.8015	876.8020	0.57	577, 603, 859
IX_o	TG(18:1/18:1/18:1)	$C_{57}H_{104}O_6$	$[M+NH_4]^+$	$C_{57}H_{108}NO_6^+$	902.8176	902.8176	0.00	603, 885
	TG(18:0/18:1/18:3-O)	$C_{57}H_{100}O_7$	$[M+Na]^+$	$C_{57}H_{100}O_7Na^+$	919.7314	919.7366	-5.65	319, 321, 599, 621, 637, 639
	TG(18:0/18:1/18:2-O)	$C_{57}H_{102}O_7$	$[M+Na]^+$	$C_{57}H_{102}O_7Na^+$	921.7417	921.7523	-11.50	319, 321, 601, 623, 639, 641
	TG(8:0/18:1/18:2)	$C_{47}H_{82}O_6$	$[M+NH_4]^+$	$C_{47}H_{86}NO_6^+$	762.6549	762.6611	-8.13	463, 465, 601, 745
	TG(8:0/18:2/18:2)	$C_{47}H_{84}O_6$	$[M+NH_4]^+$	$C_{47}H_{88}NO_6^+$	760.6395	760.6455	-7.89	463, 599, 621, 743

**compared with authentic standard*

Table 4.5 Amino acid profile in the ileum digesta. *Indicates statistical significance (*p*-value < 0.05 from non-paired two-way ANOVA test)

% (by µg/mL)	CSO	CSO-Si	HSO	HSO-Si	Heat	Silica	Heat:Silica
Alanine	1.65 ± 0.72	1.70 ± 0.72	1.49 ± 0.42	1.63 ± 0.86	0.75	0.78	0.90
Arginine	11.64 ± 1.42	12.66 ± 2.24	12.28 ± 1.27	12.63 ± 0.59	0.69	0.37	0.66
Asparagine	5.14 ± 1.12	4.93 ± 1.55	6.35 ± 1.09	6.25 ± 0.55	*	0.79	0.91
Aspartic acid	3.13 ± 0.11	3.21 ± 0.94	3.55 ± 0.40	3.49 ± 0.53	0.25	0.98	0.81
Citrulline	0.12 ± 0.13	0.31 ± 0.43	0.25 ± 0.19	0.10 ± 0.06	0.74	0.84	0.19
Glutamate	9.93 ± 1.48	10.28 ± 1.06	9.60 ± 1.03	11.35 ± 2.04	0.62	0.18	0.36
Glutamine	4.81 ± 0.61	5.09 ± 1.42	3.97 ± 1.23	4.16 ± 0.59	0.11	0.65	0.93
Glycine	3.84 ± 0.16	3.69 ± 0.15	3.98 ± 1.00	3.79 ± 0.19	0.65	0.53	0.93
Histidine	1.74 ± 0.35	1.66 ± 0.44	1.66 ± 0.29	1.68 ± 0.16	0.84	0.86	0.78
Iso/Leucine	6.54 ± 0.84	5.68 ± 0.51	5.11 ± 0.73	4.76 ± 0.75	*	0.12	0.49
Lysine	9.88 ± 1.07	9.33 ± 1.26	11.75 ± 1.85	10.96 ± 0.86	*	0.33	0.85
Methionine	2.51 ± 0.50	2.72 ± 0.29	2.14 ± 0.50	2.34 ± 0.42	0.11	0.36	0.98
Ornithine	0.03 ± 0.02	0.13 ± 0.11	0.09 ± 0.07	0.04 ± 0.04	0.63	0.45	0.07
Phenylalanine	6.63 ± 1.53	5.47 ± 1.68	5.78 ± 1.05	5.21 ± 0.40	0.40	0.20	0.65
Proline	2.67 ± 0.33	2.10 ± 0.26	2.39 ± 0.23	2.07 ± 0.40	0.35	*	0.46
Serine	5.19 ± 0.40	5.11 ± 1.36	5.21 ± 1.62	5.33 ± 0.68	0.84	0.98	0.86
Taurine	6.86 ± 2.75	10.87 ± 2.63	6.91 ± 0.60	7.01 ± 1.28	0.08	0.07	0.08
Threonine	4.22 ± 0.30	3.45 ± 0.53	4.00 ± 0.48	3.92 ± 0.44	0.60	0.08	0.15
Tryptophan	1.62 ± 0.79	0.96 ± 0.40	2.49 ± 0.96	1.98 ± 0.76	*	0.15	0.85
Tyrosine	5.89 ± 3.56	6.05 ± 1.82	5.92 ± 3.59	6.45 ± 0.97	0.87	0.80	0.89
Valine	5.99 ± 0.51	4.57 ± 0.87	5.11 ± 0.78	4.85 ± 0.83	0.45	*	0.16

Table 4.6 Amino acid profile in the cecum digesta. *Indicates statistical significance (p-value < 0.05 from non-paired two-way ANOVA test)

% (by µg/g digesta)	CSO	CSO-Si	HSO	HSO-Si	Heat	Silica	Heat:Silica
Alanine	6.86 ± 0.95	6.10 ± 0.41	6.05 ± 0.38	6.13 ± 0.49	0.22	0.28	0.19
Arginine	2.82 ± 0.95	2.69 ± 0.37	5.87 ± 2.62	4.12 ± 2.93	0.08	*	*
Asparagine	2.04 ± 0.78	3.63 ± 0.37	2.00 ± 0.53	3.29 ± 0.97	0.60	*	0.68
Aspartic acid	1.70 ± 0.28	3.31 ± 0.94	1.19 ± 0.72	1.81 ± 0.93	*	*	0.22
Citrulline	1.22 ± 0.73	2.43 ± 1.08	2.21 ± 0.31	1.56 ± 0.75	0.87	0.48	*
Glutamate	15.19 ± 3.86	17.75 ± 4.07	12.54 ± 4.40	14.01 ± 5.30	0.18	0.38	0.81
Glutamine	3.10 ± 2.04	3.09 ± 1.08	2.57 ± 0.68	6.95 ± 2.47	0.97	0.21	0.78
Glycine	3.93 ± 0.44	3.41 ± 0.18	3.85 ± 1.27	3.13 ± 0.33	0.61	0.10	0.77
Histidine	0.04 ± 0.06	0.03 ± 0.03	0.04 ± 0.03	0.04 ± 0.02	0.29	0.77	0.59
Iso/Leucine	13.91 ± 2.61	10.18 ± 2.10	13.75 ± 2.41	11.25 ± 4.48	0.77	0.06	0.69
Lysine	0.72 ± 0.43	0.61 ± 0.11	0.51 ± 0.19	0.54 ± 0.13	*	0.37	0.44
Methionine	2.47 ± 1.12	1.56 ± 0.47	1.78 ± 0.95	1.97 ± 1.02	0.77	0.45	0.25
Ornithine	2.19 ± 0.44	2.44 ± 0.25	2.12 ± 0.22	2.49 ± 0.75	0.79	0.83	0.84
Phenylalanine	9.58 ± 4.29	7.57 ± 1.54	11.41 ± 2.13	8.68 ± 2.48	0.32	0.12	0.80
Proline	3.69 ± 0.48	2.73 ± 0.23	2.53 ± 0.32	3.13 ± 0.26	*	0.30	*
Serine	4.50 ± 0.56	3.25 ± 0.41	4.20 ± 0.40	3.14 ± 1.11	0.56	*	0.78
Taurine	1.32 ± 2.14	1.52 ± 1.62	2.07 ± 3.02	4.07 ± 4.49	0.30	0.48	0.56
Threonine	4.37 ± 0.42	4.62 ± 0.16	4.15 ± 0.63	3.76 ± 1.28	0.18	0.87	0.41
Tryptophan	2.64 ± 1.50	1.83 ± 0.63	3.08 ± 0.76	2.39 ± 1.16	0.37	0.19	0.92
Tyrosine	6.22 ± 5.52	11.30 ± 1.40	7.07 ± 1.07	8.83 ± 5.50	0.69	0.11	0.42
Valine	11.48 ± 2.12	9.96 ± 2.12	11.00 ± 1.08	8.71 ± 1.83	0.36	0.06	0.68

Table 4.7 Amino acid profile in the feces. *Indicates statistical significance (p-value < 0.05 from non-paired two-way ANOVA test)

% (by µg/g feces)	CSO	CSO-Si	HSO	HSO-Si	Heat	Silica	Heat:Silica
Alanine	9.60 ± 0.49	10.60 ± 1.18	9.71 ± 0.21	7.98 ± 2.11	0.05	0.66	*
Glycine	3.56 ± 0.43	4.57 ± 1.16	4.08 ± 0.16	3.62 ± 0.67	0.48	0.54	*
Taurine	0.78 ± 0.98	1.34 ± 2.20	0.21 ± 0.12	12.79 ± 9.19	0.10	*	*
Phenylalanine	3.19 ± 0.55	3.16 ± 0.14	3.04 ± 0.10	2.54 ± 0.64	*	0.11	0.11
Glutamate	23.61 ± 5.21	19.89 ± 4.07	17.39 ± 1.16	13.97 ± 4.53	*	0.11	0.77
Serine	4.70 ± 0.45	5.18 ± 1.24	6.15 ± 0.12	4.21 ± 0.93	0.48	0.08	*
Valine	15.18 ± 2.32	13.43 ± 2.88	12.33 ± 0.94	8.16 ± 2.77	*	*	0.31
Threonine	3.96 ± 0.41	3.55 ± 0.56	4.74 ± 0.21	2.88 ± 0.85	0.43	*	*
Leucine/Isoleucine	8.53 ± 1.18	7.70 ± 1.21	7.21 ± 0.60	4.57 ± 1.53	*	*	0.10
Asparagine	1.43 ± 0.64	2.33 ± 1.57	3.42 ± 0.53	3.44 ± 1.48	*	0.21	0.61
Aspartic acid	4.05 ± 1.34	2.97 ± 0.65	3.27 ± 0.44	1.78 ± 0.65	0.07	*	0.65
Proline	2.09 ± 0.59	3.28 ± 1.56	1.87 ± 0.21	2.37 ± 0.58	0.19	0.12	0.40
Citrulline	3.57 ± 1.03	2.97 ± 1.69	2.95 ± 0.76	1.52 ± 0.76	0.10	0.08	0.36
Tyrosine	2.41 ± 0.51	2.28 ± 1.24	2.61 ± 0.29	2.61 ± 0.83	0.76	0.62	0.82
Methionine	2.31 ± 0.34	2.77 ± 0.30	2.56 ± 0.26	2.64 ± 0.42	0.89	0.20	0.25
Arginine	2.71 ± 0.77	3.48 ± 2.32	6.07 ± 0.39	9.61 ± 3.65	*	*	*
Lysine	5.47 ± 0.44	8.12 ± 0.62	8.65 ± 0.19	12.57 ± 3.17	*	*	*
Histidine	0.29 ± 0.13	0.37 ± 0.11	0.33 ± 0.07	0.33 ± 0.11	0.94	0.36	0.57
Tryptophan	0.44 ± 0.06	0.42 ± 0.08	0.33 ± 0.03	0.24 ± 0.10	*	0.08	0.18
Ornithine	0.34 ± 0.09	0.31 ± 0.06	0.32 ± 0.12	0.54 ± 0.30	0.06	0.06	*
Glutamine	1.80 ± 0.49	1.26 ± 0.84	2.75 ± 0.15	1.62 ± 0.45	*	*	0.38

Table 4.8 Bile acid profile of gallbladder. *Indicates statistical significance (*p*-value < 0.05 from non-paired two-way ANOVA test). MCA, muricholic acid; TMCA, Tauromuricholic acid; CA, cholic acid; TCA, Taurocholic acid; TDCA, Taurodeoxycholic acid; TCDCA, Taurochenodeoxycholic acid; TUDCA, Tauroursodeoxycholic acid.

% of total BA (by µg/mL)	CSO	CSO-Si	HSO	HSO-Si	Heat	Silica	Heat:Silica
CA	0.09 ± 0.03	0.15 ± 0.17	0.08 ± 0.05	0.09 ± 0.04	0.53	0.54	0.58
TCDCA	3.63 ± 0.59	2.79 ± 0.24	2.00 ± 0.46	1.76 ± 0.20	*	0.38	0.52
MCA	0.18 ± 0.07	0.18 ± 0.08	0.07 ± 0.03	0.02 ± 0.03	*	0.24	0.12
TMCA	48.22 ± 2.69	45.12 ± 1.36	47.86 ± 5.22	51.04 ± 1.85	*	*	0.19
TUDCA	8.87 ± 1.63	10.44 ± 0.65	7.28 ± 1.78	8.50 ± 0.47	*	0.43	0.30
TDCA	4.22 ± 0.28	5.72 ± 2.41	2.05 ± 0.96	1.91 ± 0.91	0.11	0.89	0.10
TCA	34.78 ± 1.81	35.61 ± 2.30	40.65 ± 3.10	36.67 ± 2.56	*	0.07	0.80

Table 4.9 Bile acid profile of ileum digesta. *Indicates statistical significance (*p*-value < 0.05 from non-paired two-way ANOVA test). MCA, muricholic acid; TMCA, Tauromuricholic acid; CA, cholic acid; TCA, Taurocholic acid; UDCA, Ursodeoxycholic acid; TDCA, Taurodeoxycholic acid; TCDCA, Taurochenodeoxycholic acid; GCA, Glycocholic acid.

% of total BA (by µg/mL)	CSO	CSO-Si	HSO	HSO-Si	Heat	Silica	Heat:Silica
MCA	1.19 ± 2.28	2.38 ± 4.49	0.37 ± 0.36	1.27 ± 1.97	0.49	0.45	0.91
TMCA	45.62 ± 6.27	41.54 ± 3.94	44.10 ± 3.87	45.44 ± 3.78	0.61	0.56	0.26
CA	2.57 ± 4.92	4.64 ± 8.69	1.46 ± 1.53	1.99 ± 2.88	0.49	0.63	0.77
TCDCA	5.14 ± 1.48	4.24 ± 2.41	1.93 ± 0.49	2.21 ± 1.07	*	0.69	0.45
GCA	0.29 ± 0.11	0.36 ± 0.07	0.29 ± 0.10	0.16 ± 0.06	*	0.49	*
TDCA	7.06 ± 2.02	9.87 ± 7.09	4.55 ± 0.63	3.41 ± 2.20	*	0.67	0.33
TCA	38.05 ± 3.91	36.79 ± 8.48	47.24 ± 1.39	45.41 ± 3.90	*	0.56	0.91
UDCA	0.08 ± 0.09	0.18 ± 0.32	0.06 ± 0.03	0.10 ± 0.13	0.60	0.43	0.71

Table 4.10 Bile acid profile of cecum digesta. *Indicates statistical significance (*p*-value < 0.05 from non-paired two-way ANOVA test) MCA, muricholic acid; TMCA, Tauromuricholic acid; CA, cholic acid; TCA, Taurocholic acid; UDCA, Ursodeoxycholic acid; TDCA, Taurodeoxycholic acid; LCA, lithocholic acid; DCA, deoxycholic acid; GCA, Glycocholic acid.

% of total BA (by µg/g digesta)	CSO	CSO-Si	HSO	HSO-Si	Heat	Silica	Heat:Silica
MCA	57.56 ± 30.60	66.11 ± 13.08	37.07 ± 3.80	42.41 ± 8.20	0.84	0.79	0.19
TMCA	10.26 ± 18.95	1.49 ± 1.60	1.87 ± 2.41	7.70 ± 9.20	0.40	0.37	0.34
LCA	0.88 ± 0.55	1.21 ± 0.28	0.51 ± 0.21	0.65 ± 0.19	*	0.20	0.60
CA	4.69 ± 4.90	4.47 ± 5.14	9.22 ± 11.15	6.99 ± 6.35	0.35	0.74	0.79
DCA	13.17 ± 7.63	19.88 ± 7.93	42.24 ± 10.00	33.19 ± 11.92	*	0.81	0.12
TDCA	0.87 ± 1.56	0.25 ± 0.29	0.71 ± 0.65	0.65 ± 0.49	0.79	0.46	0.54
TCA	7.96 ± 15.31	0.51 ± 0.24	0.83 ± 1.08	3.96 ± 5.09	0.66	0.60	0.22
UDCA	4.60 ± 3.03	6.08 ± 1.23	7.54 ± 1.46	4.46 ± 0.88	0.49	0.40	*
DCA+LCA+UDCA+MDCA / TMCA+TCA+MCA+CA	0.30 ± 0.26	0.37 ± 0.14	1.05 ± 0.38	0.64 ± 0.29	*	0.23	0.10

Table 4.11 Bile acid profile of feces. *Indicates statistical significance (p-value < 0.05 from non-paired two-way ANOVA test). MCA, muricholic acid; TMCA, Tauromuricholic acid; CA, cholic acid; TCA, Taurocholic acid; UDCA, Ursodeoxycholic acid; TDCA, Taurodeoxycholic acid; TCDCA, Taurochenodeoxycholic acid; LCA, lithocholic acid; DCA, deoxycholic acid; GCA, Glycocholic acid.

% of total BA (by µg/g feces)	CSO	CSO-Si	HSO	HSO-Si	Heat	Silica	Heat:Silica
MCA	56.99 ± 6.03	56.18 ± 15.87	34.70 ± 2.14	33.80 ± 6.46	*	0.85	0.99
TMCA	1.08 ± 0.43	5.94 ± 8.56	0.58 ± 0.25	8.08 ± 6.36	0.76	*	0.63
LCA	5.19 ± 2.05	4.28 ± 1.65	1.76 ± 0.51	0.59 ± 0.28	*	0.15	0.85
CA	4.56 ± 4.34	7.23 ± 9.37	2.95 ± 1.10	10.95 ± 8.52	0.76	0.14	0.44
DCA	23.19 ± 1.80	17.46 ± 5.59	46.74 ± 1.75	33.05 ± 11.03	*	*	0.23
TCA	0.78 ± 0.33	3.20 ± 2.89	0.78 ± 0.40	7.75 ± 6.36	0.22	*	0.22
UDCA	8.22 ± 1.81	5.71 ± 0.38	12.50 ± 1.12	5.77 ± 2.26	*	*	*
DCA+LCA+UDCA+MDCA / TMCA+TCA+MCA+CA	0.58 ± 0.07	0.38 ± 0.11	1.57 ± 0.17	0.70 ± 0.0.33	*	*	*

Table 4.12 Amino acid profile in the serum. *Indicates statistical significance (p-value < 0.05 from non-paired two-way ANOVA test)

µM	CSO	CSO-Si	HSO	HSO-Si	Heat	Silica	Heat:Silica
Alanine	106.88 ± 20.09	102.30 ± 29.17	101.83 ± 40.05	85.68 ± 9.43	0.44	0.46	0.68
Glycine	93.95 ± 25.01	103.28 ± 19.17	91.30 ± 32.75	86.50 ± 17.97	0.44	0.86	0.57
Taurine	201.00 ± 36.02	156.83 ± 105.12	235.70 ± 135.89	205.13 ± 24.15	0.37	0.42	0.88
Phenylalanine	33.50 ± 10.53	24.03 ± 5.02	29.18 ± 5.98	20.83 ± 3.36	0.29	*	0.87
Glutamate	14.63 ± 5.24	16.78 ± 3.78	20.68 ± 18.85	14.03 ± 1.19	0.75	0.66	0.40
Serine	64.40 ± 8.40	61.25 ± 15.98	64.23 ± 26.56	58.33 ± 7.36	0.85	0.59	0.87
Valine	108.03 ± 21.05	79.73 ± 25.83	96.98 ± 39.76	73.68 ± 8.60	0.53	0.07	0.85
Threonine	81.43 ± 26.50	75.50 ± 33.55	88.10 ± 42.41	80.58 ± 8.01	0.71	0.67	0.96
Iso/Leucine	34.25 ± 5.03	27.40 ± 5.87	37.88 ± 12.94	24.13 ± 4.50	0.97	*	0.40
Asparagine	25.35 ± 10.46	14.95 ± 10.99	19.30 ± 8.48	15.93 ± 4.38	0.58	0.15	0.45
Aspartic acid	3.25 ± 0.95	3.78 ± 1.26	4.80 ± 4.11	3.28 ± 0.43	0.64	0.66	0.37
Proline	75.73 ± 30.57	52.50 ± 36.54	76.50 ± 46.96	45.38 ± 10.80	0.85	0.13	0.82
Citrulline	11.08 ± 1.76	10.93 ± 3.55	11.18 ± 4.86	10.33 ± 1.93	0.88	0.77	0.83
Tyrosine	28.73 ± 14.18	18.40 ± 9.25	23.08 ± 7.54	16.20 ± 3.88	0.42	0.09	0.72
Methionine	20.68 ± 6.14	15.13 ± 7.04	22.93 ± 11.91	16.63 ± 1.71	0.63	0.15	0.92
Glutamine	246.53 ± 66.98	224.65 ± 35.86	178.73 ± 78.98	181.28 ± 19.27	0.07	0.73	0.67
Arginine	21.50 ± 3.17	21.93 ± 2.04	19.38 ± 9.21	16.90 ± 3.06	0.19	0.70	0.59
Lysine	95.68 ± 25.40	98.08 ± 36.00	74.30 ± 40.11	47.60 ± 26.53	*	0.47	0.39
Tryptophan	32.90 ± 7.51	31.48 ± 8.53	22.30 ± 3.53	21.33 ± 6.13	*	0.73	0.95
Histidine	28.00 ± 6.94	19.85 ± 5.37	20.73 ± 8.61	19.28 ± 1.69	0.23	0.15	0.30
Ornithine	9.95 ± 1.01	5.05 ± 2.48	4.78 ± 5.02	5.83 ± 4.54	0.25	0.31	0.13
Total	887.45 ± 151.93	760.58 ± 223.93	765.15 ± 324.22	636.63 ± 44.58	0.27	0.25	0.99

Table 4.13 Amino acid profile in the liver. *Indicates statistical significance (*p*-value < 0.05 from non-paired two-way ANOVA test)

µg/g liver	CSO	CSO-Si	HSO	HSO-Si	Heat	Silica	Heat:Silica
Alanine	161.74 ± 32.30	173.57 ± 18.45	169.42 ± 12.73	179.21 ± 21.97	0.57	0.36	0.93
Asparagine	54.79 ± 18.17	42.73 ± 11.66	47.55 ± 10.18	45.46 ± 15.52	0.76	0.34	0.50
Aspartic acid	31.37 ± 19.26	30.71 ± 3.66	20.45 ± 1.78	27.17 ± 3.49	0.17	0.56	0.47
Glutamate	184.19 ± 111.93	205.10 ± 35.87	126.22 ± 34.69	192.90 ± 58.12	0.32	0.22	0.51
Glutamine	284.45 ± 92.73	381.70 ± 76.67	412.52 ± 75.95	424.13 ± 75.97	0.06	0.20	0.31
Glycine	138.29 ± 20.71	146.13 ± 6.98	121.17 ± 9.53	131.22 ± 21.68	0.07	0.29	0.89
Histidine	63.79 ± 7.72	68.83 ± 4.36	77.45 ± 6.19	81.20 ± 9.76	*	0.25	0.86
Iso/Leucine	56.39 ± 14.75	54.33 ± 8.53	57.66 ± 4.06	65.28 ± 12.71	0.28	0.62	0.39
Lysine	149.98 ± 31.91	126.08 ± 21.81	117.13 ± 17.75	119.05 ± 27.08	0.14	0.40	0.33
Methionine	24.97 ± 8.76	23.61 ± 4.27	20.89 ± 4.22	26.93 ± 7.90	0.91	0.49	0.29
Ornithine	64.01 ± 23.91	49.53 ± 7.60	49.61 ± 12.98	42.40 ± 28.14	0.30	0.30	0.72
Phenylalanine	49.71 ± 12.30	48.66 ± 6.36	47.10 ± 5.68	55.49 ± 7.25	0.62	0.39	0.28
Proline	53.57 ± 15.45	47.55 ± 10.82	46.15 ± 12.31	50.07 ± 16.86	0.73	0.88	0.49
Serine	67.83 ± 14.97	73.51 ± 12.53	60.61 ± 7.43	82.02 ± 17.97	0.93	0.07	0.28
Taurine	1,663.29 ± 115.83	1,502.95 ± 134.24	1,708.53 ± 84.66	1,753.60 ± 144.85	*	0.36	0.12
Threonine	57.44 ± 9.95	60.21 ± 8.77	52.97 ± 4.93	67.22 ± 16.92	0.82	0.15	0.32
Tryptophan	7.57 ± 1.40	7.88 ± 1.95	8.07 ± 0.92	10.55 ± 2.17	0.08	0.12	0.22
Tyrosine	65.78 ± 20.63	56.47 ± 10.87	49.19 ± 5.17	66.50 ± 15.14	0.65	0.58	0.08
Valine	66.65 ± 17.09	63.02 ± 10.24	63.64 ± 5.22	70.68 ± 15.67	0.73	0.80	0.43
Total	3,245.79 ± 336.60	3,162.59 ± 166.84	3,256.32 ± 103.37	3,491.09 ± 293.91	0.19	0.55	0.22

Table 4.14 Detection of HSO-responsive urinary metabolites (n=4 in each group). The putative identities and molecular formulas of these markers were elucidated via tandem MS/MS, isotope modeling, and elemental composition analysis. *Identity confirmed by comparison with authentic standards. (DDE, 2,4-decadienal; Y = detected; ND = not detected)

Metabolite	RT (min)	Molecular formula	Adduct form of detected ion	Molecular formula of detected ion	Accurate *m/z* of detected ion	*M/Z* of major fragments	Presence in DDE gavaged mice urine
Hydroxypentenoic acid	3.47	$C_5H_8O_3$	$[M+HQ]^+$	$C_{14}H_{16}N_3O_2^+$	258.1232		Y
Hydroxyoctenoic acid	4.95	$C_8H_{14}O_3$	$[M+HQ]^+$	$C_{17}H_{22}N_3O_2^+$	300.17		Y
Suberic acid*	4.5	$C_8H_{14}O_4$	$[M+HQ]^+$	$C_{17}H_{22}N_3O_3^+$	316.1661		Y
Azelaic acid*	4.95	$C_9H_{16}O_4$	$[M+HQ]^+$	$C_{18}H_{24}N_3O_3^+$	330.1818		Y
i_U	4.84	$C_8H_{14}O_2$	$[M+HQ]^+$	$C_{17}H_{22}N_3O^+$	284.1763	266, 144, 125	ND
ii_U	5.68	$C_9H_{16}O_2$	$[M+HQ]^+$	$C_{18}H_{24}N_3O^+$	298.1919	280, 144, 130, 128	ND
iii_U	4.93	$C_{12}H_{18}O_5$	$[M+HQ]^+$	$C_{21}H_{26}N_3O_4^+$	384.1923	366, 348, 144, 126	ND
iv_U	6.07	$C_{13}H_{22}O_4$	$[M+HQ]^+$	$C_{22}H_{30}N_3O_3^+$	384.2287	366, 348, 226, 144, 128	ND
v_U	5.35	$C_{14}H_{22}O_4$	$[M+HQ]^+$	$C_{23}H_{30}N_3O_3^+$	396.2287	378, 360, 234, 144, 128	ND
Glycine conjugates of hydroxydecenoic acid	3.92, 4.0, 4.18	$C_{12}H_{22}NO_3$	$[M+H]^+$	$C_{12}H_{22}NO_4^+$	244.155		Y

Table 4.15 Detection of selected urinary markers in the digesta and organ extract of mice (n=4 in each group). N.D. = not detected in all group samples. Y = detected with the highest abundance in HSO group samples.

	RT	Detected *M/Z*	Ion adduct	Feed extract	Ileum	Cecum	Feces	Liver extract	Kidney extract	Urine
I_U	3.5003	321.2186	$[M+H]^+$	N.D.	Y	Y	Y	N.D.	N.D.	Y
II_U	2.9176	319.2026	$[M+H]^+$	N.D.	Y	Y	Y	N.D.	N.D.	Y
III_U	3.2483	308.1543	$[M+H]^+$	N.D.	N.D.	N.D.	N.D.	N.D.	N.D.	Y
IV_U	3.9951	337.2134	$[M+H]^+$	N.D.	N.D.	N.D.	N.D.	N.D.	N.D.	Y

Table 4.16 LC-MS/MS analysis of 321^+ and 319^+ ions in the urine. Parent and major fragment ions obtained from co-incubation of lysine, d_8-lysine,^{15}N-lysine, *N*α-acetyl-lysine respectively with 2,4-decadienal are listed with their putative molecular formulas. *d_8-Lysine substituted lysine for coincubation with 2,4-decadienal. $^{\#15}$N-Lysine substituted lysine for coincubation with 2,4-decadienal. $^{\#\#}$*N*α-acetyl-lysine substituted lysine for coincubation with 2,4-decadienal. ***N*ε-acetyl-lysine substituted lysine for coincubation with 2,4-decadienal.

	321$^+$		**319$^+$**		**Nα-acetyl-lysine$^{\#\#}$**	**Nε-acetyl-lysine****	**Lysine + 2,4-Decadienal**		**d_8-Lysine***	**^{15}N-Lysine$^{\#}$**	**Lysine + 2,4-Decadienal**		**d_8-Lysine***	**^{15}N-Lysine$^{\#}$**
	Ions	*Putative formula*	*Ions*	*Putative formula*	*Ions*	*Ions*	*Ions*	*Putative formula*	*Ions*	*Ions*	*Ions*	*Putative formula*	*Ions*	*Ions*
Parent ions	321^+	$C_{18}H_{29}N_2O_3^+$	319^+	$C_{18}H_{27}N_2O_3^+$	321^+	321^+	281^+	$C_{16}H_{29}N_2O_2^+$	289^+	282^+	279^+	$C_{16}H_{27}N_2O_2^+$	287^+	280^+
Major fragment ions	279^+	$C_{16}H_{27}N_2O_2^+$	277^+	$C_{16}H_{25}N_2O_2^+$	279^+									
	150^+	$C_{10}H_{16}N^+$	148^+	$C_{10}H_{14}N^+$	150^+	150^+	152^+	$C_{10}H_{18}N^+$	152^+	152^+	150^+	$C_{10}H_{16}N^+$	150^+	150^+
	130^+	$C_6H_{12}NO_2^+$	130^+	$C_6H_{12}NO_2^+$	130^+									
	84^+	$C_5H_{10}N^+$	84^+	$C_5H_{10}N^+$	84^+	84^+	84^+	$C_5H_{10}N^+$	92^+	85^+	84^+	$C_5H_{10}N^+$	92^+	85^+

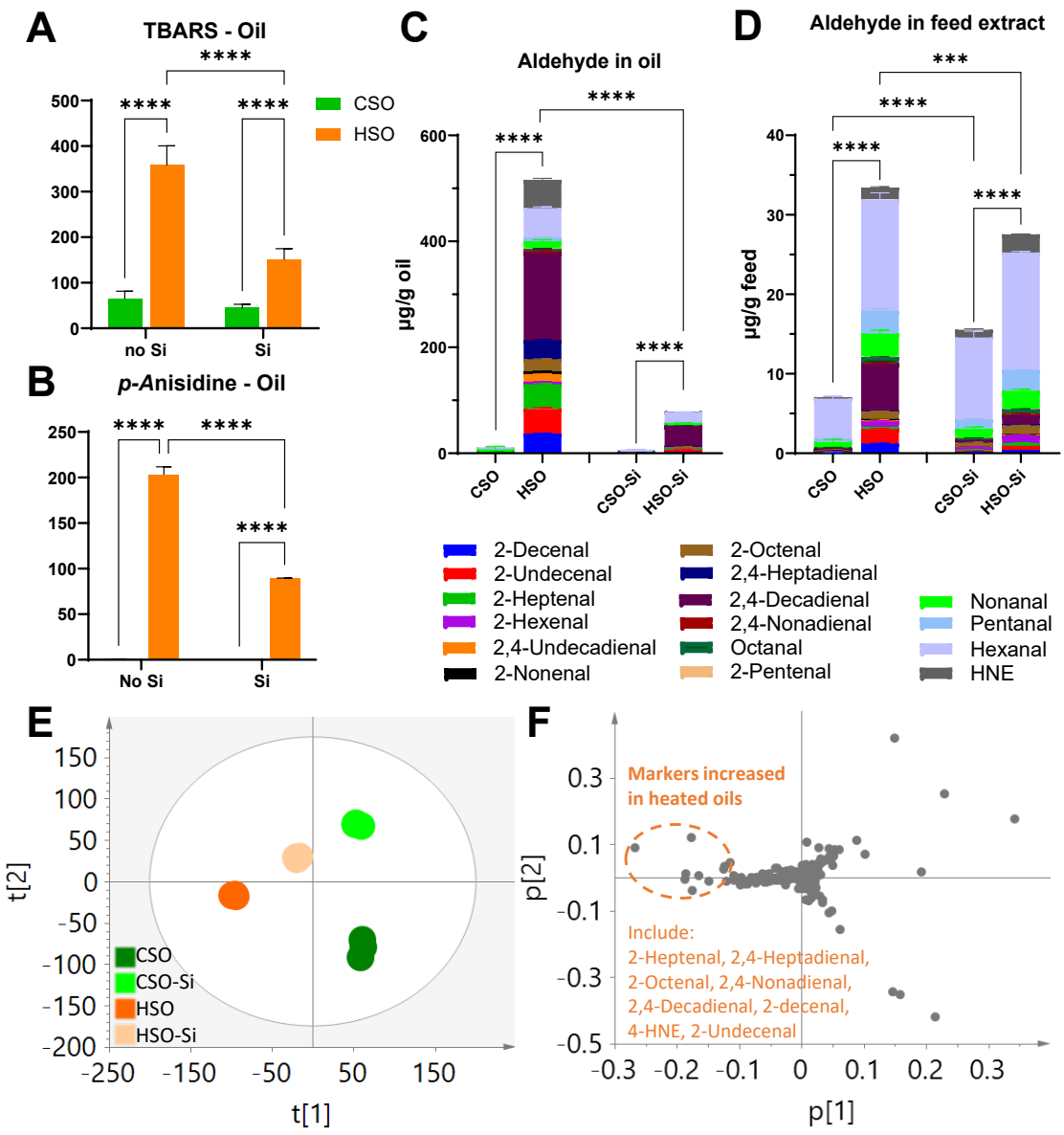

Figure 4.1 Oxidative status of the oils and feeds. A) TBARS of four oils; B) *p*-Anisidine value of four oils; C) Aldehyde concentrations in oils; D) Aldehyde concentrations in the feed extracts (n = 4 in for each oil; Two-way ANOVA tests were conducted, followed by Fisher's LSD tests for examining the difference of CSO vs HSO, and oils with and without silica treatment; ****p<0.0001). Evaluation of the lipid profile of the oils used

for mice feeding. E) The scores plot of a PCA model on CSO, CSO-Si, HSO, and HSO-Si. Data obtained from the HQ derivatization and LC-MS/MS analysis of the oils. F) The loadings plot of the PCA model in E). Markers contributing to the separation of heated oils from the non-heated oils along the direction of PC1 (x-axis) were identified and listed in **Table 4.4**

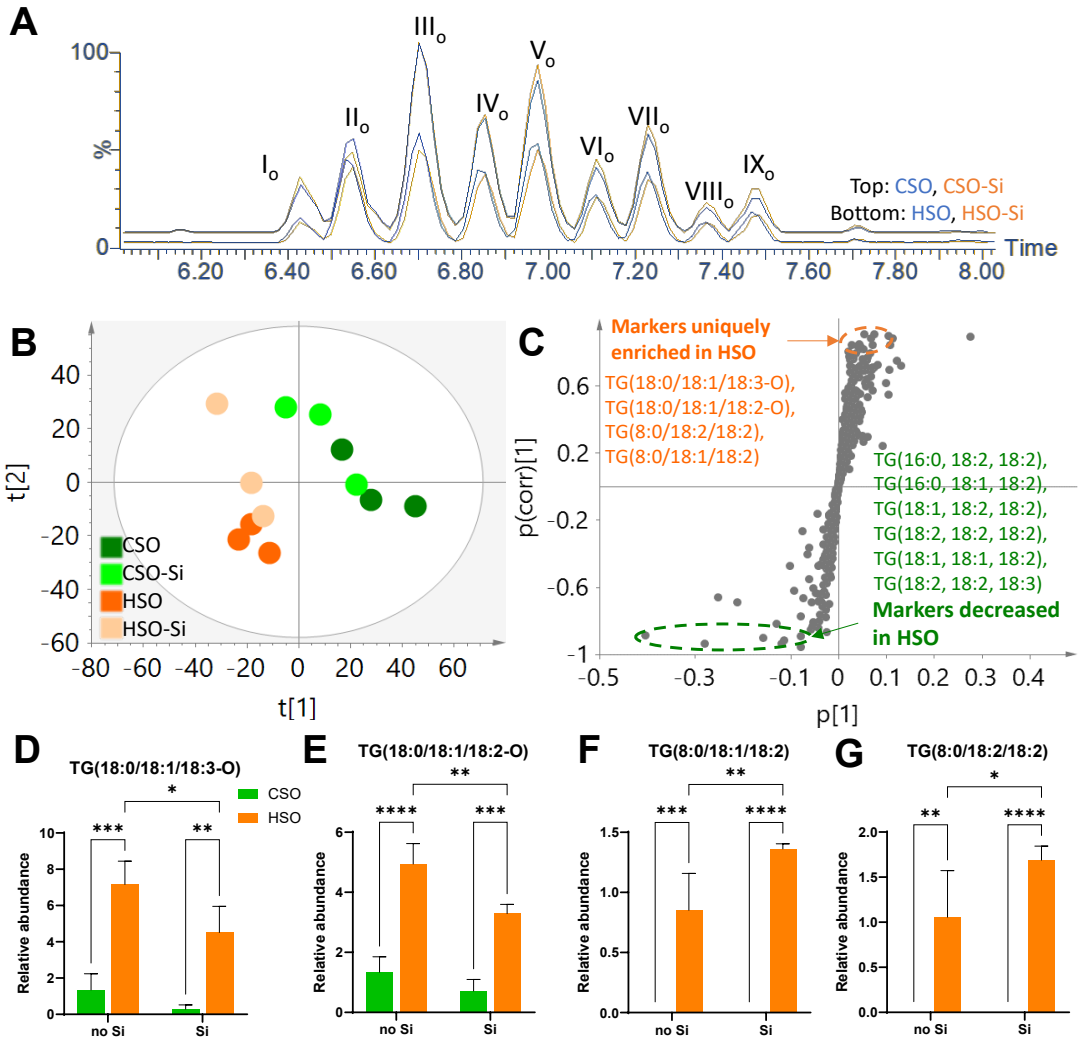

Figure 4.2 Lipidomic analysis of the four oils used in mouse feeding. A) The overlayed BPI chromatographs of oils for retention time 6-8min, normalized by the largest peak as 100%. The main peaks corresponds to TG species as determined by tandem MS/MS analysis: I_o) TG(18:2/18:2/18:3), II_o) Internal standard, tripentadecanoin, TG(15:0), III_o) TG(18:2/18:2/18:2), IV_o) TG(16:0/18:2/18:2), V_o) TG(18:1/18:2/18:2), VI_o) TG(16:0/18:1/18:2), VII_o) TG(18:1/18:1/18:2), $VIII_o$) TG(16:0/18:1/18:1), IX_o) TG(18:1/18:1/18:1). B) The scores plot of a PCA model on CSO, CSO-Si, HSO, and

HSO-Si oils. Data obtained from the LC-MS based lipidomic analysis of the oils. C) The S-plot of an OPLS-DA model of non-heated and heated oils. Markers uniquely enriched in HSO, and decreased in CSO, were identified, and listed. D-G) Relative abundance of markers uniquely enriched in HSO identified in C). n = 3 in each diet group. Two-way ANOVA tests were conducted, followed by Fisher's LSD tests for examining the difference of non-heated and heated oils, and with and without silica treatment. (*p<0.05, **p<0.01, ***p<0.001, ****p<0.0001). The identification of triglyceride species are listed in **Table 4.3**.

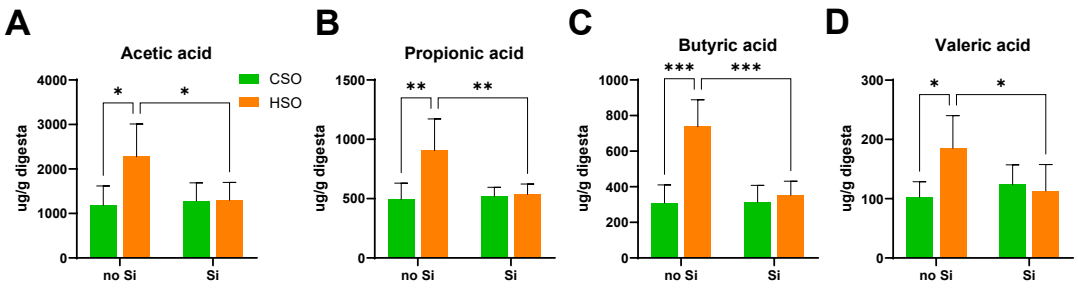

Figure 4.3 Cecum short-chain fatty acids of mice after 28-day feeding. Concentrations of A) acetic acid, B) propionic acid, C) butyric acid, D) valeric acid. (n = 4 in each diet group; Two-way ANOVA tests were conducted, followed by Fisher's LSD tests for examining the difference of CSO vs HSO, and oils with and without silica treatment; *p<0.05, **p<0.01, ***p<0.001, ****p<0.000).

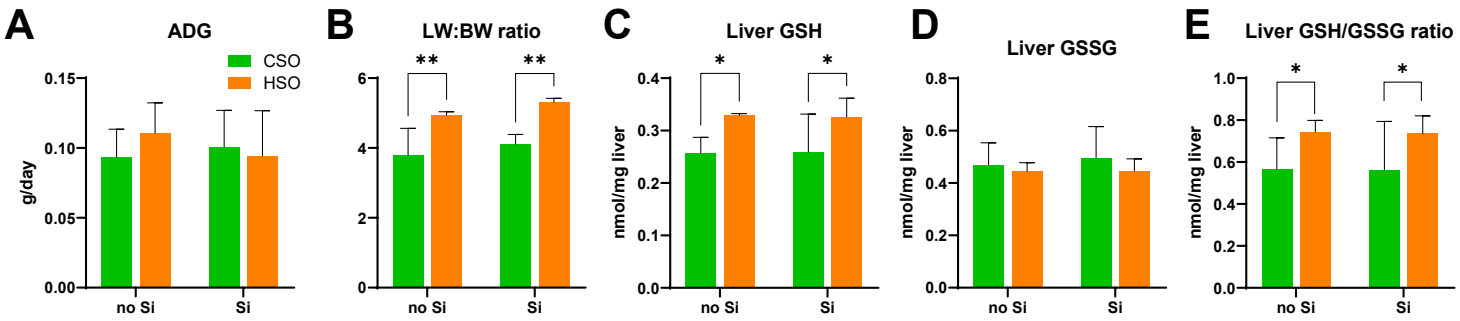

Figure 4.4 Growth performance and metabolites associated with amino acid metabolism in liver and serum. A) Average daily gain (ADG). B) Liver weight: body weight ratio (LW:BW). C) Liver glutathione (GSH) concentration. D) Liver oxidized glutathione (GSSG) concentration. E) GSH/GSSG ratio in liver. F) Amino acid profile of serum, shown as percentage of total amino acid pool. G) Concentration of tryptophan in serum. G) Concentration of lysine in serum. (n = 4 in each diet group. Two-way ANOVA tests were conducted, followed by Fisher's LSD tests examining the difference of CSO vs HSO, and oils with and without silica treatment. *p<0.05, **p<0.01, ***p<0.001, ****p<0.0001)

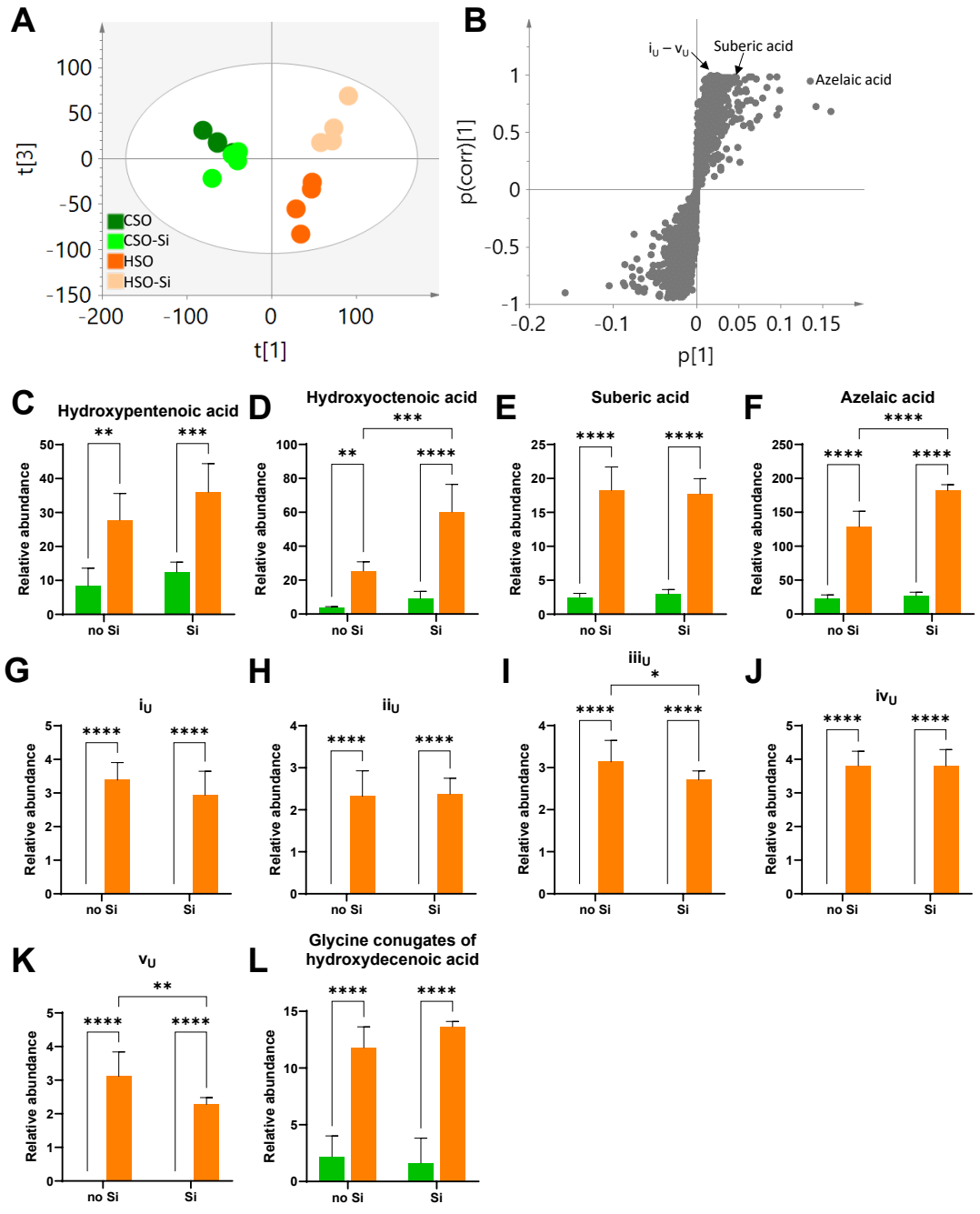

Figure 4.5 Identification of HSO-responsive urinary markers. A) PCA model of the urine from mice fed four diets for 28 days with overview of the scores plot with PC1 and PC3. Data acquired from the LC-MS analysis via BEH C18 column and with HQ

derivatization in positive ionization modes. B) S-plot of an OPLS-DA model constructed based on the PCA model in A), maximizing the differences related to the main effect of HSO. Four HSO-responsive markers consistent with the previous report were identified. The relative abundance of C) hydroxypentenoic acid, D) hydroxyoctenoic acid, E) suberic acid, and F) azelaic acid. G-K) The relative abundance of HSO-responsive markers ($i_U - v_U$) that were nearly absent in CSO and CSO-Si. L) Relative abundance of glycine conjugates of hydroxydecenoic acids. (n = 4 in each diet group. Two-way ANOVA tests were conducted, followed by Fisher's LSD tests for examining the difference of CSO vs HSO, and oils with and without silica treatment. *p<0.05, **p<0.01, ***p<0.001, ****p<0.0001).

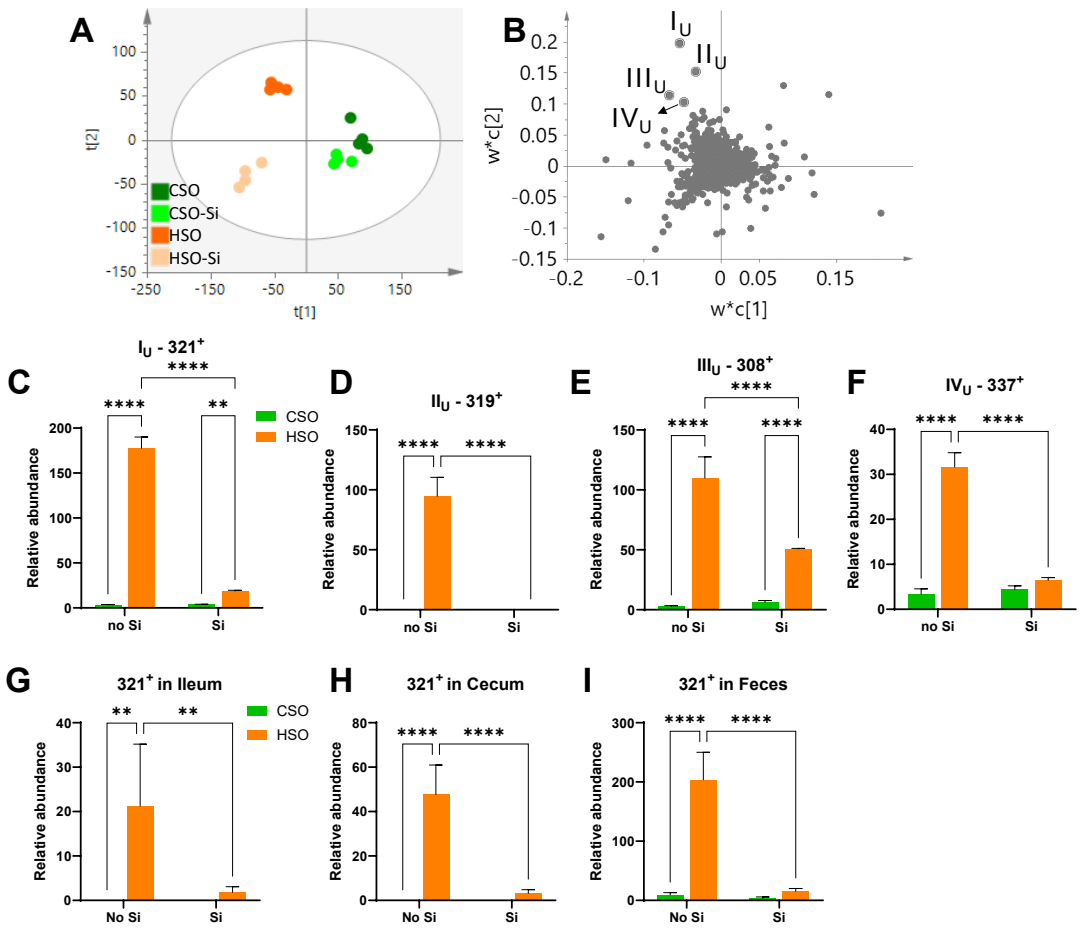

Figure 4.6 Identification of urinary marker associated with HSO intake and were responsive to HSO-Si feeding. A) Scores plot of a PLS-DA model constructed on the urine from mice fed four diets for 28 days. Data acquired from LC-MS analysis via BEH C18 column in positive and negative mode. B) Loadings plot of the PLS-DA model. Markers I_U-V_U were selected and showed good correlation to HSO exposure. C-F) The relative abundance of the selected markers in the mice urine. G-I) The relative abundance of the 321^+ ion in ileum digesta, cecum digesta, and feces (n = 4 in each diet group. Two-way ANOVA tests were conducted, followed by Fisher's LSD tests examining the

difference of CSO vs HSO, and oils with and without silica treatment. *p<0.05, **p<0.01, ***p<0.001, ****p<0.0001).

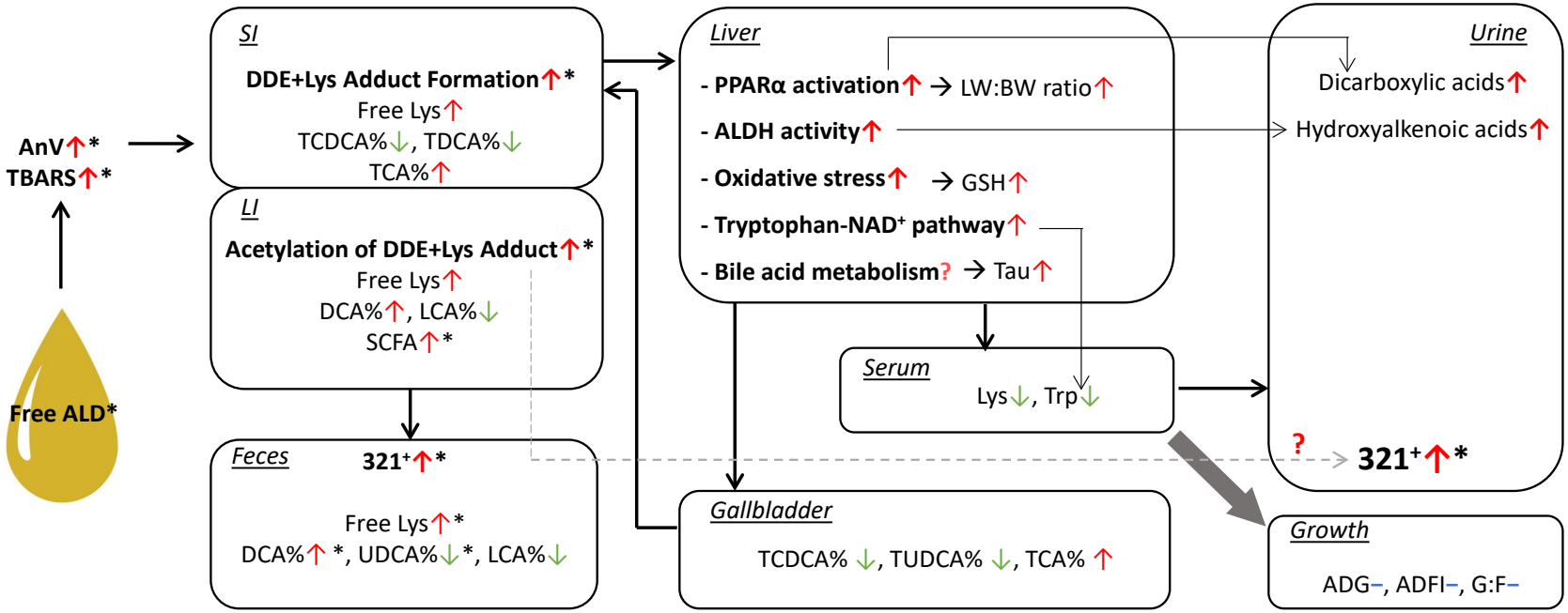

Figure 4.7 Summary of free aldehyde and other LOPs in the HSO induced metabolic changes in mice. *indicates free-aldehyde-dependent pathway and metabolites, which were changed by HSO consumption and was responsive to HSO-Si feeding. ALD, aldehyde; LOP, lipid oxidation products; SI, small intestine; LI, large intestine; Lys, lysine; Gln, glutamine; Tau, taurine; Trp, tryptophan; SCFA, short-chain fatty acids.; DDE, 2,4-decadienal.; GSH, glutathione; LW:BW, liver weight to body weight; ADG, average daily growth; ADFI, average daily feed intake; G:F daily weight gain to feed intake ratio; TCA, taurocholic acid; UDCA,

ursodeoxycholic acid; TDCA, taurodeoxycholic acid; TCDCA, taurochenodeoxycholic acid; TUDCA, tauroursodeoxycholic acid; DCA, deoxycholic acid; LCA, lithocholic acid.

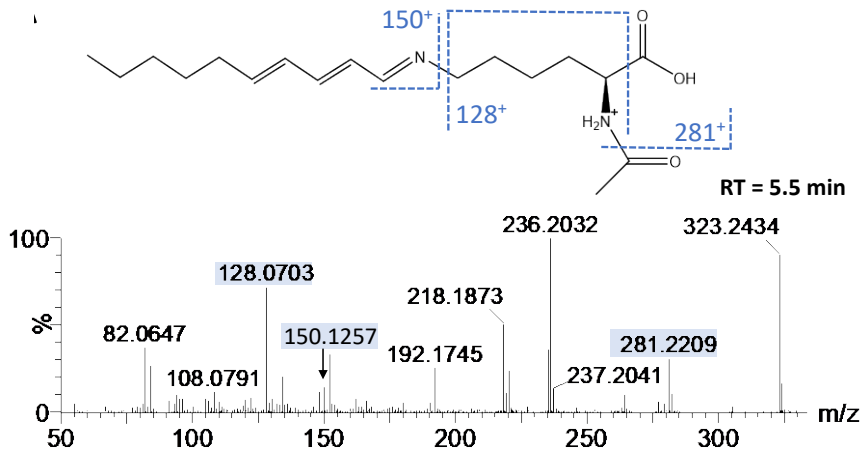
150+
128+
281+
RT = 5.5 min
236.2032
323.2434
128.0703
218.1873
82.0647
150.1257
192.1745
281.2209
108.0791
237.2041
100
%
0
50
100
150
200
250
300
m/z

B

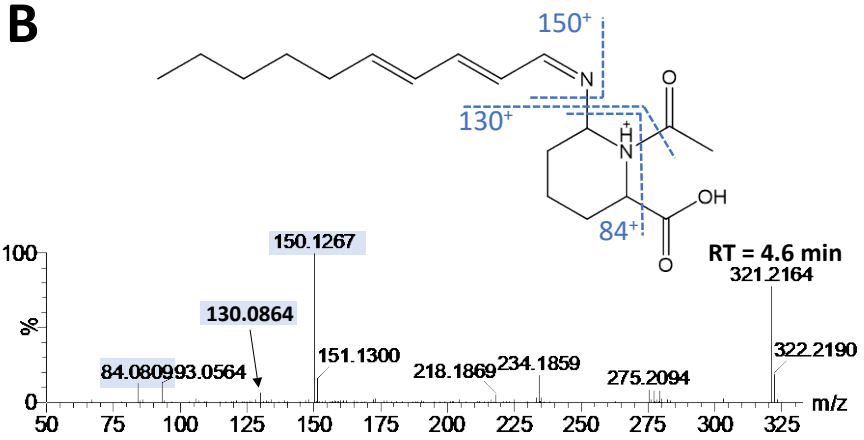
150+
130+
84+
RT = 4.6 min
150.1267
321.2164
130.0864
151.1300
322.2190
84.0809
93.0564
218.1869
234.1859
275.2094
100
%
0
50
75
100
125
150
175
200
225
250
275
300
325
m/z

C

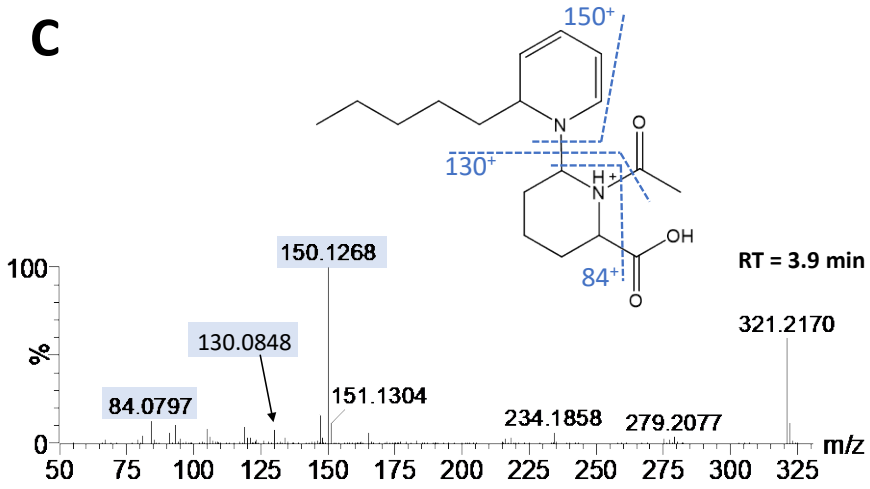
150+
130+
84+
RT = 3.9 min
150.1268
321.2170
130.0848
84.0797
151.1304
234.1858
279.2077
100
%
0
50
75
100
125
150
175
200
225
250
275
300
325
m/z

Figure 4.8 Putative structure, fragmentation pattern, and the MS/MS spectra of synthetic and urinary markers. A) A proposed structure of 323^{+}, a Schiff-type adduct between DDE and Nα -acetyl-lysine. B) Proposed structure of synthetic 321^{+}, obtained from the reaction between *N*α- or *N*ε-acetyl-lysine coincubation with DDE. C) A proposed structure of urinary 321^{+}, containing a pyridine structure. The IUPAC nomenclature is 1-acetyl-2-carboxy-6-(6-pentylpyridin-1(2H)-yl)piperidin-1-ium. DDE, 2,4-decadienal.

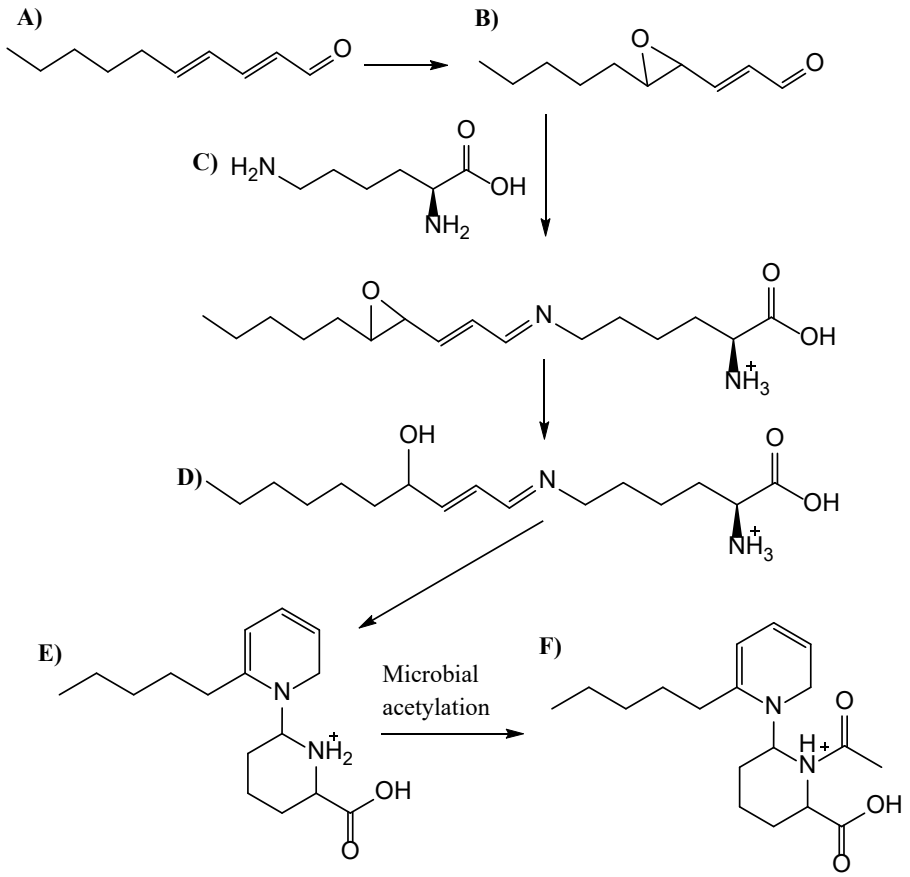

Figure 4.9 Proposed scheme of the formation of 321^{+} marker in the GI lumen. A) 2,4-decadienal. B) 4,5-epoxy-2-decenal. C) Lysine. D) Hydroxy-DDE-lysine. E) DDE-Lysine adduct, rearranged. F) Urinary 321^{+} metabolite, acetylated DDE-lysine adduct, with the IUPAC nomenclature 1-acetyl-2-carboxy-6-(6-pentylpyridin-1(2H)-yl)piperidin-1-ium.

REFERENCES

1. Kim N, Lee J, Song HS, et al. Kimchi intake alleviates obesity-induced neuroinflammation by modulating the gut-brain axis. *Food research international (Ottawa, Ont).* 2022;158:111533.
2. Khezri SS, Saidpour A, Hosseinzadeh N, Amiri Z. Beneficial effects of Apple Cider Vinegar on Weight Management, Visceral Adiposity Index and Lipid Profile in Overweight or Obese Subjects Receiving Restricted Calorie Diet: A randomized clinical trial. *Journal of Functional Foods.* 2018;43:95-102.
3. Panesar M, Shah N, Vaqar S, et al. Changes in Serum Bicarbonate Levels Caused by Acetate - Containing Bicarbonate - Buffered Hemodialysis Solution: An Observational Prospective Cohort Study. *Therapeutic Apheresis and Dialysis.* 2017;21(2):157-165.
4. Cederbaum AI. Alcohol Metabolism. *Clinics in Liver Disease.* 2012;16(4):667-685.
5. Horibata Y, Ando H, Itoh M, Sugimoto H. Enzymatic and Transcriptional Regulation of the Cytoplasmic Acetyl-CoA Hydrolase ACOT12. *Journal of Lipid Research.* 2013;54(8):2049-2059.
6. Matsunaga T, Isohashi F, Nakanishi Y, Sakamoto Y. PHYSIOLOGICAL-CHANGES IN THE ACTIVITIES OF EXTRAMITOCHONDRIAL ACETYL-COA HYDROLASE IN THE LIVER OF RATS UNDER VARIOUS METABOLIC CONDITIONS. *European journal of biochemistry.* 1985;152(2):331-336.
7. Liu X, Cooper DE, Cluntun AA, et al. Acetate Production from Glucose and Coupling to Mitochondrial Metabolism in Mammals. *Cell.* 2018;175(2):502-513.e513.
8. Lydell CP, Chan A, Wambolt RB, et al. Pyruvate dehydrogenase and the regulation of glucose oxidation in hypertrophied rat hearts. *Cardiovasc Res.* 2002;53(4):841-851.
9. McBrian MA, Behbahan IS, Ferrari R, et al. Histone Acetylation Regulates Intracellular pH. *Molecular cell.* 2013;49(2):310-321.
10. Moffett JR, Puthillathu N, Vengilote R, Jaworski DM, Namboodiri AM. Acetate Revisited: A Key Biomolecule at the Nexus of Metabolism, Epigenetics, and Oncogenesis - Part 2: Acetate and ACSS2 in Health and Disease. *Frontiers in Physiology.* 2020;11:25.
11. Den Besten G, Van Eunen K, Groen AK, Venema K, Reijngoud D-J, Bakker BM. The role of short-chain fatty acids in the interplay between diet, gut microbiota, and host energy metabolism. *Journal of Lipid Research.* 2013;54(9):2325-2340.
12. Jeon JY, Lee M, Whang SH, Kim JW, Cho A, Yun M. Regulation of Acetate Utilization by Monocarboxylate Transporter 1 (MCT1) in Hepatocellular Carcinoma (HCC). *Oncology research.* 2018;26(1):71-81.
13. Moffett JR, Puthillathu N, Vengilote R, Jaworski DM, Namboodiri AM. Acetate Revisited: A Key Biomolecule at the Nexus of Metabolism, Epigenetics and Oncogenesis-Part 1: Acetyl-CoA, Acetogenesis and Acyl-CoA Short-Chain Synthetases. *Frontiers in Physiology.* 2020;11.

14. Pietrocola F, Galluzzi L, Bravo-San Pedro JM, Madeo F, Kroemer G. Acetyl Coenzyme A: A Central Metabolite and Second Messenger. *Cell Metabolism.* 2015;21(6):805-821.
15. Fujino T, Kondo J, Ishikawa M, Morikawa K, Yamamoto TT. Acetyl-CoA synthetase 2, a mitochondrial matrix enzyme involved in the oxidation of acetate. *JOURNAL OF BIOLOGICAL CHEMISTRY.* 2001;276(14):11420-11426.
16. Wellen KE, Hatzivassiliou G, Sachdeva UM, Bui TV, Cross JR, Thompson CB. ATP-Citrate Lyase Links Cellular Metabolism to Histone Acetylation. *SCIENCE.* 2009;324(5930):1076-1080.
17. Luong A, Hannah VC, Brown MS, Goldstein JL. Molecular Characterization of Human Acetyl-CoA Synthetase, An Enzyme Regulated by Sterol Regulatory Element-binding Proteins. *Journal of Biochemical Chemistry.* 2000;275(34):26458-26466.
18. Bulusu V, Tumanov S, Michalopoulou E, et al. Acetate Recapturing by Nuclear Acetyl-CoA Synthetase 2 Prevents Loss of Histone Acetylation during Oxygen and Serum Limitation. *CELL REPORTS.* 2017;18(3):647-658.
19. Ariyannur PS, Moffett JR, Madhavarao CN, et al. Nuclear-Cytoplasmic Localization of Acetyl Coenzyme A Synthetase-1 in the Rat Brain. *JOURNAL OF COMPARATIVE NEUROLOGY.* 2010;518(15):2952-2977.
20. Schug ZT, Peck B, Jones DT, et al. Acetyl-Coa Synthetase 2 Promotes Acetate Utilization And Maintains Cancer Cell Growth Under Metabolic Stress. *Cancer Cell.* 2015;27(1):57-71.
21. Pingitore A, Gonzalez-Abuin N, Ruz-Maldonado I, Huang GC, Frost G, Persaud SJ. Short Chain Fatty Acids Stimulate Insulin Secretion and Reduce Apoptosis in Mouse and Human Islets In Vitro: Role of Free Fatty Acid Receptor 2. *Diabetes, Obesity and Metabolism.* 2019;21(2):330-339.
22. Villa SR, Priyadarshini M, Fuller MH, et al. Loss of Free Fatty Acid Receptor 2 leads to impaired islet mass and beta cell survival. *Scientific Reports.* 2016;6(1):28159.
23. Xu M, Jiang Z, Wang C, et al. Acetate attenuates inflammasome activation through GPR43-mediated Ca(2+)-dependent NLRP3 ubiquitination. *Exp Mol Med.* 2019;51(7):1-13.
24. Maslowski KM, Vieira AT, Ng A, et al. Regulation of Inflammatory Responses by Gut Microbiota and Chemoattractant Receptor GPR43. *Nature.* 2009;461(7268):1282-U1119.
25. Richards RH, Vreman HJ, Zager P, Feldman C, Blaschke T, Weiner MW. Acetate Metabolism In Normal Human Subjects. *American Journal of Kidney Disease.* 1982;2(1):47-57.
26. Ullrich KJ, Rumrich G, Klöss S. Reabsorption of monocarboxylic acids in the proximal tubule of the rat kidney. *Pflügers Archiv European Journal of Physiology.* 1982;395(3):212-219.
27. Morris ME, Kwatra NV. Monocarboxylic Acid Transporters. *Drug Transporters*2022:143-164.

28. Den Besten G, Bleeker A, Gerding A, et al. Short-Chain Fatty Acids Protect Against High-Fat Diet–Induced Obesity via a PPARγ-Dependent Switch From Lipogenesis to Fat Oxidation. *Diabetes.* 2015;64(7):2398-2408.
29. Yamashita H, Fujisawa K, Ito E, et al. Improvement of Obesity and Glucose Tolerance by Acetate in Type 2 Diabetic Otsuka Long-Evans Tokushima Fatty (OLETF) Rats. *Biosci Biotechnol Biochem.* 2007;71(5):1236-1243.
30. Kondo T, Kishi M, Fushimi T, Kaga T. Acetic Acid Upregulates the Expression of Genes for Fatty Acid Oxidation Enzymes in Liver to Suppress Body Fat Accumulation. *Journal of Agricultural and Food Chemistry.* 2009;57(13):5982-5986.
31. Nakajima A, Nakatani A, Hasegawa S, et al. The Short Chain Fatty Acid Receptor GPR43 Regulates Inflammatory Signals In Adipose Tissue M2-Type Macrophages. *PloS one.* 2017;12(7):e0179696.
32. Maryam IY, Adel MS, Ahmad B. Effect of apple cider vinegar on blood glucose level in diabetic mice. *Pharmaceutical Sciences.* 2014;20:163-168.
33. Mitrou P, Petsiou E, Papakonstantinou E, et al. The role of acetic acid on glucose uptake and blood flow rates in the skeletal muscle in humans with impaired glucose tolerance. *European Journal of Clinical Nutrition.* 2015;69(6):734-739.
34. Kausar S, Abbas MA, Ahmad NH, et al. Effect of apple cider vinegar in type 2 diabetic patients with poor glycemic control: a randomized placebo controlled design®. *Health Sciences.* 2019;8(2):149-159.
35. Gheflati A, Bashiri R, Ghadiri-Anari A, Reza JZ, Kord MT, Nadjarzadeh A. The Effect of Apple Vinegar Consumption On Glycemic Indices, Blood Pressure, Oxidative Stress, and Homocysteine in Patients With Type 2 Diabetes And Dyslipidemia: A Randomized Controlled Clinical Trial. *Clinical nutrition ESPEN.* 2019;33:132-138.
36. Wu D, Kimura F, Takashima A, et al. Intake of vinegar beverage is associated with restoration of ovulatory function in women with polycystic ovary syndrome. *The Tohoku Journal of Experimental Medicine.* 2013;230(1):17-23.
37. Perry RJ, Peng L, Barry NA, et al. Acetate Mediates a Microbiome–brain–β-cell Axis to Promote Metabolic Syndrome. *Nature.* 2016;534(7606):213-217.
38. Schug ZT, Vande Voorde J, Gottlieb E. The Metabolic Fate Of Acetate In Cancer. *Nature Reviews Cancer.* 2016;16(11):708-717.
39. Wang Y, Liu F, Sun L, et al. Association Between Human Blood Metabolome and The Risk of Breast Cancer. *Breast Cancer Research.* 2023;25(1):9.
40. Gabutti L, Lucchini B, Marone C, Alberio L, Burnier M. Citrate- Vs. Acetate-Based Dialysate In Bicarbonate Haemodialysis: Consequences On Haemodynamics, Coagulation, Acid-Base Status, And Electrolytes. *BMC nephrology.* 2009;10:7.
41. Shi X, Yao D, Chen C. Identification Of N-Acetyltaurine As A Novel Metabolite Of Ethanol Through Metabolomics-Guided Biochemical Analysis. *Journal of Biological Chemistry.* 2012;287(9):6336-6349.
42. Feron V, Til H, De Vrijer F, Woutersen R, Cassee F, Van Bladeren P. Aldehydes: occurrence, carcinogenic potential, mechanism of action and risk assessment. *Mutation Research/Genetic Toxicology.* 1991;259(3-4):363-385.

43. Yuan J. Aldehydes in oxidized oils and fried foods and their associations with animal growth performance. University of Minnesota; 2020.
44. Grootveld M, Percival BC, Leenders J, Wilson PB. Potential Adverse Public Health Effects Afforded by the Ingestion of Dietary Lipid Oxidation Product Toxins: Significance of Fried Food Sources. *Nutrients.* 2020;12(4):974.
45. Lopachin RM, Gavin T. Molecular mechanisms of aldehyde toxicity: a chemical perspective. *Chemical Research in Toxicology.* 2014;27(7):1081-1091.
46. Zhong H, Yin H. Role of lipid peroxidation derived 4-hydroxynonenal (4-HNE) in cancer: focusing on mitochondria. *Redox biology.* 2015;4:193-199.
47. Chen HJ, Gonzalez FJ, Shou M, Chung FL. 2,3-epoxy-4-hydroxynonanal, a potential lipid peroxidation product for etheno adduct formation, is not a substrate of human epoxide hydrolase. *Carcinogenesis.* 1998;19(5):939-943.
48. Aguilar Diaz De Leon J, Borges CR. Evaluation of Oxidative Stress in Biological Samples Using the Thiobarbituric Acid Reactive Substances Assay. *Journal of visualized experiments : JoVE.* 2020(159).
49. Irwin JW, Hedges N. 13 - Measuring lipid oxidation. In: Steele R, ed. *Understanding and Measuring the Shelf-Life of Food*: Woodhead Publishing; 2004:289-316.
50. Kanazawa K, Ashida H. Dietary hydroperoxides of linoleic acid decompose to aldehydes in stomach before being absorbed into the body. *Biochimica et Biophysica Acta (BBA) - Lipids and Lipid Metabolism.* 1998;1393(2):349-361.
51. Sinharoy P, Mcallister SL, Vasu M, Gross ER. Environmental Aldehyde Sources and the Health Implications of Exposure. *Aldehyde Dehydrogenases*: Springer Singapore; 2019:35-52.
52. Adams TB, Gavin CL, Taylor SV, et al. The FEMA GRAS assessment of α,β-unsaturated aldehydes and related substances used as flavor ingredients. *Food and Chemical Toxicology.* 2008;46(9):2935-2967.
53. Tandon KS, Baldwin EA, Shewfelt RL. Aroma perception of individual volatile compounds in fresh tomatoes (Lycopersicon esculentum, Mill.) as affected by the medium of evaluation. *Postharvest Biology and Technology.* 2000;20(3):261-268.
54. Karagul Yuceer Y, Tuncel B, Guneser O, et al. Characterization of aroma-active compounds, sensory properties, and proteolysis in Ezine cheese. *Journal of Dairy Science.* 2009;92(9):4146-4157.
55. Saijyo R, Takeo T. The importance of linoleic acid and linolenic acid as precursors of hexanal and trans-2-hexenal in black tea. *Plant and Cell Physiology.* 1972;13(6):991-998.
56. Shahidi F, Pegg RB. Hexanal as an indicator of the flavor deterioration of meat and meat products. ACS Publications; 1994.
57. Meng HY, Piccand M, Fuchsmann P, et al. Formation of 3-Methylbutanal and 3-Methylbutan-1-ol Recognized as Malty during Fermentation in Swiss Raclette-Type Cheese, Reconstituted Milk, and de Man, Rogosa, and Sharpe Broth. *Journal of Agricultural and Food Chemistry.* 2021;69(2):717-729.
58. Ledauphin J, Basset B, Cohen S, Payot T, Barillier D. Identification of trace volatile compounds in freshly distilled Calvados and Cognac: Carbonyl and sulphur compounds. *Journal of Food Composition and Analysis.* 2006;19(1):28-40.

59. Smit BA, Engels WJM, Smit G. Branched chain aldehydes: production and breakdown pathways and relevance for flavour in foods. *Applied Microbiology and Biotechnology.* 2009;81(6):987-999.
60. Counet C, Callemien D, Ouwerx C, Collin S. Use of gas chromatography−olfactometry to identify key odorant compounds in dark chocolate. Comparison of samples before and after conching. *Journal of Agricultural and Food Chemistry.* 2002;50(8):2385-2391.
61. Guillen MD, Uriarte PS. Aldehydes contained in edible oils of a very different nature after prolonged heating at frying temperature: Presence of toxic oxygenated alpha,beta unsaturated aldehydes. *Food Chemistry.* 2012;131(3):915-926.
62. Guillensans R, Guzmanchozas M. ALDEHYDES IN FOOD AND ITS RELATION WITH THE TEA TEST FOR RANCIDITY. *Fett Wissenschaft Technologie-Fat Science Technology.* 1995;97(7-8):285-286.
63. Katsuta I, Shimizu M, Yamaguchi T, Nakajima Y. Emission of volatile aldehydes from DAG-rich and TAG-rich oils with different degrees of unsaturation during deep-frying. *Journal of the American Oil Chemists Society.* 2008;85(6):513-519.
64. Rohleder AR, Scherf KA, Schieberle P, Koehler P. Quantitative Analyses of Key Odorants and Their Precursors Reveal Differences in the Aroma of Gluten-Free Rice Bread and Wheat Bread. *Journal of Agricultural and Food Chemistry.* 2019;67(40):11179-11186.
65. Galliard T. Lipids of potato tubers. 1. Lipid and fatty acid composition of tubers from different varieties of potato. *Journal of the Science of Food and Agriculture.* 1973;24(5):617-622.
66. Wang L, Csallany AS, Kerr BJ, Shurson GC, Chen C. Kinetics of forming aldehydes in frying oils and their distribution in French fries revealed by LC–MS-based chemometrics. *Journal of Agricultural and Food Chemistry.* 2016;64(19):3881-3889.
67. Adams TB, Cohen SM, Doull J, et al. The FEMA GRAS assessment of cinnamyl derivatives used as flavor ingredients. *Food and chemical toxicology.* 2004;42(2):157-185.
68. Kanner J. Dietary advanced lipid oxidation endproducts are risk factors to human health. *Molecular Nutrition & Food Research.* 2007;51(9):1094-1101.
69. Kanner J, Lapidot T. The stomach as a bioreactor: dietary lipid peroxidation in the gastric fluid and the effects of plant-derived antioxidants. *Free Radical Biology and Medicine.* 2001;31(11):1388-1395.
70. Márquez-Ruiz G, García-Martínez MC, Holgado F. Changes and Effects of Dietary Oxidized Lipids in the Gastrointestinal Tract. *Lipid Insights.* 2008;2:LPI.S904.
71. Kanazawa K, Ashida H. Catabolic fate of dietary trilinoleoylglycerol hydroperoxides in rat gastrointestines. *Biochimica et Biophysica Acta (BBA) - Lipids and Lipid Metabolism.* 1998;1393(2):336-348.
72. Márquez-Ruiz G, Holgado F, Ruiz-Méndez MV, Velasco J. Chemical changes of hydroperoxy-, epoxy-, keto- and hydroxy-model lipids under simulated gastric conditions. *Foods.* 2021;10(9):2035.
73. Alberdi-Cedeño J, Ibargoitia ML, Guillén MD. Study of the In Vitro Digestion of Olive Oil Enriched or Not with Antioxidant Phenolic Compounds. Relationships

between Bioaccessibility of Main Components of Different Oils and Their Composition. *Antioxidants.* 2020;9(6):543.
74. Grootveld M. Evidence-Based Challenges to the Continued Recommendation and Use of Peroxidatively-Susceptible Polyunsaturated Fatty Acid-Rich Culinary Oils for High-Temperature Frying Practises: Experimental Revelations Focused on Toxic Aldehydic Lipid Oxidation Products. *Frontiers in Nutrition.* 2022;8(1173).
75. Frankel EN, Neff WE, Brooks DD, Fujimoto K. FLUORESCENCE FORMATION FROM THE INTERACTION OF DNA WITH LIPID OXIDATION DEGRADATION PRODUCTS. *Biochimica et biophysica acta.* 1987;919(3):239-244.
76. Ayala A, Munoz MF, Arguelles S. Lipid Peroxidation: Production, Metabolism, and Signaling Mechanisms of Malondialdehyde and 4-Hydroxy-2-Nonenal. *Oxidative Medicine and Cellular Longevity.* 2014;2014.
77. Moldovan L, Moldovan NI. Oxygen free radicals and redox biology of organelles. *Histochemistry and Cell Biology.* 2004;122(4):395-412.
78. Chung FL, Chen HJ, Nath RG. Lipid peroxidation as a potential endogenous source for the formation of exocyclic DNA adducts. *Carcinogenesis.* 1996;17(10):2105-2111.
79. Elisia I, Kitts DD. Quantification of hexanal as an index of lipid oxidation in human milk and association with antioxidant components. *Journal of Clinical Biochemistry and Nutrition.* 2011;49(3):147-152.
80. Ishino K, Wakita C, Shibata T, et al. Lipid Peroxidation Generates Body Odor Component trans-2-Nonenal Covalently Bound to Protein in Vivo. *Journal of Biological Chemistry.* 2010;285(20):15302-15313.
81. Balogh LM, Atkins WM. Interactions of glutathione transferases with 4-hydroxynonenal. *Drug metabolism reviews.* 2011;43(2):165-178.
82. Guillén MD, Ruiz A. Monitoring of heat-induced degradation of edible oils by proton NMR. *European Journal of Lipid Science and Technology.* 2008;110(1):52-60.
83. Haywood RM, Claxson AWD, Hawkes GE, et al. DETECTION OF ALDEHYDES AND THEIR CONJUGATED HYDROPEROXYDIENE PRECURSORS IN THERMALLY-STRESSED CULINARY OILS AND FATS - INVESTIGATIONS USING HIGH-RESOLUTION PROTON NMR-SPECTROSCOPY. *Free Radical Research.* 1995;22(5):441-482.
84. Moumtaz S, Percival BC, Parmar D, Grootveld KL, Jansson P, Grootveld M. Toxic aldehyde generation in and food uptake from culinary oils during frying practices: peroxidative resistance of a monounsaturate-rich algae oil. *Scientific Reports.* 2019;9.
85. Velasco J, Marmesat S, Bordeaux O, Marquez-Ruiz G, Dobarganes C. Formation and evolution of monoepoxy fatty acids in thermoxidized olive and sunflower oils and quantitation in used frying oils from restaurants and fried-food outlets. *Journal of Agricultural and Food Chemistry.* 2004;52(14):4438-4443.
86. Wang GW, Guo YR, Vondriska TM, et al. Acrolein consumption exacerbates myocardial ischemic injury and blocks nitric oxide-induced PKC epsilon signaling

and cardioprotection. *Journal of Molecular and Cellular Cardiology.* 2008;44(6):1016-1022.
87. Health And Environmental Effects Profile for Acrolein. 2004.
88. Jiang K, Huang C, Liu F, et al. Origin and Fate of Acrolein in Foods. *Foods.* 2022;11(13):1976.
89. Briefel RR, Johnson CL. Secular trends in dietary intake in the United States. *Annu Rev Nutr.* 2004;24:401-431.
90. Wells HF, Buzby JC. *Dietary assessment of major trends in US food consumption, 1970-2005.* U.S. Department of Agriculture;2008.
91. Sapkota AR, Lefferts LY, McKenzie S, Walker P. What do we feed to food-production animals? A review of animal feed ingredients and their potential impacts on human health. 2007;115(5):663-670.
92. Haumann F. Renderers give new life to waste restaurant fats. *International news on fats, oils and related materials (USA).* 1990.
93. Westendorf ML. Food waste as animal feed: an introduction. *Food waste to animal feed.* 2000:3-16.
94. Canakci M. The potential of restaurant waste lipids as biodiesel feedstocks. *Bioresource Technology.* 2007;98(1):183-190.
95. Kerr BJ, Kellner TA, Shurson GC. Characteristics of lipids and their feeding value in swine diets. *Journal of Animal Science and Biotechnology.* 2015;6(1).
96. Shurson GC, Kerr BJ, Hanson AR. Evaluating the quality of feed fats and oils and their effects on pig growth performance. *Journal of Animal Science and Biotechnology.* 2015;6.
97. van Kempen TA, McComas S. Infrared Spectroscopy as a Tool for Assessing Fat Quality. *Journal of Applied Poultry Research.* 2002;11(2):191-201.
98. Hotel D. Department of Animal Science at the New York State College of Agriculture and Life Sciences (A Statutory College of the State University of New York) Cornell University. 2011.
99. Gao Y, Meng Q, Qin J, Zhao Q, Shi B. Resveratrol alleviates oxidative stress induced by oxidized soybean oil and improves gut function via changing gut microbiota in weaned piglets. *Journal of Animal Science and Biotechnology.* 2023;14(1).
100. Yan H, Zhou P, Zhang Y, Zhang Z, Liu J, Zhang H. Short-chain fructo-oligosaccharides alleviates oxidized oil-induced intestinal dysfunction in piglets associated with the modulation of gut microbiota. *Journal of Functional Foods.* 2020;64:103661.
101. Rosero DS, Odle J, Moeser AJ, Boyd RD, Van Heugten E. Peroxidised dietary lipids impair intestinal function and morphology of the small intestine villi of nursery pigs in a dose-dependent manner. *British Journal of Nutrition.* 2015;114(12):1985-1992.
102. Yuan J, Kerr BJ, Curry SM, Chen C. Identification of C9-C11 unsaturated aldehydes as prediction markers of growth and feed intake for non-ruminant animals fed oxidized soybean oil. *Journal of Animal Science and Biotechnology.* 2020;11(1).

103. Kerr BJ, Lindblom SC, Overholt MF. Influence of feeding thermally peroxidized soybean oil on growth performance, digestibility, gut integrity, and oxidative stress in nursery pigs. *Journal of Animal Science.* 2020;98(2).
104. Lindblom SC, Gabler NK, Dilger RN, Olson ZF, Loving CL, Kerr BJ. Influence of feeding thermally peroxidized soybean oil on oxidative status in growing pigs. *Journal of Animal Science.* 2018.
105. Hung YT, Hanson AR, Shurson GC, Urriola PE. Peroxidized lipids reduce growth performance of poultry and swine: A meta-analysis. *Animal Feed Science and Technology.* 2017;231:47-58.
106. Choe E, Min D. Chemistry of deep‐fat frying oils. *Journal of food science.* 2007;72(5):R77-R86.
107. Frankel EN. *Lipid oxidation.* Elsevier; 2014.
108. Amat Sairin M, Abd Aziz S, Yoke Mun C, Khaled AY, Rokhani FZ. Analysis and prediction of the major fatty acids in vegetable oils using dielectric spectroscopy at 5-30 MHz. *PLoS One.* 2022;17(5):e0268827.
109. Yuan J. *Aldehydes in oxidized oils and fried foods and their associations with animal growth performance* [Dissertation]: Food Science and Nutrition, University of Minnesota; 2020.
110. Frankel E, Neff W, Weisleder D. Determination of methyl linoleate hydroperoxides by 13C nuclear magnetic resonance spectroscopy. *Methods in enzymology.* Vol 186: Elsevier; 1990:380-387.
111. Frankel EN, Neff WE, Rohwedder WK, Khambay BP, Garwood RF, Weedon BC. Analysis of autoxidized fats by gas chromatography-mass spectrometry: II. Methyl linoleate. *Lipids.* 1977;12(11):908-913.
112. Sergeant S, Rahbar E, Chilton FH. Gamma-linolenic acid, Dihommo-gamma linolenic, Eicosanoids and Inflammatory Processes. *Eur J Pharmacol.* 2016;785:77-86.
113. Fan Y-Y, Chapkin RS. Importance of Dietary γ-Linolenic Acid in Human Health and Nutrition. *The Journal of Nutrition.* 1998;128(9):1411-1414.
114. Hernandez EM, Sanders TAB. 4 - Specialty oils. Functional and nutraceutical properties. In: Sanders TAB, ed. *Functional Dietary Lipids (Second Edition)*: Woodhead Publishing; 2024:69-97.
115. Wang L. *Chemometric and Metabolomic Investigations of Thermal Treatment-Induced Chemical and metabolic Events in Heat Stress, Preparation and Consumption of Heated Vegetable Oils*: Food Science and Nutrition, University of Minnesota; 2016.
116. Choe E, Min DB. Mechanisms and Factors for Edible Oil Oxidation. *Comprehensive Reviews in Food Science and Food Safety.* 2006;5(4):169-186.
117. Ho C-T, Chen Q. Lipids in Food Flavors. *Lipids in Food Flavors.* Vol 558: American Chemical Society; 1994:2-14.
118. Bax S, Hakka MH, Glaude P-A, Herbinet O, Battin-Leclerc F. Experimental study of the oxidation of methyl oleate in a jet-stirred reactor. *Combustion and Flame.* 2010;157(6):1220-1229.

119. Fullana A, Carbonell-Barrachina AA, Sidhu S. Comparison of Volatile Aldehydes Present in the Cooking Fumes of Extra Virgin Olive, Olive, and Canola Oils. *Journal of Agricultural and Food Chemistry.* 2004;52(16):5207-5214.
120. Wang X, Ho C-T, Shahidi F. Flavor Components of Fats and Oils. *Bailey's Industrial Oil and Fat Products*2020:1-25.
121. Xiao L, Li C, Chai D, et al. Volatile compound profiling from soybean oil in the heating process. *Food science & nutrition.* 2020;8(2):1139-1149.
122. Zhuang Y, Dong J, He X, et al. Impact of Heating Temperature and Fatty Acid Type on the Formation of Lipid Oxidation Products During Thermal Processing. *Frontiers in Nutrition.* 2022;9.
123. Yuan JY, Kerr BJ, Curry SM, Chen C. Identification of C9-C11 unsaturated aldehydes as prediction markers of growth and feed intake for non-ruminant animals fed oxidized soybean oil. *Journal of Animal Science and Biotechnology.* 2020;11(1).
124. Zamora R, Navarro JL, Aguilar I, Hidalgo FJ. Lipid-derived aldehyde degradation under thermal conditions. *Food Chemistry.* 2015;174:89-96.
125. Dasgupta A, Klein K. Chapter 2 - Methods for Measuring Oxidative Stress in the Laboratory. In: Dasgupta A, Klein K, eds. *Antioxidants in Food, Vitamins and Supplements*. San Diego: Elsevier; 2014:19-40.
126. Almandó s ME, Giannini DH, Ciarlo AS, Boeri RL. Formaldehyde as an interference of the 2-thiobarbituric acid test. *Journal of the Science of Food and Agriculture.* 1986;37(1):54-58.
127. Buttkus H, Bose RJ. Amine-malonaldehyde condensation products and their relative color contribution in the thiobarbituric acid test. *Journal of the American Oil Chemists' Society.* 1972;49(7):440-443.
128. Ma L, Liu G, Liu X. Amounts of malondialdehyde do not accurately represent the real oxidative level of all vegetable oils: a kinetic study of malondialdehyde formation. *International Journal of Food Science & Technology.* 2019;54(2):412-423.
129. Gordon MH. 7 - Factors affecting lipid oxidation. In: Steele R, ed. *Understanding and Measuring the Shelf-Life of Food*: Woodhead Publishing; 2004:128-141.
130. Guo Y, Wang L, Hanson A, Urriola PE, Shurson GC, Chen C. Identification of protective amino acid metabolism events in nursery pigs fed thermally oxidized corn oil. *Metabolites.* 2023;13(1):103.
131. Barriuso B, Astiasarán I, Ansorena D. A review of analytical methods measuring lipid oxidation status in foods: a challenging task. *European Food Research and Technology.* 2013;236(1):1-15.
132. Shellie RA. Gas Chromatography. In: Siegel JA, Saukko PJ, Houck MM, eds. *Encyclopedia of Forensic Sciences (Second Edition)*. Waltham: Academic Press; 2013:579-585.
133. Qian MC, Peterson DG, Reineccius GA. Gas Chromatography. In: Nielsen SS, ed. *Food Analysis*. Boston, MA: Springer US; 2010:513-537.
134. Pontes H, Guedes de Pinho P, Casal S, et al. GC Determination of Acetone, Acetaldehyde, Ethanol, and Methanol in Biological Matrices and Cell Culture. *Journal of Chromatographic Science.* 2009;47(4):272-278.

135. Liu X, Wang S, Tamogami S, Chen J, Zhang H. An Evaluation Model for the Quality of Frying Oil Using Key Aldehyde Detected by HS-GC/MS. *Foods.* 2022;11(16).
136. Wang X, Xu R, Tong X, et al. Characterization of different meat flavor compounds in Guangdong small-ear spotted and Yorkshire pork using two-dimensional gas chromatography–time-of-flight mass spectrometry and multi-omics. *LWT.* 2022;169:114010.
137. Mayr CM, Capone DL, Pardon KH, Black CA, Pomeroy D, Francis IL. Quantitative Analysis by GC-MS/MS of 18 Aroma Compounds Related to Oxidative Off-Flavor in Wines. *Journal of Agricultural and Food Chemistry.* 2015;63(13):3394-3401.
138. Yuwono SS, Hanasasmita N, Sunarharum WB, Harijono. Effect of different aroma extraction methods combined with GC-MS on the aroma profiles of coffee. *IOP Conference Series: Earth and Environmental Science.* 2019;230(1):012044.
139. Dator RP, Solivio MJ, Villalta PW, Balbo S. Bioanalytical and Mass Spectrometric Methods for Aldehyde Profiling in Biological Fluids. *Toxics.* 2019;7(2):32.
140. Berdyshev EV. Mass spectrometry of fatty aldehydes. *Biochimica et Biophysica Acta (BBA) - Molecular and Cell Biology of Lipids.* 2011;1811(11):680-693.
141. Spiteller G, Kern W, Spiteller P. Investigation of aldehydic lipid peroxidation products by gas chromatography–mass spectrometry. *Journal of Chromatography A.* 1999;843(1-2):29-98.
142. Schmarr HG, Sang W, Ganss S, et al. Analysis of aldehydes via headspace SPME with on-fiber derivatization to their O-(2,3,4,5,6-pentafluorobenzyl)oxime derivatives and comprehensive 2D-GC-MS. *Journal of separation science.* 2008;31(19):3458-3465.
143. Li N, Deng C, Yin X, Yao N, Shen X, Zhang X. Gas chromatography-mass spectrometric analysis of hexanal and heptanal in human blood by headspace single-drop microextraction with droplet derivatization. *Anal Biochem.* 2005;342(2):318-326.
144. Hanff E, Eisenga MF, Beckmann B, Bakker SJ, Tsikas D. Simultaneous pentafluorobenzyl derivatization and GC-ECNICI-MS measurement of nitrite and malondialdehyde in human urine: Close positive correlation between these disparate oxidative stress biomarkers. *J Chromatogr B Analyt Technol Biomed Life Sci.* 2017;1043:167-175.
145. Stalikas CD, Konidari CN. Analysis of malondialdehyde in biological matrices by capillary gas chromatography with electron-capture detection and mass spectrometry. *Anal Biochem.* 2001;290(1):108-115.
146. Cighetti G, Debiasi S, Paroni R, Allevi P. Free and total malondialdehyde assessment in biological matrices by gas chromatography-mass spectrometry: what is needed for an accurate detection. *Anal Biochem.* 1999;266(2):222-229.
147. Osório VM, de Lourdes Cardeal Z. Determination of acrolein in french fries by solid-phase microextraction gas chromatography and mass spectrometry. *Journal of chromatography A.* 2011;1218 21:3332-3336.

148. Yashin YI, Yashin AY. Chapter 10 - Liquid Chromatography. In: Picó Y, ed. *Chemical Analysis of Food: Techniques and Applications*. Boston: Academic Press; 2012:285-310.
149. Liu S, Xu J, Sun J, Jiang X, Lv M, Wang L. Rapid HPLC–MS/MS Detection of Aliphatic Aldehyde Formation in Four Vegetable Oils from Different Frying Processes. *Food Analytical Methods.* 2021;14(12):2651-2659.
150. Lu Y, Yao D, Chen C. 2-Hydrazinoquinoline As A Derivatization Agent For LC-MS-Based Metabolomic Investigation Of Diabetic Ketoacidosis. *Metabolites.* 2013;3(4):993-1010.
151. Csallany AS, Han I, Shoeman DW, Chen C. 4-hydroxynonenal (HNE), a toxic aldehyde, in French fries from fast food restaurants in the USA. *Free Radical Biology and Medicine.* 2012;53:S250-S250.
152. Dator R, Carrà A, Maertens L, Guidolin V, Villalta PW, Balbo S. A High Resolution/Accurate Mass (HRAM) Data-Dependent MS(3) Neutral Loss Screening, Classification, and Relative Quantitation Methodology for Carbonyl Compounds in Saliva. *Journal of the American Society for Mass Spectrometry.* 2017;28(4):608-618.
153. Chiu H-H, Kuo C-H. Gas chromatography-mass spectrometry-based analytical strategies for fatty acid analysis in biological samples. *Journal of Food and Drug Analysis.* 2020;28(1):60-73.
154. Rohman A. Infrared spectroscopy for quantitative analysis and oil parameters of olive oil and virgin coconut oil: A review. *International Journal of Food Properties.* 2017;20(7):1447-1456.
155. Simon J, Tsetsgee O, Iqbal NA, et al. A fast method to measure the degree of oxidation of dialdehyde celluloses using multivariate calibration and infrared spectroscopy. *Carbohydrate Polymers.* 2022;278:118887.
156. Navarra G, Cannas M, D'Amico M, et al. Thermal oxidative process in extra-virgin olive oils studied by FTIR, rheology and time-resolved luminescence. *Food Chemistry.* 2011;126(3):1226-1231.
157. Wójcicki K, Khmelinskii I, Sikorski M, Sikorska E. Near and mid infrared spectroscopy and multivariate data analysis in studies of oxidation of edible oils. *Food chemistry.* 2015;187:416-423.
158. Alshuiael SM, Al-Ghouti MA. Multivariate analysis for FTIR in understanding treatment of used cooking oil using activated carbon prepared from olive stone. *PLoS One.* 2020;15(5):e0232997.
159. Goicoechea E, Guillen MD. Analysis of Hydroperoxides, Aldehydes and Epoxides by 1H Nuclear Magnetic Resonance in Sunflower Oil Oxidized at 70 and 100 °C. *Journal of Agricultural and Food Chemistry.* 2010;58(10):6234-6245.
160. Ahmed Laskar A, Younus H. Aldehyde toxicity and metabolism: the role of aldehyde dehydrogenases in detoxification, drug resistance and carcinogenesis. *Drug metabolism reviews.* 2019;51(1):42-64.
161. Stott-Miller M, Neuhouser ML, Stanford JL. Consumption of deep-fried foods and risk of prostate cancer. *The prostate.* 2013;73(9):960-969.

162. Sayon-Orea C, Martinez-Gonzalez M, Gea A, Flores-Gomez E, Basterra-Gortari F, Bes-Rastrollo M. Consumption of fried foods and risk of metabolic syndrome: the SUN cohort study. *Clinical nutrition.* 2014;33(3):545-549.
163. Sun Y, Liu B, Snetselaar LG, et al. Association of fried food consumption with all cause, cardiovascular, and cancer mortality: prospective cohort study. *BMJ.* 2019:k5420.
164. Zhang T, Song SS, Liu M, Park S. Association of Fried Food Intake with Gastric Cancer Risk: A Systemic Review and Meta-Analysis of Case-Control Studies. *Nutrients.* 2023;15(13).
165. Lin J, Zhang SM, Cook NR, Lee IM, Buring JE. Dietary fat and fatty acids and risk of colorectal cancer in women. *American journal of epidemiology.* 2004;160(10):1011-1022.
166. Stott-Miller M, Neuhouser ML, Stanford JL. Consumption of deep-fried foods and risk of prostate cancer. *Prostate.* 2013;73(9):960-969.
167. Hanson AR, Urriola PE, Wang L, Johnston LJ, Chen C, Shurson GC. Dietary peroxidized maize oil affects the growth performance and antioxidant status of nursery pigs. *Animal Feed Science and Technology.* 2016;216:251-261.
168. Wang L, Yao D, Urriola PE, et al. Identification of activation of tryptophan–NAD+ pathway as a prominent metabolic response to thermally oxidized oil through metabolomics-guided biochemical analysis. *The Journal of nutritional biochemistry.* 2018;57:255-267.
169. Shafaeizadeh S, Jamalian J, Owji AA, et al. The effect of consuming oxidized oil supplemented with fiber on lipid profiles in rat model. *Journal of research in medical sciences : the official journal of Isfahan University of Medical Sciences.* 2011;16(12):1541-1549.
170. Suomela J-P, Ahotupa M, Kallio H. Triacylglycerol oxidation in pig lipoproteins after a diet rich in oxidized sunflower seed oil. 2005;40(5):437-444.
171. Keller J, Baradat M, Jouanin I, Debrauwer L, Gueraud F. "Twin peaks": searching for 4-hydroxynonenal urinary metabolites after oral administration in rats. *Redox biology.* 2015;4:136-148.
172. Van Dijk SJ, Feskens EJ, Bos MB, et al. A saturated fatty acid–rich diet induces an obesity-linked proinflammatory gene expression profile in adipose tissue of subjects at risk of metabolic syndrome. *The American journal of clinical nutrition.* 2009;90(6):1656-1664.
173. Schaur RJ. Basic aspects of the biochemical reactivity of 4-hydroxynonenal. *Molecular Aspects of Medicine.* 2003;24(4):149-159.
174. Castegna A, Drake J, Pocernich C, Butterfield DA. Protein Carbonyl Levels– An Assessment of Protein Oxidation. *Methods in Biological Oxidative Stress*: Humana Press; 2003:161-168.
175. Lopachin RM, Gavin T, Decaprio A, Barber DS. Application of the Hard and Soft, Acids and Bases (HSAB) Theory to Toxicant–Target Interactions. *Chemical Research in Toxicology.* 2012;25(2):239-251.
176. Doorn JA, Petersen DR. Covalent adduction of nucleophilic amino acids by 4-hydroxynonenal and 4-oxononenal. 2003;143-144:93-100.

177. Sousa BC, Pitt AR, Spickett CM. Chemistry and analysis of HNE and other prominent carbonyl-containing lipid oxidation compounds. *Free Radical Biology and Medicine.* 2017;111:294-308.
178. Isom AL, Barnes S, Wilson L, Kirk M, Coward L, Darley-Usmar V. Modification of Cytochrome c by 4-hydroxy- 2-nonenal: Evidence for histidine, lysine, and arginine-aldehyde adducts. 2004;15(8):1136-1147.
179. Aslebagh R, Pfeffer BA, Fliesler SJ, Darie CC. Mass spectrometry-based proteomics of oxidative stress: Identification of 4-hydroxy-2-nonenal (HNE) adducts of amino acids using lysozyme and bovine serum albumin as model proteins. 2016;37(20):2615-2623.
180. Czerny C, Eder E, Rünger TM. Genotoxicity and mutagenicity of the α,β-unsaturated carbonyl compound crotonaldehyde (butenal) on a plasmid shuttle vector. 1998;407(2):125-134.
181. Aitken RJ, Whiting S, De Iuliis GN, McClymont S, Mitchell LA, Baker MA. Electrophilic Aldehydes Generated by Sperm Metabolism Activate Mitochondrial Reactive Oxygen Species Generation and Apoptosis by Targeting Succinate Dehydrogenase. 2012;287(39):33048-33060.
182. Weng M-W, Lee H-W, Park S-H, et al. Aldehydes are the predominant forces inducing DNA damage and inhibiting DNA repair in tobacco smoke carcinogenesis. *Proceedings of the National Academy of Sciences.* 2018;115(27):E6152-E6161.
183. Prakasham K, Gurrani S, Wu C-F, et al. Rapid identification and monitoring of cooking oil fume-based toxic volatile organic aldehydes in lung tissue for predicting exposure level and cancer risks. *Chemosphere.* 2023;339:139704.
184. Pizzimenti S, Ciamporcero E, Daga M, et al. Interaction of aldehydes derived from lipid peroxidation and membrane proteins. *Frontiers in Physiology.* 2013;4.
185. Bhatnagar A. Environmental Cardiology. *Circulation Research.* 2006;99(7):692-705.
186. Ringseis R, Piwek N, Eder K. Oxidized fat induces oxidative stress but has no effect on NF-κB-mediated proinflammatory gene transcription in porcine intestinal epithelial cells. 2007;56(3):118-125.
187. Ambreen G, Siddiq A, Hussain K. Association of long-term consumption of repeatedly heated mix vegetable oils in different doses and hepatic toxicity through fat accumulation. *Lipids in Health and Disease.* 2020;19(1).
188. Overholt MF, Dilger AC, Boler DD, Kerr BJ. Influence of feeding thermally peroxidized soybean oil on growth performance, digestibility, and gut integrity in finishing pigs. *Journal of Animal Science.* 2018.
189. Dalle-Donne I, Rossi R, Giustarini D, Milzani A, Colombo R. Protein carbonyl groups as biomarkers of oxidative stress. *Clinica Chimica Acta.* 2003;329(1-2):23-38.
190. Grimsrud PA, Xie H, Griffin TJ, Bernlohr DA. Oxidative Stress and Covalent Modification of Protein with Bioactive Aldehydes. *Journal of Biological Chemistry.* 2008;283(32):21837-21841.
191. Schaich KM. Toxicity of lipid oxidation products consumed in the diet. *Bailey's Industrial Oil and Fat Products; John Wiley & Sons: Hoboken, NJ, USA.* 2020:1-88.

192. Varady J, Gessner DK, Most E, Eder K, Ringseis R. Dietary moderately oxidized oil activates the Nrf2 signaling pathway in the liver of pigs. *Lipids in Health and Disease.* 2012;11(1):31.
193. Ma Q. Role of Nrf2 in Oxidative Stress and Toxicity. *Annual Review of Pharmacology and Toxicology.* 2013;53(1):401-426.
194. O'Brien PJ, Siraki AG, Shangari N. Aldehyde sources, metabolism, molecular toxicity mechanisms, and possible effects on human health. *Critical Reviews in Toxicology.* 2005;35(7):609-662.
195. Hartley DP, Ruth JA, Petersen DR. The hepatocellular metabolism of 4-hydroxynonenal by alcohol dehydrogenase, aldehyde dehydrogenase, and glutathione S-transferase. *Arch Biochem Biophys.* 1995;316(1):197-205.
196. Ray S, Ray M. Purification and characterization of NAD and NADP-linked alpha-ketoaldehyde dehydrogenases involved in catalyzing the oxidation of methylglyoxal to pyruvate. *J Biol Chem.* 1982;257(18):10566-10570.
197. Siems WG, Zollner H, Grune T, Esterbauer H. Metabolic fate of 4-hydroxynonenal in hepatocytes: 1,4-dihydroxynonene is not the main product. *J Lipid Res.* 1997;38(3):612.
198. Hanna PE, Anders MW. The mercapturic acid pathway. *Critical Reviews in Toxicology.* 2019;49(10):819-929.
199. Grootveld M, Atherton MD, Sheerin AN, et al. In vivo absorption, metabolism, and urinary excretion of alpha, beta-unsaturated aldehydes in experimental animals. Relevance to the development of cardiovascular diseases by the dietary ingestion of thermally stressed polyunsaturate-rich culinary oils. *The Journal of clinical investigation.* 1998;101(6):1210-1218.
200. Sidell KR, Montine KS, Picklo MJ, Olsen SJ, Amarnath V, Montine TJ. Mercapturate Metabolism of 4-Hydroxy-2-Nonenal in Rat and Human Cerebrum. 2003;62(2):146-153.
201. Alary J, Fernandez Y, Debrauwer L, Perdu E, Guéraud F. Identification of Intermediate Pathways of 4-Hydroxynonenal Metabolism in the Rat. 2003;16(3):320-327.
202. Alary J, Gueraud F, Cravedi JP. Fate of 4-hydroxynonenal in vivo: disposition and metabolic pathways. *Mol Aspects Med.* 2003;24(4-5):177-187.
203. Kuiper HC, Miranda CL, Sowell JD, Stevens JF. Mercapturic acid conjugates of 4-hydroxy-2-nonenal and 4-oxo-2-nonenal metabolites are in vivo markers of oxidative stress. *The Journal of biological chemistry.* 2008;283(25):17131-17138.
204. Boleda MD, Julià P, Moreno A, Parés X. Role of extrahepatic alcohol dehydrogenase in rat ethanol metabolism. *Archives of biochemistry and biophysics.* 1989;274(1):74-81.
205. Chiang C-P, Jao S-W, Lee S-P, et al. Expression pattern, ethanol-metabolizing activities, and cellular localization of alcohol and aldehyde dehydrogenases in human large bowel: association of the functional polymorphisms of ADH and ALDH genes with hemorrhoids and colorectal cancer. *Alcohol.* 2012;46(1):37-49.
206. Kozminski KD, Selimkhanov J, Heyward S, Zientek MA. Contribution of Extrahepatic Aldehyde Oxidase Activity to Human Clearance. *Drug Metab Dispos.* 2021;49(9):743-749.

207. Wang Y, He W. Chapter 21 - Endogenous Mitochondrial Aldehyde Dehydrogenase-2 as an Antioxidant in Liver. In: Patel VB, Rajendram R, Preedy VR, eds. *The Liver*. Boston: Academic Press; 2018:247-259.
208. Cui JY, Li CY. 2.08 - Regulation of Xenobiotic Metabolism in the Liver☆. In: McQueen CA, ed. *Comprehensive Toxicology (Third Edition)*. Oxford: Elsevier; 2018:168-214.
209. Liu Z, Liu M, Lyu C, et al. Effect of Heat Treatment on Oxidation of Hazelnut Oil. *Journal of Oleo Science.* 2022;71(12):1711-1723.
210. Xu L, Wu G, Zhang Y, et al. Evaluation of glycerol core aldehydes formation in edible oils under restaurant deep frying. *Food Research International.* 2020;137:109696.
211. Hu Q, Zhang J, Li G, Wei L, Zhong C, Chen Y. Oxidative lipidomics to elucidate the non-volatile derivatives of four typical triglycerides in vegetable oils under simulated frying conditions. *Food Chemistry.* 2023;410:135414.
212. Steenhorst - Slikkerveer L, Louter A, Janssen HG, Bauer - Plank C. Analysis of nonvolatile lipid oxidation products in vegetable oils by normal - phase high - performance liquid chromatography with mass spectrometric detection. *Journal of the American Oil Chemists' Society.* 2000;77(8):837.
213. Khor YP, Hew KS, Abas F, et al. Oxidation and Polymerization of Triacylglycerols: In-Depth Investigations towards the Impact of Heating Profiles. *Foods.* 2019;8(10).
214. Paul S, Mittal GS. Regulating the use of degraded oil/fat in deep-fat/oil food frying. *Crit Rev Food Sci Nutr.* 1997;37(7):635-662.
215. Berdeaux O, Dutta PC, Dobarganes MC, Sébédio JL. Analytical Methods for Quantification of Modified Fatty Acids and Sterols Formed as a Result of Processing. *Food Analytical Methods.* 2009;2(1):30-40.
216. Bruhl L, Weisshaar R, Matthaus B. Epoxy fatty acids in used frying fats and oils, edible oils and chocolate and their formation in oils during heating. *European Journal of Lipid Science and Technology.* 2016;118(3):425-434.
217. Kalogeropoulos N, Salta FN, Chiou A, Andrikopoulos NK. Formation and distribution of oxidized fatty acids during deep - and pan - frying of potatoes. *European Journal of Lipid Science and Technology.* 2007;109(11):1111-1123.
218. Cao WM, Zhang KY, Xue B, Chen FX, Jin QZ, Wang XG. Determination of Oxidized Triacylglycerol Polymers by Preparative Flash Chromatography and High-Performance Size-Exclusion Chromatography. *Asian Journal of Chemistry.* 2013;25(16):9189-9194.
219. Sun J, Hu P, Lyu C, et al. Targeted Lipidomics Analysis of Oxylipids in Hazelnut Oil during Storage by Liquid Chromatography Coupled to Tandem Mass Spectrometry. *Journal of Agricultural and Food Chemistry.* 2022;70(5):1715-1723.
220. Koelmel JP, Aristizabal-Henao JJ, Ni Z, et al. A Novel Technique for Redox Lipidomics Using Mass Spectrometry: Application on Vegetable Oils Used to Fry Potatoes. *Journal of the American Society for Mass Spectrometry.* 2021;32(7):1798-1809.
221. Hamosh M. Lingual and gastric lipases. *Nutrition.* 1990;6(6):421-428.

222. Márquez-Ruiz G, Guevel G, Dobarganes MC. Applications of chromatographic techniques to evaluate enzymatic hydrolysis of oxidized and polymeric triglycerides by pancreatic lipase in vitro. *Journal of the American Oil Chemists' Society.* 1998;75(2):119-126.
223. Giuffrida F, Destaillats F, Robert F, Skibsted LH, Dionisi F. Formation and hydrolysis of triacylglycerol and sterols epoxides: Role of unsaturated triacylglycerol peroxyl radicals. *Free Radical Biology and Medicine.* 2004;37(1):104-114.
224. Miyamoto S, Dupas C, Murota K, Terao J. Phospholipid hydroperoxides are detoxified by phospholipase A2 and GSH peroxidase in rat gastric mucosa. *Lipids.* 2003;38(6):641-649.
225. Golding M, Wooster TJ. The influence of emulsion structure and stability on lipid digestion. *Current Opinion in Colloid & Interface Science.* 2010;15(1-2):90-101.
226. Nieva-Echevarría B, Goicoechea E, Manzanos MJ, Guillén MD. (1)H NMR and SPME-GC/MS study of hydrolysis, oxidation and other reactions occurring during in vitro digestion of non-oxidized and oxidized sunflower oil. Formation of hydroxy-octadecadienoates. *Food research international (Ottawa, Ont).* 2017;91:171-182.
227. Matsushita S. Specific interactions of linoleic acid hydroperoxides and their secondary degraded products with enzyme proteins. *J Agric Food Chem.* 1975;23(2):150-154.
228. Li X, Liu Y-j, Nian B-b, et al. Molecular dynamics revealed the effect of epoxy group on triglyceride digestion. *Food Chemistry.* 2022;373:131285.
229. Aw TY, Williams MW, Gray L. Absorption and lymphatic transport of peroxidized lipids by rat small intestine in vivo: role of mucosal GSH. *The American journal of physiology.* 1992;262(1 Pt 1):G99-106.
230. Sherratt PJ, Hayes JD. Glutathione S-transferases. *Enzyme Systems that Metabolise Drugs and Other Xenobiotics*2001:319-352.
231. White BA, Mackie RI. Gastrointestinal microbiology. Vol. 1, Gastrointestinal ecosystems and fermentations. 1997.
232. Hussain MM. Intestinal lipid absorption and lipoprotein formation. *Current opinion in lipidology.* 2014;25(3):200-206.
233. Márquez-Ruiz G, Dobarganes MC. Changes in endogenous lipid excretion in rats fed diets containing non-heated and thermally oxidized olive oils. *Scandinavian journal of gastroenterology.* 1992;27(12):1069-1076.
234. Márquez-Ruiz G, Dobarganes MC. Assessments on the digestibility of oxidized compounds from [1-14C] linoleic acid using a combination of chromatographic techniques. *Journal of chromatography B, Biomedical applications.* 1996;675(1):1-8.
235. El-Sherbeni AA, El-Kadi AO. The role of epoxide hydrolases in health and disease. *Archives of toxicology.* 2014;88:2013-2032.
236. Decker M, Adamska M, Cronin A, et al. EH3 (ABHD9): the first member of a new epoxide hydrolase family with high activity for fatty acid epoxides. *Journal of lipid research.* 2012;53(10):2038-2045.

237. Greene JF, Newman JW, Williamson KC, Hammock BD. Toxicity of epoxy fatty acids and related compounds to cells expressing human soluble epoxide hydrolase. *Chemical Research in Toxicology.* 2000;13(4):217-226.
238. Ringseis R, Eder K. Regulation of genes involved in lipid metabolism by dietary oxidized fat. 2011;55(1):109-121.
239. Chao P-M, Chao C-Y, Lin F-J, Huang C-J. Oxidized Frying Oil Up-Regulates Hepatic Acyl-CoA Oxidase and Cytochrome P450 4 A1 Genes in Rats and Activates PPARα. *The Journal of Nutrition.* 2001;131(12):3166-3174.
240. Suzuki H, Yamada J, Watanabe T, Suga T. Compartmentation of dicarboxylic acid β-oxidation in rat liver: importance of peroxisomes in the metabolism of dicarboxylic acids. 1989;990(1):25-30.
241. Houten SM, Denis S, Argmann CA, et al. Peroxisomal L-bifunctional enzyme (Ehhadh) is essential for the production of medium-chain dicarboxylic acids. *Journal of Lipid Research.* 2012;53(7):1296-1303.
242. Miura Y. The biological significance of ^|^omega;-oxidation of fatty acids. *Proceedings of the Japan Academy, Series B.* 2013;89(8):370-382.
243. Holden P, Tugwood J. Peroxisome proliferator-activated receptor alpha: role in rodent liver cancer and species differences. *Journal of molecular endocrinology.* 1999;22(1):1-8.
244. Dingels NK. Oxidized soybean oil alters the expression of PPAR gamma and target genes in 3T3-L1 cells. 2012.
245. Ahmadian M, Suh JM, Hah N, et al. PPARγ signaling and metabolism: the good, the bad and the future. *Nature Medicine.* 2013;19(5):557-566.
246. Hong F, Pan S, Guo Y, Xu P, Zhai Y. PPARs as Nuclear Receptors for Nutrient and Energy Metabolism. *Molecules.* 2019;24(14):2545.
247. Koch A, KöNig B, Spielmann J, Leitner A, Stangl GI, Eder K. Thermally Oxidized Oil Increases the Expression of Insulin-Induced Genes and Inhibits Activation of Sterol Regulatory Element-Binding Protein-2 in Rat Liver. *The Journal of Nutrition.* 2007;137(9):2018-2023.
248. König B, Koch A, Spielmann J, Hilgenfeld C, Stangl GI, Eder K. Activation of PPARα lowers synthesis and concentration of cholesterol by reduction of nuclear SREBP-2. 2007;73(4):574-585.
249. Liu P, Chen C, Kerr BJ, Weber TE, Johnston LJ, Shurson GC. Influence of thermally oxidized vegetable oils and animal fats on growth performance, liver gene expression, and liver and serum cholesterol and triglycerides in young pigs1. *Journal of Animal Science.* 2014;92(7):2960-2970.
250. Xiao W, Wang R-S, Handy DE, Loscalzo J. NAD(H) and NADP(H) Redox Couples and Cellular Energy Metabolism. *Antioxidants & Redox Signaling.* 2018;28(3):251-272.
251. Oliphant K, Allen-Vercoe E. Macronutrient metabolism by the human gut microbiome: major fermentation by-products and their impact on host health. *Microbiome.* 2019;7(1):91.
252. Zhou Z, Wang Y, Jiang Y, et al. Deep-fried oil consumption in rats impairs glycerolipid metabolism, gut histology and microbiota structure. *Lipids in health and disease.* 2016;15(1):86.

253. Kwek E, Yan C, Ding H, et al. Effects of thermally-oxidized frying oils (corn oil and lard) on gut microbiota in hamsters. *Antioxidants.* 2022;11(9):1732.
254. Ruan M, Bu Y, Wu F, et al. Chronic consumption of thermally processed palm oil or canola oil modified gut microflora of rats. *Food Science and Human Wellness.* 2021;10(1):94-102.
255. Ruan M, Zhang Z, Yuan X, et al. Effects of deep frying vegetable oils rich in <scp>PUFAs</scp> on gut microbiota in rats. *International Journal of Food Science & Technology.* 2023;58(1):37-44.
256. Bailey RL. Overview of dietary assessment methods for measuring intakes of foods, beverages, and dietary supplements in research studies. *Current opinion in biotechnology.* 2021;70:91-96.
257. Harnack L. Nutrition Data System for Research (NDSR). In: Gellman MD, Turner JR, eds. *Encyclopedia of Behavioral Medicine*. New York, NY: Springer New York; 2013:1348-1350.
258. USDA Approved Nutrient Analysis Software. In: USDA, ed.
259. Clarke ED, Rollo ME, Pezdirc K, Collins CE, Haslam RL. Urinary biomarkers of dietary intake: a review. *Nutr Rev.* 2020;78(5):364-381.
260. Lin P, Lee H-L, Cheng H-I, Chen C-Y, Tsai M-H, Liu H-J. Metabolomic profiling of mice urine and serum associated with trans-trans 2, 4-decadienal induced lung lesions by liquid chromatography-mass spectrometry. *Analytical and Bioanalytical Chemistry.* 2014;406(17):4287-4297.
261. Camargo SM, Bockenhauer D, Kleta R. Aminoacidurias: Clinical and molecular aspects. *Kidney Int.* 2008;73(8):918-925.
262. Alary J, Debrauwer L, Fernandez Y, Cravedi J-P, Rao D, Bories G. 1,4-Dihydroxynonene Mercapturic Acid, the Major End Metabolite of Exogenous 4-Hydroxy-2-nonenal, Is a Physiological Component of Rat and Human Urine. *Chemical Research in Toxicology.* 1998;11(2):130-135.
263. Alary J, Gueraud F, Cravedi J-P. Fate of 4-hydroxynonenal in vivo: Disposition and metabolic pathways. *Molecular Aspects of Medicine.* 2003;24(4-5):177-187.
264. Jamin EL, Costantino R, Mervant L, et al. Global Profiling of Toxicologically Relevant Metabolites in Urine: Case Study of Reactive Aldehydes. *Analytical Chemistry.* 2020;92(2):1746-1754.
265. Keller J, Baradat M, Jouanin I, Debrauwer L, Guéraud F. "Twin peaks": Searching for 4-hydroxynonenal urinary metabolites after oral administration in rats. *Redox biology.* 2015;4:136-148.
266. Wang L, Csallany AS, Kerr BJ, Shurson GC, Chen C. Kinetics of Forming Aldehydes in Frying Oils and Their Distribution in French Fries Revealed by LC-MS-Based Chemometrics. *Journal of Agricultural and Food Chemistry.* 2016;64(19):3881-3889.
267. Schlager KJ, Ruchti TL. Overview of chemometrics. Paper presented at: Ultrasensitive Instrumentation for DNA Sequencing and Biochemical Diagnostics1995.
268. Yang K, Han X. Lipidomics: Techniques, Applications, and Outcomes Related to Biomedical Sciences. *Trends in biochemical sciences.* 2016;41(11):954-969.

269. Chen H, Wei F, Dong X-y, Xiang J-q, Quek S-y, Wang X. Lipidomics in food science. *Current Opinion in Food Science.* 2017;16:80-87.
270. Luo Y, Gao B, Zhang Y, Yu LL. Detection of olive oil adulteration with vegetable oils by ultra-performance convergence chromatography-quadrupole time-of-flight mass spectrometry (UPC(2)-QTOF MS) coupled with multivariate data analysis based on the differences of triacylglycerol compositions. *Food science & nutrition.* 2020;8(7):3759-3767.
271. Liu H, Guo X, Zhao Q, Qin Y, Zhang J. Lipidomics analysis for identifying the geographical origin and lactation stage of goat milk. *Food Chemistry.* 2020;309:125765.
272. Grüneis V, Fruehwirth S, Zehl M, et al. Simultaneous analysis of epoxidized and hydroperoxidized triacylglycerols in canola oil and margarine by LC-MS. *J Agric Food Chem.* 2019;67:10174.
273. Neff WE, Byrdwell WC. Characterization of model triacylglycerol (triolein, trilinolein and trilinolenin) autoxidation products via high-performance liquid chromatography coupled with atmospheric pressure chemical ionization mass spectrometry. *Journal of Chromatography A.* 1998;818(2):169-186.
274. Petronilho S, Neves B, Melo Tn, et al. Characterization of non-volatile oxidation products formed from triolein in a model study at frying temperature. *J Agric Food Chem.* 2021;69:3466.
275. Guasch-Ferré M, Bhupathiraju SN, Hu FB. Use of metabolomics in improving assessment of dietary intake. *Clinical chemistry.* 2018;64(1):82-98.
276. Chen C, Gonzalez FJ, Idle JR. LC-MS-based metabolomics in drug metabolism. *Drug metabolism reviews.* 2007;39(2-3):581-597.
277. Clish CB. Metabolomics: An Emerging But Powerful Tool For Precision Medicine. *Molecular Case Studies.* 2015;1(1):a000588.
278. Yuan L, Jiang F, Cao X, Liu Y, Xu Y-J. Metabolomics reveals the toxicological effects of polar compounds from frying palm oil. *Food & function.* 2020;11(2):1611-1623.
279. Liu Z-Y, Hu Y-Y, Zhao M-T, et al. Formation and disappearance of aldehydes during simulated gastrointestinal digestion of fried clams. *Food & function.* 2020;11(4):3483-3492.
280. Wang Y, Cao X, Shi J, Li X, Liu Y, Xu Y-J. Tracking the dynamics of epoxy triglycerides during thermal oxidation by liquid chromatography-mass spectrometry. *Food Control.* 2023;146:109523.
281. Buckley BM, Williamson DH. Origins of Blood Acetate in Rat. *Biochemical Journal.* 1977;166(3):539-545.
282. Gill PA, Bogatyrev A, Van Zelm MC, Gibson PR, Muir JG. Delivery of Acetate to the Peripheral Blood after Consumption of Foods High in Short-Chain Fatty Acids. *Molecular Nutrition & Food Research.* 2021;65(4):2000953.
283. Luginbühl M, Rutjens S, König S, Furrer J, Weinmann W. N-Acetyltaurine As A Novel Urinary Ethanol Marker In A Drinking Study. *Analytical and Bioanalytical Chemistry.* 2016;408(26):7529-7536.
284. Miyazaki T, Ishikura K, Honda A, et al. Increased N-Acetyltaurine In Serum And Urine After Endurance Exercise In Human. Paper presented at: Taurine 92015.

285. Miyazaki T, Nakamura-Shinya Y, Ebina K, et al. N-acetyltaurine and Acetylcarnitine Production for the Mitochondrial Acetyl-CoA Regulation in Skeletal Muscles during Endurance Exercises. *Metabolites.* 2021;11(8).
286. Mathew R. Progress toward Acetate Supplementation Therapy for Canavan Disease: Glyceryl Triacetate Administration Increases Acetate, but Not N-Acetylaspartate, Levels in Brain. *Journal of Pharmacology and Experimental Therapeutics.* 2005;315(1):297-303.
287. Larsen LH, Ørstrup LKH, Hansen SH, Grunnet N, Quistorff B, Mortensen OH. The Effect of Long-Term Taurine Supplementation and Fructose Feeding on Glucose and Lipid Homeostasis in Wistar Rats. Paper presented at: Taurine 82013; New York, NY.
288. Jellum E, Horn L, Thoresen O, Kvittingen EA, Stokke O. Urinary Excretion Of N-Acetyl Amino Acids In Patients With Some Inborn Errors Of Amino Acid Metabolism. *Scandinavian journal of clinical and laboratory investigation Supplementum.* 1986;184:21-26.
289. Tsai G, Coyle JT. N-Acetylaspartate in Neuropsychiatric Disorders. *Progress in Neurobiology.* 1995;46(5):531-540.
290. Gronwald W, Klein MS, Zeltner R, et al. Detection of Autosomal Dominant Polycystic Kidney Disease By NMR Spectroscopic Fingerprinting Of Urine. *Kidney International.* 2011;79(11):1244-1253.
291. Bhandari S, Bisht KS, Merkler DJ. The Biosynthesis and Metabolism of the N-Acylated Aromatic Amino Acids: N-Acylphenylalanine, N-Acyltyrosine, N-Acyltryptophan, and N-Acylhistidine. *Frontiers in Molecular Biosciences.* 2022;8.
292. Hayes KC, Sturman JA. Taurine in Metabolism. *The Annual Review of Nutrition.* 1981;1:401-425.
293. Han X, Budreau AM, Chesney RW. Functional Expression Of Rat Renal Cortex Taurine Transporter In Xenopus Laevis Oocytes: Adaptive Regulation By Dietary Manipulation. *Pediatric Research.* 1997;41(5):624-631.
294. Chesney RW, Friedman AL, Albright PW, Gusowski N. Fasting Reverses The Renal Adaptation To Altered Dietary Sulfur Amino Acid Intake. Paper presented at: The Society for Experimental Biology and Medicine; Sep, 1982.
295. Hsieh Y-L, Yeh Y-H, Lee Y-T, Huang C-Y. Effect of Taurine in Chronic Alcoholic Patients. *Food Funct.* 2014;5(7):1529-1535.
296. Trachtman H, Futterweit S, Maesaka J, et al. Taurine Ameliorates Chronic Streptozocin-Induced Diabetic Nephropathy In Rats. *American Journal of Physiology.* 1995;269(3 Pt 2):F429-438.
297. Gill PA, Bogatyrev A, van Zelm MC, Gibson PR, Muir JG. Delivery of Acetate to the Peripheral Blood after Consumption of Foods High in Short-Chain Fatty Acids. *Mol Nutr Food Res.* 2021;65(4):e2000953.
298. Mueller NT, Zhang M, Juraschek SP, Miller ER, Appel LJ. Effects Of High-Fiber Diets Enriched With Carbohydrate, Protein, Or Unsaturated Fat On Circulating Short Chain Fatty Acids: Results From The Omniheart Randomized Trial. *American Journal of Clinical Nutrition.* 2020;111(3):545-554.

299. Neavyn MJ, Boyer EW, Bird SB, Babu KM. Sodium Acetate as a Replacement for Sodium Bicarbonate in Medical Toxicology: a Review. *Journal of Medical Toxicology.* 2013;9(3):250-254.
300. Tollinger CD, Vreman HJ, Weiner MW. Measurement Of Acetate In Human Blood By Gas Chromatography: Effects Of Sample Preparation, Feeding, And Various Diseases. *Clinical Chemistry.* 1979;25(10):1787-1790.
301. Imenez Silva PH, Mohebbi N. Kidney Metabolism and Acid-base Control: Back To The Basics. *Pflugers Archiv : European journal of physiology.* 2022;474(8):919-934.
302. Hauet T, Baumert H, Gibelin H, Godart C, Carretier M, Eugene M. Citrate, Acetate and Renal Medullary Osmolyte Excretion in Urine as Predictor of Renal Changes after Cold Ischaemia and Transplantation. *Clin Chem Lab Med.* 2000;38(11):1093-1098.
303. Sison RC, Collado A, Dedeles JI, et al. Diagnostic Significance of Urine Acetic Acid Level Among Pregnant Women with Bacterial Urinary Tract Infection. *American Journal of Clinical Pathology.* 2015;144(suppl_2):A216-A216.
304. Abeyrathne E, Nam K, Ahn DU. Analytical methods for lipid oxidation and antioxidant capacity in food systems. *Antioxidants (Basel, Switzerland).* 2021;10(10).
305. Guillen MD, Goicoechea E. Oxidation of corn oil at room temperature: Primary and secondary oxidation products and determination of their concentration in the oil liquid matrix from 1H nuclear magnetic resonance data. *Food Chemistry.* 2009;116(1):183-192.
306. Ramis-Ramos G. Antioxidants | Synthetic Antioxidants. In: Caballero B, ed. *Encyclopedia of Food Sciences and Nutrition (Second Edition)*. Oxford: Academic Press; 2003:265-275.
307. Dobarganes MC, Márquez-Ruiz G. Formation and analysis of oxidized monomeric, dimeric, and higher oligomeric triglycerides. *Deep Frying*: Elsevier; 2007:87-110.
308. Zhou Z, Li Y-L, Zhao F, et al. Unraveling the Thermal Oxidation Products and Peroxidation Mechanisms of Different Chemical Structures of Lipids: An Example of Molecules Containing Oleic Acid. *Journal of Agricultural and Food Chemistry.* 2022;70(51):16410-16423.
309. Yuan L, Xu Z, Tan C-P, Liu Y, Xu Y-J. Biohazard and dynamic features of different polar compounds in vegetable oil during thermal oxidation. *LWT.* 2021;146:111450.
310. Li X, Yu X, Sun D, et al. Effects of polar compounds generated from the deep-frying process of palm oil on lipid metabolism and glucose tolerance in Kunming mice. *Journal of agricultural and food chemistry.* 2017;65(1):208-215.
311. Bligh EG, Dyer WJ. A rapid method of total lipid extraction and purification. *Canadian journal of biochemistry and physiology.* 1959;37(8):911-917.
312. Tanaka T, Metori K, Mineo S, Hirotani M, Furuya T, Kobayashi S. Inhibitory effects of berberine-type alkaloids on elastase. *Planta medica.* 1993;59(03):200-202.
313. Liu K. Soybean trypsin inhibitor assay: further improvement of the standard method approved and reapproved by American Oil Chemists' Society and

American Association of Cereal Chemists International. *Journal of the American Oil Chemists' Society.* 2019;96(6):635-645.
314. Minekus M, Alminger M, Alvito P, et al. A standardised staticin vitrodigestion method suitable for food – an international consensus. *Food Funct.* 2014;5(6):1113-1124.
315. Estévez M, Díaz-Velasco S, Martínez R. Protein carbonylation in food and nutrition: a concise update. *Amino Acids.* 2022;54(4):559-573.
316. Colombo G, Clerici M, Garavaglia ME, et al. A step-by-step protocol for assaying protein carbonylation in biological samples. *J Chromatogr B Analyt Technol Biomed Life Sci.* 2016;1019:178-190.
317. Feldman E. Thiobarbituric acid reactive substances (TBARS) assay. *AMDCC Protocols, Version.* 2004;50:1.
318. Jakimiuk K, Gesek J, Atanasov AG, Tomczyk M. Flavonoids as inhibitors of human neutrophil elastase. *Journal of enzyme inhibition and medicinal chemistry.* 2021;36(1):1016-1028.
319. Gass J, Vora H, Hofmann AF, Gray GM, Khosla C. Enhancement of dietary protein digestion by conjugated bile acids. *Gastroenterology.* 2007;133(1):16-23.
320. Clemente TE, Cahoon EB. Soybean oil: genetic approaches for modification of functionality and total content. *Plant Physiol.* 2009;151(3):1030-1040.
321. Frankel EN, Neff WE, Selke E. Analysis of autoxidized fats by gas chromatography-mass spectrometry: VII. Volatile thermal decomposition products of pure hydroperoxides from autoxidized and photosensitized oxidized methyl oleate, linoleate and linolenate. *Lipids.* 1981;16(5):279-285.
322. Shahidi F, Hossain A. Role of lipids in food flavor generation. *Molecules.* 2022;27(15):5014.
323. Martin-Rubio AS, Sopelana P, Ibargoitia ML, Guillén MD. 1H NMR Study of the In Vitro Digestion of Highly Oxidized Soybean Oil and the Effect of the Presence of Ovalbumin. *Foods.* 2021;10(7):1573.
324. Lee JH, Pangloli P. Volatile Compounds and Storage Stability of Potato Chips Fried in Mid-Oleic Sunflower Oil. *International Journal of Food Properties.* 2013;16(3):563-573.
325. Toishimanov M, Nurgaliyeva M, Serikbayeva A, et al. Comparative analysis and determination of the fatty acid composition of Kazakhstan's commercial vegetable oils by GC-FID. *Applied Sciences.* 2023;13(13):7910.
326. Papamandjaris AA, Macdougall DE, Jones PJH. Medium chain fatty acid metabolism and energy expenditure: Obesity treatment implications. *Life Sciences.* 1998;62(14):1203-1215.
327. Brühl L. Fatty acid alterations in oils and fats during heating and frying. *European Journal of Lipid Science and Technology.* 2014;116(6):707-715.
328. Frankel EN. Lipid oxidation. *Progress in Lipid Research.* 1980;19(1):1-22.
329. Kim TS, Yeo J, Kim JY, Kim M-J, Lee J. Determination of the degree of oxidation in highly-oxidised lipids using profile changes of fatty acids. *Food Chemistry.* 2013;138(2):1792-1799.
330. Kurz A, Seifert J. Factors influencing proteolysis and protein utilization in the intestine of pigs: a review. *Animals.* 2021;11(12):3551.

331. Fedkiv O, Rengman S, Westrom BR, Pierzynowski SG. Growth is dependent on the exocrine pancreas function in young weaners but not in growing-finishing pigs. *Journal of physiology and pharmacology : an official journal of the Polish Physiological Society.* 2009;60 Suppl 3:55-59.
332. Liu X, Huang X, Fu Y, Wang Y, Lu Z. The positive effects of exogenous pancreatin on growth performance, nutrient digestion and absorption, and intestinal microbiota in piglets. *Frontiers in Physiology.* 2022;13.
333. Schubert DC, Mößeler A, Ahlfänger B, et al. Influences of exocrine pancreatic insufficiency on nutrient digestibility, growth parameters as well as anatomical and histological morphology of the intestine in a juvenile pig model. *Frontiers in Medicine.* 2022;9.
334. Hedstrom L. Serine protease mechanism and specificity. *Chemical Reviews.* 2002;102(12):4501-4524.
335. Billinger E, Viljanen J, Lind SB, Johansson G. Inhibition properties of free and conjugated leupeptin analogues. *FEBS Open Bio.* 2020;10(12):2605-2615.
336. Macfarlane GT, Cummings JH, Macfarlane S, Gibson GR. Influence of retention time on degradation of pancreatic enzymes by human colonic bacteria grown in a 3-stage continuous culture system. *The Journal of applied bacteriology.* 1989;67(5):520-527.
337. Lam KW, Leeds J. How to manage: patient with a low faecal elastase. *Frontline gastroenterology.* 2021;12(1):67-73.
338. Li T, Han K, Feng G, et al. Bile acid profile influences digestion resistance and antigenicity of soybean 7S protein. *Journal of Agricultural and Food Chemistry.* 2023;71(6):2999-3009.
339. Cremers CM, Knoefler D, Vitvitsky V, Banerjee R, Jakob U. Bile salts act as effective protein-unfolding agents and instigators of disulfide stress in vivo. *Proceedings of the National Academy of Sciences.* 2014;111(16):E1610-E1619.
340. Nielsen HK, Finot PA, Hurrell RF. Reactions of proteins with oxidizing lipids. 1985;53(01):75.
341. Maj MA, Burrin DG, Manjarín R. Decreased FXR Agonism in the Bile Acid Pool Is Associated with Impaired FXR Signaling in a Pig Model of Pediatric NAFLD. *Biomedicines.* 2023;11(12):3303.
342. Jiang L, Zhang H, Xiao D, Wei H, Chen Y. Farnesoid X receptor (FXR): Structures and ligands. *Comput Struct Biotechnol J.* 2021;19:2148-2159.
343. Chiang JYL. Bile acids: regulation of synthesis. *Journal of Lipid Research.* 2009;50(10):1955-1966.
344. Modica S, Gadaleta RM, Moschetta A. Deciphering the nuclear bile acid receptor FXR paradigm. *Nuclear receptor signaling.* 2010;8:e005.
345. Khan-Merchant N, Penumetcha M, Meilhac O, Parthasarathy S. Oxidized Fatty Acids Promote Atherosclerosis Only in the Presence of Dietary Cholesterol in Low-Density Lipoprotein Receptor Knockout Mice. *The Journal of Nutrition.* 2002;132(11):3256-3262.
346. Xie C, Takahashi S, Brocker CN, et al. Hepatocyte peroxisome proliferator-activated receptor α regulates bile acid synthesis and transport. *Biochimica et biophysica acta Molecular and cell biology of lipids.* 2019;1864(10):1396-1411.

347. Zheng X, Chen T, Jiang R, et al. Hyocholic acid species improve glucose homeostasis through a distinct TGR5 and FXR signaling mechanism. *Cell Metabolism.* 2021;33(4):791-803.e797.
348. Albert BB, Vickers MH, Gray C, et al. Oxidized fish oil in rat pregnancy causes high newborn mortality and increases maternal insulin resistance. *American Journal of Physiology-Regulatory, Integrative and Comparative Physiology.* 2016;311(3):R497-R504.
349. Liao C-H, Shaw H-M, Chao P-M. Impairment of glucose metabolism in mice induced by dietary oxidized frying oil is different from that induced by conjugated linoleic acid. *Nutrition.* 2008;24(7-8):744-752.
350. Li T, Chiang JYL. Bile Acid Metabolism in Health and Disease. *The Liver*2020:269-285.
351. Madkour LH. Chapter 12 - Endoplasmic reticulum stress-induced cell death mechanism. In: Madkour LH, ed. *Reactive Oxygen Species (ROS), Nanoparticles, and Endoplasmic Reticulum (ER) Stress-Induced Cell Death Mechanisms*: Academic Press; 2020:299-342.
352. Miyazaki T, Sasaki S-i, Toyoda A, et al. The effects of taurine depletion on bile acid composition and its amino acid-conjugation in the bile of cats. *The FASEB Journal.* 2019;33(S1):765.761-765.761.
353. Konikoff FM, Leikin-Frenkel A, Goldiner I, et al. Biliary and systemic effects of fatty acid bile acid conjugates. *European journal of gastroenterology & hepatology.* 2003;15(6):649-655.
354. Jin X-Y, Zhu C-B, Fan S-Y, et al. Novel hypolipidemic conjugates of fatty acid and bile acid with lysine for linkage. *Drug Development and Industrial Pharmacy.* 2019;45(6):995-998.
355. Takei H, Narushima S, Suzuki M, et al. Characterization of long-chain fatty acid-linked bile acids: a major conjugation form of 3β-hydroxy bile acids in feces. *Journal of Lipid Research.* 2022;63(10):100275.
356. Sugai T, Takizawa M, Bakke M, Ohtsuka Y, Ohta H. Efficient lipase-catalyzed preparation of long-chain fatty acid esters of bile acids: biological activity and synthetic application of the products. *Biosci Biotechnol Biochem.* 1996;60(12):2059-2063.
357. Li Z, Vance DE. Thematic Review Series: Glycerolipids. Phosphatidylcholine and choline homeostasis. *Journal of Lipid Research.* 2008;49(6):1187-1194.
358. Corbin KD, Zeisel SH. Choline metabolism provides novel insights into nonalcoholic fatty liver disease and its progression. *Current opinion in gastroenterology.* 2012;28(2):159-165.
359. Barrios JM, Lichtenberger LM. Role of biliary phosphatidylcholine in bile acid protection and NSAID injury of the ileal mucosa in rats. *Gastroenterology.* 2000;118(6):1179-1186.
360. Yue HY, Wang J, Qi XL, et al. Effects of dietary oxidized oil on laying performance, lipid metabolism, and apolipoprotein gene expression in laying hens. *Poultry Science.* 2011;90(8):1728-1736.
361. Siddiq A, Ambreen G, Hussain K, Baig SG. Oxidative stress and lipid per-oxidation with repeatedly heated mix vegetable oils in different doses in comparison with

single time heated vegetable oils. *Pakistan journal of pharmaceutical sciences.* 2019;32(5):2099-2105.
362. Patrignani F, Iucci L, Belletti N, Gardini F, Guerzoni ME, Lanciotti R. Effects of sub-lethal concentrations of hexanal and 2-(E)-hexenal on membrane fatty acid composition and volatile compounds of Listeria monocytogenes, Staphylococcus aureus, Salmonella enteritidis and Escherichia coli. *Int J Food Microbiol.* 2008;123(1-2):1-8.
363. Lim L-T. Gases and Vapors Used in Food. In: Melton L, Shahidi F, Varelis P, eds. *Encyclopedia of Food Chemistry*. Oxford: Academic Press; 2019:114-120.
364. Yoon B, Jackman J, Valle-González E, Cho N-J. Antibacterial free fatty acids and monoglycerides: biological activities, experimental testing, and therapeutic applications. *International Journal of Molecular Sciences.* 2018;19(4):1114.
365. Kohlmeier M. Chapter 8 - Amino Acids and Nitrogen Compounds. In: Kohlmeier M, ed. *Nutrient Metabolism (Second Edition)*. San Diego: Academic Press; 2015:265-477.
366. Bahri S, Zerrouk N, Aussel C, et al. Citrulline: From metabolism to therapeutic use. *Nutrition.* 2013;29(3):479-484.
367. Lo C-J, Ko Y-S, Chang S-W, et al. Metabolic signatures of muscle mass loss in an elderly Taiwanese population. *Aging (Albany NY).* 2021;13(1):944.
368. Kersten S, Mandard S, Escher P, et al. The peroxisome proliferator-activated receptor α regulates amino acid metabolism. *FASEB Journal.* 2001;15(11):1971-1978.
369. Reddy JK. Peroxisome proliferators and peroxisome proliferator-activated receptor alpha: biotic and xenobiotic sensing. *Am J Pathol.* 2004;164(6):2305-2321.
370. Pierozan CR, Agostini PS, Gasa J, et al. Factors affecting the daily feed intake and feed conversion ratio of pigs in grow-finishing units: the case of a company. *Porcine health management.* 2016;2:7.
371. Honerlaw JP, Ho Y-L, Nguyen X-MT, et al. Fried food consumption and risk of coronary artery disease: The Million Veteran Program. *Clinical Nutrition.* 2020;39(4):1203-1208.
372. Reeves PG, Nielsen FH, Fahey GC. AIN-93 Purified Diets for Laboratory Rodents: Final Report of the American Institute of Nutrition Ad Hoc Writing Committee on the Reformulation of the AIN-76A Rodent Diet. *The Journal of Nutrition.* 1993;123(11):1939-1951.
373. Firestone D. Official methods and recommended practices of the AOCS. *(No Title).* 2009.
374. Durán Merás I, Periañez Llorente C, Pilo Ramajo J, Martín Tornero E, Espinosa-Mansilla A. Optimization of the thiobarbituric acid-malonaldehyde reaction in non-aqueous medium. Direct analysis of malonaldehyde in oil samples by HPLC with fluorimetric detection. *Microchemical Journal.* 2020;159:105318.
375. Wang Y, Cui P. Reactive Carbonyl Species Derived from Omega-3 and Omega-6 Fatty Acids. *Journal of Agricultural and Food Chemistry.* 2015;63(28):6293-6296.
376. Liu P, Kerr BJ, Chen C, Weber TE, Johnston LJ, Shurson GC. Methods to create thermally oxidized lipids and comparison of analytical procedures to characterize peroxidation1. *Journal of Animal Science.* 2014;92(7):2950-2959.

377. Sjövall O, Kuksis A, Kallio H. Formation of triacylglycerol core aldehydes during rapid oxidation of corn and sunflower oils with tert - butyl hydroperoxide/Fe²⁺. *Lipids.* 2002;37(1):81-94.
378. Ren R, Hashimoto T, Mizuno M, et al. A lipid peroxidation product 9-oxononanoic acid induces phospholipase A2 activity and thromboxane A2 production in human blood. *Journal of Clinical Biochemistry and Nutrition.* 2013;52(3):228-233.
379. Comai S, Bertazzo A, Brughera M, Crotti S. Chapter Five - Tryptophan in health and disease. In: Makowski GS, ed. *Advances in Clinical Chemistry.* Vol 95: Elsevier; 2020:165-218.
380. Michael AF, Drummond KN, Doeden D, Anderson JA, Good RA. TRYPTOPHAN METABOLISM IN MAN. *J Clin Invest.* 1964;43(9):1730-1746.
381. Van Raalte DH, Li M, Pritchard PH, Wasan KM. Peroxisome Proliferator-Activated Receptor (PPAR)- : A Pharmacological Target with a Promising Future. *Pharmaceutical Research.* 2004;21(9):1531-1538.
382. Luci S, König B, Giemsa B, et al. Feeding of a deep-fried fat causes PPARα activation in the liver of pigs as a non-proliferating species. *British Journal of Nutrition.* 2007;97(5):872-882.
383. Volker D, Fitzgerald P, Major G, Garg M. Efficacy of fish oil concentrate in the treatment of rheumatoid arthritis. *The Journal of rheumatology.* 2000;27(10):2343-2346.
384. Sethi S, Ziouzenkova O, Ni H, Wagner DD, Plutzky J, Mayadas TN. Oxidized omega-3 fatty acids in fish oil inhibit leukocyte-endothelial interactions through activation of PPARα. *Blood, The Journal of the American Society of Hematology.* 2002;100(4):1340-1346.
385. Singh R, Lemire J, Mailloux RJ, Appanna VD. A novel strategy involved in [corrected] anti-oxidative defense: the conversion of NADH into NADPH by a metabolic network. *PLoS One.* 2008;3(7):e2682.
386. Chatuphonprasert W, Sriset Y, Jarukamjorn K. Continuous consumption of reused palm oil induced hepatic injury, depletion of glutathione stores, and modulation of cytochrome P450 profiles in mice. *Polish Journal of Food and Nutrition Sciences.* 2019;69(1).
387. Degroote J, Wang W, Vergauwen H, De Smet S, Van Ginneken C, Michiels J. Impact of a dietary challenge with peroxidized oil on the glutathione redox status and integrity of the small intestine in weaned piglets. *animal.* 2019;13(8):1641-1650.
388. Saka S, Aouacheri W, Abdennour C. The capacity of glutathione reductase in cell protection from the toxic effect of heated oils. *Biochimie.* 2002;84(7):661-665.
389. Ammouche A, Rouaki F, Bitam A, Bellal MM. Effect of Ingestion of Thermally Oxidized Sunflower Oil on the Fatty Acid Composition and Antioxidant Enzymes of Rat Liver and Brain in Development. *Annals of Nutrition and Metabolism.* 2002;46(6):268-275.
390. Narayanankutty A, Manalil JJ, Suseela IM, et al. Deep fried edible oils disturb hepatic redox equilibrium and heightens lipotoxicity and hepatosteatosis in male Wistar rats. *Human & Experimental Toxicology.* 2016;36(9):919-930.

391. Bröer S. Amino Acid Transport Across Mammalian Intestinal and Renal Epithelia. *Physiological reviews.* 2008;88(1):249-286.
392. Bröer S. The role of the neutral amino acid transporter B0AT1 (SLC6A19) in Hartnup disorder and protein nutrition. *IUBMB Life.* 2009;61(6):591-599.
393. Włodek L. The reaction of sulfhydryl groups with carbonyl compounds. *Acta Biochim Pol.* 1988;35(4):307-317.
394. Neis E, Dejong C, Rensen S. The Role of Microbial Amino Acid Metabolism in Host Metabolism. *Nutrients.* 2015;7(4):2930-2946.
395. Honda A, Miyazaki T, Iwamoto J, et al. Regulation of bile acid metabolism in mouse models with hydrophobic bile acid composition. *J Lipid Res.* 2020;61(1):54-69.
396. Li T, Chiang JYL. Bile acids as metabolic regulators: an update. *Current opinion in gastroenterology.* 2023;39(3):249-255.
397. Nowiński A, Chabowski D, Giebułtowicz J, Aleksandrowicz M, Ufnal M. Deoxycholic Acid, a Secondary Bile Acid, Increases Cardiac Output and Blood Pressure in Rats. *Nutrients.* 2024;16(1).
398. Kawano A, Ishikawa H, Kamano T, et al. Significance of fecal deoxycholic acid concentration for colorectal tumor enlargement. *Asian Pacific journal of cancer prevention : APJCP.* 2010;11(6):1541-1546.
399. Stenman LK, Holma R, Forsgård R, Gylling H, Korpela R. Higher Fecal Bile Acid Hydrophobicity Is Associated with Exacerbation of Dextran Sodium Sulfate Colitis in Mice. *The Journal of Nutrition.* 2013;143(11):1691-1697.
400. Raimondi F, Santoro P, Barone MV, et al. Bile acids modulate tight junction structure and barrier function of Caco-2 monolayers via EGFR activation. *American Journal of Physiology-Gastrointestinal and Liver Physiology.* 2008;294(4):G906-G913.
401. David LA, Maurice CF, Carmody RN, et al. Diet rapidly and reproducibly alters the human gut microbiome. *Nature.* 2014;505(7484):559-563.
402. Stenman LK, Holma R, Korpela R. High-fat-induced intestinal permeability dysfunction associated with altered fecal bile acids. *World journal of gastroenterology: WJG.* 2012;18(9):923.
403. Bortolotti M, Kreis R, Debard C, et al. High protein intake reduces intrahepatocellular lipid deposition in humans2. *The American journal of clinical nutrition.* 2009;90(4):1002-1010.
404. Martin-Rubio AS, Sopelana P, Nakashima F, Shibata T, Uchida K, Guillén MD. A Dual Perspective of the Action of Lysine on Soybean Oil Oxidation Process Obtained by Combining 1H NMR and LC–MS: Antioxidant Effect and Generation of Lysine–Aldehyde Adducts. *Antioxidants.* 2019;8(9):326.
405. Sigolo CAO, Mascio PD, Medeiros MHG. Covalent Modification of Cytochrome c Exposed to trans,trans-2,4-Decadienal. *Chemical Research in Toxicology.* 2007;20(8):1099-1110.
406. Zhang Y, Ho CT. Volatile compounds formed from thermal interaction of 2,4-decadienal with cysteine and glutathione. *Journal of Agricultural and Food Chemistry.* 1989;37(4):1016-1020.

407. Van Lancker F, Adams A, De Kimpe N. Chemical Modifications of Peptides and Their Impact on Food Properties. *Chemical Reviews.* 2011;111(12):7876-7903.
408. Zamora R, Gallardo E, Hidalgo FJ. Strecker Degradation of Phenylalanine Initiated by 2,4-Decadienal or Methyl 13-Oxooctadeca-9,11-dienoate in Model Systems. *Journal of Agricultural and Food Chemistry.* 2007;55(4):1308-1314.
409. Zhou A, Boatright WL. Formation of 2‐Pentyl Pyridine During Processing of Soybean Protein Isolates as Affected by pH. *Journal of Food Science.* 1999;64(5):852-854.
410. Zhu X, Tang X, Zhang J, Tochtrop GP, Anderson VE, Sayre LM. Mass spectrometric evidence for the existence of distinct modifications of different proteins by 2(E),4(E)-decadienal. *Chem Res Toxicol.* 2010;23(3):467-473.
411. Adams A, Kitryte V, Venskutonis R, De Kimpe N. Model studies on the pattern of volatiles generated in mixtures of amino acids, lipid-oxidation-derived aldehydes, and glucose. *J Agric Food Chem.* 2011;59:1449.
412. Lin L, Zhang K, Xiong Q, et al. Gut microbiota in pre-clinical rheumatoid arthritis: From pathogenesis to preventing progression. *Journal of Autoimmunity.* 2023:103001.
413. McGirr LG, Hadley M, Draper HH. Identification of N alpha-acetyl-epsilon-(2-propenal)lysine as a urinary metabolite of malondialdehyde. *Journal of Biological Chemistry.* 1985;260(29):15427-15431.
414. Zhang Q, Ke J, Long P, et al. Formation of Furan from Linoleic Acid Thermal Oxidation: (E,E)-2,4-Decadienal as a Critical Intermediate Product. *Journal of Agricultural and Food Chemistry.* 2024;72(8):4384-4392.
415. Lin J, Fay LB, Welti DH, Blank I. Quantification of key odorants formed by autoxidation of arachidonic acid using isotope dilution assay. *Lipids.* 2001;36(7):749-756.
416. Meijboom PW, Stroink JBA. 2-trans,4-cis,7-cis-Decatrienal, the fishy off-flavor occurring in strongly autoxidized oils containing linolenic acid or ω 3,6,9, etc., fatty acids. *Journal of the American Oil Chemists Society.* 1972;49(10):555-558.
417. Pan K-L, Huang W-J, Hsu M-H, et al. Identification of trans,trans-2,4-Decadienal Metabolites in Mouse and Human Cells Using Liquid Chromatography–Mass Spectrometry. *Chemical Research in Toxicology.* 2014;27(10):1707-1719.
418. Wahlström A, Sayin Sama I, Marschall H-U, Bäckhed F. Intestinal Crosstalk between Bile Acids and Microbiota and Its Impact on Host Metabolism. *Cell Metabolism.* 2016;24(1):41-50.

APPENDIX

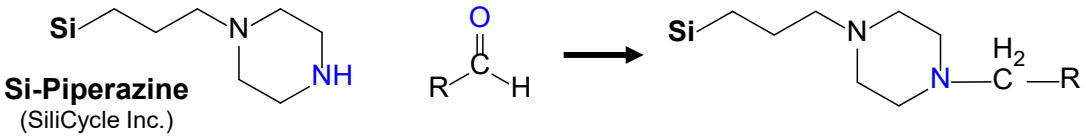

Appendix Figure A1 Scheme of reaction between a functionalized silica (Si-Piperazine) with an aldehyde.